AN ABSTRACT OF THE DISSERTATION OF

Kelsey Shea Swieca for the degree of Doctor of Philosophy in Integrative Biology presented on May 6, 2022.

Title: Influence of Regional Oceanography on the Distributions, Trophic Interactions, Growth, and Survival of the Early Life History Stages of Fishes

Abstract approved: _____

Su Sponaugle

Most marine fishes experience high rates of mortality during their early life history stages with far reaching consequences for adult population dynamics. Within a few weeks of hatching, relatively small changes in larval growth and mortality rates can lead to orders of magnitude variability in year-class strength. Growth and survival during this phase are contingent upon the ability of larvae to find food and avoid predation in a physically and biologically heterogeneous environment. Here, we coupled biological sampling and fine-scale *in situ* plankton imaging to examine the influence of regional oceanography on larval fish distributions, feeding, and growth in the context of their zooplankton prey and predators in the northern California Current (NCC). Larval fish were strongly affected by two highly dynamic regional oceanographic features in the NCC: coastal upwelling and the Columbia River Plume. While the NCC supports major fisheries whose larval and juvenile stages depend on upwelling driven primary and secondary production, coastal upwelling is highly variable in space and time. In Chapter 2, diet and otolith microstructure analysis showed that the condition of a dominant myctophid (*Stenobrachius leucopsarus*) reflected the prevailing upwelling conditions. During reduced upwelling, recent growth was substantially slower, guts less full, and diets dominated by low trophic level prey. In contrast, during active upwelling, faster-growing northern lampfish fed on higher quality copepod prey. Yet, larvae exhibited reduced feeding and growth in the most intense upwelling, revealing a dome-shaped relationship with the fastest growth occurring in moderate upwelling conditions. Further, high zooplanktivorous predation pressure on larval northern lampfish led to above

average growth, which may indicate the selective loss of slower-growing larvae. Chapter 3 revealed that upwelling also influenced the larval growth of another forage fish, northern anchovy (*Engraulis mordax*). Northern anchovy otolith-derived recent growth was spatially variable and related to the location of the summer upwelling front. When the front was restricted nearshore, inshore larval anchovy grew significantly faster than offshore. Conversely, when a period of prolonged active upwelling pushed the front to the edge of the continental shelf, offshore anchovy larvae grew significantly faster than inshore. Larval anchovy growth may be constrained by cross-shelf temperature differences and the distribution of nutritious copepod prey that are restricted to the nearshore environment off Oregon in summer. Embedded within the highly dynamic NCC, the tidally modulated Columbia River Plume is an important spawning and nursery ground for many fishes (e.g., northern anchovy, *E. mordax*). In Chapter 4, data illustrated how the strength and location of the plume front exposed larval fishes to a diversity of unique prey and predator fields over the progression of a tidal cycle. While the plume region provided a substantially higher concentration of prey that are important for the feeding of young fishes occupying this area, this region was also characterized by enhanced spatial overlap of larval fishes and their zooplankton predators relative to oceanic waters. In a separate study, and in partial fulfillment of the National Science Foundation Research Traineeship (NRT) program at Oregon State University, Chapter 5 switched focus from larval fishes to another component of the plankton: Dungeness crab larvae. Mortality during the early life history stages of Dungeness crab is considered a bottleneck for fishery production, but information on the offshore distribution of the most vulnerable pelagic larval stages is lacking. Fine-scale depth discrete biological sampling over two years revealed that Dungeness crab larvae were not uniformly distributed in time or space, but exhibited distinct spatial distributions within the water column, over the continental shelf, and across latitudes, with larval abundance significantly negatively correlated with *in situ* temperature and salinity throughout ontogeny. Taken together, this body of work demonstrates that local and regional oceanographic features contribute to variable zooplankton distributions as well as growth and mortality patterns for larval fishes by affecting their trophic interactions. This dissertation illustrates the importance

of incorporating food-web dynamics and local and regional oceanographic processes when predicting the response of fish and crab populations to ecosystem variability.

Influence of Regional Oceanography on the Distributions, Trophic Interactions, Growth, and Survival of the Early Life History Stages of Fishes

by
Kelsey Shea Swieca

A DISSERTATION

submitted to

Oregon State University

in partial fulfillment of
the requirements for the
degree of

Doctor of Philosophy

Presented May 6, 2022
Commencement June 2022

Doctor of Philosophy dissertation of Kelsey Shea Swieca presented on May 6, 2022

APPROVED:

Major Professor, representing Integrative Biology

Head of the Department of Integrative Biology

Dean of the Graduate School

I understand that my dissertation will become part of the permanent collection of Oregon State University libraries. My signature below authorizes release of my dissertation to any reader upon request.

Kelsey Shea Swieca, Author

ACKNOWLEDGEMENTS

I am sincerely grateful to many colleagues, friends, and family for their continued support and encouragement through my graduate studies. First and foremost, I'd like to acknowledge my advisor, Su Sponaugle, for her commitment to my development as a scientist. I am incredibly thankful for her genuine approach to mentorship, unwavering support, and thoughtful advice. Additionally, I want to thank my quasi co-advisor Bob Cowen, who has always provided perspective in a sea of madness (literally and figuratively). His ability to innovate and lead have been particularly impactful. Together, Su and Bob have fostered a lab family that has carried me through my PhD and I am lucky to have studied under them.

My work has greatly benefited from the contributions of three additional committee members. Ric Brodeur has been a mentor and an invaluable knowledge source, continually sharing his California Current expertise. In addition to his ability to quickly recall literature, I'm thankful for his warm demeanor. I also thank Lorenzo Ciannelli for being remarkably generous with his time and guiding me through quantitative analyses. Finally, I thank Francis Chan for his support and 'big picture' perspective as a member of my committee.

I could not have completed my PhD without those who helped at-sea and in the lab. Most importantly, my lab mates, who became some of my greatest friends: Kelia Axler, Miram Gleiber, Will Fennie, Megan Wilson, Moritz Schmid, Jami Ivory, Christian Briseño-Avena, and Dani Ottmann. It is difficult to express how grateful I am to have shared ideas and laughs with each member of this wonderful crew. In addition to their intellectual and moral support, I'd also like to acknowledge the significant amount of time (up to 40 d) many of them spent at-sea collecting the data used in this project. I also thank Jessica Luo, Kelly Robinson, and Clare Hansen. Although we didn't share the lab for long, I greatly appreciated your kindness and encouragement at the start of my graduate journey. Finally, I'm happy to have had the opportunity to collaborate with the Sutherland Lab at University of Oregon. Their humor and excitable nature made many long shifts at-sea enjoyable. Thank you, all.

Next, I thank the Department of Integrative Biology (IB) and Hatfield Marine Science Center (HMSC) for the continual financial and logistical support throughout my degree. I'm indebted to the 4 T's from IB and the Director's Office staff at HMSC, in particular. The funding opportunities provided from each institution, as well as Hatfield Student Organization, have been immensely helpful. Further, I'd like to thank the BI 20x teaching team for their flexibility as we navigated long distance instruction and the army of IB undergraduates (n=18) who have contributed to the lab work for my project.

While at OSU, I had the opportunity to participate in a National Research Traineeship (NRT) program which was instrumental in my development as a scientist. Through its interdisciplinary approach, the NRT expanded my understanding of coupled human-natural systems and showed me how I could better incorporate the human dimension into my ecological work. Most importantly, however, this program highlighted the benefits of effective collaborative research and encouraged me to pursue meaningful collaborations throughout my academic career. I am proud to have been part of the 'Crab Team' and am honored to have been able to work so closely with Caitlin Magel, Liz Lee, Astrea Stawn, and Andrew Jensen. Many thanks to the NRT program leads, especially Lorenzo Ciannelli and Katherine Hoffman, for their guidance and financial support.

Now, I thank the most important people of all – my family. While some are biological, some chosen, and some canine, each has played a special role in my development as a scientist. My parents, Chris and Sara Swieca, who have blindly supported me and my endeavors since day one. Thank you…for everything. Thank you for sacrificing for me, thank you for believing in me. I'm continually grateful for encouragement from my sisters, Megan and Sadie, and Megan's husband, Matt, as well as my in-laws and niece and nephew. I also need to thank my grandmas, whose stories from home and adventures to fill the bouillabaisse stock were a natural history lesson all in their own. Finally, my husband, John, and dog, Mack, who have been a source of comfort since long before this journey. Thank you for walking through this with me. You have scarified a lot for my dream and it didn't go unnoticed.

CONTRIBUTION OF AUTHORS

Chapters 2 & 3: Kelsey Swieca conducted all laboratory analyses, data analysis, and manuscript preparation; Su Sponaugle served as co-PI, advised Kelsey Swieca and edited manuscript drafts; Robert Cowen was a co-PI and chief scientist during all field work; Moritz Schmid facilitated image processing; Jami Ivory sorted plankton samples. Kelsey Swieca, Robert Cowen, Moritz Schmid, and Jami Ivory participated in field work.

Chapter 4: Kelsey Swieca conducted data analysis and manuscript preparation; Su Sponaugle and Robert Cowen served as co-PIs, advised Kelsey Swieca and edited manuscript drafts; Richard Brodeur was chief scientist during field work; Christian Briseño-Avena and Moritz Schmid facilitated image processing. Kelsey Swieca, Robert Cowen, Richard Brodeur, Christian Briseño-Avena, and Moritz Schmid participated in fieldwork.

Chapter 5: Kelsey Swieca conducted data analysis and manuscript preparation; Su Sponaugle served as co-PI, advised Kelsey Swieca and edited manuscript drafts; Robert Cowen was a co-PI and chief scientist; Jami Ivory sorted plankton samples; Kelsey Swieca, Robert Cowen, and Jami Ivory participated in field work.

TABLE OF CONTENTS

TABLE OF CONTENTS (Continued)

Page

LIST OF FIGURES

LIST OF FIGURES (Continued)

LIST OF FIGURES (Continued)

LIST OF TABLES

LIST OF APPENDICES

LIST OF APPENDICES (Continued)

Appendix Page

CHAPTER 1: General introduction

Most marine fishes experience high rates of mortality during their early life history stages with far reaching consequences for adult population dynamics. Within a few weeks of hatching, larvae that experience relatively small changes in growth and mortality rates can lead to orders of magnitude variability in year-class strength (Houde 1987, Leggett & Deblois 1994, Houde 2008). As such, identifying the factors influencing larval growth and survival is a core goal of fisheries oceanographers (Hare 2014).

Over a century of work has emphasized that larval fish growth and survival are contingent upon the ability to find food and avoid predation in the physically and biologically heterogeneous pelagic environment. Starvation during the early larval stages was initially recognized as a bottleneck for fishery production in Hjort's (1914) *Critical Period Hypothesis.* Building on this seminal work, a number of foundational hypotheses were developed to help explain how mortality during the early life history stages affects recruitment to the adult population. Notably, the *Stable Ocean* (Lasker 1978, 1981) and *Optimal Environmental Window Hypotheses* (Cury & Roy 1989, Roy et al. 1992) emphasize the interaction between oceanography and feeding success. The former suggests calm periods in upwelling systems promote the aggregation of prey resources needed to support sufficient larval feeding. The latter posits that there is a dome-shaped relationship between upwelling intensity and recruitment with the highest survivorship occurring during moderate upwelling conditions. Finally, the *Growth-Mortality Hypotheses* (Anderson 1988) signify an important shift in the understanding of fish recruitment and highlights the implication of poor feeding on larval vulnerability to predation. Taken together, these works illustrate that recruitment variability is the result of complex food-web dynamics, which are subject to the prevailing oceanographic conditions (Houde 2008). However, the specific mechanisms underlying these hypotheses remain unclear and appear to be system-, scale-, and species-specific.

Physical features that increase productivity and/or aggregate prey resources are thought to heighten survival through the early life history stages and positively affect year-class strength (Lasker 1975, Anderson 1988, Miller et al. 1988, Hare & Cowen 1997). It is generally asserted that enhanced prey availability leads to high feeding

success, fast growth, and large size-at-age (Sponaugle et al. 2009, Pepin et al. 2015). Following this logic, oceanographic features that increase food availability are often considered a hallmark for superior larval growth and survival. However, recent studies have challenged this idea by demonstrating that larvae exhibit strong preferences for specific prey taxa and selectively feed on ambient prey fields, sometimes distinguishing among prey of different species (Robert et al. 2014). Further, many oceanographic processes that increase production also lead to turbulent mixing which can reduce foraging success by disrupting prey aggregations (Lasker 1978, 1981, Cury & Roy 1989). Thus, the degree to which increased production confers enhanced larval fish feeding success is debatable. Feeding success is more likely a function of local productivity and the factors that influence encounter rates between larvae and their preferred prey (Pepin et al. 2015).

In addition to the biological consequences of preferred prey availability, predator concentrations influence larval fish survival. Unfortunately, the same physical mechanisms that aggregate prey resources also concentrate known larval fish predators (Luo et al. 2014). Yet, the potential for co-occurring predator abundances to offset the perceived advantages of heightened larval feeding is not well understood. Foundational theories in the field of fisheries oceanography suggest that that predation is the primary agent of larval mortality, though it is mediated by feeding success (Bailey & Houde 1989). Specifically, the *Growth-Mortality Hypothesis* and its three corollaries (*bigger-is-better*, *stage duration*, and *growth-selective predation*), suggest that larger size, faster growth, and quicker development reduces vulnerability to predation (Anderson 1988). Because baseline prey levels necessary for survival may have historically been over-estimated (Houde 2008) and many fish larvae are satiated in the wild, even in oligiotrophic environments (Llopiz & Cowen 2008), predation is likely an important factor determing recruitment to adult populations.

Larval fish predators encompass many taxa, including older conspecifics (Ciannelli et al. 2007). However, gelatinous zooplankton have received special attention because of their propensity to undergo population 'blooms' that have the potential to cause significant larval mortality. There are two types of gelatinous zooplankton blooms: 'true blooms' that occur due to population growth, and 'apparent blooms' that result from

the aggregation of their highly-buoyant bodies at density discontinuities (e.g., fronts, eddies, etc.; Graham et al. 2001, Purcell & Arai 2001, McClatchie et al. 2012, Luo et al. 2014). Chaetognaths (semi-gelatinous), ctenophores, hydromedusae, and siphonophores have been shown to consume fish larvae (Alvarino 1985, Purcell & Grover 1990). While some studies in the northern California Current have anecdotally recorded predation events by these taxa (Auth & Brodeur 2006), others have quantitatively demonstrated that fish larvae can account for >90% of the diet of some gelatinous taxa (Purcell 1985). Gelatinous zooplankton clearly play an important role in larval fish food-web dynamics and the need to understand the implications of their predation is greater than ever, as the abundance of potential gelatinous predators is increasing in many systems (e.g., the northern California Current; Brodeur et al. 2019).

In short, both predation and starvation are thought to be the dominant causes of larval fish mortality (Houde 1987, 2008). Predation may be the main direct source of larval mortality (Bailey & Houde 1989) while food limitation can act directly through starvation, or indirectly by slowing larval growth rates thereby increasing predation-induced mortality (Houde 1987). Both larva-prey and larva-predator encounter rates are mediated by physical processes that dictate the amount of food available in the water column and affect the spatial distributions of larvae, their prey, and their potential predators. Understanding the implications of variable prey and predation densities is necessary for a comprehensive examination of the forces guiding larval growth, survival, and recruitment to the adult population.

Study system: The northern California Current (NCC)

The northern California Current (NCC) is a highly productive Eastern boundary current within the broader California Current Large Marine Ecosystem. It is an ideal study system to examine the influence of physical oceanographic features on planktonic trophic interactions as it exhibits strong physical and ecosystem variability spatially and on seasonal and interannual timescales (Checkley & Barth 2009). Two dynamic regional oceanographic features dominate the NCC coastal ocean: upwelling and the Columbia River Plume.

Coastal wind-driven upwelling occurs when prevailing equatorward winds drive surface waters offshore, allowing cooler, nutrient rich water to rise into the euphotic zone. There are strong latitudinal gradients in the intensity and seasonality of coastal upwelling in the NCC. While the central coast of Oregon has distinct downwelling (winter) and upwelling (summer) seasons, northern California typically experiences stronger and more persistent upwelling with a higher degree of interannual variability. In both locations, upwelling is typically intermittent, occurring on time scales of 3-10 d separated by the presence of weak winds (Bograd et al. 2009, Checkley & Barth 2009, García-Reyes & Largier 2012). Strong and sustained periods of upwelling-favorable winds increase the cross-shelf region of cold and productive upwelled waters (Castelao et al. 2005). Within this broader pattern, local environments are influenced by land-wind interactions which also impact the cross-shelf extent of upwelling. For example, topographic features (i.e., headlands) along the coast deflect the upwelling jet offshore, creating discrete upwelling cells which broaden the region influenced by upwelling-induced production (Checkley & Barth 2009). Embedded within the NCC, the Oregon-Washington coastal ecosystem is further complicated by significant freshwater inputs from the Columbia River. In addition to promoting high primary and secondary production, the tidally-modulated Columbia River Plume is marked by sharp physical gradients at the plume fronts that structure the coastal ecological community (Morgan et al. 2005, Peterson & Peterson 2008, 2009, Henderikx Freitas et al. 2018).

The NCC supports major fisheries whose larval and juvenile stages depend on upwelling driven primary and secondary production. Yet, most NCC fishes spawn in winter when the system is downwelling or experiencing reduced upwelling, and some fish (e.g., northern lampfish, *Stenobrachius leucopsarus*) have protracted spawning seasons that encompass both winter (downwelling) and summer (upwelling) conditions. Only a few species (northern anchovy, *Engraulis mordax* and Pacific sardine, *Sardinops sagax*) are considered summer spawners and their spawning habitat is thought to be restricted to waters influenced by the Columbia River Plume (Richardson 1973, Richardson & Pearcy 1977, Auth & Brodeur 2006, Auth et al. 2007, Brodeur et al. 2008, Auth 2009). In Ekman-type upwelling systems, there is a tradeoff between access to productivity and favorable transport. Upwelling induced offshore advection in the NCC

poses a risk for larval fish feeding as well as life cycle closure, especially for species that recruit to nearshore habitats (Parrish et al. 1981). A hypothesized solution to this problem is that fishes develop reproductive strategies that place larvae in the pelagic realm during periods or locations that minimize the probability of offshore advection (Parrish et al. 1981) while providing enough production for sustenance and slower, but sufficient growth for survival.

Larval success in the NCC has historically been linked to the timing and location of preferred prey availability and the degree of offshore transport; however, we lack information on how variable species distributions may or may not translate to realized biological consequences (i.e., diet, feeding success, and growth data) in this system. While a vast body of research is dedicated to studying the diets and growth of planktonic marine fish larvae, most of this work is concentrated at high- and low-latitudes. Of the 204 studies included in a recent review of larval diets, only 10 were from the California Current and two from the NCC (Llopiz 2013). Larval fish feeding and growth are rarely quantified at mid-latitude upwelling intensive environments where many of the world's most abundant fisheries occur (e.g., the NCC). Seminal work examining the gut contents of larvae off Oregon suggested that larvae selectively feed on ambient prey fields and successful prey capture is impacted by prevailing upwelling conditions. Specifically, English sole (Pleuronectidae, *Parophrys vetulus)* have been observed with higher gut contents in calm, reduced upwelling conditions (spatially and temporally) when their preferred prey, appendicularians, were aggregated in high abundance (Alldredge 1982, Gadomski & Boehlert 1984).

Recently, the California Current experienced a severe marine heat wave with sea surface temperatures up to 6.2 °C above average and primary productivity anomalously low in many regions (Gentemann et al. 2017, Kahru et al. 2018, Thompson et al. 2019). These conditions impacted larval fish spawning phenology (Auth et al. 2018) and zoo- and ichthyoplankton community structure (Brodeur et al. 2019, Thompson et al. 2019). Novel and unanticipated biological responses under these anomalous conditions have made it abundantly clear that there are gaps in our knowledge about the specific mechanisms linking physical oceanographic conditions to biological responses in the California Current. While the implications of the marine heat wave can be observed in

spatial and temporal distributional data, a lack of information on the basic tenants of ichthyoplankton life histories, including their diets and growth rates and the relationship between these metrics and variable oceanographic conditions limits our ability to predict the impact of the marine heat wave on the economically and ecologically important species in the NCC.

Foundational theories in the field of fisheries oceanography suggest that larval fish prey availability and predation pressure dictate growth and survival, yet few studies explicitly address these interactions in this study system. Nonetheless, variability in upwelling and plume characteristics (i.e., intensity, phenology, spatial extent) likely contribute to complex patterns of feeding, growth, and subsequent survival of young fishes. An examination of the biological consequences of spatial and temporal variability in larval fishes, their prey, and their potential predator densities will help to build a comprehensive understanding of success at the base of the NCC marine food-web.

Sampling technologies

The zooplankton community is notoriously challenging to sample. Many constituents of this group have patchy distributions and fragile morphologies making them difficult to capture, let alone quantify. Nevertheless, an accurate description of mesozooplankton fine-scale distributions is necessary to understand the factors regulating larval fish trophic interactions and subsequent survival. Traditional net-based sampling techniques have limited our ability to resolve these interactions, as integrating over large spatial (horizontal and vertical) scales obscures relationships between the environment, prey availability, feeding success, and predation events.

In this dissertation, I use two technologies to quantify distributions and trophic interactions at the base of the NCC marine food-web: (1) the high resolution *In situ* Ichthyoplankton Imaging System (ISIIS; Cowen & Guigand 2008) and (2) a coupled Multiple Opening/Closing Net and Environmental Sensing System (MOCNESS; Guigand et al. 2005). ISIIS is uniquely designed to sample large volumes of water, which increases the ability to simultaneously capture relatively rare planktonic organisms such as larval fishes and their more abundant prey and predators. Recent studies using ISIIS have elucidated the role of a number of oceanographic features in structuring planktonic

communities including mesoscale eddies in the Straits of Florida (Schmid et al. 2020), internal waves and oceanic fronts in the Atlantic Ocean (Greer et al. 2014, 2015), river plumes in the Gulf of Mexico (Greer et al. 2016, Axler et al. 2020), and fronts and thin layers in the Pacific Ocean (McClatchie et al. 2012, Greer et al. 2013, Luo et al. 2014). ISIIS imagery is generally coupled with depth-discrete MOCNESS tows to collect representative organisms to quantify the biological consequences (i.e., feeding and growth) of oceanographic features on larval fish trophic interactions.

Dissertation outline

My dissertation explores how local oceanography influences the trophic interactions, growth, and success of planktonic larvae in the NCC. In Chapter 2, I examine how the trophic environment impacts the feeding and growth of a dominant myctophid (northern lampfish, *Stenobrachius leucopsarus*) in four distinct NCC upwelling regimes. Chapter 3 focuses on how the spatial extent of upwelling and cross-shelf position of the upwelling front affects northern anchovy (*Engraulis mordax*) growth by altering *in situ* prey and predator distributions. Chapter 4 investigates the influence of the tidally modulated Columbia River Plume on the fine-scale horizontal and vertical distributions of larval fishes, their prey, and their potential predators. Finally, and in partial fulfillment of the requirements for Oregon State University's NSF Research Traineeship (NRT) program and Risk and Uncertainty Quantification in Earth Systems graduate minor, Chapter 5 describes the poorly understood offshore distribution of Dungeness crab larvae, including a description of their latitudinal, cross-shelf, vertical, and diel distributions and stage-specific relationships to oceanographic parameters. It is part of a broader transdisciplinary collaboration aimed at understanding the implications (both ecological and social) of a potential Dungeness crab range shift in the California Current. Overall, the ultimate over-arching goal of my dissertation is to further our understanding of the specific mechanisms through which variability in the environment translates into variability in the recruitment of organisms that play an important role in the larger ecosystem. With this knowledge, we can more accurately predict how fishes and crabs will respond to changing ocean conditions into the future.

REFERENCES

Alldredge AL (1982) Aggregation of spawning appendicularians in surface windrows. Bull Mar Sci 32:250–254

Alvarino A (1985) Predation in the plankton realm; mainly with reference to fish larvae. Inv Mar CICIMAR 2:1–122

Anderson JT (1988) A review of size dependent survival during pre-recruit stages of fishes in relation to recruitment. J Northwest Atl Fish Sci 8:55–66

Auth TD (2009) Importance of far-offshore sampling in evaluating the ichthyoplankton community in the northern California Current. Calif Coop Ocean Fish Investig Reports 50:107–117

Auth TD, Brodeur RD (2006) Distribution and community structure of ichthyoplankton off the coast of Oregon, USA, in 2000 and 2002. Mar Ecol Prog Ser 319:199–213

Auth TD, Brodeur RD, Fisher KM (2007) Diel variation in vertical distribution of an offshore ichthyoplankton community off the Oregon coast. Fish Bull 105:313–326

Auth TD, Daly EA, Brodeur RD, Fisher JL (2018) Phenological and distributional shifts in ichthyoplankton associated with recent warming in the northeast Pacific Ocean. Glob Chang Biol 24:259–272

Axler K, Sponaugle S, Briseño-Avena C, Hernandez Jr. F, Warner S, Dzwonkowski B, Dykstra S, Cowen R (2020) Variability in fine-scale distributions and predator-prey relationships of larval fishes during a high discharge event in the northern Gulf of Mexico. Mar Ecol Prog Ser 650:37–61

Bailey K, Houde E (1989) Predation on eggs and larvae of marine fishes and the recruitment problem. Adv Mar Biol 25:1–83

Bograd SJ, Schroeder I, Sarkar N, Qiu X, Sydeman WJ, Schwing FB (2009) Phenology of coastal upwelling in the California Current. Geophys Res Lett 36:1–5

Brodeur RD, Auth TD, Phillips A (2019) Major shifts in pelagic micronekton and macrozooplankton community structure in an upwelling ecosystem related to an unprecedented marine heatwave. Front Mar Sci 6:212

Brodeur RD, Peterson WT, Auth TD, Soulen HL, Parnel MM, Emerson AA (2008) Abundance and diversity of coastal fish larvae as indicators of recent changes in ocean and climate conditions in the Oregon upwelling zone. Mar Ecol Prog Ser 366:187–202

Castelao RM, Barth JA, Mavor TP (2005) Flow-topography interactions in the northern California Current System observed from geostationary satellite data. Geophys Res Lett 32:1–4

Checkley Jr. DM, Barth JA (2009) Patterns and processes in the California Current System. Prog Oceanogr 83:49–64

Ciannelli L, Dingsør GE, Bogstad B, Ottersen G, Chan K, Gjøsæter H, Stiansen JE, Stenseth NC (2007) Spatial anatomy of species survival: effects of predation and climate-driven environmental variability. Ecology 88:635–646

Cowen RK, Guigand CM (2008) *In situ* Ichthyoplankton Imaging System (ISIIS): system design and preliminary results. Limnol Oceanogr Methods 6:126–132

Cury P, Roy C (1989) Optimal environmental window and pelagic fish recruitment success in upwelling areas. Can J Fish Aquat Sci 46:670–680

Gadomski DM, Boehlert GW (1984) Feeding ecology of pelagic larvae of English sole *Parophrys vetulus* and butter sole *Isopsetta isolepis* off the Oregon coast. Mar Ecol

Prog Ser 20:1–12
García-Reyes M, Largier J (2012) Seasonality of coastal upwelling off central and northern California: New insights, including temporal and spatial variability. J Geophys Res Ocean 117:1–17
Gentemann CL, Fewings MR, García-Reyes M (2017) Satellite sea surface temperatures along the West Coast of the United States during the 2014–2016 northeast Pacific marine heat wave. Geophys Res Lett 44:312–319
Graham WM, Pagès F, Hamner WM (2001) A physical context for gelatinous zooplankton aggregations: a review. Hydrobiologia 451:199-212
Greer AT, Cowen RK, Guigand CM, Hare JA (2015) Fine-scale planktonic habitat partitioning at a shelf-slope front revealed by a high-resolution imaging system. J Mar Syst 142:111–125
Greer AT, Cowen RK, Guigand CM, Hare JA, Tang D (2014) The role of internal waves in larval fish interactions with potential predators and prey. Prog Oceanogr 127:47–61
Greer AT, Cowen RK, Guigand CM, McManus MA, Sevadjian JC, Timmerman AH (2013) Relationships between phytoplankton thin layers and the fine-scale vertical distributions of two trophic levels of zooplankton. J Plankton Res 35:939–956
Greer AT, Woodson CB, Smith CE, Guigand CM, Cowen RK (2016) Examining mesozooplankton patch structure and its implications for trophic interactions in the northern Gulf of Mexico. J Plankton Res 38:1115–1134
Guigand CM, Cowen RK, Llopiz JK, Richardson DE (2005) A coupled asymmetrical multiple opening closing net with environmental sampling system. Mar Technol Soc J 39:22–24
Hare JA, Cowen RK (1997) Size, growth, development, and survival of the planktonic larvae of *Pomatomus saltatrix* (Pisces: Pomatomidae). Ecology 78:2415–2431
Hare JA (2014) The future of fisheries oceanography lies in the pursuit of multiple hypotheses. ICES J Mar Sci 74: 2343–2356
Henderikx Freitas F, Saldías GS, Goni M, Shearman RK, White AE (2018) Temporal and spatial dynamics of physical and biological properties along the endurance array of the California Current ecosystem. Oceanography 31:80–89
Hjort J (1914) Fluctuations in the great fisheries of northern Europe viewed in the light of biological research. Rapp Procès-Verbaux 20:1–228
Houde E (1987) Fish early life dynamics and recruitment variability. Am Fish Soc Symp 2:17–29
Houde ED (2008) Emerging from Hjort's shadow. Fish Sci J Northw Atl Fish Sci 41:53–70
Kahru M, Jacox MG, Ohman MD (2018) CCE1: Decrease in the frequency of oceanic fronts and surface chlorophyll concentration in the California Current System during the 2014–2016 northeast Pacific warm anomalies. Deep Sea Res Part I Oceanogr Res Pap 140:4–13
Lasker R (1975) Field criteria for survival of anchovy larvae: the relation between inshore chlorophyll maximum layers and successful first feeding. Fish Bull US 73:453–462
Lasker R (1978) The relation between oceanographic conditions, and larval anchovy food in the California Current: Identification of factors contributing to recruitment failure.

Rapp P-V Reun Cons Int Explo Mer 173:212–230
Lasker R (1981) Factors contributing to variable recruitment of the nothern anchovy (*Engraulis mordax*) in the California Current: Contrasting years,1975 through 1978. Rapp P-V Reun Cons Int Explo Mer 178:375–388
Leggett W, Deblois E (1994) Recruitment in marine fishes: is it regulated by starvation and predation in the egg and larval stages? Netherlands J Sea Res 32:119–134
Llopiz JK (2013) Latitudinal and taxonomic patterns in the feeding ecologies of fish larvae: a literature synthesis. J Mar Syst 109–110:69–77
Llopiz JK, Cowen RK (2008) Precocious, selective and successful feeding of larval billfishes in the oceanic Straits of Florida. Mar Ecol Prog Ser 358:231–244
Luo JY, Grassian B, Tang D, Irisson J-O, Greer AT, Guigand CM, McClatchie S, Cowen RK (2014) Environmental drivers of the fine-scale distribution of a gelatinous zooplankton community across a mesoscale front. Mar Ecol Prog Ser 510:129–149
McClatchie S, Cowen R, Nieto K, Greer A, Luo JY, Guigand C, Demer D, Griffith D, Rudnick D (2012) Resolution of fine biological structure including small narcomedusae across a front in the Southern California Bight. J Geophys Res Ocean 117:1–18
Miller TJ, Crowder LB, Rice JA, Marschall EA (1988) Larval size and recruitment mechanisms in fishes: toward a conceptual framework. Can J Fish Aquat Sci 45:1657–1670
Morgan CA, Robertis A De, Zabel RW (2005) Columbia River plume fronts. I. Hydrography, zooplankton distribution, and community composition. Mar Ecol Prog Ser 299:19–31
Parrish RH, Nelson CS, Bakun A (1981) Transport mechanisms and reproductive success of fishes in the California Current. Biol Oceanogr 1:175–203
Pepin P, Robert D, Bouchard C, Dower JF, Falardeau M, Fortier L, Jenkins GP, Leclerc V, Levesque K, Llopiz JK, Meekan MG, Murphy HM, Ringuette M, Sirois P, Sponaugle S (2015) Once upon a larva: revisiting the relationship between feeding success and growth in fish larvae. ICES J Mar Sci 72:359–373
Peterson JO, Peterson WT (2008) Influence of the Columbia River plume (USA) on the vertical and horizontal distribution of mesozooplankton over the Washington and Oregon shelf. ICES J Mar Sci 65:477–483
Peterson JO, Peterson WT (2009) Influence of the Columbia River plume on cross-shelf transport of zooplankton. J Geophys Res 114:1–11
Purcell JE (1985) Predation on fish eggs and larvae by pelagic cnidarians and ctenophores. Bull Mar Sci 37:739–755
Purcell JE, Arai MN (2001) Interactions of pelagic cnidarians and ctenophores with fish: a review. Hydrobiologia 451:27–44
Purcell JE, Grover JJ (1990) Predation and food limitation as causes of mortality in larval herring at a spawning ground in British Columbia. Mar Ecol Prog Ser 59:55–61
Richardson SL (1973) Abundance and distribution of larval fishes in waters off Oregon, May - October 1969, with special emphasis on the northern anchovy, *Engraulis mordax.* Fish Bull 71:697–711
Richardson SL, Pearcy WG (1977) Coastal and oceanic fish larvae in an area of upwelling off Yaquina Bay, Oregon. Fish Bull 75:125–145
Robert D, Murphy H, Jenkins G, Fortier L (2014) Poor taxonomical knowledge of larval

fish prey preference is impeding our ability to assess the existence of a “critical period” driving year-class strength. ICES J Mar Sci 71:2042–2052

Roy C, Cury P, Kifani S (1992) Pelagic fish recruitment success and reproductive strategy in upwelling areas: environmental compromises. South African J Mar Sci 12:135–146

Schmid MS, Cowen RK, Robinson K, Luo JY, Briseño-Avena C, Sponaugle S (2020) Prey and predator overlap at the edge of a mesoscale eddy: fine-scale, in-situ distributions to inform our understanding of oceanographic processes. Sci Rep 10:921

Sponaugle S, Llopiz JK, Havel LN, Rankin TL (2009) Spatial variation in larval growth and gut fullness in a coral reef fish. Mar Ecol Prog Ser 383:239–249

Thompson AR, Schroeder ID, Bograd SJ, Hazen EL, Jacox MG, Leising A, Wells BK, Largier JL, Fisher JL, Jacobson KC, Zeman SM, Bjorktedt EP, Robertson RR, Kahru M, Goericke R, Peabody CE, Baumgartner T, Lavaniegos BE, Miranda LE, Gómez-Ocampo E, Gómez-Valdés J, Authy TD, Daly EA, Morgan CA, Burke JB, Field JC, Sakuma K, Weber ED, Watson W, Porquez JM, Dolliver J, Lyons DE, Orben RA, Zamon J, Warybok P, Jahncke J, Santora JA, Thompson SA, Hoover B, Sydeman WJ, Melin S (2019) State of the California current 2018-19: a novel anchovy regime and a new marine heat wave? CalCOFI Rep 60:1–65

CHAPTER 2: Shedding light on lanternfish: growth and diet of a larval myctophid across distinct upwelling regimes in the California Current

Abstract

Eastern Boundary Current Systems support major fisheries whose larval and juvenile stages depend on upwelling driven primary and secondary production. However, within these larger systems, upwelling can be highly variable at the regional scale, which likely results in complex patterns of feeding, growth, and survival for taxa who are broadly distributed in space and time. The northern California Current (NCC) is characterized by strong latitudinal variability in the seasonality and intensity of coastal upwelling: Oregon has distinct downwelling (winter) and upwelling (summer) seasons, while northern California experiences stronger and more persistent upwelling. We examined the diet and larval growth of a dominant myctophid (northern lampfish, *Stenobrachius leucopsarus*) in the context of their *in situ* prey and potential predators in distinct seasonal (winter, summer) and latitudinal (Oregon, northern California) upwelling regimes in the NCC. Larvae exhibited significant differences in diet and growth, with greater seasonal than latitudinal variability. In winter reduced upwelling, growth was substantially slower, guts less full, and diets dominated by copepod nauplii. In contrast, during summer upwelling, faster-growing larvae had guts that were more full from feeding on calanoid copepods and relying less heavily on lower trophic level prey (i.e., copepod nauplii and protists). Yet, our findings revealed a dome-shaped relationship with the fastest growth occurring at moderate upwelling intensity. Finally, high zooplanktivorous predation pressure was correlated to above average growth, which may indicate the selective loss of slower-growing larvae. Our results suggest that species whose spatio-temporal distributions encompass multiple regional upwelling regimes experience unique feeding and predation environments throughout their range with implications for larval survivorship.

In preparation for submission to: *ICES Journal of Marine Science*

1. INTRODUCTION

The early life history stages of marine fishes are generally considered a bottleneck for year-class strength and fishery production (Hjort 1914, Anderson 1988, Houde 2008). Survival through these critical periods is largely determined by the ability of larvae to find food and avoid predation in the highly dynamic pelagic environment (Lasker 1975, Bailey & Houde 1989). One key physical mechanism that may influence trophic interactions and the subsequent growth, survival, and recruitment (entry into the adult population) of the early life history stages of fishes is upwelling. Coastal wind-driven upwelling occurs when prevailing equatorward winds drive surface waters offshore, allowing cooler, nutrient rich water to rise into the euphotic zone. Coastal upwelling can influence the survival of the early life history stages of fishes directly, by dictating the amount of food available in the water column and, indirectly, by affecting the spatial distributions and encounter rates between larvae, their prey, and their potential predators.

Coastal upwelling is often considered a hallmark for increased food availability, as it promotes enhanced biological productivity (Checkley & Barth 2009 and references therein). For pelagic larval fishes, high prey availability can lead to high feeding success, fast growth, and large size-at-age of larvae (Sponaugle et al. 2009, Pepin et al. 2015). Typically, these traits are thought to increase survival through the vulnerable early life history stages and positively affect year-class strength (Lasker 1975, Anderson 1988, Miller et al. 1988, Hare & Cowen 1997). However, larvae feed selectively on available prey fields and the degree to which increased production confers increasing feeding is unclear (Robert et al. 2014). Further, in addition to increasing potential food availability, coastal upwelling leads to turbulent mixing of the nutrient rich upper water column and offshore transport of the surface layer. Both of these processes have the potential to indirectly affect larval survival by modifying larva-prey and larva-predator encounter rates (Lasker 1975, 1978, 1981, Parrish et al. 1981, Gadomski & Boehlert 1984).

The effect of upwelling on the early life history stages of fishes is highly variable and appears to be system, scale, and taxon dependent. Foundational hypotheses in the field of fisheries oceanography suggest that upwelling may be necessary to replenish surface nutrients, but too much upwelling can disrupt larval food aggregations and/or advect larvae into more oligotrophic conditions offshore ('Stable Ocean Hypothesis';

Lasker 1978, 1981, 'Optimal Environmental Window'; Cury & Roy 1989, Roy et al. 1992). Hence, there may be a dome-shaped relationship between upwelling intensity and recruitment with the highest survivorship occurring during moderate upwelling conditions when foraging success is high (due to nutrient inputs from upwelled waters coupled with moderate turbulence induced increased encounter rates) and advection losses are low. In addition to upwelling intensity, upwelling phenology may be an important characteristic impacting larval survival, especially in seasonal upwelling systems. For example, in the northern California Current (NCC), a delayed onset of the upwelling season (i.e., the spring transition) resulted in slower growth of northern anchovy (*Engraulis mordax*) larvae, with implication for recruitment (Takahashi et al. 2012). In the NCC, the onset and length of the upwelling season is tightly linked to the arrival and maintenance of a lipid-rich copepod community which likely serves as important prey base for this species (Hooff & Peterson 2006).

Variability in upwelling characteristics (i.e., intensity, duration, phenology) leads to complex patterns of feeding, growth, and survival of young fish. Yet, explicit studies of variability in larval and juvenile growth and feeding across upwelling regimes with differing intensity and phenology are rare. Further, it is typically challenging to simultaneously incorporate the influence of predation on survival because of the difficulty in sampling some taxa (i.e., gelatinous predators) with net-based systems. Nonetheless, feeding opportunities are often spatially correlated to predation risk (Purcell & Arai 2001, Bakun 2006, Fiksen et al. 2007, McClatchie et al. 2012, Luo et al. 2014) and predation may be the primary agent of larval mortality (Bailey & Houde 1989). In the present study, we analyze larval growth and feeding patterns of a common yet understudied fish relative to prey availability and co-occurring predation pressure in four distinct NCC upwelling regimes.

The NCC is characterized by strong latitudinal gradients in the intensity and seasonality of coastal upwelling. While the central coast of Oregon has distinct downwelling (winter) and upwelling (summer) seasons, northern California typically experiences stronger and more persistent upwelling with a higher degree of interannual variability. In both locations, occasional winter storms cause deep mixing of the water column and strong turbulence in the surface layer (Bograd et al. 2009, Checkley & Barth

2009, García-Reyes & Largier 2012). In the NCC, upwelling is frequently associated with high production and offshore transport of surface waters, while downwelling leads to decreased production, reduced water column stratification, and onshore transport (Husby & Nelson 1982, Checkley & Barth 2009). Variability in regional upwelling leads to changes in the community structure of zoo- and ichthyoplankton (Hooff & Peterson 2006, Auth 2008), with implications for species interactions and survival of young fishes.

Widely distributed from northern Baja California (~30° N) to the Bering Sea (~55° N; Matarese et al. 1989, Beamish et al. 1999, Brodeur & Yamamura 2005), the northern lampfish (*Stenobrachius leucopsarus*, Myctophidae) is frequently one of the most abundant larval fish in the California Current (Richardson 1973, Richardson & Pearcy 1977, Auth & Brodeur 2006, McClatchie et al. 2018). They are small bodied as adults, short lived, and can be considered a forage fish. Mature northern lampfish have a protracted spawning season throughout their range, which typically peaks in March each year (Fast 1960, Smoker & Pearcy 1970). Although an early study suggested that their spawning season is shorter off Oregon (October - March; Smoker & Pearcy 1970), larval northern lampfish are found in high abundances in spring and summer sampling (April/May - September/October; Richardson 1973, Richardson & Pearcy 1977, Auth & Brodeur 2006, Auth et al. 2007, Auth 2009) indicating that Oregon spawning likely extends further into summer than previously noted. Northern lampfish eggs are infrequently sampled due to a delicate chorion so exact size at hatch is unknown, but flexion and metamorphosis occur ~6.5 mm and 18 mm SL, respectively (Fast 1960, Smoker & Pearcy 1970, Matarese et al. 1989).

Latitudinal variability in the intensity and phenology of upwelling within the range of northern lampfish make this system and species ideal to tease apart relationships between upwelling, trophic interactions, growth, and subsequent survival of young fish. Though myctophids are not currently commercially harvested, they represent an important trophic link between zooplankton (e.g., copepods and euphausiids) and large marine predators (e.g., tuna, salmon, seabirds, and marine mammals; Brodeur & Yamamura 2005). Their sheer biomass points to the critical role northern lampfish play in NCC oceanic food-webs, yet they are the focus of relatively few studies. Knowledge of

their larval stage is particularly scant, with only one study examining larval growth (last 3d growth only; Methot 1981) in the literature.

We hypothesize that variability in the growth and diet of larval northern lampfish is related to the degree of upwelling and its influence on prey availability and potential predation pressure. To test this, we coupled otolith-derived measures of growth, gut content analysis, and *in situ* plankton imagery in four distinct NCC upwelling regimes: Oregon winter (typically downwelling), Oregon summer (typically moderate upwelling), northern California winter (typically upwelling), and northern California summer (typically strong upwelling). We expected growth to vary seasonally and latitudinally, with higher growth occurring during summer upwelling compared to winter downwelling (or reduced upwelling) conditions and in moderate Oregon upwelling compared to the more intense upwelling off of northern California where food webs might be disrupted by high turbulence.

2. MATERIALS AND METHODS

2.1 Field sampling

Biological net samples and *in situ* plankton imagery were collected during four research cruises in the northern California Current (NCC) over a period of 2 years, with two seasonal cruises in 2018 and two replicate cruises in 2019: winter 2018 (W18; Feb 15-23), summer 2018 (S18; Jul 3-11), winter 2019 (W19; Mar 3-11), and summer 2019 (S19; Jul 16-25).

During each cruise, we typically deployed nets at five stations and continuously towed the plankton imager along two historically sampled cross-shelf transects, the Newport Hydrographic Line (NH; seasonal upwelling) and the Trinidad Head Line (TR; continuous upwelling) (Fig. 2.1). Station locations were selected to capture shelf, shelf-break, and offshore environments on each transect. All sampling occurred during daylight hours.

2.1.1 Biological sample collection

Biological samples were collected with a coupled Multiple Opening/Closing Net and Environmental Sensing System (MOCNESS; Guigand et al. 2005) at every station. MOCNESS simultaneously sampled with five sets of paired nets: 4-m^2 nets fit with 1-mm

mesh and 1-m^2 nets fit with 333-µm mesh. The first set of nets were towed obliquely from the surface to depth (max 100 m) and the remaining four sets were triggered remotely to sample discrete 25 m depth bins. This system was towed behind the ship at 2.5 m s^{-1} and was fit with a flowmeter and conductivity, temperature, and depth sensors. Replicate MOCNESS tows were performed at every station, except for the W18 cruise when sampling was limited by winter storm conditions. In addition to MOCNESS sampling, to sample prey that might be excluded from the MOCNESS nets, a 0.2 m^2 vertical ring-net fit with 100-µm mesh and a flowmeter was deployed to 25 m depth at every other station.

Immediately after MOCNESS and ring-net retrieval, nets were rinsed with seawater, sieved, and individually preserved in 95% ethanol. Ethanol was changed within 48 h of collection and again within two months to properly preserve otoliths for growth analysis. Fish larvae collected by MOCNESS were sorted in the laboratory, enumerated, and identified to the lowest possible taxonomic level. Northern lampfish were placed in individual vials for future growth and diet analyses. Ring-net samples were processed following Postel et al. (2000), with subsamples of 1-5 mL and >200 individuals taken with a Stempel pipette. Zooplankton were enumerated and identified to the lowest possible taxonomic level. Taxa concentrations were calculated for MOCNESS northern lampfish (ind 1000 m^{-3}) and ring-net zooplankton (ind m^{-3}) by dividing biological counts from each net by the volume of water filtered through the net.

2.1.2 Imagery data collection

Zooplankton imagery data were collected using the *In situ* Ichthyoplankton Imaging System (ISIIS; Cowen & Guigand 2008) which was continuously towed the length of each transect within 24 h of every biological sample collection. ISIIS is a low turbulence, high-resolution *in situ* shadowgraph imaging system with a large sample volume (150-180 L s^{-1}) and a pixel resolution of 68 µm. Additionally, ISIIS has a large field of view (13 x 13 x 50 cm), allowing it to capture fragile gelatinous taxa that can be important predators of larval fishes but are difficult to quantify with traditional net-based sampling techniques (McClatchie et al. 2012, Luo et al. 2014, 2018). ISIIS was towed at a speed of 2.5 m s^{-1} in a tight undulating fashion from the surface to 100 m depth or

within a few meters of the seafloor in shallower regions. It was fit with multiple sensors to simultaneously collect physical data including CTD (Sea-Bird SBE49 FastCAT), dissolved oxygen (Sea-Bird 43), fluorescence (Wetlabs FLRT), and photosynthetically active radiation (EPAR; Biospherical QCP-2300). ISIIS data were transferred to ship-board computers via a fiber optic cable.

2.2 Growth analysis

We used otolith microstructure analysis to investigate the age and daily growth patterns of larval northern lampfish. While this is the first study to examine the full otolith-based larval growth history of this species, daily increment deposition has been confirmed for two similar myctophids in the region (*Diaphus theta* and *Tarletonbenia crenularis*: Moku et al. 2001, Bystydzieńska et al. 2010, respectively) and other studies measured the widths of the outer three complete otolith increments under the assumption of daily increment deposition (Methot 1981).

To reduce any variability associated with depth and because we had sufficiently large sample sizes during most cruises, we restricted our growth analyses to MOCNESS larvae collected in the top 50 m of the water column. A random subset of those larvae (n = 2620) were measured for standard length (SL) and body depth to the nearest 0.01 mm using a Leica MZ16 dissecting microscope with a QImaging camera and Image Pro Premier 9.1 software. Random subsamples of ~ 30 individual northern lampfish were selected from the NH and TR Lines on each cruise for otolith microstructure analysis, except for winter 2018 TR where larvae were heavily damaged due to conditions at sea and all larvae with intact otoliths were used (n = 6; total n = 216). Larvae < 5 mm SL were excluded from otolith analysis (Fig. A1).

Sagittal otoliths were dissected and stored in immersion oil on a glass slide for approximately 3 d to ‘clear’ prior to reading. Prepared otoliths were read along the longest axis at 400x magnification using a Zeiss Axio compound microscope fit with a QImaging camera and Image Pro Premier 9.1 software. Each otolith was read twice by the same reader without access to any sampling data. If the two reads differed by ≤5%, one read was randomly chosen for analysis. If reads differed by >5%, the otolith was read

a third time. Otoliths where the three reads differed by >5% were removed from analysis (n=1; Sponaugle 2009).

We enumerated daily increments to provide an estimate of age and used two metrics to analyze growth patterns: (1) mean daily growth (MDG) which is the average increment width of each day of life and (2) mean recent growth (MRG) which is the average increment widths of each individual over the last three full days of life. We used the latter to best align with sampled environmental conditions because it is unknown how long larvae had been associated with the environmental conditions (including prey and predators) at the time of collection.

Because otolith increment width increases with the age of the fish (Baumann et al. 2003), we detrended the last three increment widths for age by calculating a detrended growth index:

$$DG_{ij} = (G_{ij} - G_j)\, SD_j^{-1} \quad (1)$$

Where DG_{ij} is the detrended growth of individual i at age j, G_{ij} is otolith-based growth (increment width) for individual i at age j, G_j is the mean otolith-based growth of all individuals at age j, and SD is the standard deviation of G. Detrending growth of the last three full days of life (i.e., last three complete increment widths) for age allows us to compare the MRG of differently aged larvae (Robert et al. 2009, Sponaugle et al. 2010).

We compared MRG across cruises and locations using analysis of covariance (ANCOVA) with age as a covariate. There were no significant interactions between age and cruise or location prohibiting the interpretation of ANCOVA results. ANCOVAs were followed by a Tukey HSD post-hoc test, when applicable.

2.3 Diet analysis

We examined the gut contents of all larval northern lampfish used in otolith analysis that had intact guts (n = 174). Most larvae collected during winter 2018 storm conditions had some gut damage, so fish from this cruise (W18) were not included in the diet analysis.

Larval guts were dissected in a few drops of glycerol on a microscope slide under a Leica MZ16 dissecting scope. We removed the entire gastrointestinal tract and then gently teased out prey using minutien pins, starting with the anterior end (Llopiz &

Cowen 2008). Prey were identified to the lowest taxonomic level possible, enumerated, and measured along the longest dimension (prosome length, carapace length, or total length) under the Leica MZ16 dissecting microscope with a QImaging camera and Image Pro Premier 9.1 software. Prey lengths were converted to biomass with published length to dry weight conversions, using temperate system conversions whenever possible (Uye 1982, Berggreen et al. 1988, Webber & Roff 1995, Lindley et al. 1999, Kaeriyama & Tsutomu 2002, Cornet-Barthaux et al. 2007, Nakamura et al. 2017). When copepod order could not be discerned, we used the conversion provided for the pooled copepod community ('total copepodia'; Uye 1982). Unknown crustacean biomass was estimated with the mean of the conversions used for all crustacean prey groups.

We calculated feeding incidence as the percentage of larval northern lampfish with prey in their gut. Larvae with no prey in their gut were excluded from all other diet analyses (n = 38). Three metrics were used to describe larval diet composition: frequency of occurrence (%FO; percent of larvae with a particular prey type in gut), numerical percentage (%N; percent of each prey type out of all prey types consumed), and relative biomass (%B; percent biomass of each prey type out of total consumed prey biomass). These metrics were calculated for every prey type in each season (winter, summer) and location (NH Line, TR Line). Because larvae had a broader size range in summer (5.3 – 12.0 mm SL) compared to winter (5.1 – 7.9 mm SL), summer larvae were split into small (< 8 mm SL) and large (> 8 mm SL) size classes to investigate differences in feeding incidence and diet composition across season considering potential ontogenetic changes in feeding habits.

Consumed prey biomass was calculated for each larva by summing the dry weights of all consumed prey. We divided this value by larval SL^3 to account for increased gut capacity with larval size. These calculations were also performed for each individual prey group. Finally, we calculated standardized gut fullness as the residuals of the linear relationship between consumed prey biomass and larval SL^3 (Dower et al. 1998). We use SL^3 instead of SL, which is traditionally used (Sponaugle et al. 2009, Gleiber et al. 2020), because post-flexion growth in northern lampfish entails a substantial increase in body depth (more so than length). Thus, body volume (SL^3) likely more accurately captures increased gut capacity than length in this species. Mean

standardized consumed prey biomass and gut fullness were compared across seasons (winter, summer) and locations (NH Line, TR Line) using Wilcoxon rank sum tests (non-parametric) and Welch's t-tests (parametric), respectively. T-tests were used to compare gut fullness because one group (NH winter) had a parametric distribution and t-tests are robust to non-normality as long as sample size is large (n = ~ 30). There was no significant difference in total standardized consumed prey biomass or gut fullness between years ($p = 0.12$ and $p = 0.22$, respectively) or size classes ($p = 0.42$ and $p = 0.13$, respectively) in summer so these groups were pooled.

2.4 Prey availability and potential predation pressure

ISIIS imagery data were processed, trained, and tested for automated classification following Luo et al. (2018), Briseño-Avena et al. (2020), Schmid et al. (2020), and Swieca et al. (2020), with the full pipeline code open-sourced in Schmid et al. (2021). After image processing, corrected taxa concentration estimates and co-collected physical data were kriged onto a grid equal to the length of each transect at 2 m vertical and 500 m horizontal resolution.

Prey groups of interest were selected based on gut content analysis (present study). Because we were interested in how northern lampfish diets and growth vary in different upwelling regimes, we focused our analysis on prey taxa that appeared to vary substantially in their importance to larval diets across seasons and/or locations: calanoid copepods, copepod nauplii, and protists (Table 2.2). While copepod nauplii are an important prey resource for northern lampfish (see Results), they are not quantitatively captured by ISIIS due to their indistinct morphology. Thus, biological ring-net samples were used to supplement imagery data to capture the copepod nauplii group. Since all prey groups were standardized to concentration, the nauplii data could be easily integrated for a more holistic evaluation of prey availability.

There is a paucity of data on predation upon larval fishes in the NCC to inform potential predator selection. Predation by zooplankton, in particular, is rarely quantified because of the variety of potential predators (Bailey & Houde 1989) and the difficulty in sampling some taxa (i.e., gelatinous taxa) with net-based systems. Yet, several studies indicate that larval fishes may make up a significant portion of the diets of some taxa

including chaetognaths, ctenophores, siphonophores, and hydromedusae (reviewed in Alvarino 1985, Purcell 1985). Anecdotally, northern lampfish have been observed in the gastric cavities of ctenophores (Auth & Brodeur 2006) and chaetognaths (the present study) in the NCC, so these taxa were selected as the potential predator groups for analysis.

Mean prey and potential predator concentrations (ind m^{-3}) were calculated for shelf and offshore portions of each transect (delineated by the shelf break, 200 m isobath). For the imagery data, mean taxa concentration was computed for each 1-m vertical bin down to 50 m depth. For the ring-net data, mean taxa concentration was computed for all net tows on the shelf and off the shelf along each transect.

2.5 Statistical modelling

We used Generalized additive models (GAMs) to examine the effect of upwelling, prey availability, and potential predation pressure on the recent larval growth of northern lampfish. The response variable in this model was the individual mean recent growth (MRG; last three full days) of 174 northern lampfish, which was the subset of larvae used in growth analysis with intact guts. The covariates were upwelling (continuous), *in situ* temperature (continuous), and protist (continuous, log transformed), copepod nauplii (continuous, log transformed), calanoid copepod (continuous, log transformed), and predator (continuous, log transformed) concentrations. We also incorporated an early growth parameter (mean increment width over the first third of each fish's life), as an individual's recent growth is likely impacted by their growth history (i.e., fish that grow fast as early in life are more likely to continue growing fast later in life; Dower et al. 2008, Robert et al. 2014, Pepin et al. 2015). Finally, we tested the use of a random effect (intercept) of net tow to account for the fact that individuals from the same MOCNESS tow are more likely to have similar growth, but model selection indicated that models without the random intercept were best.

Upwelling was the cumulative daily Coastal Upwelling Transport Index (CUTI; https://mjacox.com/upwelling-indices/) 10 d prior to capture. This period was selected to account for the lag between physical forcing and phyto- and zooplankton abundance. It is thought that phyto- and zooplankton lag wind stress by ~7 d and ~13-16 d, respectively

(Spitz & Allen 2005). Because CUTI is a measure of vertical transport following wind stress, we chose the intermediate lag of 10 d. Temperature was calculated from MOCNESS environmental data, as the mean per net associated with each fish collection. We included temperature in the model to examine the role of upwelling after taking into account the well documented effect of temperature on metabolically-induced growth (Gillooly et al. 2001). This is important to account for in upwelling systems where temperature and production often have an inverse relationship. Mean concentrations of protists (imagery data), copepod nauplii (ring-net data), calanoid copepods (imagery data), and predators (ctenophores and chaetognaths combined; imagery data) used corresponded to the location of fish collection on each transect. Predator taxa were pooled due to collinearity.

Variance inflation factors (VIF) indicated that correlations between covariates were not a cause for concern (values ≤ 3; Zuur et al. 2010). Smoothing functions were applied to each covariate and the number of knots was restricted to 4 to avoid model overfitting. We then used a backward stepwise approach for model selection, comparing full and reduced versions of the models with Akaike's information criterion (AIC) and generalized cross validation (GCV). The model with the lowest AIC and GCV values was chosen as the best model if it was the reduced (simpler) version. However, if the model with the lowest AIC and GCV was the more complex model, it was only selected if it was significantly different (ANOVA, $p < 0.05$) from the reduced version. Model residuals were checked for deviations from normality, homogeneity of variance, and other abnormalities. All modeling analyses were conducted using the R software (v 4.0.4) package 'mgcv' (Wood 2021).

3. RESULTS

3.1 Environmental setting

Upwelling varied seasonally and latitudinally throughout sampling. In general, and consistent with expectations, upwelling was stronger in summer compared to winter and in northern California (Trinidad Head Line; TR) relative to Oregon (Newport Hydrographic Line; NH). Cumulative upwelling 10 d prior to sampling ranged from 0.81 to 21.02 m^3s^{-1} (Table 2.1). Mean cumulative upwelling was lowest during W19 in both locations. Off Oregon (NH), the strongest upwelling 10 d prior to sampling occurred

during S19, while northern California (TR) experienced the most intense upwelling during S18, which was more than 3x greater than the following summer (S18 = 19.59 m^3s^{-1}, S19 = 6.20 m^3s^{-1}). Both locations experienced interannual variability in upwelling within each season, but the magnitude of variability was much greater in TR relative to NH (Fig. 2.2).

Kriged temperature profiles align well with expectations based on the upwelling experienced during each sampling event. The water column was well mixed throughout winter sampling, but vertical thermal stratification existed during summer sampling with the thermocline shoaling toward the shelf in NH and TR both years. Vertical stratification was especially strong along the NH Line where surface waters (< 10 m) were up to ~5-9 ◦C warmer than those at depth (~ 50 m). The summer water column was moderately more well mixed along TR. Summer surface temperatures were fairly uniform across the shelf in TR, while NH exhibited cooler inshore and warmer offshore surface waters, which may denote the location of the upwelling front (Fig. A2).

3.2 Northern lampfish distribution

Northern lampfish were the most abundant larval fish throughout our sampling (n = 6563), accounting for 13.7% of the total abundance of larval fishes in the winter and 32.3% in the summer. The overall mean concentration of larval northern lampfish was 27.7 (± 3.3) ind. 1000 m^{-3} and ranged from 2.2 (± 1.3; W18) to 55.0 (± 8.7; S18) ind. 1000 m^{-3} across cruises (Table A2). Concentrations were generally higher in summer than in winter and at TR relative to NH (Table 2.1). Larvae were broadly distributed across the shelf throughout our sampling effort (Fig. 2.1). While they were concentrated in the upper 75 m of the water column, larvae were also found in lower abundances to our maximum sampling depth (100 m).

3.3 Northern lampfish size, age, and growth

Larvae subject to growth analysis ranged in size from 5.0 to 12.04 mm SL and were 2 to 55 d post hatch (dph). Though the largest (> 9 mm SL, > 1.75 mm body depth) and oldest (>45 dph) larvae were only present in the summer, there was general coherence in size and age across seasons (Fig. 2.3). Less than 6% of larvae were ≥40 dph. The overall population somatic growth rate was 0.11 mm d^{-1}.

Larval northern lampfish otoliths were visible through the top of the cranium prior to dissection and growth increments well defined. Otolith microstructure revealed three distinct growth regions after a prominent hatch-check: (1) fast growth and wide increments for approximately 3-7 d, (2) consistently slow growth and narrow increments for about 12 d, followed by (3) increasing growth increments to the otolith's edge (Fig. 2.4). There was a significant positive relationship between fish size vs. age, otolith size vs. age, and the fish size-at-age residuals vs. otoliths size-at-age residuals in all years, seasons, and locations except for W18 TR, due to low sample size (n = 6; Table A1).

MRG (mean growth over the last three full days of life) was significantly slower in winter than in summer during both years in NH ($p < 0.001$) and in 2019 in TR ($p < 0.001$; Fig. 2.5). The non-significant difference in MRG between 2018 seasons in TR ($p = 0.39$) is likely due to small sample size (W18, n = 6). There was no significant within-season interannual variability in MRG, except for TR summer when MRG was significantly faster in S19 than in S18 ($p = 0.001$; Fig. 2.5B). Finally, there was no significant difference in MRG between locations during any cruise ($p = 0.26$, $p = 0.72$, $p = 0.67$, $p = 0.41$ for W18, S18, W19, and S19, respectively).

Similarly, MDG (mean increment widths for each day of life) and size-at-age (otolith radius-at-age) varied by season; in both years, fish grew faster and attained larger sizes-at-age in summer than in winter (Fig. 2.6). This variability was apparent at all ages. At ~ 15 dph, larvae at TR were growing significantly faster and were larger at age in S19 relative to S18 (Fig. 2.6B, D). Winter interannual differences could not be examined in TR due to low sample size. At NH within season interannual variability in MDG and size-at-age was minimal (Fig. 2.6A, C).

3.4 Northern lampfish diet

Northern lampfish feeding incidence was, on average, 20.9% higher in summer than in winter. Feeding incidence was similar across locations in both seasons, differing by no more than 5.2% between NH and TR (Table 2.2). Similarly, standardized consumed prey biomass, gut fullness, and diet composition varied across cruises with diet differences greater between seasons than among locations.

Larval northern lampfish consumed more prey and had fuller guts in summer compared to winter, with significantly higher standardized ingested prey biomass (NH $p = 0.04$, TR $p < 0.001$) and gut fullness (NH $p = 0.04$, TR $p = 0.003$) in both locations (Fig. 2.7). There was no significant difference in standardized ingested prey biomass or gut fullness between years ($p = 0.12$ and $p = 0.22$, respectively) or summer larval fish size classes ($p = 0.42$ and $p = 0.13$, respectively).

In winter, northern lampfish larvae primarily consumed euphausiid calyptopis (46.3%) and copepod nauplii (45.0%), which comprised >90% of their total ingested biomass. In summer, while larvae continued to consume these taxa, they also incorporated calanoid copepods into their diets. Calanoid copepods (26.1%) were the second largest contributor to summer total ingested biomass and were important for both larger (>8mm SL; 41.3%) and smaller (<8mm SL; 7.5%) larvae (Fig. 2.8B). However, the size of ingested calanoid copepods differed between summer size classes, with larger larvae consuming significantly larger calanoid copepods (0.58 ± 0.03 mm prosome length) than smaller larvae (0.45 ± 0.04 mm prosome length; $p = 0.01$). Ostracods were regularly ingested throughout the year and protists were consumed only in winter, as reflected in ingested prey counts (Fig. 2.8A).

Larvae ingested a significantly higher biomass of copepod nauplii and protists in both locations in winter (NH $p = 0.002$, TR $p < 0.001$ and NH $p = 0.03$, TR $p = 0.02$, respectively) and calanoid copepods in summer (NH $p = 0.03$, TR $p = 0.01$; Fig. 2.9A, B). Interannual differences in ingested biomass were only apparent in TR, where larvae consumed a substantially higher biomass of calanoid copepods in S19 compared to S18 and a moderately higher biomass of ostracods in S18 compared to S19 (Fig. 2.9C, D).

3.5 Prey availability and potential predation pressure

Prey availability differed more between seasons than locations, with the concentration of protists and calanoid copepods roughly 1.5 - 2x higher in summer than in winter ($p = 0.02$ and $p = 0.002$, respectively). There was no significant difference in copepod nauplii abundance between summer and winter ($p = 0.08$), as they attained high concentrations throughout our sampling effort (Table 2.1). This seasonal pattern largely held within each location, except for calanoid copepods at TR in 2018 ($p=0.90$) and

protists at NH ($p = 0.94$). The typical seasonal pattern of higher summer calanoid abundance was evident at TR in 2019 ($p = 0.03$; Table A2). Predation pressure also varied seasonally, but only in TR where predators (chaetognaths and ctenophores) were more abundant in summer ($p = 0.03$; Table 2.1).

Within each season, there was no significant locational difference in protist or copepod nauplii concentration (winter $p = 0.09$, summer $p = 0.48$; winter $p = 0.66$, summer $p = 0.58$, respectively), but calanoid copepods were significantly more abundant at NH than TR in summer ($p = 0.008$). The same was true for predators in winter ($p = 0.008$; Table 2.1).

Finally, there were no significant within-season interannual differences in protist, copepod nauplii, and calanoid copepod availability in either location, but predators were more abundant in S19 than in S18 at TR ($p = 0.03$; Table A2).

3.5 Recent growth modelling

The MRG of northern lampfish was influenced by environmental conditions, prey availability, and potential predation pressure (Fig. 2.10; deviance explained = 48.6%). MRG displayed a dome-shaped relationship with upwelling intensity ($p < 0.001$): growth was lower than average during the weakest upwelling and rapidly increased to a peak at intermediate values before decreasing, but largely remaining above average, at the most intense upwelling experienced in TR during S18 (Fig. 2.10A). However, we note that interpretation of predicted MRG at intermediate upwelling values is challenged by low sample size. MRG was strongly and positively affected by temperature ($p < 0.001$), with above average growth at temperatures > 11 ˚C (Fig. 2.10B). When environmental calanoid copepod concentrations were low, northern lampfish larvae had below average MRG, whereas they had above average MRG at high calanoid copepod concentrations ($p = 0.002$; Fig. 2.10D). The opposite was true for copepod nauplii concentrations, which had a weaker and negative impact on MRG ($p = 0.009$; Fig. 2.10C). Finally, northern lampfish growth was consistently below average at increasing predator concentrations but increased quickly at the highest predator concentrations experienced throughout sampling ($p = 0.005$; Fig. 2.10E).

4. DISCUSSION

Myctophid larvae are ubiquitous in the world's oceans and northern lampfish (*Stenobrachius leucopsarus*) are typically the most abundant ichthyoplankton in the northern California Current (NCC; Richardson 1973, Richardson & Pearcy 1977, Auth & Brodeur 2006). Upwelling phenology and intensity are highly variable throughout their broad spatio-temporal range providing the unique opportunity to investigate the relationships between upwelling, feeding, and growth within this seasonal system.

Northern lampfish larvae exhibited significant differences in growth and diet across NCC upwelling regimes, with greater seasonal than latitudinal variability. Growth was generally faster in the summer, when upwelling was stronger and larvae consumed more calanoid copepods, fewer copepod nauplii and protists, and had substantially higher gut fullness, than in the winter. In contrast, during reduced upwelling in the winter, slower-growing larvae had guts that were less full and diets that were dominated by lower trophic level prey (i.e., protists and copepod nauplii). These patterns resulted in summer larvae that were significantly larger-at-age than winter larvae. However, when summer upwelling was the most intense, and despite comparable environmental prey availability, larval northern lampfish consumed fewer calanoid copepods, grew more slowly, and were smaller-at-age than in more moderate upwelling conditions. Finally, high zooplanktivorous predation pressure was correlated to above average growth, which may indicate a selective loss of slower-growing larvae that are less able to escape predation.

4.1 Larval northern lampfish otolith microstructure

Larval northern lampfish grew at a rate of 0.11 mm d^{-1}, which is comparable to other slower-growing, high-latitude myctophids (Methot 1981, Moku et al. 2001). Their otoliths were comprised of well-defined bands with three distinct growth regions after a prominent hatch-check: (1) fast growth and wide bands for approximately 3-7 d, (2) consistently slow growth and thin bands for about 12 d, followed by (3) increasing growth increments to the otolith's edge. Nishimura et al. (fig. 4B, 1999) also observed this growth pattern on the interior section of adult northern lampfish otoliths and a similar growth history is evident in another larval myctophid in the region, *Tarletonbeania crenularis* (fig. 3, Bystydzieńska et al. 2010). Interestingly, despite having very similar

morphology and growth rates (0.13 mm d^{-1}), the growth pattern of larval *Diaphus theta* is quite different, with increments gradually increasing in width from the core to the otolith edge (fig. 1A, Moku et al. 2001). The discrepancy in larval growth patterns between northern lampfish and *D. theta* may provide a mechanism to confidently discern between morphologically similar species. Finally, the only other study that examined the larval growth of northern lampfish in the NCC noted the inability to discern the inner-most increments without polishing which limited their study to examining the last three complete increments (Methot 1981). With the advent of higher-powered microscopes and advanced imaging technology, we did not encounter this barrier.

4.2 Seasonal variability in larval northern lampfish diet and growth

Similar to other larval myctophids, the diet composition of northern lampfish consisted of protists, ostracods, larval euphausiids, copepod nauplii, and cyclopoid and calanoid copepods (Conley & Hopkins 2004, Sassa & Kawaguchi 2005). However, larval diets were affected by seasonal variability in the plankton community. Of particular importance is the environmental abundance of copepod nauplii and calanoid copepods relative to their seasonal importance in northern lampfish diets. During reduced upwelling in winter, northern lampfish primarily consumed copepod nauplii. They continued to feed on nauplii in summer upwelling conditions, but also incorporated calanoid copepods into their diets. This resulted in northern lampfish with a substantially greater relative biomass of nauplii in their guts in winter compared to summer. Yet, copepod nauplii were equally available in the environment in both seasons. In contrast, when the availability of calanoid copepods increased in summer, their biomass in larval northern lampfish diets significantly increased. These patterns suggest that larval northern lampfish respond opportunistically to increases in calanoid copepods. Although larger northern lampfish consume more calanoid copepods, preferential feeding on calanoids cannot be attributed to an ontogenetic shift in diet, as this pattern holds for winter and summer larvae in the same size class (5 - 8 mm SL). Preference for calanoid copepods has been observed for multiple species of larval fish in a variety of systems including, among others, larval tunas (*Thunnus atlanticus*) in the Straits of Florida (Gleiber et al. 2020), Atlantic cod (*Gadus morhua*) in the Gulf of St. Lawrence (Robert et

al. 2011), and European hake (*Merluccius merluccius*) in the Catalan Sea (Morote et al. 2011). Further evidence for dietary selection is evident in larval consumption of the lowest trophic level prey (i.e., protists). Protist ingestion was restricted to the less productive winter season even though they were twice as abundant in summer.

Our findings indicate that northern lampfish larvae can respond to the more productive food-web during enhanced summer upwelling by selectively feeding on higher trophic level prey (i.e., calanoid copepods). Heightened copepod abundance in summer is well documented in this seasonal system (Peterson & Miller 1977). In addition to seasonal variability in overall copepod abundance, the copepod community also shifts between seasons. The winter downwelling community is typically dominated by warm water copepods that are transported poleward in the Davidson Current. Conversely, the summer upwelling community is characterized by the presence of cold-water species transported south to the NCC from subarctic source waters (Peterson & Miller 1977, Hooff & Peterson 2006). Given their northern affinity, these copepods tend to be lipid-rich and are an important prey base for many predator taxa (Logerwell et al. 2003, Peterson & Schwing 2003, Hooff & Peterson 2006, Tomaro et al. 2012, Peterson et al. 2014). While the adult forms of these species are likely too large (> 3mm prosome length) to be consumed by fish larvae in this study (5 – 12 mm SL), their smaller, younger, but still lipid-rich, life stages may provide superior nutrition for larval northern lampfish in summer (Peterson 1986, Mclaren et al. 1988, Liu & Hopcroft 2007).

Consumption of calanoids appears to be beneficial for northern lampfish growth and survival. A high reliance on nauplii biomass in winter resulted in reduced growth and smaller-at-age larvae, while less dependence on nauplii and the incorporation of calanoid copepods in summer led to faster growing and larger-at-age larvae. In seasonally productive systems, some prey taxa (i.e., copepod nauplii) are likely important for sustenance year-round, while other high value taxa (i.e., calanoid copepods) confer enhanced growth when available during more productive conditions (i.e., summer upwelling). Because northern lampfish have a protracted spawning season that places larvae in the pelagic water column during both optimal (summer) and suboptimal (winter) feeding environments, there are likely effects on larval survivorship as well as possibly carry-over effects on growth and survival later in life. More work is needed to examine

the implications of northern lampfish seasonal feeding and growth patterns across life history stages.

4.3 Interannual variability in larval northern lampfish diet and growth

Modelling individual recent growth across NCC upwelling regimes revealed a dome-shaped relationship with growth peaking at intermediate upwelling intensities. Recent growth was below average when upwelling was minimal, but rapidly increased with moderate upwelling conditions leading to above average growth. Growth then decreased at the highest upwelling intensity (as measured in 2018 on the Trinidad Head line). During that time, upwelling 10 d prior to sampling was 3x greater than at this location the following year. Despite interannual variability in summer upwelling intensity at this location, ambient calanoid copepod abundances remained relatively consistent. Yet, fish consumed an order of magnitude lower calanoid copepod biomass resulting in significantly slower larval growth than they did the following year. Together these findings suggest that there may be a physical mechanism limiting feeding.

Theoretical models suggest larval fish feeding is not only influenced by ambient food availability but also larvae-prey encounter rates. Upwelling is typically accompanied by turbulent mixing of the nutrient-rich upper water column. When intense, upwelling-induced turbulence can negatively impact encounter rates between larval fishes and their prey, thereby reducing feeding success (Bakun & Parrish 1982, Cury & Roy 1989, Roy et al. 1992, MacKenzie et al. 1994). The negative effects of too much upwelling-induced turbulence have been demonstrated for other species in the California Current. A common pleuronectid in the region (English sole, *Parophrys vetulus*) attains high feeding success in reduced upwelling conditions when their preferred prey, appendicularians, are aggregated. Turbulent upwelling conditions disperse their appendicularian prey and decrease larval feeding success (Alldredge 1982, Gadomski & Boehlert 1984). A similar relationship has been demonstrated for larval northern anchovy (*Engraulis mordax*). Too much upwelling-induced turbulence is thought to disrupt their planktonic food aggregations that may be necessary for sufficient larval feeding (Lasker 1978, 1981). While empirical evidence for subsequent effects on recruitment to the adult population remain equivocal (Peterman & Bradford 1987, Peterman et al. 1988) and

responses to upwelling related turbulence appear to be system, scale, and taxon (both predator and prey) dependent, our findings are consistent with the conceptional model that at low upwelling intensity, feeding is production limited while at high upwelling intensity it is turbulence limited.

4.4 Early life history success in seasonally driven systems

The NCC supports major fisheries whose larval and juvenile stages depend on upwelling driven primary and secondary production. Yet, most NCC fishes spawn in winter when the system is downwelling or experiencing reduced upwelling and some, such as northern lampfish, have protracted spawning seasons that encompass both winter (downwelling) and summer (upwelling) conditions (Richardson 1973, Richardson & Pearcy 1977, Auth & Brodeur 2006, Auth et al. 2007, Brodeur et al. 2008, Auth 2009).

We found that northern lampfish consumed fewer and lower trophic level prey in the winter than in the summer, with significant effects on growth. This begs the question: what is the benefit of winter spawning? One possibility is that the need for larval retention outweighs the need for fast growth. Because nutrient supply is linked to offshore transport in upwelling systems, fishes must find a balance between transport/retention, feeding, and growth during their vulnerable early life history stages. A hypothesized solution to this problem is that fishes develop reproductive strategies that place larvae in the pelagic realm during periods or locations that minimize the probability of offshore advection (Parrish et al. 1981) while providing enough production for sustenance and slower, but sufficient growth for survival.

Another possibility is that winter-spawned northern lampfish confer a survival advantage later in life. In this system the biological spring transition (typically April-May) follows the onset of upwelling and marks the arrival of a copepod community that is dominated by cold-water species which are transported south into the NCC from subarctic source waters. As previously noted, these copepods tend to be large and lipid-rich (Hooff & Peterson 2006). Numerous studies suggest that the presence of this highly nutritious prey base is vital for the feeding and survival of the early life history stages of NCC fishes (Logerwell et al. 2003, Peterson & Schwing 2003, Hooff & Peterson 2006, Tomaro et al. 2012, Peterson et al. 2014). However, these studies largely focused on the

juvenile stage when fish can theoretically consume adult cold-water copepods with a prosome length of ~3 mm (Peterson 1986, Mclaren et al. 1988, Liu & Hopcroft 2007). Most marine fishes, including larvae, are gape-limited: larvae are initially constrained to small prey, with the breadth of prey sizes available to them generally increasing as they grow, especially for mid-to-high latitude taxa (Pepin & Penney 1997, Llopiz 2013). At the biological spring transition, surviving winter-spawned larvae would be several months old. Although slower-growing, these older individuals might be large enough to overcome some gape limitation and capitalize on the largest (adult) lipid-rich prey base typical of summer.

We found a significant ontogenetic shift in ingested calanoid copepod prey size, with larger larvae consuming larger calanoid copepods. Back-calculated birthdates suggest that at the biological spring transition (29 May, 2018 and 5 June, 2019), surviving winter-spawned northern lampfish from our samples would have been 3.5-4.5 mo. old (Jan 13 – Feb 17 birthdates) in 2018 and 3-4 mo. old (Feb 3 – Mar 7) in 2019. While the larval duration for this species is unknown, an abrupt change in adult northern lampfish otolith microstructure at approximately 70 dph (Nishimura et al. 1999) may indicate metamorphosis (Sponaugle 2009). Additionally, a similar species in the region is estimated to be 71 dph at juvenile transformation (*Diaphus theta*, Moku et al. 2001), thus we can reasonably deduce that winter-spawned northern lampfish are likely to be at or near transition to the juvenile stage at the time of the biological spring transition. Therefore, while winter-spawned northern lampfish have substantially lower feeding success and consequently slower larval growth than summer-spawned fish, winter-spawning may lead to a survival advantage for the juvenile stage in summer coinciding with availability of large, nutritious adult copepod prey. Such a tradeoff between fast and slow larval growth and subsequent juvenile success may underlie the persistence of a protracted spawning behavior in seasonally driven systems. How this tradeoff carries over to successful recruitment to the adult population is unclear, though likely varies among years.

4.5 Predation

Predator (chaetognaths and ctenophores) abundances significantly influenced measured northern lampfish larval growth. After factoring in prey availability and environmental conditions, the partial effect of predators indicates that larval growth was consistently below average at low-to-mid range predator abundances, and was above average at the highest concentration of predators. While the abundance of these potential predators only varied seasonally at TR during our sampling, other multi-year studies have documented higher chaetognath and ctenophore abundances at NH in summer compared to winter (Peterson & Miller 1976, Keister & Peterson 2003). Further, other potential gelatinous predators, such as hydromedusae, can increase in abundance during upwelling conditions (Miglietta et al. 2008). Such increased predator abundances may lead to enhanced summer predation pressure on northern lampfish. The 'growth-mortality' hypothesis and its three corollaries ('bigger-is-better', 'stage duration', and 'growth-selective predation'), suggest that larger size, faster growth, and quicker development reduces vulnerability to predation (Anderson 1988). Thus, fast larval growth may be important to the survival of summer-spawned larvae in the high-predator environment typical of summer. Although predation pressure will also be enhanced for winter-spawned northern lampfish at this time, they may be better suited to escape predation due their older age, larger size, and advanced developmental stage when they encounter the high-predator summer environment.

In situ imagery allowed us evaluate predator distributions that could offset the perceived advantages of heightened feeding under certain upwelling regimes. Traditional net-based sampling techniques have limited our ability to resolve zooplanktivorous predation on larval fishes, especially for fragile gelatinous taxa. Nonetheless, predation may be the primary agent of larval mortality (Bailey & Houde 1989) and understanding the implications of variable predation pressure across upwelling regimes is necessary for a comprehensive examination of the influence of upwelling on larval survival. The need to understand the role of predation in larval survival is greater than ever, as the abundance of some potential gelatinous predators is increasing in the NCC (Brodeur et al. 2019).

5. CONCLUSIONS

In the northern California Current, most fishes spawn during winter downwelling or reduced upwelling and some have protracted spawning that encompasses both seasons. For the latter, understanding the growth and feeding repercussions of spawning phenology via its impacts on the upwelling environments experienced by fish larvae is important in elucidating the mechanisms underlying recruitment variability in this seasonal system. Our findings demonstrate variability in larval northern lampfish feeding and growth across upwelling regimes, with moderate upwelling conditions conferring the fastest growth. While we suggest that winter spawned larvae with slower larval growth may experience enhanced juvenile success once upwelling commences, this is likely to vary across years and extension of this work across life history stages is needed to tease apart these relationships. Finally, as interest in harvesting mesopelagic resources grows (Hidalgo & Browman 2019), it is imperative that we understand the basic tenants of myctophid early life histories including their growth and diets, and the relationship between these metrics and variable oceanographic conditions. Their role in the pelagic food web of such productive systems is understudied yet likely to be highly important.

6. ACKNOWLEDGEMENTS

We are grateful for the captains and crews of the R/V Sikuliaq, R/V Atlantis, and R/V Sally Ride for their contributions to at-sea sampling. We are especially indebted to H. William Fennie, Megan Wilson, Kelia Axler, Miram Gleiber, and Christian Briseño-Avena for their dedication to this study, which included spending up to 40 d at sea. This project was greatly improved through input on larval fish identification by T. Auth as well as modeling guidance from L. Ciannelli. Finally, we thank the Center for Quantitative Life Sciences (formerly Center for Genome Research and Biocomputing) and the army of undergraduate volunteers at Oregon State University who contributed to the processing of plankton samples: L. Nepstad, A. Branka, A. Bolm, C. Watson, B. Anders, A. Pulscak, L. Wetchler, J. Knowlton, N. Baker, R. Hartley, K. Bowditch, K. Rorvig, H. Woodwick, K. Bauer, Z. Sallada, S. Knodel, M. Sandmeier, H. Woodruff, Z. Thomas, and B. Rothman. This study was funded by NSF OCE 1737399. KS was also supported through the HMSC Markham Award, the Walter G. Jones Fishery Development Award, the Hannah-Jones Award, and Integrative Biology Research Funds.

7. REFERENCES

Alldredge AL (1982) Aggregation of spawning appendicularians in surface windrows. Bull Mar Sci 32:250–254

Alvarino A (1985) Predation in the plankton realm; mainly with reference to fish larvae. Inv Mar CICIMAR 2:1–122

Anderson JT (1988) A review of size dependent survival during pre-recruit stages of fishes in relation to recruitment. J Northwest Atl Fish Sci 8:55–66

Auth T (2008) Distribution and community structure of ichthyoplankton from the northern and central California Current in May 2004-06. Fish Oceanogr 17:316–331

Auth TD (2009) Importance of far-offshore sampling in evaluating the ichthyoplankton community in the northern California Current. Calif Coop Ocean Fish Investig Reports 50:107–117

Auth TD, Brodeur RD (2006) Distribution and community structure of ichthyoplankton off the coast of Oregon, USA, in 2000 and 2002. Mar Ecol Prog Ser 319:199–213

Auth TD, Brodeur RD, Fisher KM (2007) Diel variation in vertical distribution of an offshore ichthyoplankton community off the Oregon coast. Fish Bull 105:313–326

Bailey K, Houde E (1989) Predation on eggs and larvae of marine fishes and the recruitment problem. Adv Mar Biol 25:1–83

Bakun A (2006) Fronts and eddies as key structures in the habitat of marine fish larvae: opportunity, adaptive response and competitive advantage. Sci Mar 70:105–122

Bakun A, Parrish RH (1982) Turbulence, transport, and fish in the California and Peru Current systems. CalCOFI Rep 23:99–112

Baumann H, Pepin P, Davidson FJ., Mowbray F, Schnack D, Dower JF (2003) Reconstruction of environmental histories to investigate patterns of larval radiated shanny (*Ulvaria subbifurcata*) growth and selective survival in a large bay of Newfoundland. ICES J Mar Sci 60:243–258

Beamish RJ, Leask KD, Ivanov OA, Balanov AA, Orlov AM, Sinclair B (1999) The ecology, distribution, and abundance of midwater fishes of the Subarctic Pacific gyres. Prog Oceanogr 43:399–442

Berggreen U, Hansen B, Kiorboe T (1988) Food size spectra, ingestion and growth of the copepod *Acartia tonsa* during development: implications for determination of copepod prodcution. Mar Biol 99:341–352

Bograd SJ, Schroeder I, Sarkar N, Qiu X, Sydeman WJ, Schwing FB (2009) Phenology of coastal upwelling in the California Current. Geophys Res Lett 36:1–5

Briseño-Avena C, Schmid M, Swieca K, Sponaugle S, Brodeur R, Cowen R (2020) Three-dimensional cross-shelf zooplankton distributions off the Central Oregon Coast during anomalous oceanographic conditions. Prog Oceanogr 188:102436

Brodeur RD, Auth TD, Phillips A (2019) Major shifts in pelagic micronekton and macrozooplankton community structure in an upwelling ecosystem related to an unprecedented marine heatwave. Front Mar Sci 6:212

Brodeur RD, Peterson WT, Auth TD, Soulen HL, Parnel MM, Emerson AA (2008) Abundance and diversity of coastal fish larvae as indicators of recent changes in ocean and climate conditions in the Oregon upwelling zone. Mar Ecol Prog Ser 366:187–202

Brodeur RD, Yamamura O (2005) Micronekton of the North Pacific. PICES Scientific Report No. 30: 1–107

Bystydzieńska ZE, Phillips AJ, Linkowski TB (2010) Larval stage duration, age and growth of blue lanternfish *Tarletonbeania crenularis* (Jordan and Gilbert, 1880) derived from otolith microstructure. Environ Biol Fishes 89:493–503

Checkley Jr. DM, Barth JA (2009) Patterns and processes in the California Current System. Prog Oceanogr 83:49–64

Conley WJ, Hopkins TL (2004) Feeding ecology of lanternfish (Pisces: Myctophidae) larvae: prey preferences as a reflection of morphology. Bull Mar Sci 75:361–379

Cornet-Barthaux V, Armand L, Quéguiner B (2007) Biovolume and biomass estimates of key diatoms in the Southern Ocean. Aquat Microb Ecol 48:295–308

Cowen RK, Guigand CM (2008) *In situ* ichthyoplankton imaging system (ISIIS): system design and preliminary results. Limnol Oceanogr Methods 6:126–132

Cury P, Roy C (1989) Optimal environmental window and pelagic fish recruitment success in upwelling areas. Can J Fish Aquat Sci 46:670–680

Dower J, Pepin P, Kim G (2008) Covariation in feeding success, size-at-age and growth in larval radiated shanny (*Ulvaria subbifurcata*): insights based on individuals. J Plankton Res 31:235–247

Dower JF, Pepin P, Leggett WC (1998) Enhanced gut fullness and an apparent shift in size selectivity by radiated shanny (*Ulvaria subbifurcata*) larvae in response to increased turbulence. Can J Fish Aquat Sci 55:128–142

Fast TN (1960) Some aspects of the natural history of *Stenobrachius leucopsarus* Eigenmann and Eigenmann. PhD Dissertation, Stanford University, Stanford, CA

Fiksen Ø, Jørgensen C, Kristiansen T, Vikebø F, Huse G (2007) Linking behavioural ecology and oceanography: larval behaviour determines growth, mortality and dispersal. Mar Ecol Prog Ser 347:195–206

Gadomski DM, Boehlert GW (1984) Feeding ecology of pelagic larvae of English sole *Parophrys vetulus* and butter sole *Isopsetta isolepis* off the Oregon coast. Mar Ecol Prog Ser 20:1–12

García-Reyes M, Largier J (2012) Seasonality of coastal upwelling off central and northern California: New insights, including temporal and spatial variability. J Geophys Res Ocean 117:1–17

Gillooly J, Brown J, West G, Savage V, Charnov E (2001) Effects of size and temperature on metabolic rate. Science 293:2248–2251

Gleiber MR, Sponaugle S, Cowen RK (2020) Some like it hot, hungry tunas do not! Implications of temperature and plankton food web dynamics on growth and diet of tropical tuna larvae. ICES J Mar Sci 77:3058–3073

Guigand CM, Cowen RK, Llopiz JK, Richardson DE (2005) A coupled asymmetrical multiple opening closing net with environmental sampling system. Mar Technol Soc J 39:22–24

Hare JA, Cowen RK (1997) Size, growth, development, and survival of the planktonic larvae of *Pomatomus saltatrix* (Pisces: Pomatomidae). Ecology 78:2415–2431

Hidalgo M, Browman HI (2019) Developing the knowledge base needed to sustainably manage mesopelagic resources. ICES J Mar Sci 76:609–615

Hjort J (1914) Fluctuations in the great fisheries of northern Europe viewed in the light of biological research. Rapp Procès-Verbaux 20:1–228

Hooff RC, Peterson WT (2006) Copepod biodiversity as an indicator of changes in ocean and climate conditions of the northern California current ecosystem. Limnol

Oceanogr 51:2607–2620
Houde ED (2008) Emerging from Hjort's shadow. Fish Sci J Northw Atl Fish Sci 41:53–70
Husby DM, Nelson CS (1982) Turbulence and vertical stability in the California Current. CalCOFI Reports XXIII
Kaeriyama H, Tsutomu I (2002) Body allometry and developmental characteristics of the three dominant pelagic ostracods (*Discoconchoecia pseudodiscophora*, *Orthoconchoecia haddoni* and *Metaconchoecia skogsbergi*) in the Oyashio region, western North Pacific. Plankt Biol Ecol 49:97–100
Keister JE, Peterson WT (2003) Zonal and seasonal variations in zooplankton community structure off the central Oregon coast, 1998–2000. Prog Oceanogr 57:341–361
Lasker R (1975) Field criteria for survival of anchovy larvae: the relation between inshore chlorophyll maximum layers and successful first feeding. Fish Bull US 73:453–462
Lasker R (1978) The relation between oceanographic conditions, and larval anchovy food in the California Current: identification of factors contributing to recruitment failure. Rapp P-V Reun Cons Int Explo Mer 173:212–230
Lasker R (1981) Factors contributing to variable recruitment of the nothern anchovy (*Engraulis mordax*) in the California Current: Contrasting years,1975 through 1978. Rapp P-V Reun Cons Int Explo Mer 178:375–388
Lindley J, Robins D, Williams R (1999) Dry weight carbon and nitrogen content of some euphausiids from the north Atlantic Ocean and the Celtic Sea. J Plankton Res 21:2053–2066
Liu H, Hopcroft RR (2007) A comparison of seasonal growth and development of the copepods *Calanus marshallae* and *C. pacificus* in the northern Gulf of Alaska. J Plankton Res 29:569–581
Llopiz JK (2013) Latitudinal and taxonomic patterns in the feeding ecologies of fish larvae: a literature synthesis. J Mar Syst 109–110:69–77
Llopiz JK, Cowen RK (2008) Precocious, selective and successful feeding of larval billfishes in the oceanic Straits of Florida. Mar Ecol Prog Ser 358:231–244
Logerwell E., Mantua N, Lawson P, Francis R, Agostini V (2003) Tracking environmental processes in the coastal zone for understanding and predicting Oregon coho (*Oncorhynchus kisutch*) marine survival. Fish Oceanogr 12:554–568
Luo JY, Grassian B, Tang D, Irisson J-O, Greer AT, Guigand CM, McClatchie S, Cowen RK (2014) Environmental drivers of the fine-scale distribution of a gelatinous zooplankton community across a mesoscale front. Mar Ecol Prog Ser 510:129–149
Luo JY, Irisson J-O, Graham B, Guigand C, Sarafraz A, Mader C, Cowen RK (2018) Automated plankton image analysis using convolutional neural networks. Limnol Oceanogr Methods 16:814–827
MacKenzie BR, Miller TJ, Cyr S, Leggett WC (1994) Evidence for a dome-shaped relationship between turbulence and larval fish ingestion rates. Limnol Oceanogr 39:1790–1799
Matarese A, Kendall Jr. A, Blood D, Vinter B (1989) Laboratory guide to early life history stages of northeast Pacific fishes. NOAA Tech Rep NMFS 80:1–652
McClatchie S, Cowen R, Nieto K, Greer A, Luo JY, Guigand C, Demer D, Griffith D, Rudnick D (2012) Resolution of fine biological structure including small

narcomedusae across a front in the Southern California Bight. J Geophys Res Ocean 117:1–18

McClatchie S, Gao J, Drenkard EJ, Thompson AR, Watson W, Ciannelli L, Bograd SJ, Thorson JT (2018) Interannual and secular variability of larvae of mesopelagic and forage fishes in the southern California Current system. J Geophys Res 123:6277–6295

Mclaren I, Sevigny J, Corkett C (1988) Body sizes, development rates, and genome sizes among *Calanus* species. Hydrobiologia:275–284

Methot RD (1981) Spatial covariation of daily grow th rates of larval northern anchovy, *Engraulis mordax*, and larval northern lampfish, *Stenobrachius leucopsarus*. Rapp Proces-verbaux des Réunions Cons Int pour l'Éxploration la Mer 178:424–431

Miglietta MP, Rossi M, Collin R (2008) Hydromedusa blooms and upwelling events in the Bay of Panama, Tropical East Pacific. J Plankton Res 30:783–793

Miller TJ, Crowder LB, Rice JA, Marschall EA (1988) Larval size and recruitment mechanisms in fishes: Toward a conceptual framework. Can J Fish Aquat Sci 45:1657–1670

Moku M, Ishimaru K, Kawaguchi K (2001) Growth of larval and juvenile *Diaphus theta* (Pisces: Myctophidae) in the transitional waters of the western North Pacific. Ichthyol Res 48:385–390

Morote E, Olivar MP, Bozzano A, Villate F (2011) Feeding selectivity in larvae of the European hake (*Merluccius merluccius*) in relation to ontogeny and visual capabilities. Mar Biol 158:1349–1361

Nakamura A, Matsuno K, Abe Y, Shimada H, Yamaguchi A (2017) Length-weight relationships and chemical composition of the dominant mesozooplankton taxa/species in the subarctic pacific, with special reference to the effect of lipid accumulation in copepoda. Zool Stud 56:13

Nishimura A, Nagasawa K, Asanuma T, Aoki H, Kubota T (1999) Age, growth, and feeding habits of lanternfish, *Stenobrachius leucopsarus* (myctophidae), collected from the near-surface layer in the Bering Sea. Fish Sci 65:11–15

Parrish RH, Nelson CS, Bakun A (1981) Transport mechanisms and reproductive success of fishes in the California Current. Biol Oceanogr 1:175–203

Pepin P, Penney R (1997) Patterns of prey size and taxonomic composition in larval fish: are there general size-dependent models? J Fish Biol 51:84–100

Pepin P, Robert D, Bouchard C, Dower JF, Falardeau M, Fortier L, Jenkins GP, Leclerc V, Levesque K, Llopiz JK, Meekan MG, Murphy HM, Ringuette M, Sirois P, Sponaugle S (2015) Once upon a larva: revisiting the relationship between feeding success and growth in fish larvae. ICES J Mar Sci 72:359–373

Peterman R, Bradford M (1987) Wind Speed and mortality rate of a marine fish, the northern anchovy (*Engraulis mordax*). Science 235:354–356

Peterman RM, Bradford MI, Lo NCH, Methot RD (1988) Contribution of early life stages to interannual recruitment of northern anchovy (*Engraulis mordax*). Can J Fish Aquat Sci 45:8–16

Peterson W (1986) Development, growth, and survivorship of the copepod *Calanus marshallae* in the laboratory. Mar Ecol Prog Ser 29:61–72

Peterson W, Fisher J, Peterson J, Morgan C, Burke B, Fresh K (2014) Applied fisheries oceanography: ecosystem indicators of ocean conditions inform fisheries

management in the California Current. Oceanography 27:80–89
Peterson WT, Miller C (1976) Zooplankton along the continential shelf off Newport, Oregon, 1969-1972: distribution, abundance, seasonal cycle, and year-to-year variations. Sea Grant Report: 1–114
Peterson WT, Miller CB (1977) Seasonal cycle of zooplankton abundance and species composition along the central Oregon coast. Fish Bull 75:717–724
Peterson WT, Schwing FB (2003) A new climate regime in northeast pacific ecosystems. Geophys Res Lett 30:1–4
Postel L, Fock H, Hagen W (2000) Biomass and Abundance. In: Harris R, Wiebe P, Skjoldal H, Huntdley M (eds) Zooplankton Methodology Manual, ICES. Academic Press, London, p 83–192
Purcell JE (1985) Predation on fish eggs and larvae by pelagic cnidarians and ctenophores. Bull Mar Sci 37:739–755
Purcell JE, Arai MN (2001) Interactions of pelagic cnidarians and ctenophores with fish: a review. Hydrobiologia 451:27–44
Richardson SL (1973) Abundance and distribution of larval fishes in waters off Oregon, May - October 1969, with special emphasis on the northern anchovy, *Engraulis mordax*. Fish Bull 71:697–711
Richardson SL, Pearcy WG (1977) Coastal and oceanic fish larvae in an area of upwelling off Yaquina Bay, Oregon. Fish Bull 75:125–145
Robert D, Castonguay M, Fortier L (2009) Effects of preferred prey density and temperature on feeding success and recent growth in larval mackerel of the southern Gulf of St. Lawrence. Mar Ecol Prog Ser 377:227–237
Robert D, Levesque K, Gagné JA, Fortier L (2011) Change in prey selectivity during the larval life of Atlantic cod in the southern Gulf of St Lawrence. J Plankton Res 33:195–200
Robert D, Murphy H, Jenkins G, Fortier L (2014) Poor taxonomical knowledge of larval fish prey preference is impeding our ability to assess the existence of a “critical period” driving year-class strength. ICES J Mar Sci 71:2042–2052
Robert D, Pepin P, Dower J, Fortier L (2014) Individual growth history of larval Atlantic mackerel is reflected in daily condition indices. ICES J Mar Sci 71:1001–1009
Roy C, Cury P, Kifani S (1992) Pelagic fish recruitment success and reproductive strategy in upwelling areas: environmental compromises. South African J Mar Sci 12:135–146
Sassa C, Kawaguchi K (2005) Larval feeding habits of *Diaphus theta*, *Protomyctophum thompsoni*, and *Tarletonbeania taylori* (Pisces: Myctophidae) in the transition region of the western North Pacific. Mar Ecol Prog Ser 298:261–276
Schmid M, Cowen R, Robinson K, Luo J, Briseño-Avena C, Sponaugle S (2020) Prey and predator overlap at the edge of a mesoscale eddy: fine-scale, in-situ distributions to inform our understanding of oceanographic processes. Sci Rep 10:921
Schmid MS, Daprano D, Jacobson KM, Sullivan C, Briseño-Avena C, Luo JY, Cowen RK (2021) A Convolutional Neural Network based high-throughput image classification pipeline - code and documentation to process plankton underwater imagery using local HPC infrastructure and NSF’s XSEDE. Zenodo https://zenodo.org/record/4641158#.YdeGIxPMJD0
Smoker W, Pearcy WG (1970) Growth and reproduction of the lanternfish *Stenobrachius*

leucopsarus. Fish Res Board Canada 27:1265–1275
Spitz Y, Allen J (2005) Modeling of ecosystem processes on the Oregon shelf during the 2001 summer upwelling. J Geophys Res 110:C10S17
Sponaugle S (2009) Daily otolith increments in the early stages of tropical fish. In: Green B, Mapstone B, Carlos G, Begg G (eds) Tropical Fish Otoliths: Information for the Assessment, Management and Ecology. Springer, Netherlands, p 93–132
Sponaugle S, Llopiz JK, Havel LN, Rankin TL (2009) Spatial variation in larval growth and gut fullness in a coral reef fish. Mar Ecol Prog Ser 383:239–249
Sponaugle S, Walter KD, Denit KL, Llopiz JK, Cowen RK (2010) Variation in pelagic larval growth of Atlantic billfishes: the role of prey composition and selective mortality. Mar Biol 157:839–849
Swieca K, Sponaugle S, Briseño-Avena C, Schmid M, Brodeur R, Cowen R (2020) Changing with the tides: fine-scale larval fish prey availability and predation pressure near a tidally modulated river plume. Mar Ecol Prog Ser 650:217–238
Takahashi M, Checkley Jr. DM, Litz MN, Brodeur RD, Peterson WT (2012) Responses in growth rate of larval northern anchovy (*Engraulis mordax*) to anomalous upwelling in the northern California Current. Fish Oceanogr 21:393–404
Tomaro L, Teel D, Peterson W, Miller J (2012) When is bigger better? Early marine residence of middle and upper Columbia River spring Chinook salmon. Mar Ecol Prog Ser 452:237–252
Uye S (1982) Length-weight relationships of important zooplankton from the inland Sea of Japan. J Oceanogr Soc Japan 38:149–158
Webber M, Roff J (1995) Annual biomass and production of the oceanic copepod community off Discovery Bay, Jamaica. Mar Biol 123:481–495
Wood S (2021) mgcv. R package version 1.8-38. https://cran.r project.org/web/packages/mgcv /mgcv.pdf
Zuur AF, Leno EN, Elphick CS (2010) A protocol for data exploration to avoid common statistical problems. Methods Ecol Evol 1:3–14

Table 2.1. Northern lampfish (*Stenobrachius leucopsarus*) concentration, upwelling during sampling, and concentrations of environmental prey (select protists, copepod nauplii, and calanoid copepods) and predators (chaetognaths and ctenophores) sampled along the Newport Hydrographic Line (NH) and Trinidad Head Line (TR) during the winters and summers of 2018 and 2019.

	Winter			Summer		
	All	**NH**	**TR**	**All**	**NH**	**TR**
Northern lampfish (ind. 1000 m^{-3})	17.1 (±4.7)	15.3 (±4.3)	19.1 (±8.6)	34.0 (±4.5)	21.0 (±6.3)	46.0 (±6.2)
Upwelling (CUTI; m^3s^{-1})	4.1 (0.8 - 12.9)	2.5 (0.8 - 4.3)	6.3 (2.9 - 12.9)	8.2 (3.0 - 21.0)	3.4 (3.0 - 3.9)	12.9 (5.5 - 21.0)
Prey						
Protists (ind. m^{-3})	9.8 (±1.6)	12.7 (±2.1)	6.9 (±2.0)	21.1 (±3.2)	17.8 (±6.5)	23.5 (±3.2)
Copepod nauplii (ind. m^{-3})	3754.7 (±644.5)	4146.3 (±1298.0)	3363.1 (±488.6)	6995.2 (±1088.6)	6673.8 (±1742.0)	7316.5 (±1462.3)
Calanoid copepods (ind. m^{-3})	29.0 (± 16.7)	17.1 (± 3.7)	40.9 (± 31.8)	44.0 (± 9.2)	70.8 (± 15.5)	23.9 (± 3.7)
Predators						
Chaetognaths, ctenophores (ind. m^{-3})	2.9 (±0.5)	4.4 (±0.5)	1.3 (±0.3)	3.4 (±0.5)	2.9 (±0.7)	3.7 (±0.8)

Northern lampfish were sampled with a MOCNESS, copepod nauplii with a ring net, and all other taxa with the *In situ* Ichthyoplankton Imaging System (ISIIS). Upwelling values are the cumulative daily CUTI (Coastal Upwelling Transport Index; https://mjacox.com/upwelling-indices/) 10 d prior to each sampling event. Concentrations are reported as mean ± SE and upwelling is mean and range. Data are separated by year in Table A2.

Table 2.2. Summary of diet data for larval northern lampfish (*Stenobrachius leucopsarus*) collected in the northern California Current in the winter of 2019 and summers of 2018 and 2019 along the Newport Hydrographic (NH) Line and the Trinidad Head (TR) Line

	Winter						Summer (<8 mm SL)						Summer (>8 mm SL)					
	All		NH		TR		All		NH		TR		All		NH		TR	
Larvae, n =	58		28		30		75		38		37		41		20		21	
Prey, n =	146		78		68		190		107		83		159		81		78	
Fish size (mm SL)	5.1 - 7.9		5.1 - 7.9		5.2 - 7.6		5.3 - 8.0		5.5 - 7.9		5.3 - 8.0		8.1 - 12.0		8.1 - 12.0		8.2 - 11.8	
Feeding incidence (%)	65.5		67.9		63.3		80.0		78.9		81.1		92.7		90		95.2	
Prey type	**%N**	**%FO**	**%N**	**%FO**	**%N**	**%FO**	**%N**	**%FO**	**%N**	**%FO**	**%N**	**%FO**	**%N**	**%FO**	**%N**	**%FO**	**%N**	**%FO**
Copepoda																		
Calanoida	0.0	0.0	0.0	0.0	0.0	0.0	5.8	14.2	2.8	7.5	9.6	22.9	23.3	57.9	24.7	53.1	21.8	62.8
Cyclopoida	0.7	2.7	1.3	5.1	0.0	0.0	2.1	6.3	3.7	11.2	0.0	0.0	4.4	25.2	4.9	37.0	3.8	12.8
Unknown	0.7	2.7	1.3	5.1	0.0	0.0	1.6	7.9	0.9	1.9	2.4	15.7	1.3	11.9	1.2	8.6	1.3	15.4
Nauplius	70.5	87.7	62.8	84.6	79.4	91.2	38.4	69.5	45.8	75.7	28.9	61.4	34.6	68.6	30.9	64.2	38.5	73.1
Euphausiacea																		
Calyptopis	8.9	24.7	11.5	34.6	5.9	13.2	26.8	61.1	27.1	62.6	26.5	59.0	13.8	46.5	11.1	48.1	16.7	44.9
Ostracoda																		
Ostracoda	11.0	37.7	15.4	47.4	5.9	26.5	15.8	42.6	10.3	39.3	22.9	47.0	15.7	50.3	19.8	54.3	11.5	46.2
Protists	6.8	9.6	5.1	7.7	8.8	11.8	0.0	0.0	0.0	0.0	0.0	0.0	0.0	0.0	0.0	0.0	0.0	0.0
Unknown crustacean	1.4	4.1	2.6	7.7	0.0	0.0	8.4	30.0	7.5	30.8	9.6	28.9	6.9	35.2	7.4	54.3	6.4	15.4
Unknown	0.0	0.0	0.0	0.0	0.0	0.0	1.1	2.1	1.9	3.7	0.0	0.0	0.0	0.0	0.0	0.0	0.0	0.0

Feeding incidence is the percentage of larvae that consumed at least one prey item, and the diet is described with both numerical percentages of prey types (%N) and the frequencies of occurrence of prey types (%FO), defined as the percentage of feeding larvae with the prey type present. Summer data are split by size class.

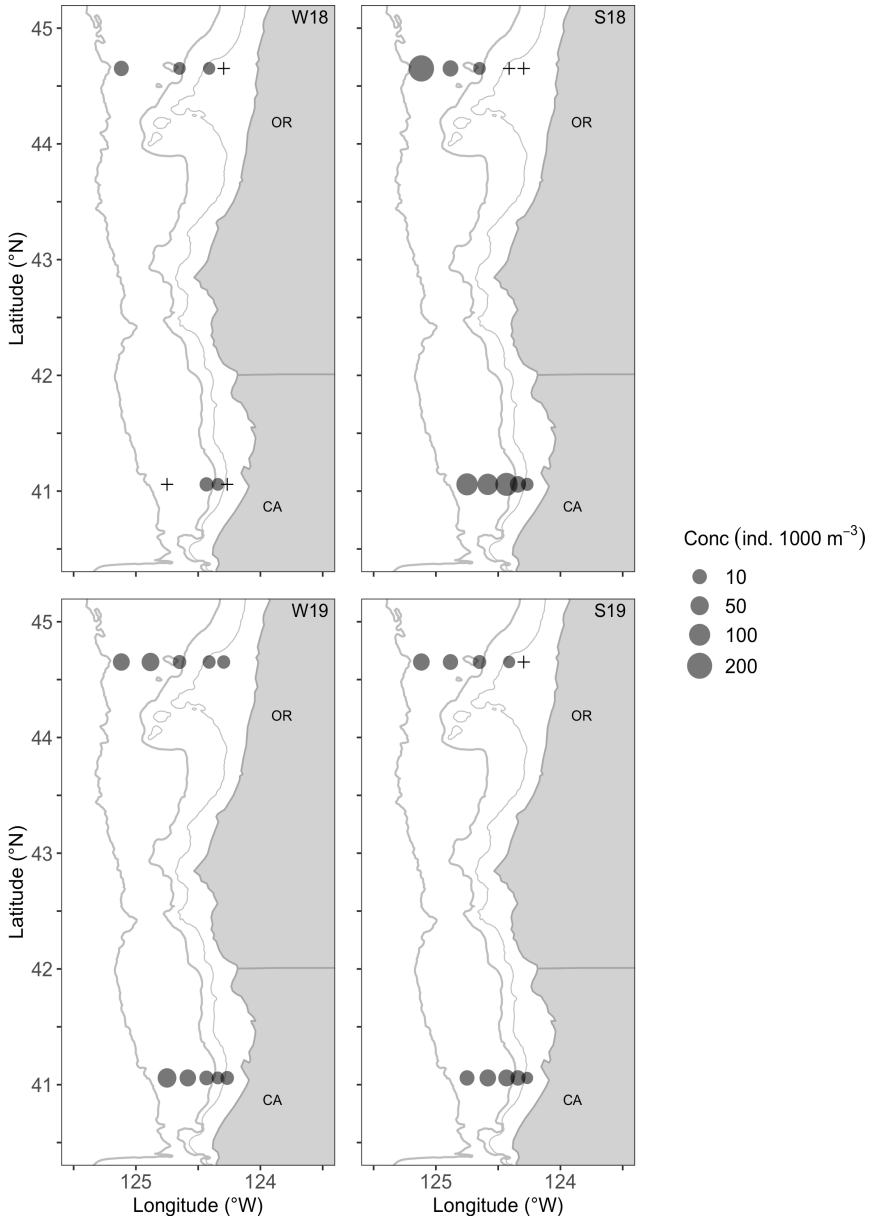

Fig. 2.1. Mean concentration of northern lampfish (*Stenobrachius leucopsarus*) larvae (individuals 1000 m $^{-3}$) sampled along the Newport Hydrographic Line (NH) off the coast of Oregon (OR) and the Trinidad Head Line (TR) off the coast of California (CA) in winter 2018 (W18; Feb 15-23), summer 2018 (S18; Jul 3-11), winter 2019 (W19; Mar 3-11), and summer 2019 (S19; Jul 16-25). '+' denotes true zeros and contour lines represent the 100-, 200-, and 2000-m isobaths

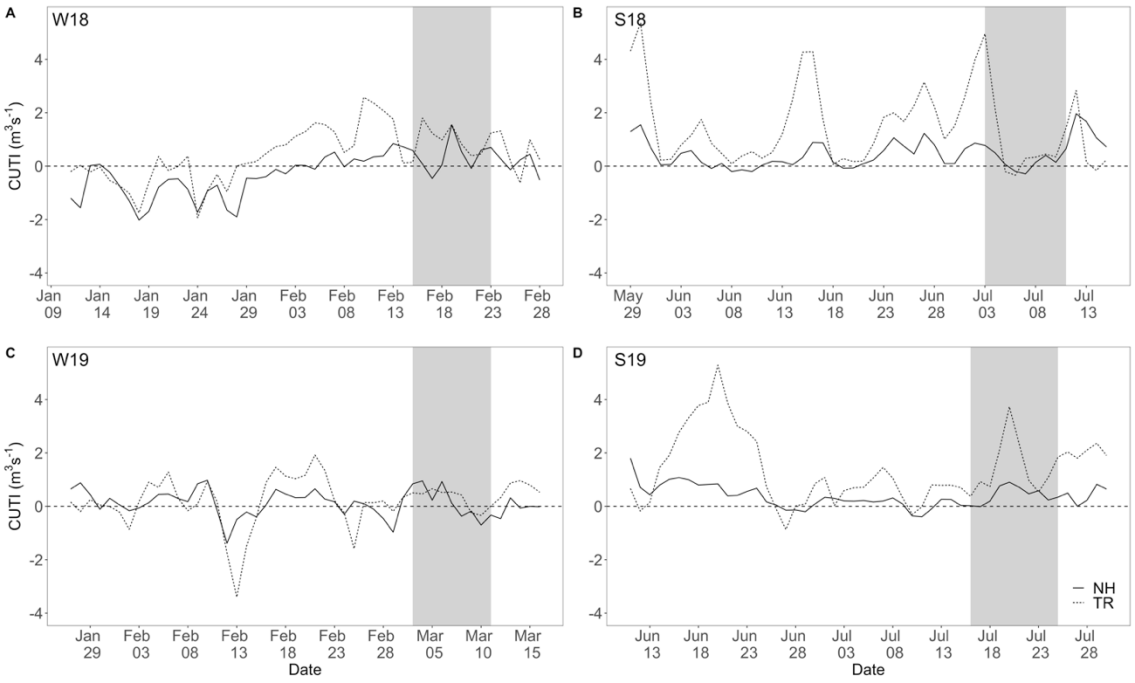

Fig. 2.2. Daily Coastal Upwelling Transport Index (CUTI) for the Newport Hydrographic Line (NH; 45° N; solid line) and the Trinidad Head Line (TR; 41° N; dotted line) during (A) winter 2018 (W18), (B) summer 2018 (S18), (C) winter 2019 (W19), and (D) summer 2019 (S19), with sampling dates highlighted in grey. Positive values signify upwelling, zero are neutral conditions, and negative values are downwelling

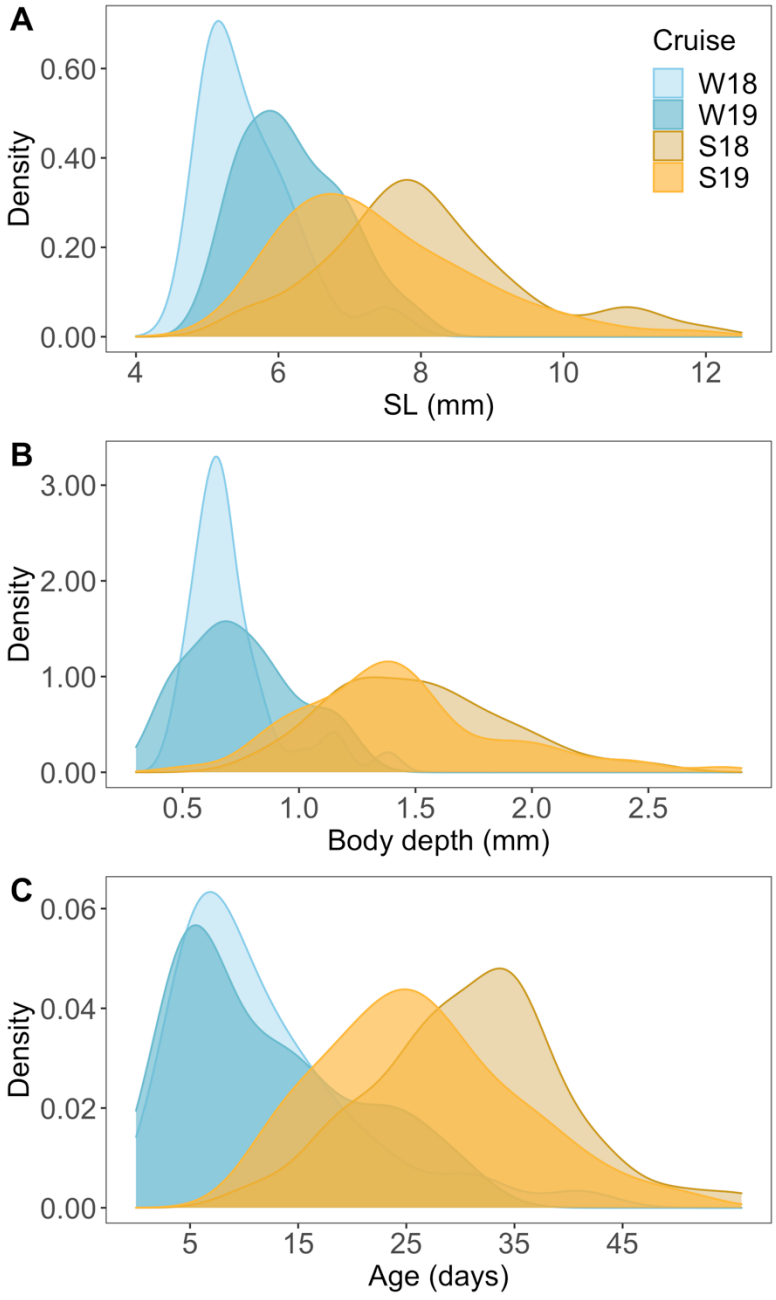

Fig. 2.3. (A) Size (standard length; SL), (B) body depth, and (C) age frequency distributions of northern lampfish (*Stenobrachius leucopsarus*) examined for otolith and gut content analysis. Fish were sampled from the northern California Current during the winters (blues) and summers (golds) of 2018 and 2019. W18 = winter 2018, W19 = winter 2019, S18 = summer 2018, S19 = summer 2019

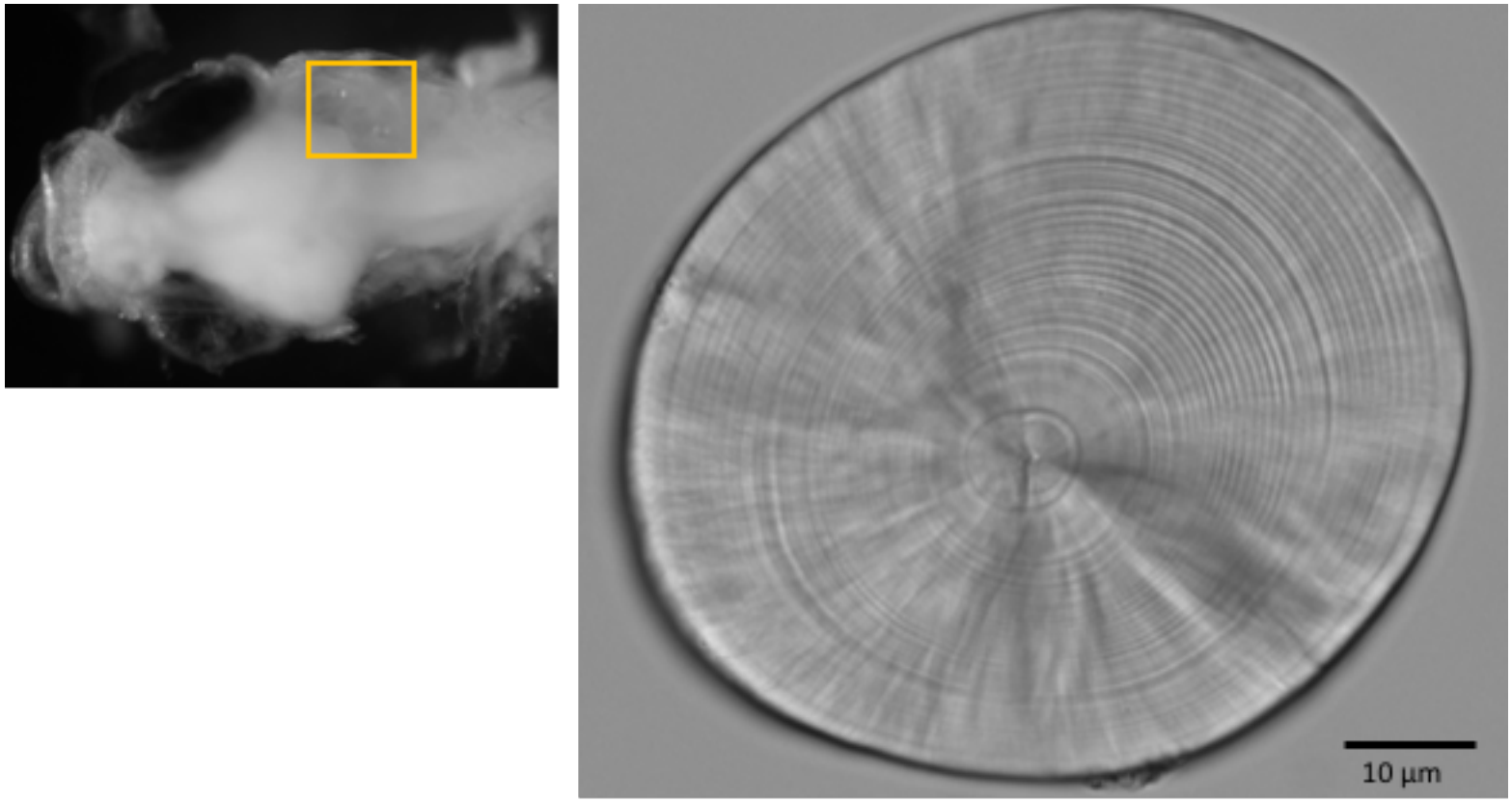

Fig. 2.4. Photograph of larval northern lampfish (*Stenobrachius leucopsarus*) otoliths with right sagitta and lapillus visible in the orange square (left) and a sagittal otolith under 400x magnification (right)

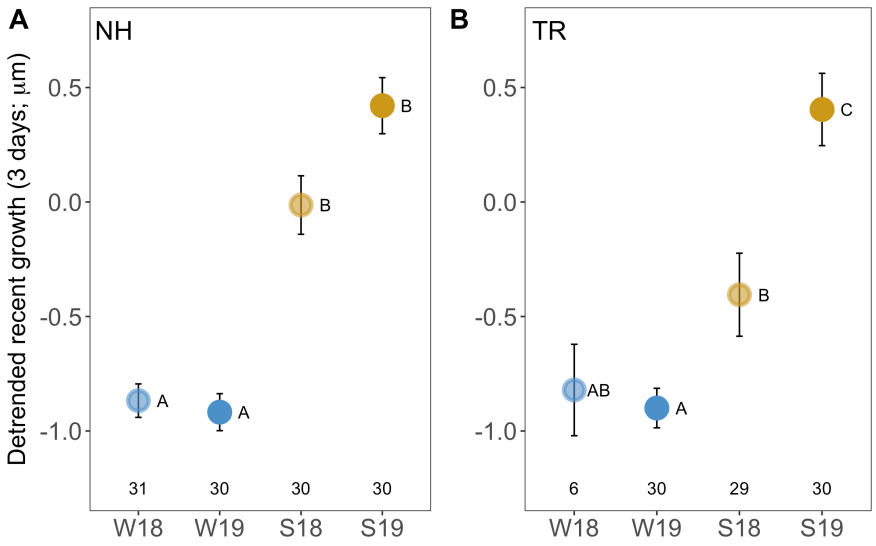

Fig. 2.5. Mean ± SE detrended growth during the last three complete days of life (mean recent growth) of northern lampfish (*Stenobrachius leucopsarus*) collected in the winter (blues) and summer (golds) of 2018 and 2019 along the (A) Newport Hydrographic Line (NH) and the (B) Trinidad Head Line (TR). Significance is indicated to the right of each data point, with points sharing letters not significantly different from each other ($p \geq 0.05$). Sample sizes are indicated above the x-axis. W18 = winter 2018, W19 = winter 2019, S18 = summer 2018, S19 = summer 2019

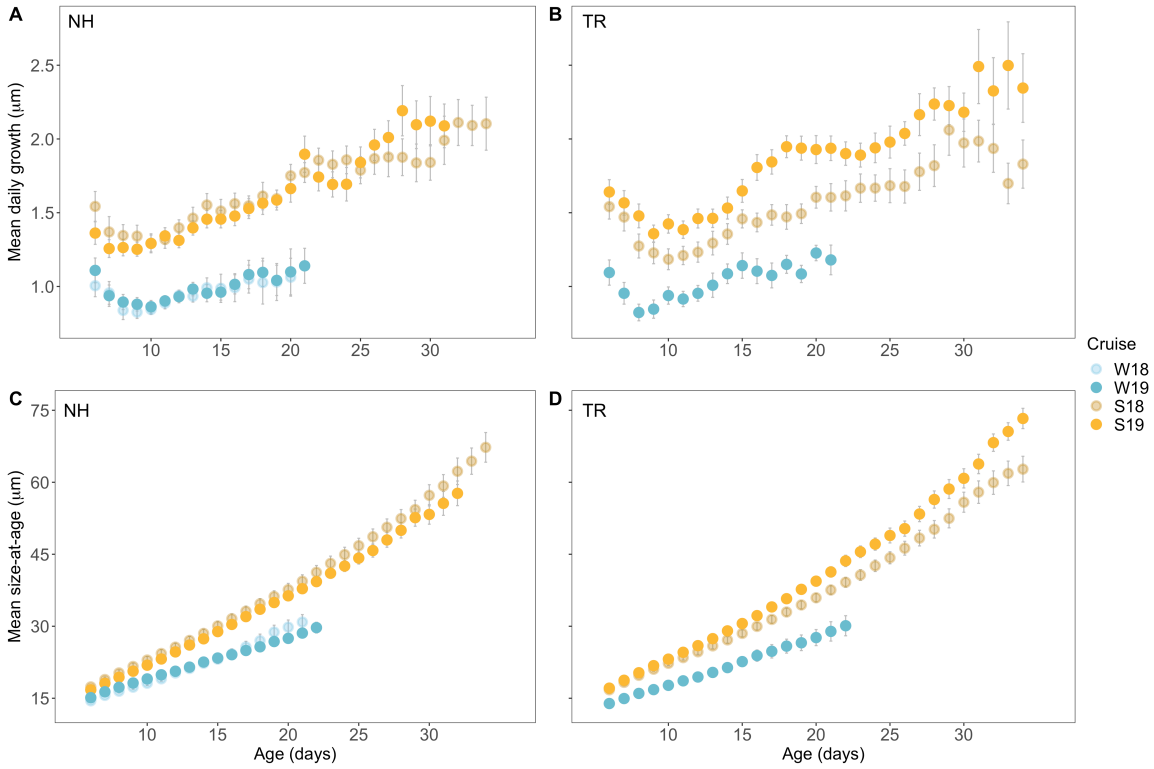

Fig. 2.6. Mean ± SE (A,B) daily growth (otolith increment width) and (C,D) size-at-age (otolith radius-at-age) of larval northern lampfish (*Stenobrachius leucopsarus*) collected in the northern California Current in winter (blues) and summer (golds) of 2018 and 2019 on the (A,C) Newport Hydrographic Line (NH) and the (B,D) Trinidad Head Line (TR). Ages were truncated when n < 5 observations. W18 = winter 2018, W19 = winter 2019, S18 = summer 2018, S19 = summer 2019

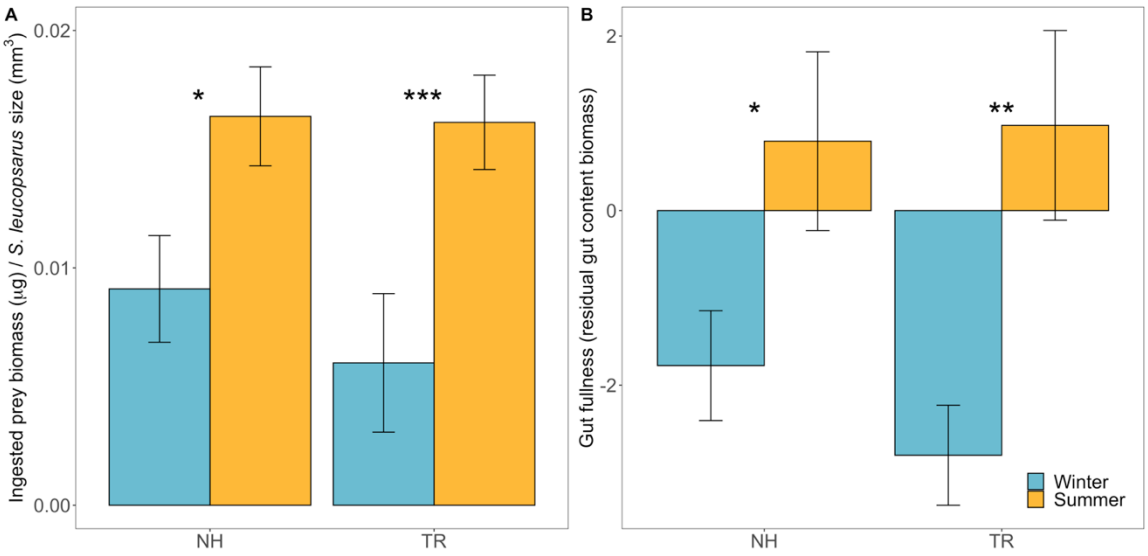

Fig. 2.7. *Stenobrachius leucopsarus* (A) mean standardized total consumed prey biomass [µg dry weight / *S. leucopsarus* SL^3 (mm^3)] and (B) mean gut fullness expressed as residual gut content biomass (residuals of total consumed prey biomass vs. SL^3) of larvae collected on the Newport Hydrographic Line (NH) and the Trinidad Head Line (TR) during the winter (blue) and summer (gold) of 2018 and 2019. ***$p < 0.001$, **$p < 0.01$, *$p<0.05$

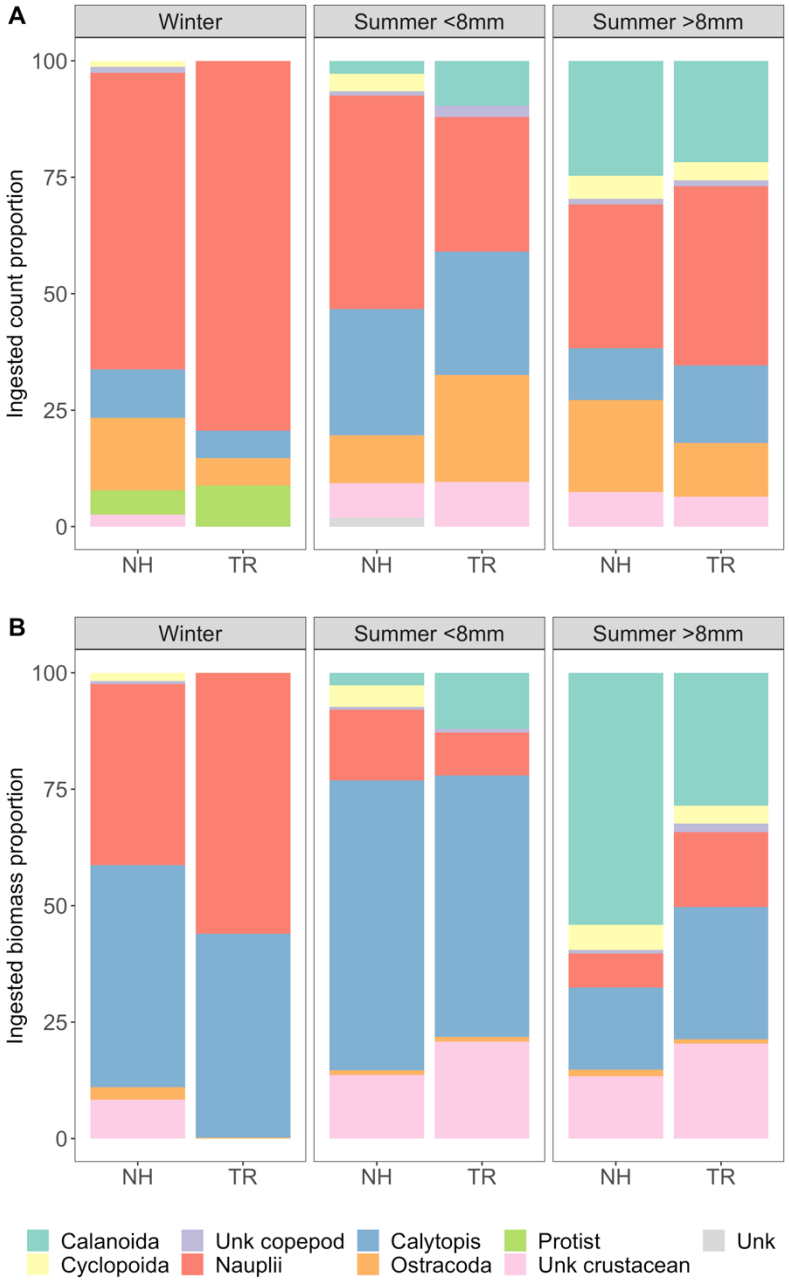

Fig. 2.8. *Stenobrachius leucopsarus* larvae ingested prey (A) count and (B) biomass [µg dry weight], presented as proportion of all consumed prey collected along the Newport Hydrographic Line (NH) and the Trinidad Head Line (TR). Summer fish are separated into small (<8 mm SL) and large (>8 mm SL) categories to account for seasonal size differences. n = 58 (winter), n = 75 (summer <8mm), and n = 41 (summer >8 mm). Unk = unknown

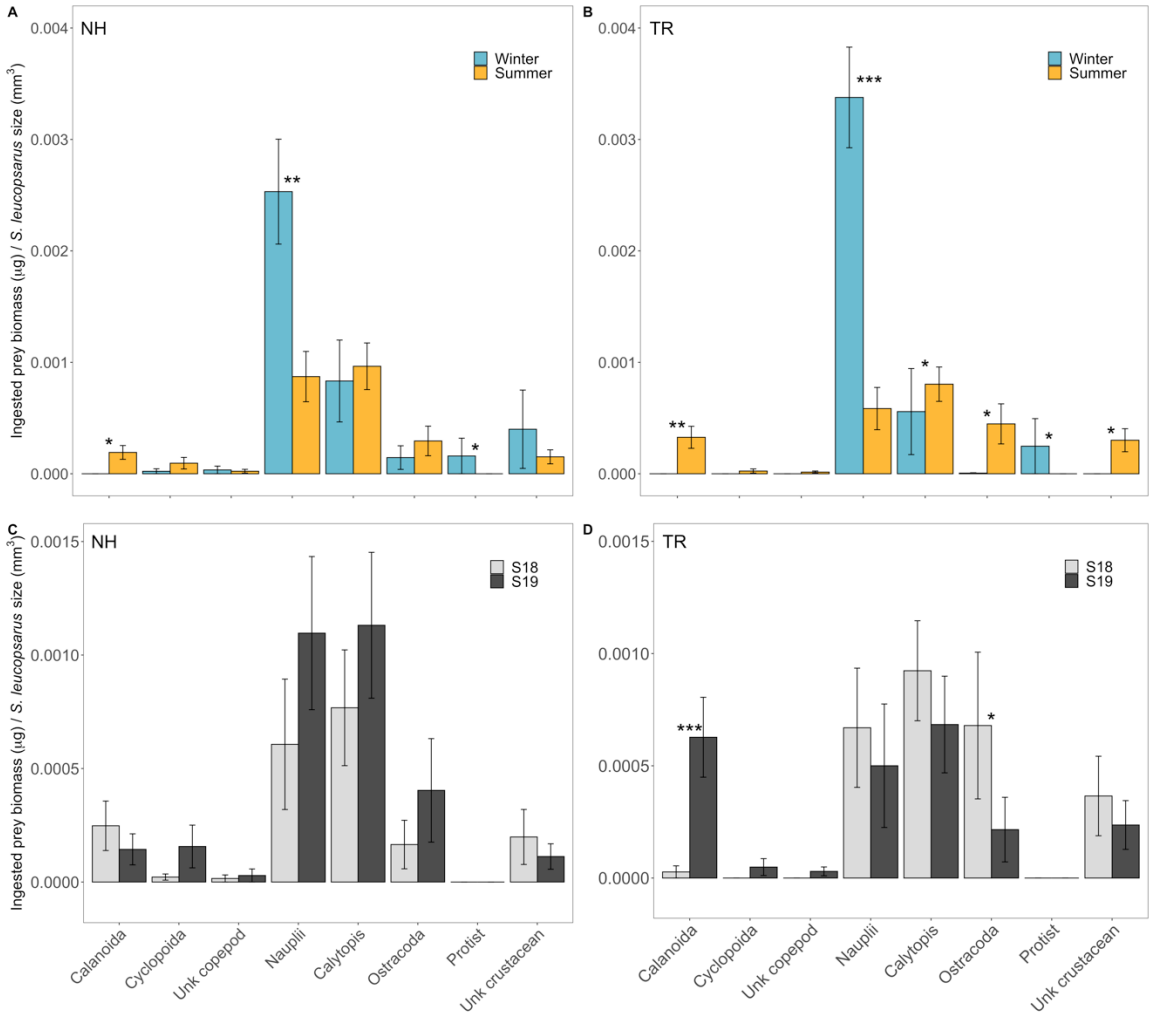

Fig. 2.9. Seasonal (A,B) and interannual (C,D) northern lampfish (*Stenobrachius leucopsarus*) mean standardized total consumed prey biomass [µg dry weight / *S. leucopsarus* SL (mm^3)] of individual prey groups on the (A,C) Newport Hydrographic Line (NH) and the (B,D) Trinidad Head Line (TR). S18 = summer 2018, S19 = summer 2019. ***$p < 0.001$, **$p < 0.01$, *$p<0.05$

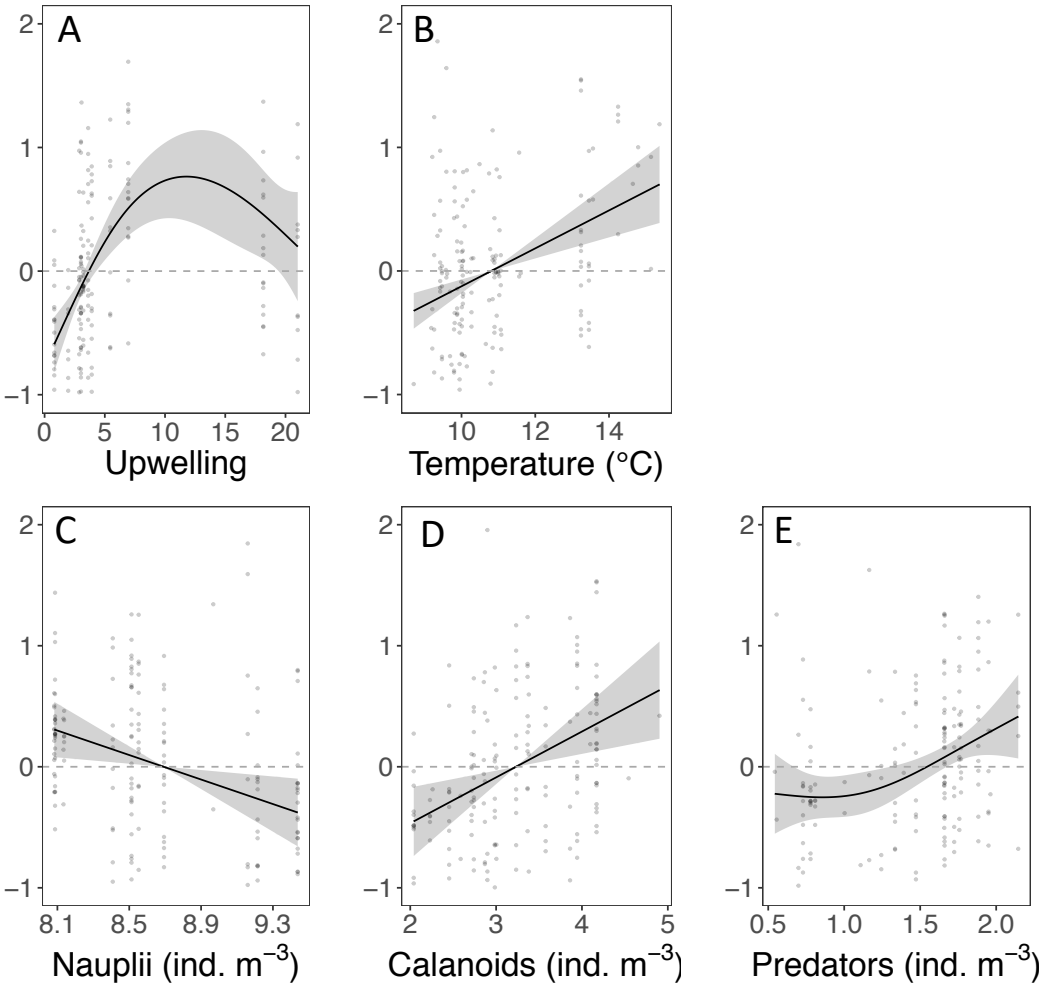

Fig. 2.10. GAM smooth functions showing the partial effects of each covariate after accounting for the other covariate effects on the mean recent growth (MRG; last 3 complete days) of individual larval northern lampfish (*Stenobrachius leucopsarus*; n= 174). Upwelling is the cumulative CUTI ($m^3 s^{-1}$) 10 d prior to each fish collection and taxa concentrations are all log+1 transformed. 95% confidence intervals (grey shading) and partial residuals (points) are shown for each covariate. Model AIC = 362.8, deviance explained = 48.6%

CHAPTER 3: Oceanographic and trophodynamic underpinnings of anchovy success in the northern California Current

Abstract

Anchovy and sardine typically display asynchronous population fluctuations with anchovy dominating during cool periods and sardine dominating during warm periods. However, the anchovy-sardine cold-warm paradigm has recently broken down in the California Current, suggesting that recruitment may not be a simple reflection of large-scale physical drivers. Instead, consideration of larval fish trophodynamics together with local oceanography is likely necessary to mechanistically relate survival and recruitment to the physical environment. We examined otolith-derived metrics of northern anchovy (*Engraulis mordax*) growth in the context of local oceanography and anchovy *in situ* prey and zooplankton predators in the northern California Current (NCC). Anchovy growth was spatially variable and the regions that conferred heighted growth differed based on the cross-shelf extent of upwelled waters. When upwelling was restricted to the nearshore environment, anchovy grew significantly faster inshore than offshore. Conversely, when the upwelling front moved farther offshore following sustained upwelling, offshore anchovy grew significantly faster than inshore anchovy. Modelling individual anchovy growth revealed that growth was affected by ambient copepod prey availability and gelatinous zooplankton predation pressure, with growth peaking at intermediate prey availability and the highest abundance of predators. Fast growth under high predation pressure may be indicative of the selective loss of slow growing larvae. Notably, anchovy abundances were high offshore but diminished immediately inshore of the upwelling front regardless of its cross-shelf position. This suggests that the upwelling front may act as a shoreward boundary for anchovy larvae which would affect their access to the highly nutritious prey base typical of the Oregon continental shelf waters in summer. Variation in anchovy growth with local oceanographic conditions and fine-scale distributions of prey and predators provides a mechanistic understanding of food-web dynamics which will enhance our ability to predict the response of forage fishes to ecosystem variability.

In preparation for submission to: *Frontiers in Marine Science*

1. INTRODUCTION

Most marine fishes experience high rates of mortality during their early life history stages with far reaching consequences for adult population dynamics. Within a few weeks of hatching, relatively small changes in larval growth and mortality rates can lead to orders of magnitude variability in year-class strength (Houde 1987, 2008, Leggett & Deblois 1994). As such, identifying the factors influencing larval survival is a core goal of fisheries oceanography.

Efforts to understand and predict year-class strength have been particularly robust for forage fishes, as these organisms play an important ecological role in coastal ecosystems (Cury et al. 2000, Koehn et al. 2016). Similar to other upwelling regions, anchovy (*Engraulis mordax*; northern anchovy) and sardine (*Sardinops sagax*; Pacific sardine) dominate the forage community in the California Current where their populations are characterized by dramatic boom and bust cycles (Baumgartner et al. 1992, Brodeur et al. 2005, Emmett et al. 2005). It is generally asserted that anchovy dominate during cool, productive periods while sardine dominate during warm periods (Lluch-Belda et al. 1989, Schwartzlose et al. 1999, Chavez et al. 2003). Yet, this theoretical anchovy-sardine cold-warm relationship has not held up under recent novel conditions in the California Current (Muhling et al. 2020). Contrary to expectations, northern anchovy abundance and larval survival reached record highs during and following the 2014 - 2016 severe marine heat wave, when sea surface temperatures were up to 6.2 °C above average and primary productivity was anomalously low in many regions (Gentemann et al. 2017, Kahru et al. 2018, Thompson et al. 2019). This suggests that recruitment to the adult population is probably not a simple reflection of large-scale physical drivers as previously postulated. Instead, consideration of larval fish trophodynamics together with local and regional oceanography is likely necessary to mechanistically relate northern anchovy survival and recruitment to the physical environment.

Growth and survival of pelagic larval fishes is determined by their ability to find food and avoid predation, which is tightly linked to the prevailing oceanographic conditions (Lasker 1975, Bailey & Houde 1989). Wind-driven upwelling has been implicated as a prominent oceanographic process affecting northern anchovy success in

the California Current (Lasker 1975, 1978, 1981, Takahashi et al. 2012). This type of upwelling occurs when equatorward winds drive the surface layer offshore allowing cool, nutrient rich water to rise into the coastal euphotic zone. Coastal upwelling can influence the survival of the early life history stages of northern anchovy in two primary ways: (1) by dictating the quantity and quality of prey available in the water column and (2) by affecting the spatial distributions and encounter rates of larvae with their prey and potential predators.

Empirical relationships between northern anchovy success and upwelling intensity are thought to be dome-shaped, with optimal conditions for larval feeding occurring at moderate upwelling intensity. Larvae may be production limited when upwelling is weak, but too much upwelling may disrupt larval food aggregations necessary for sufficient feeding ('Stable Ocean Hypothesis'; Lasker 1978, 1981, 'Optimal Environmental Window'; Cury & Roy 1989, Roy et al. 1992). Additionally, a lack of upwelling-favorable winds reduces the nutritional quality of northern anchovy's prey-field resulting in slower larval growth (Takahashi et al. 2012). Because fast larval growth and large size-at-age are thought to increase survival and year-class strength of most fishes (Anderson 1988, Miller et al. 1988, Hare & Cowen 1997), the influence of upwelling on prey availability and composition are likely important factors regulating northern anchovy populations. Yet, prey supply is linked to offshore transport in upwelling systems. During periods of sustained upwelling favorable winds, coastal larvae inhabiting surface waters can be advected into more oligotrophic conditions offshore. Upwelling induced offshore transport poses a risk for larval feeding as well as life cycle closure, especially for species that recruit to nearshore habitats (Parrish et al. 1981). Given the impact of upwelling on larval success, variability in the spatial extent of upwelled waters may contribute to complex patterns of northern anchovy feeding, growth, and survival. Presently, however, little is known about the degree to which anchovy vital rates vary across space and the potential effect on recruitment variability.

During summer in the northern California Current (NCC), north alongshore winds drive upwelling and the establishment of an upwelling front where lower density (warmer, fresher) offshore waters meet higher density (colder, saltier) upwelled waters. Local upwelling intensity affects the strength and position of the upwelling front. As a

result, the cross-shelf extent of upwelling influenced waters is highly variable in space and time (Castelao et al. 2005, Sato et al. 2018). For example, topographic features along the Oregon coast deflect the upwelling jet offshore, broadening the region influenced by upwelling-induced production (Checkley & Barth 2009). Likewise, the front gets pushed farther offshore following sustained periods of upwelling- favorable winds along the coast thereby widening the region of cold and productive upwelled waters. A narrow band of upwelled waters is restricted nearshore at the initiation of upwelling or during weakly favorable winds (Castelao et al. 2005).

Either due to passive transport or physiological temperature limitations, the location of the upwelling front and extent of upwelled waters affects the cross-shelf distribution of larval and juvenile fishes, including northern anchovy (Miller & Shanks 2004, Auth 2008, Sato et al. 2018). While the hydrodynamics of the upwelling front can help retain coastal taxa nearshore (Bjorkstedt et al. 2002), the front can also simultaneously act as a shoreward boundary to offshore species (Sato et al. 2018). Off central Oregon, larval northern anchovy are typically concentrated in warm, low salinity offshore water originating from the Columbia River Plume (Richardson 1973, Auth & Brodeur 2006). However, when upwelling is weak, larvae tend to be evenly distributed between coastal and offshore regions and can even be concentrated close to shore during periods of downwelling (Auth 2008). Moreover, during the recent extended marine heatwave in the NCC, spawning occurred throughout much of the year and closer to shore than previously observed (Auth et al. 2018). Variability in the cross-shelf distribution of anchovy under different upwelling scenarios likely affects their access to the highly abundant and lipid-rich prey base characteristic of shelf waters in summer in this system (Morgan et al. 2003), with implications for larval feeding and survival.

Northern anchovy are broadly distributed from southern Canada to Baja Mexico, with three distinct subpopulations throughout their range (Baxter 1966, Vrooman et al. 1981). While the central subpopulation is quite well studied, we focus on the northern subpopulation which ranges from northern California to British Columbia and is thought to spawn primarily in the summer upwelling season (May – Aug) near the Oregon-Washington border where it also supports a small bait fishery (Richardson 1981, Litz et al. 2008, Parnel et al. 2008). Anchovy hatch from eggs quickly after spawning and larvae

are generally surface oriented and primarily found in Columbia River Plume-influenced waters offshore with sea surface temperatures ranging from 13 – 17.4 °C (Baxter 1966, Richardson 1981, Auth & Brodeur 2006). Larvae are phyto- and zooplanktivorous, becoming more zooplanktivorous as they grow (Baxter 1966, Arthur 1976). Similar to other anchovy species (Morote et al. 2010), copepod post-nauplii (adults and copepodites) become an important prey source for northern anchovy when they are ~7 mm, standard length (SL; Berner 1959, Arthur 1976).

We examined spatial variability in northern anchovy growth in the context of local oceanography and their *in situ* prey and zooplankton predators in the NCC. Specifically, we coupled otolith-based metrics of larval growth and *in situ* plankton imagery to elucidate how northern anchovy, their prey, and their predators are affected by the intensity and cross-shelf extent of local upwelling. Understanding the oceanographic and trophodynamics underpinning of larval anchovy success is necessary to more accurately predict the response of this important forage fish to ecosystem variability.

2. MATERIALS AND METHODS

2.1 Field sampling

To relate larval northern anchovy (*Engraulis mordax*) growth to the fine-scale distributions of their zooplankton prey and potential predators, we coupled depth-discrete net sampling and fine-scale *in situ* plankton imaging. Sampling was conducted during two research cruises off the coast of Oregon in the summers of 2018 (Jul 3-11) and 2019 (Jul 16-25). During each cruise, larval northern anchovy were collected at 5 stations along the Newport Hydrographic Line, which is just south of the spawning location of the northern subpopulation of northern anchovy (Fig. 3.1; Richardson 1981). Station locations were chosen to capture shelf (n=2), shelf-break (n=1), and offshore (n=2) environments. We sampled each station twice per cruise and continuously towed a plankton imager along the same cross-shelf transect within 24 h of each biological sample collection. All sampling occurred during daylight hours.

Larval northern anchovy were collected at each station using a coupled Multiple Opening/Closing Net and Environmental Sensing System (MOCNESS; Guigand et al. 2005). The MOCNESS sampled discrete 25 m depth bins from the surface to depth (max

100 m) using five paired nets (4 m^2 and 1 m^2) fit with 1-mm and 333-μm mesh, respectively. The system was fit with a flowmeter and conductivity, temperature, and depth sensors and was towed behind the ship at 2.5 m s^{-1}. Nets were rinsed, sieved, and individually preserved in 95% ethanol immediately following MOCNESS retrieval. Sample ethanol was changed at-sea within 48 h of collection and again within two months to ensure proper preservation of otoliths for microstructure analysis. In the laboratory, fish larvae were sorted, enumerated, and identified to the lowest possible taxonomic level and northern anchovy were separated out in individual vials for growth analysis. Northern anchovy concentrations (ind. 1000 m^{-3}) were calculated by dividing counts from each net by the volume of water filtered through the net.

Three-dimensional prey and predator plankton distribution data were acquired using the *In situ* Ichthyoplankton Imaging System (ISIIS; Cowen & Guigand 2008). ISIIS is a low turbulence, high-resolution *in situ* shadowgraph imager with a large sample volume (150-180 s^{-1}), a pixel resolution of 68 μm, and a large field of view (13 x 13 x 50 cm). This system captures organisms roughly ranging from 200 μm to 12 cm in length. These characteristics make it an ideal system to sample small plankters that have been shown to be key prey taxa for larval northern anchovy and fragile gelatinous zooplankton that can be important predators of larval fishes but are difficult to quantify with traditional net-based sampling techniques (McClatchie et al. 2012, Luo et al. 2014, 2018). ISIIS was towed in a tight undulating fashion from surface to 100 m depth, or within a few meters of the seafloor in shallower regions, allowing for fine-scale horizontal and vertical spatial analyses. Imagery and co-collected physical data from CTD (Sea-Bird SBE49 FastCAT), dissolved oxygen (Sea-Bird 43), fluorescence (Wetlabs FLRT), and photosynthetically active radiation (EPAR; Biospherical QCP-2300) sensors were transferred to ship-based computers via fiber optic cable.

2.2 Physical data analysis

All MOCNESS and ISIIS raw sensor data were converted to environmental variables of interest based on factory calibrations. To understand how local oceanography influences larval anchovy we quantified the strength of upwelling immediately prior to sample collection and the cross-shelf location of the upwelling front during each

sampling event. We use the cumulative daily Coastal Upwelling Transport Index (CUTI; https://mjacox.com/upwelling-indices/) 10 d and 30 d prior to sampling as a measure of upwelling strength. The first time period was selected to account for the lag between physical wind-stress and phyto- and zooplankton abundances. Off Oregon, this lag is thought to be approximately 7 d and 13-16 d, respectively (Spitz & Allen 2005). The latter time period was selected to represent the upwelling experienced by larvae throughout the lifetime of our fish, as our oldest fish was 28 d.

Geopotential anomaly fields ($\Delta\Phi$; dynamic height multiplied by the acceleration of gravity) can be used to determine the location of the upwelling front in the NCC (Barth et al. 2000). ISIIS physical data were kriged onto a grid equal to the length of each transect at 2-m vertical and 500-m horizontal resolution. Mean temperature, salinity, and pressure data per grid cell were used to estimate the geopotential anomaly at 10 m relative to 80 m depth for each ISIIS transect using the R software (v 4.0.4) package 'gsw' (Kelley & Richards 2021). Similar to previous studies in this region (Sato et al. 2018), we define the upwelling front as $\Delta\Phi = 1.8\ m^2\ s^{-2}$.

2.3 Growth analysis

We used otolith microstructure analysis to examine the spatio-temporal age and daily growth patterns of larval northern anchovy. To reduce variability that might be associated with depth and because anchovy are generally surface oriented, we restricted our growth analysis to MOCNESS larvae collected in the top 50 m of the water column. A random subset of those larvae (n = 734) were measured for standard length (SL) to the nearest 0.01 mm using a Leica MZ16 dissecting microscope with a QImaging camera and Image Pro Premier 9.1 software. Due to low sample sizes at some stations, particularly in 2019, stations were categorized into inshore (n=2), shelf-break (n=1), and offshore (n=2) locations (Fig. 3.1) to analyze cross-shelf variability in otolith-based traits. Larvae from each year and cross-shelf location were randomly selected for otolith analysis (n = 270). Daily growth increments have been validated in northern anchovy and daily increment deposition begins near yolk-sac absorption (~4.2 mm SL ; Brothers et al. 1976, Methot & Kramer 1979). Because at least three increments are needed to estimate recent daily

growth (by definition), larvae < 5.5 mm SL were excluded from otolith analysis (Fig. B1).

Sagittal otoliths were dissected and stored in immersion oil on a glass slide for approximately 1-3 h to 'clear' prior to reading. Prepared otoliths were read along the longest axis at 400x magnification using a Zeiss Axio compound microscope fit with a QImaging camera and Image Pro Premier 9.1 software. Each otolith was read twice by the same reader without access to any sampling data. If reads differed by >5%, the otolith was read a third time. If reads differed by ≤5%, one read was randomly chosen for analysis. Otoliths where all three reads differed by >5% would have been removed from analysis (Sponaugle 2009), but none fit this criterion.

Daily growth increments were enumerated to provide an estimate of age. The period from hatching to the first daily ring deposition varies with temperature and ranges from 3 to 9 d post hatch (dph; Methot & Kramer 1979). In the NCC, larval northern anchovy typically occur in regions where sea surface temperature is 13 -16 °C (Richardson 1981). In this study, we collected northern anchovy at a mean water temperature of ~13.5 °C. Thus, similar to other studies in the region (Takahashi et al. 2012), the first daily otolith increment was assumed to have been deposited 5 dph and final ages were calculated by adding 5 d to the total otolith increment count.

We used two metrics to analyze northern anchovy growth patterns: (1) mean daily growth (MDG) which is the average increment width of each day of life and (2) mean recent growth (MRG) which is the average increment width of each individual over the last three full days of life. We use the latter because it is unknown how long larvae have been associated with the environmental and prey and predator conditions measured at the time of collection.

Otolith increment widths increase with age (Baumann et al. 2003). To account for this, we detrended the last three increment widths for age by calculating a detrended growth index:

$$DG_{ij} = (G_{ij} - G_j)\, SD_j^{-1} \qquad (1)$$

Where DG_{ij} is the detrended growth of individual i at age j, G_{ij} is otolith-based growth (increment width) for individual i at age j, G_j is the mean otolith-based growth of all

individuals at age j, and SD is the standard deviation of G. Detrending for age allows us to investigate the spatio-temporal variability in MRG of differently aged northern anchovy larvae (Robert et al. 2009, Sponaugle et al. 2010).

We compared MRG across years and cross-shelf locations using analysis of covariance (ANCOVA) with age as a covariate. If a significant interaction between age and year or location precluded the interpretation of ANCOVA results, fish were split roughly in half into young (<14 d) and old (≥14 d) age groups and a separate ANCOVA with age as a covariate was conducted for each group. When applicable, ANCOVAs were followed by a Tukey HSD post-hoc test.

2.4 Imagery analysis

To investigate the relationships between MRG and the distributions of northern anchovy and their potential prey and predators we coupled growth analyses with *in situ* imagery. ISIIS data were processed, trained, and tested for automated classification following Luo et al. (2018), Briseño-Avena et al. (2020), Schmid et al. (2020), and Swieca et al. (2020), with the full pipeline code open-sourced in Schmid et al. (2021). After image processing, corrected taxa concentration estimates were kriged onto a grid equal to the length of each transect at 2-m vertical and 500-m horizontal resolution.

Although species of Clupeiformes larvae cannot be quantitatively discerned by ISIIS due to their indistinct morphology, co-collected net samples can be used to determine the constituents of this imagery group. During net sampling, we collected two Clupeiformes species: northern anchovy (*Engraulis mordax*) and Pacific sardine (*Sardinops sagax*), with northern anchovy comprising 98.4% of the Clupeiformes caught. Larval Pacific sardine were entirely absent in 2018 and were rare (1.6% Clupeiformes catch) in 2019. Thus, for our purposes, Clupeiformes imagery data can reasonably be used to represent the fine-scale distribution of northern anchovy larvae.

Prey groups of interest were selected based on field studies of northern anchovy diet analysis in the literature. Protists and calanoid and cyclopoid copepods of various life stages are frequently found in the guts of northern anchovy larvae (Berner 1959, Baxter 1966, Arthur 1976). Similar to other anchovy species, copepodites and adult copepods (i.e., copepod post-nauplii) become important prey items for northern anchovy around

6.5-7 mm SL (Arthur 1976, Morote et al. 2010). Because the mean size of larvae used in our growth analysis was 8.9 mm SL, we focused our examination of potential prey availability on the distributions of post-naupliar calanoid and cyclopoid copepods.

Although a large body of work emphasizes the importance of top-down predation on northern anchovy, zooplanktivorous predation on larval fishes is rarely quantified to inform the selection of potential predators. This is likely due to the variety of potential zooplanktivorous predators (Bailey & Houde 1989) and the difficulty in sampling some taxa (i.e., gelatinous taxa) with net-based systems. Nonetheless, several studies suggest that larval fishes are important prey for chaetognaths, ctenophores, hydromedusae, and siphonophores (Alvarino 1980, 1985, Purcell 1985). Further, larval fishes have been anecdotally observed in the guts of chaetognaths and ctenophores on the Newport Hydrographic Line (Auth & Brodeur 2006), so these taxa were selected as the potential predator groups for our analysis.

The mean concentration (ind m^{-3}) of larval northern anchovy and their potential prey and predators was calculated for every sampling station as the mean taxa concentration per 2-m depth bin from the station waypoint to 500 m seaward and within the top 50 m of the water column. Station values were summarized into their respective inshore, shelf-break, and offshore cross-shelf locations each year. Vertical distribution plots of mean taxa concentration per 2-m depth bin were constructed for all cross-shelf locations each year. Vertically integrated taxa concentrations were compared among cross-shelf locations each year using non-parametric Kruskal-Wallis tests followed by a Dunn post-hoc test, when applicable.

We also explicitly investigated the effect of local oceanography on northern anchovy by examining their distributions and the distributions of their potential zooplankton prey and predators relative to the upwelling front for each year. For the length of each transect, vertically integrated taxa concentrations were binned into 5-km horizontal segments and the distance from each segment to the position of the upwelling front was calculated. Mean (±SE) segment concentrations were normalized to the maximum transect value and were centered on the position of the upwelling front such that negative distances denoted concentrations inshore of the upwelling front and positive distances offshore of the upwelling front. The data were non-parametric so Wilcoxon

rank sum tests were used to determine if differences between taxa concentrations inshore and offshore of the upwelling front each year were significant. Then, every plankton imagery frame (13 x 13 x 50 cm) containing a northern anchovy larva (n = 1444) was extracted and the mean number of selected prey and predator taxa co-occurring within the anchovy frame was plotted along the length of the transect. Plots were constructed for each sampling year, with the location of the upwelling front noted, to provide an estimate of anchovy overlap with their prey and predators on scales relevant to trophic interactions.

2.5 Statistical modeling

We quantified the effect of local oceanography and potential prey availability and predation pressure on the recent larval growth of northern anchovy using generalized additive models (GAMs). In these models, the response variable was the individual mean recent growth (MRG; last three full days of life) of 270 northern anchovy and the covariates were *in situ* temperature (continuous) and concentrations of protists (continuous, log transformed), copepod post-nauplii (continuous, log transformed), and predators (continuous, log transformed). Additionally, an early growth parameter (mean increment width over the first third of each fish's life) was incorporated to account for the fact that an individual's recent growth is likely impacted by their growth history (i.e., fish that grow fast early in life are more likely to continue growing fast later in life; Dower et al. 2008, Robert et al. 2014, Pepin et al. 2015). We also address the possible effect of density dependence on recent growth by incorporating a larval density term (mean concentration of northern anchovy per net tow) in the model. Finally, we included a random effect (intercept) of net tow, as individuals from the same MOCNESS tow are more likely to have similar growth patterns, but model selection indicated that models without the random intercept performed better.

MOCNESS environmental data were used to calculate mean *in situ* temperature per MOCNESS net (25-m depth bin) associated with each fish collected. Mean concentrations of protists, copepod post-nauplii (calanoid copepods, cyclopoid copepods), and predators (chaetognaths, ctenophores) were the mean ISIIS concentrations corresponding to the station where fish were collected on each transect.

Calanoid and cyclopoid copepods as well as chaetognaths and ctenophores were pooled due to collinearity.

After pooling, variance inflation factors (VIF) indicated that collinearity between covariates would not preclude the interpretation of model results (values ≤ 3.5; Zuur et al. 2010). We applied a smoothing function to each covariate, restricting the number of knots to 4 to avoid model overfitting. Then, we used a backward stepwise approach for model selection and compared full and reduced versions of the models with Akaike's information criterion (AIC) and generalized cross validation (GCV). The model with the lowest AIC and GCV values was chosen as the best model if it was the reduced (simpler) version. However, if the model with the lowest AIC and GCV was the more complex model, it was only selected if it was significantly different (ANOVA, $p < 0.05$) from the reduced version. Model residuals were checked for deviations from normality, homogeneity of variance, and other abnormalities. All modeling analyses were conducted using the R software (v 4.0.4) package 'mgcv' (Wood 2017).

3. RESULTS

3.1 Environmental setting

We measured interannual and spatial variability in the physical environment along the Newport Hydrographic Line. In 2018, the month preceding sampling was marked by strong and persistent upwelling. Approximately 5 d prior to sampling, upwelling winds weakened and sample collection occurred during a brief relaxation period (Fig. 3.2A). In contrast, in 2019 we sampled during the onset of active upwelling following nearly a month-long relaxation event (Fig. 3.2B). Cumulative CUTI upwelling values 30 d and 10 d prior to sampling were 10.67 m^3s^{-1} and 3.05 m^3s^{-1} in 2018 and 5.90 m^3s^{-1} and 3.77 m^3s^{-1} in 2019, respectively. Interannual variability in upwelling strength resulted in a ~12 km difference in the cross-shelf position of the upwelling front ($\Delta\Phi = 1.8\ m^2\ s^{-2}$), with the front located just ~3 km shoreward of the shelf-break (200 m isobath) in 2018, while it was ~15 km shoreward of the shelf break in 2019.

Both *in situ* collected physical data and satellite derived surface maps show the effect of upwelling on the environment each year and align well with expectations based on the position of the upwelling front. Surface waters were generally cooler inshore and

warmer offshore, but cooler surface water protruded farther across the shelf in 2018 compared to 2019 (Figs. 3.1, B2). Similarly, high concentrations of chlorophyll *a* were widely distributed in all cross-shelf environments in 2018, while high chlorophyll *a* concentrations were restricted to only the nearshore in 2019 (Fig. 3.1, Table 3.1). During this time, the concentration of chlorophyll *a* nearshore was almost 3x higher than at the shelf-break and was 5x higher than offshore. Finally, the chlorophyll max was substantially shallower in 2018 than in 2019 and deeper offshore than inshore each year, ranging from 5.8 – 17.8 m in 2018 and 14.1 – 31.5 m in 2019 (Table 3.1).

3.2 Northern anchovy distributions

Northern anchovy was a dominant member the ichthyoplankton assemblage during sampling (n = 1928), accounting for 37.4% of the total larval fish abundance in 2018 and 11.7% in 2019. Overall, the mean concentration of larval northern anchovy in the top 50 m of the water column was 75.3 (± 27.3) ind. 1000 m^{-3}, ranging from 233.3 (±90.8) ind. 1000 m^{-3} in 2018 to 32.9 (±8.5) ind. 1000 m^{-3} in 2019 (Table 3.1). Concentrations were generally higher at the offshore (2018) and shelf-break (2019) locations compared to inshore each year, but larvae were collected at each station during both sampling years (Table 3.1, Fig. 3.1). Regardless of the cross-shelf position of the upwelling front, larval northern anchovy were substantially more abundant offshore than inshore of the front (Wilcoxon rank sum test: $p < 0.001$ both years), with abundances steadily declining immediately shoreward of the frontal boundary (Fig. 3.3). Finally, northern anchovy larvae were heavily concentrated in the top 50 m of the water column. MOCNESS catches below this depth were negligible (n = 20 individuals; data not presented).

3.3 Northern anchovy size, age, and growth

Northern anchovy used for growth analysis ranged in size from 5.6 to 14.9 mm SL and were 10 to 28 dph. There was a fair degree of coherence in northern anchovy size and age across years and cross-shelf locations (Fig. B3). The overall population somatic growth rate was 0.58 mm d^{-1}.

Larval otolith increments were well defined following a distinct first-feeding check. The growth region between the visible hatch and first-feeding checks typically had 2-5 faint and often irregular increments (Fig. 3.4), as has been previously described for this species which begins regular increment deposition close to yolk-sac absorption and first-feeding (Methot & Kramer 1979). There was a significant positive relationship between fish size vs. age, otolith size vs. age, and the fish size-at-age residuals vs. otolith size-at-age residual in all years and locations (Table B1).

Early larval growth was spatially variable and the cross-shelf regions that conferred elevated growth differed between years. MDG (mean increment widths for each day of life) was similar across space until ~11 dph in 2018 and ~13 dph in 2019 when growth diverged such that offshore northern anchovy grew significantly faster than inshore larvae in 2018 (Fig. 3.5A) whereas the reverse occurred in 2019 (Fig. 3.5B). At the shelf-break, growth tended to be intermediate between the inshore and offshore larvae, though the MDG of shelf-break larvae did not differ significantly from their slower growing counterparts each year (inshore 2018, offshore 2019; Fig. 3.5A,B). Finally, growth was generally faster in 2019 compared to 2018, as the growth of slower growing larvae in 2019 was substantially higher than the growth of the slower growing larvae the previous year (Fig. B4).

MRG (mean growth over the last three full days of life) followed a similar pattern to MDG. However, in 2018 there was a significant interaction between age and cross-shelf location requiring the division of old (≥14 dph) and young (<14 dph) age larval groups for ANCOVA analysis. In 2018, the MRG of young fish did not differ among cross-shelf locations, but old fish grew significantly faster at the shelf-break ($p = 0.01$) and offshore ($p < 0.001$) compared to inshore (Fig. 3.6A). Conversely, in 2019, northern anchovy had significantly faster growth inshore compared to the shelf-break ($p = 0.001$) and offshore ($p = 0.02$) locations (Fig. 3.6B). There was no significant difference in the growth of old and young anchovy larvae at any location in 2019 (Fig. B5).

3.4 Recent growth modeling

Northern anchovy recent growth (MRG) was influenced by prey availability and potential predation pressure (Fig. 3.7; deviance explained = 39.9%). Model results

indicate that MRG had a dome-shaped relationship with ambient copepod (calanoid and cyclopoid) abundance ($p < 0.001$). Northern anchovy growth was below average at the lowest concentrations of copepods, reached a peak at intermediate values before decreasing to below average growth at the highest concentration of copepods (Fig. 3.7A). Growth was also significantly affected by potential predator (chaetognaths, ctenophores) abundance ($p < 0.001$), with average growth at low predator concentrations, below average growth at mid-range values, and above average growth at the maximum predator abundances measured (Fig. 3.7B). Finally, *in situ* temperature in the top 50 m of the water column, protist concentrations, and northern anchovy density did not significantly impact MRG.

3.5 Prey availability and potential predation pressure

Prey availability was generally higher in 2018 than 2019 ($p < 0.001$, all prey taxa), but differed substantially across space within each year. In contrast to northern anchovy abundance patterns, high calanoid and cyclopoid copepod abundances were observed inshore of and across the upwelling front, with abundance decreasing roughly 20 – 25 km seaward of the position of the front throughout sampling. As such, relatively high abundances of copepods were present up to 25 km seaward of the shelf-break (200 m isobath) in 2018, but only 5 – 10 km seaward of the shelf-break in 2019 (Fig. 3.8).

During 2018, there was no significant difference in cyclopoid copepod abundance inshore and offshore of the upwelling front ($p = 0.19$; Fig. 3.8B) or among inshore, shelf-break, and offshore sampling locations ($p = 0.70$-0.93; Table 3.1). While calanoid copepod concentrations were higher inshore than offshore of the upwelling front ($p < 0.001$), high abundances of calanoid copepods were present 10s of kms beyond the front with a considerable decrease in abundance occurring only > 25 km seaward of the front (Fig. 3.8A). Maximum copepod concentrations occurred at ~10 km seaward of the upwelling front, especially for cyclopoids (Fig. 3.8A,B).

In 2019, calanoid and cyclopoid copepods were considerably more abundant inshore than offshore of the upwelling front ($p < 0.001$). Peak abundances of both taxa occurred 15-20 km shoreward of the front (Fig. 3.8C,D). Calanoid copepods were especially restricted nearshore, and their concentration inshore significantly exceeded

their concentration at the shelf-break ($p = 0.001$) and offshore ($p < 0.001$; Table 3.1). There was no significant difference in the abundance of cyclopoid copepods at inshore and shelf-break locations ($p = 0.42$; Table 3.1), but a sharp decrease in abundance occurred immediately seaward of the shelf-break (Fig. 3.8D). The 2019 offshore copepod concentrations were the lowest observed throughout all of the sampling, and were 1.5 – 2x lower than the offshore location the previous year (Table 3.1).

Predators were nearly 3x more abundant in 2019 compared to 2018 ($p < 0.001$), but they displayed a similar cross-shelf pattern within each year, with offshore abundances up to 5x higher than those at the shelf-break ($p < 0.001$, both years) and inshore locations ($p < 0.001$, both years; Table 3.1).

Finally, in both years, northern anchovy had the highest fine-scale overlap (mean number of ind. in a 13 x 13 x 50 cm frame with a larval fish) with their copepod prey in the region seaward (~20 km) of the upwelling front. Given the position of the front relative to the shelf-break, this resulted in the highest anchovy-copepod overlap offshore of the shelf-break in 2018 (Fig. 3.9A), but not in 2019. Instead, 2019 anchovy-copepod overlap was greatest in the region between the upwelling front and the shelf-break (Fig. 3.9B). Notably, anchovy-predator overlap was almost entirely restricted to seaward of the shelf-break, especially in 2018 (Fig. 3.9).

3.6 Taxa vertical distributions

Northern anchovy were fairly evenly distributed from the surface to 50 m depth at inshore and shelf-break sampling locations (Fig 3.10A,B,D,E). Offshore, they displayed distinct concentration peaks at approximately 12 m depth in 2018 (Fig. 3.10C) and 25 m depth in 2019 (Fig. 3.10F). On both occasions, peaks occurred just above the chlorophyll max. Copepod vertical distributions were more nuanced. In general, copepod concentrations peaked below the chlorophyll max, with the exception of 2019 offshore, whereas neither calanoid or cyclopoid copepods displayed a clear concentration peak within the top 50 m of the water column (Fig. 3.10).

4. DISCUSSION

We examined otolith-derived metrics of larval northern anchovy (*Engraulis mordax*) growth in the context of local oceanography and their *in situ* prey and potential zooplankton predators in the northern California Current (NCC). Our 2 years of sampling occurred during strikingly different summer conditions, providing insight into how the strength and spatial extent of upwelling influences larval northern anchovy. Anchovy abundances were high offshore but diminished immediately inshore of the upwelling front regardless of its cross-shelf position. Zooplankton prey and predator concentrations relative to the upwelling front were more nuanced. As a result, anchovy growth was spatially variable and the regions that conferred higher growth differed between years. Following sustained upwelling in 2018, anchovy both offshore and at the shelf-break grew significantly faster than those inshore. Copepods were widely distributed, and the anchovy-copepod overlap peaked seaward of the shelf-break (200 m isobath). Conversely, in 2019 when upwelled waters were restricted to nearshore locations, copepod abundances and the anchovy-copepod overlap were both substantially higher on the continental shelf compared to offshore, resulting in significantly faster growth inshore than at the shelf-break or offshore.

4.1 Larval northern anchovy otolith microstructure

The early larval growth rate of northern anchovy was 0.58 mm d^{-1}, which is within the range, but toward the high-end, of what has previously been reported for this species (Methot & Kramer 1979, Methot 1981, Butler 1989). Growth was similar across space until approximately 12 dph, when northern anchovy began to exhibit spatial variability in their growth. The mean size of larvae at this age was 7.25 mm SL. Interestingly, this is near the size of flexion (6.5 – 13.5 mm SL; Moser 1996) and also roughly coincides with the size at which larval anchovies begin to incorporate significant numbers of copepodites and adult copepods (copepod post-nauplii) into their diets. While the majority of studies investigating the diets of northern anchovy focused on first-feeding larvae in controlled lab-based experiments (Hunter 1972, Lasker 1975, Scura & Jerde 1977), a few studies provide insights into the ontogenetic diet composition of this species in the wild. By 7 mm SL, northern anchovy larvae in the California Current undergo a diet shift away from protist consumption and toward late-stage copepods.

Copepod nauplii appear to be an important component of northern anchovy diet throughout early ontogeny (Berner 1959, Arthur 1976). Growth divergence at roughly the size of a shift in diet suggests that copepod availability and consumption likely underlie this spatial variability in northern anchovy growth.

Copepods are widely recognized as a nutritious prey source for fish larvae (Llopiz 2013, Jackson & Lenz 2016) and higher copepod ingestion has been shown to increase larval growth rates in a variety of systems and species including bluehead wrasse (*Thalassoma bifasciatum*) and blue marlin (*Makaira nigricans*) in the Straits of Florida (Sponaugle et al. 2009, 2010), walleye pollock (*Gadus chalcogrammus*, formerly *Theragra chalcogramma*) in the Gulf of Alaska (Bailey et al. 1995), and northern lampfish (*Stenobrachius leucopsarus*) in the NCC (Swieca et al. *in prep*). For northern anchovy, feeding on copepods increases larval condition and survival (Scura & Jerde 1977, Hakanson 1989), and presumably growth (Takahashi et al. 2012). By contributing to fast growth, copepod consumption may also help northern anchovy escape predation (Anderson 1988).

4.2 Distribution of northern anchovy larvae

Larval northern anchovy abundances were consistently high offshore and diminished immediately inshore of the upwelling front regardless of its cross-shelf position. This observation suggests that the upwelling front may act as a shoreward boundary to northern anchovy larvae. In this system, northern anchovy larvae are typically concentrated in warm, low salinity offshore water originating from the Columbia River Plume (Richardson 1973, Auth & Brodeur 2006). However, Auth (2008) found that during weak upwelling seasons larvae are evenly distributed across coastal and offshore regions. Because the upwelling front is positioned closer to shore during weak upwelling (Castelao et al. 2005), this anecdotal finding provides support for the notion that the location of the upwelling front and the extent of upwelled waters limits the shoreward distribution of northern anchovy larvae.

It is difficult to distinguish the mechanisms driving this observation because of the variety of co-varying physical properties near upwelling fronts and the dynamic nature of upwelling systems. Northern anchovy larvae are generally concentrated in the

top 10s of meters of the water column and thus are subject to passive cross-shelf transport in surface currents such as those generated by wind-driven upwelling and downwelling processes (Parrish et al. 1981). Temperature may also be an important factor regulating larval distributions. Similar to its effect on larval anchovy, the upwelling front functions as a shoreward boundary for adult planktivorous fish in the NCC and it is hypothesized that surface temperature ultimately limits the distribution of these taxa, as they are strongly temperature dependent, and the upwelling front marks the transition from warm offshore water to cool upwelled water inshore (Sato et al. 2018). While anchovy may be more cold tolerant than other planktivorous fishes (Baxter 1966, Checkley et al. 2000), they are generally confined to regions of relatively warm water where sea surface temperatures range from ~13 – 17.4 °C (Baxter 1966, Richardson 1981, Auth & Brodeur 2006). Poor swimming larvae likely have less control over their horizontal distribution than their adult counterparts, but a shift in adult spawning distributions relative to the upwelling front could help explain the observed larval distributions. Indeed, reduced upwelling has been shown to lead to a shoreward expansion of northern anchovy spawning habitat and consequently larval distributions off Oregon (Brodeur et al. 1985). Whether due to passive transport, physiological limitation, or shifting spawning habitats, variability in the cross-shelf distribution of anchovy under different upwelling scenarios likely affects their access to the highly abundant and lipid-rich prey base characteristic of summer shelf waters in this system (Morgan et al. 2003).

4.3 Prey availability and northern anchovy growth

Anchovy growth was spatially variable and the regions that conferred heightened growth differed based on the cross-shelf extent of upwelled waters. When upwelling was restricted to the nearshore environment, anchovy grew significantly faster inshore than at the shelf-break or offshore. Conversely, when the upwelling front was located farther offshore following sustained upwelling, offshore and shelf-break anchovy grew significantly faster than those inshore. The spatial extent of upwelling differentially impacted the distribution of northern anchovy larvae and their copepod prey, with implications for trophodynamics.

Unlike northern anchovy who were concentrated offshore of the upwelling front, high calanoid and cyclopoid copepod abundances occurred inshore of and across the upwelling front both years. This is consistent with expectations, as copepod biomass during summer in the NCC can be nearly 3x greater on the continental shelf compared to off the shelf (Morgan et al. 2003, Lamb & Peterson 2005). Interestingly, copepod distributions appear to be less affected by the position of the upwelling front than larval anchovy. We observed persistently high copepod concentrations roughly 20 - 25 km seaward of the upwelling front throughout sampling. Variable fish and zooplankton responses to the upwelling front have been observed by other studies in this system (Sato et al. 2018) and contrasting responses of anchovy and copepods may explain the spatial variability in northern anchovy larval growth.

Following sustained upwelling in 2018, the upwelling front was located farther offshore and high copepod abundances and fine-scale overlap with anchovy were observed up to 25 km seaward of the shelf-break (200 m isobath). When upwelling was restricted to only nearshore locations in 2019, high anchovy-copepod overlap occurred over the entire continental shelf, but peaked 10s of kms inshore of the shelf-break. Enhanced prey availability offshore of the shelf-break in 2018, but inshore of the shelf-break in 2019 likely contributed to the contrasting patterns of fast growth between years.

In addition to spatial variability in copepod abundance, copepod community composition exhibits cross-shelf zonation during summer in the NCC, which also likely impacted larval anchovy growth. Continental shelf waters are characterized by the presence of 'cold water' copepod species transported south to the NCC from subarctic source waters. In contrast, the off-shelf community is dominated by 'warm water' copepods that either reside in coastal zones during winter and are advected offshore at the start of the upwelling season or are transported from the Transition Zone (Peterson & Miller 1977, Morgan et al. 2003, Hooff & Peterson 2006). Given their affinities, 'cold water' inshore copepods are thought to be lipid-rich and serve as an important prey base for many coastal taxa, while 'warm water' offshore copepods are relatively lipid-poor (Peterson & Schwing 2003, Hooff & Peterson 2006, Tomaro et al. 2012, Peterson et al. 2014). It is generally asserted that 'cold water' copepods are retained on the shelf through ontogenetic vertical migrations that limit offshore advection during the upwelling season.

However, only late-stage copepods (C3 copepodite - adult) undergo vertical migration, and nauplii through mid-stage copepodites are concentrated in the top 20 m of the water column where they are more frequently subject to cross-shelf transport in the surface layer, although late-stage copepods can also be transported offshore during especially strong upwelling (Morgan et al. 2003, Lamb & Peterson 2005). It is possible that the younger life stages of lipid-rich 'cold water' copepods were transported offshore with sustained upwelling in 2018 contributing to fast offshore anchovy growth that year. When upwelling was reduced in 2019, this highly nutritious prey base was likely restricted to the nearshore environment, the region of fast anchovy growth that year.

4.4 Impact of predation pressure on northern anchovy growth

Larval northern anchovy growth is also significantly related to the abundance of zooplankton predators (chaetognaths and ctenophores). After accounting for the influence of prey availability, the partial effect of predators indicates that growth was just above average at low predator abundance, decreased to slower than average at mid-range predator abundance, then rapidly increased to above average growth at the highest abundance of predators. Contrasting effects of predation on northern anchovy growth is not entirely surprising and may be the result of shifting predator composition across years or cross-shelf locations. Foundational theories in the field of fisheries oceanography suggest that faster-growing larvae experience enhanced survivorship because their quick development reduces vulnerability to predation (Houde 1987, Anderson 1988). However, selection against fast growing larvae also occurs (Sponaugle et al. 2011, Takasuka et al. 2017) highlighting that patterns of selective mortality are species (prey and predator) and habitat dependent. The predators included in our model have drastically different modes of predation - chaetognaths are aggressive ambush predators (Feigenbaum & Maris 1984) while ctenophores often do not actively attack their prey (Purcell 1985) - and exhibited different cross-shelf distributions throughout our sampling. As such, the variable growth response may reflect the relative composition of each type of predator and the effect of their predation on anchovy growth.

Although we were unable to incorporate all predator taxa in the model due to collinearity, high abundances of chaetognaths and ctenophores generally co-occurred

with high abundances offshore of hydromedusae and siphonophores. This pattern resulted in offshore predator abundances that were up to 5x greater than the shelf-break and inshore regions in both years. Consequently, larval anchovy-predator overlap was also higher offshore with implication for larval mortality rates and selective loss of larvae with particular traits such as slower growth.

Both bottom-up and top-down controls have been used to explain northern anchovy population fluctuations. Studies that focus on the latter emphasize the effect of predation on eggs and age-0 anchovy from piscivorous fishes, seabirds, and marine mammals as well as cannibalism from adult conspecifics (Hunter & Kimbrell 1980, Folkvord & Hunter 1986, Glaser 2011, Sydeman et al. 2020). These studies provide substantial evidence to suggest that predation can exert some level of control on northern anchovy populations. Yet, studies investigating the potential role of zooplanktivorous predation on the early life history stages of northern anchovy are scant. This may be due, in part, to the variety of potential zooplankton predators (Bailey & Houde 1989) and the difficulty in sampling gelatinous taxa with net-based systems. Nonetheless, seminal work in this realm suggests that larval fishes comprise a significant portion of the diet of many zooplankton predators (Alvarino 1985, Purcell 1985, Purcell & Grover 1990, Purcell et al. 1994, Purcell & Arai 2001). Our results build upon these findings and demonstrate that predation is a key parameter affecting northern anchovy larval growth. Because larval growth and size-at-age strongly impact survival and year-class strength (Lasker 1975, Anderson 1988, Miller et al. 1988, Hare & Cowen 1997), zooplanktivorous predation on larval anchovy must be considered to holistically address the factors regulating northern anchovy populations. Quantifying the effects of predation on northern anchovy survival is becoming even more important in the context of changing ocean conditions in the NCC which have historically favored gelatinous predator taxa (Brodeur et al. 2019).

5. CONCLUSIONS

Under recent novel oceanographic conditions, it has become abundantly clear that there are gaps in our knowledge about the specific mechanisms through which variability in the environment translates into northern anchovy recruitment variability. We

integrated three tools (depth discrete biological sampling, *in situ* underwater imaging, and otolith microstructure analysis) to reveal that ocean habitats are not equal at promoting growth, and presumably survival, of larval northern anchovy. Importantly, the regions that conferred heighted growth differed between years and was related to upwelling variability. In particular, the spatial extent of cool, productive upwelled waters led to variability in the trophic environment experienced by northern anchovy with implications for their growth and survival. Our findings illustrate the importance of examining local oceanographic conditions and food-web dynamics when predicting the response of forage fish to ecosystem variability.

6. ACKNOWLEDGEMENTS

We thank all who contributed to at-sea sampling, including the captains and crews of the R/V Atlantis and the R/V Sally Ride, H. William Fennie, Megan Wilson, Jami Ivory, Kelia Axler, Miram Gleiber, and Christian Briseño-Avena. This work was strengthened by input on larval fish identification from T. Auth and modeling guidance from L. Ciannelli. Finally, we acknowledge the Center for Quantitative Life Sciences and the many undergraduate volunteers at Oregon State University who contributed to the processing of imagery data and biological samples: L. Nepstad, A. Branka, A. Bolm, C. Watson, B. Anders, A. Pulscak, L. Wetchler, J. Knowlton, N. Baker, R. Hartley, K. Bowditch, K. Rorvig, H. Woodwick, K. Bauer, Z. Sallada, S. Knodel, M. Sandmeier, H. Woodruff, Z. Thomas, and B. Rothman. This project was funded by NSF OCE 1737399. KS was also supported through the HMSC Markham Award, the Walter G. Jones Fishery Development Award, the Hannah-Jones Award, and Integrative Biology Research Funds.

7. REFERENCES

Alvarino A (1980) The relation between the distribution of zooplankton predators and anchovy larvae. CalCOFI Rep 21:150–160

Alvarino A (1985) Predation in the plankton realm; mainly with reference to fish larvae. Inv Mar CICIMAR 2:1–122

Anderson JT (1988) A review of size dependent survival during pre-recruit stages of fishes in relation to recruitment. J Northwest Atl Fish Sci 8:55–66

Arthur D (1976) The food and feeding of larvae of three fishes occurring in the California Current, *Sardinops sagax*, *Engraulis mordax*, and *Trachurus symmetricus*. Fish Bull 74:517–530

Auth T (2008) Distribution and community structure of ichthyoplankton from the northern and central California Current in May 2004-06. Fish Oceanogr 17:316–331

Auth TD, Brodeur RD (2006) Distribution and community structure of ichthyoplankton off the coast of Oregon, USA, in 2000 and 2002. Mar Ecol Prog Ser 319:199–213

Bailey KM, Canino MF, Napp JM, Spring SM, Brown AL (1995) Contrasting years of prey levels, feeding conditions and mortality of larval walleye pollock *Theragra chalcogramma* in the western Gulf of Alaska. Mar Ecol Prog Ser Mar Ecol Prog Ser 119:11–23

Bailey K, Houde E (1989) Predation on eggs and larvae of marine fishes and the recruitment problem. Adv Mar Biol 25:1–83

Barth JA, Pierce SD, Smith RL (2000) A separating coastal upwelling jet at Cape Blanco, Oregon and its connection to the California Current System. Deep Sea Res Part II Top Stud Oceanogr 47:783–810

Baumann H, Pepin P, Davidson FJ., Mowbray F, Schnack D, Dower JF (2003) Reconstruction of environmental histories to investigate patterns of larval radiated shanny (*Ulvaria subbifurcata*) growth and selective survival in a large bay of Newfoundland. ICES J Mar Sci 60:243–258

Baumgartner T, Soutar A, Ferreira-Bartina V (1992) Reconstruction of the history of Pacific sardine and northern anchovy populations over the past two millennia from sediments of Santa Barbara Basin, California. CalCOFI Reports 33:24–40

Baxter JL (1966) Summary of biological information on the northern anchovy *Engraulis mordax* Girard. CalCOFI Rep 11:110–116

Berner L (1959) The food of the larvae of the northern anchovy, *Engraulis mordax*. Inter-American Trop Tuna Com Bull 4:1–22

Bjorkstedt E, Rosenfeld L, Grantham B, Shkedy Y, Roughgarden J (2002) Distributions of larval rockfishes *Sebastes* spp. across nearshore fronts in a coastal upwelling region. Mar Ecol Prog Ser 242:215–228

Briseño-Avena C, Schmid M, Swieca K, Sponaugle S, Brodeur R, Cowen R (2020) Three-dimensional cross-shelf zooplankton distributions off the Central Oregon Coast during anomalous oceanographic conditions. Prog Oceanogr 188:102436

Brodeur RD, Auth TD, Phillips A (2019) Major shifts in pelagic micronekton and macrozooplankton community structure in an upwelling ecosystem related to an unprecedented marine heatwave. Front Mar Sci 6:212

Brodeur RD, Fisher JP, Emmett RL, Morgan CA, Casillas E (2005) Species composition and community structure of pelagic nekton off Oregon and Washington under variable oceanographic conditions. Mar Ecol Prog Ser 298:41–57

Brodeur RD, Gadomski DM, Pearcy WG, Batchelder HP, Miller CB (1985) Abundance and distribution of ichthyoplankton in the upwelling zone off Oregon during anomalous El Nino conditions. Estuar Coast Shelf Sci 21:365–378

Brothers EB, Mathews CP, Lasker R (1976) Daily growth increments in otoliths from larval and adult fishes. Fish Bull 74:1–8

Butler JL (1989) Growth during the larval and juvenile stages of the northern anchovy, *Engraulis mordax*, in the California Current during 1980-84. Fish Bull 87:645–652

Castelao RM, Barth JA, Mavor TP (2005) Flow-topography interactions in the northern California Current System observed from geostationary satellite data. Geophys Res Lett 32:1–4

Chavez F, Ryan J, Lluch-Cota S, Niquen M (2003) From anchovies to sardines and back: multidecadal change in the Pacific Ocean. Science 299:217–221

Checkley DM, Dotson RC, Griffith DA (2000) Continuous, underway sampling of eggs of Pacific sardine (*Sardinops sagax*) and northern anchovy (*Engraulis mordax*) in spring 1996 and 1997 off southern and central California. Deep Sea Res Part II Top Stud Oceanogr 47:1139–1155

Checkley Jr. DM, Barth JA (2009) Patterns and processes in the California Current System. Prog Oceanogr 83:49–64

Cowen RK, Guigand CM (2008) *In situ* ichthyoplankton imaging system (ISIIS): system design and preliminary results. Limnol Oceanogr Methods 6:126–132

Cury P, Bakun A, M Crawford RJ, Jarre A, Quiñ ones RA, Shannon LJ, Verheye HM (2000) Small pelagics in upwelling systems: patterns of interaction and structural changes in 'wasp-waist' ecosystems. ICES J Mar Sci 57:603–618

Cury P, Roy C (1989) Optimal environmental window and pelagic fish recruitment success in upwelling areas. Can J Fish Aquat Sci 46:670–680

Dower J, Pepin P, Kim G (2008) Covariation in feeding success, size-at-age and growth in larval radiated shanny (*Ulvaria subbifurcata*): Insights based on individuals. J Plankton Res 31:235–247

Emmett RL, Brodeur RD, Miller TW, Pool SS, Krutzikowsky GK, Bentley PJ, McCrae J (2005) Pacific sardine (*Sardinops sagax*) abundance, distribution, and ecological relationships in the Pacific Northwest. CalCOFI Rep 46:122–143

Feigenbaum D, Maris R (1984) Feeding in the chaetognatha. Oceanogr Mar Biol Annu Rev 22:343–392

Folkvord A, Hunter J (1986) Size specific vulnerability of northern anchovy (*Engraulis mordax*) larvae to predation by fishes. Fish Bull US 84:859–869

Gentemann CL, Fewings MR, García-Reyes M (2017) Satellite sea surface temperatures along the West Coast of the United States during the 2014–2016 northeast Pacific marine heat wave. Geophys Res Lett 44:312–319

Glaser SM (2011) Do albacore exert top-down pressure on northern anchovy? Estimating anchovy mortality as a result of predation by juvenile north pacific albacore in the California current system. Fish Oceanogr 20:242–257

Guigand CM, Cowen RK, Llopiz JK, Richardson DE (2005) A coupled asymmetrical multiple opening closing net with environmental sampling system. Mar Technol Soc J 39:22–24

Hakanson J (1989) Condition of larval anchvy (*Engraulis mordax*) in the Southern California Bight, as measured through lipid analysis. Mar Biol 102:153–159

Hare JA, Cowen RK (1997) Size, growth, development, and survival of the planktonic larvae of *Pomatomus saltatrix* (Pisces: Pomatomidae). Ecology 78:2415–2431

Hooff RC, Peterson WT (2006) Copepod biodiversity as an indicator of changes in ocean and climate conditions of the northern California current ecosystem. Limnol Oceanogr 51:2607–2620

Houde E (1987) Fish early life dynamics and recruitment variability. Am Fish Soc Symp 2:17–29

Houde ED (2008) Emerging from Hjort's shadow. Fish Sci J Northw Atl Fish Sci 41:53–70

Hunter JR (1972) Swimming and feeding behavior of larval anchovy *Engraulis mordax*. Fish Bull 70:821–838

Hunter J, Kimbrell C (1980) Egg cannibalism in the northern anchovy, *Engraulis mordax*. Fish Bull US 78:811–816

Jackson JM, Lenz PH (2016) Predator-prey interactions in the plankton: larval fish feeding on evasive copepods. Nat Publ Gr

Kahru M, Jacox MG, Ohman MD (2018) CCE1: Decrease in the frequency of oceanic fronts and surface chlorophyll concentration in the California Current System during the 2014–2016 northeast Pacific warm anomalies. Deep Sea Res Part I Oceanogr Res Pap 140:4–13

Kelley D, Richards C (2021) gsw. R package version 1.0-6.

Koehn LE, Essington TE, Marshall KN, Kaplan IC, Sydeman WJ, Szoboszlai AI, Thayer JA (2016) Developing a high taxonomic resolution food web model to assess the functional role of forage fish in the California Current ecosystem. Ecol Modell 335:87–100

Lamb J, Peterson W (2005) Ecological zonation of zooplankton in the COAST study region off central Oregon in June and August 2001 with consideration of retention mechanisms. J Geophys Res 110:C10S15

Lasker R (1975) Field criteria for survival of anchovy larvae: the relation between inshore chlorophyll maximum layers and successful first feeding. Fish Bull US 73:453–462

Lasker R (1978) The relation between oceanographic conditions, and larval anchovy food in the California Current: Identification of factors contributing to recruitment failure. Rapp P-V Reun Cons Int Explo Mer 173:212–230

Lasker R (1981) Factors contributing to variable recruitment of the nothern anchovy (*Engraulis mordax*) in the California Current: Contrasting years,1975 through 1978. Rapp P-V Reun Cons Int Explo Mer 178:375–388

Leggett W, Deblois E (1994) Recruitment in marine fishes: is it regulated by starvation and predation in the egg and larval stages? Netherlands J Sea Res 32:119–134

Litz MN, Emmett RL, Heppell SS, Brodeur RD (2008) Ecology and distribution of the Northern subpopulation of Northern anchovy (*Engraulis mordax*) off the U.S. West Coast. CalCOFI Rep 49:167–182

Llopiz JK (2013) Latitudinal and taxonomic patterns in the feeding ecologies of fish larvae: a literature synthesis. J Mar Syst 109–110:69–77

Lluch-Belda D, Crawford R, Kawasaki T, Maccall A, Parrish R, Schwartzlose R, Smith P (1989) World-wide fluctuations of sardine and anchovy stocks: the regime problem. South African J Mar Sci 8:195–205

Logerwell E., Mantua N, Lawson P, Francis R, Agostini V (2003) Tracking environmental processes in the coastal zone for understanding and predicting Oregon coho (*Oncorhynchus kisutch*) marine survival. Fish Oceanogr 12:554–568

Luo JY, Grassian B, Tang D, Irisson J-O, Greer AT, Guigand CM, McClatchie S, Cowen RK (2014) Environmental drivers of the fine-scale distribution of a gelatinous zooplankton community across a mesoscale front. Mar Ecol Prog Ser 510:129–149

Luo JY, Irisson J-O, Graham B, Guigand C, Sarafraz A, Mader C, Cowen RK (2018) Automated plankton image analysis using convolutional neural networks. Limnol Oceanogr Methods 16:814–827

McClatchie S, Cowen R, Nieto K, Greer A, Luo JY, Guigand C, Demer D, Griffith D, Rudnick D (2012) Resolution of fine biological structure including small narcomedusae across a front in the Southern California Bight. J Geophys Res Ocean 117:1–18

Methot RD (1981) Spatial covariation of daily grow th rates of larval northern anchovy, *Engraulis mordax*, and larval northern lampfish, *Stenobrachius leucopsarus*. Rapp Proces-verbaux des Réunions Cons Int pour l'Éxploration la Mer 178:424–431

Methot RD, Kramer D (1979) Growth of northern anchovy, *Engraulis mordax*, larvae in the sea. Fish Bull 77:413–423

Miller T, Crowder L, Rice J, Marschall E (1988) Larval size and recruitment mechanisms in fishes: toward a conceptual framework. Can J Fish Aquat Sci 45:1657–1670

Miller JA, Shanks AL (2004) Ocean-estuary coupling in the Oregon upwelling region: abundance and transport of juvenile fish and of crab megalopae. Mar Ecol Prog Ser 271:267–279

Morgan CA, Peterson WT, Emmett RL (2003) Onshore-offshore variations in copepod community structure off the Oregon coast during the summer upwelling season. Mar Ecol Prog Ser 249:223–236

Morote E, Olivar MP, Villate F, Uriarte I (2010) A comparison of anchovy (*Engraulis encrasicolus*) and sardine (*Sardina pilchardus*) larvae feeding in the Northwest Mediterranean: influence of prey availability and ontogeny. ICES J Mar Sci 67:897–908

Moser H (1996) The early life stages of fishes in the California Current Region, California Cooperative Oceanic Fisheries Investigations Atlas No. 33 (CALCOFI). Sponsored by the United States Department of Commerce National Oceanic and Atmospheric Administration National Marine Fisheries Service Southwest Fisheries Science Center

Muhling BA, Brodie S, Smith JA, Tommasi D, Gaitan CF, Hazen EL, Jacox MG, Auth TD, Brodeur RD (2020) Predictability of species distributions deteriorates under novel environmental conditions in the California Current System. Front Mar Sci 7:589

Parnel MM, Emmett RL, Brodeur RD (2008) Ichthyoplankton community in the Columbia River plume off Oregon: effects of fluctuating oceanographic conditions. Fish Bull 106:161–173

Parrish RH, Nelson CS, Bakun A (1981) Transport mechanisms and reproductive success of fishes in the California Current. Biol Oceanogr 1:175–203

Pepin P, Robert D, Bouchard C, Dower JF, Falardeau M, Fortier L, Jenkins GP, Leclerc V, Levesque K, Llopiz JK, Meekan MG, Murphy HM, Ringuette M, Sirois P,

Sponaugle S (2015) Once upon a larva: revisiting the relationship between feeding success and growth in fish larvae. ICES J Mar Sci 72:359–373
Peterson WT, Fisher JL, Peterson JO, Morgan CA, Burke BJ, Fresh KL (2014) Applied fisheries oceanography: ecosystem indicators of ocean conditions inform fisheries management in the california current. Oceanography 27:80–89
Peterson WT, Miller CB (1977) Seasonal cycle of zooplankton abundance and species composition along the central Oregon coast. Fish Bull 75:717–724
Peterson WT, Schwing FB (2003) A new climate regime in northeast pacific ecosystems. Geophys Res Lett 30:1–4
Purcell JE (1985) Predation on fish eggs and larvae by pelagic cnidarians and ctenophores. Bull Mar Sci 37:739–755
Purcell JE, Arai MN (2001) Interactions of pelagic cnidarians and ctenophores with fish: a review. Hydrobiologia 451:27–44
Purcell JE, Grover JJ (1990) Predation and food limitation as causes of mortality in larval herring at a spawning ground in British Columbia. Mar Ecol Prog Ser 59:55–61
Purcell J, Nemazie D, Dorsey S, Houde E, Gamble J (1994) Predation mortality of bay anchovy *Anchoa mitchilli* eggs and larvae due to scyphomedusae and ctenophores in Chesapeake Bay. Mar Ecol Prog Ser 114:47–58
Richardson SL (1973) Abundance and distribution of larval fishes in waters off Oregon, May - October 1969, with special emphasis on the northern anchovy, *Engraulis mordax*. Fish Bull 71:697–711
Richardson SL (1981) Spawning biomass and early life of northern anchovy, *Engraulis mordax*, in the northern subpopulation off Oregon and Washington. Fish Bull 78:855–876
Robert D, Castonguay M, Fortier L (2009) Effects of preferred prey density and temperature on feeding success and recent growth in larval mackerel of the southern Gulf of St. Lawrence. Mar Ecol Prog Ser 377:227–237
Robert D, Pepin P, Dower J, Fortier L (2014) Individual growth history of larval Atlantic mackerel is reflected in daily condition indices. ICES J Mar Sci 71:1001–1009
Roy C, Cury P, Kifani S (1992) Pelagic fish recruitment success and reproductive strategy in upwelling areas: environmental compromises. South African J Mar Sci 12:135–146
Sato M, Barth JA, Benoit-Bird KJ, Pierce SD, Cowles TJ, Brodeur RD, Peterson WT (2018) Coastal upwelling fronts as a boundary for planktivorous fish distributions. Mar Ecol Prog Ser 595:171–186
Schmid MS, Cowen RK, Robinson K, Luo JY, Briseño-Avena C, Sponaugle S (2020) Prey and predator overlap at the edge of a mesoscale eddy: fine-scale, in-situ distributions to inform our understanding of oceanographic processes. Sci Rep 10:921
Schmid MS, Daprano D, Jacobson KM, Sullivan C, Briseño-Avena C, Luo JY, Cowen RK (2021) A Convolutional Neural Network based high-throughput image classification pipeline - code and documentation to process plankton underwater imagery using local HPC infrastructure and NSF's XSEDE. Zenodo
Schwartzlose RA, Alheit J, Bakun A, Baumgartner TR, Cloete R, Crawford RJM, Fletcher WJ, Green-Ruiz Y, Hagen E, Kawasaki T, Lluch-Belda D, Lluch-Cota SE, Maccall AD, Matsuura Y, Nevárez-Martínez MO, Parrish RH, Roy C, Serra R,

Shust K V, Ward MN, Zuzunaga JZ (1999) Worldwide large-scale fluctuations of sardine and anchovy populations. South African J Mar Sci 21:289–347

Scura E, Jerde C (1977) Various species of phytoplankton as food for larval northern anchovy, *Engraulis mordax*, and relative nutritional value of the dinoflagellates *Gymnodinium splendens* and *Gonyaulax polyedra*. Fish Bull 75:577–583

Spitz Y, Allen J (2005) Modeling of ecosystem processes on the Oregon shelf during the 2001 summer upwelling. J Geophys Res 110:C10S17

Sponaugle S, Boulay J, Rankin T (2011) Growth- and size-selective mortality in pelagic -larvae of a common reef fish. Aquat Biol 13:263–273

Sponaugle S, Llopiz JK, Havel LN, Rankin TL (2009) Spatial variation in larval growth and gut fullness in a coral reef fish. Mar Ecol Prog Ser 383:239–249

Sponaugle S, Walter KD, Denit KL, Llopiz JK, Cowen RK (2010) Variation in pelagic larval growth of Atlantic billfishes: the role of prey composition and selective mortality. Mar Biol 157:839–849

Swieca K, Sponaugle S, Briseño-Avena C, Schmid M, Brodeur R, Cowen R (2020) Changing with the tides: fine-scale larval fish prey availability and predation pressure near a tidally modulated river plume. Mar Ecol Prog Ser 650:217–238

Swieca K, Sponaugle S, Schmid M, Cowen R (*in prep*) Shedding light on lanternfish: growth and diet of a larval myctophid across dinstinct upwelling regimes in the California Current

Sydeman WJ, Dedman S, García-Reyes M, Thompson SA, Thayer JA, Bakun A, MacCall AD (2020) Sixty-five years of northern anchovy population studies in the southern California Current: a review and suggestion for sensible management. ICES J Mar Sci 77:486–499

Takahashi M, Checkley Jr. DM, Litz MN, Brodeur RD, Peterson WT (2012) Responses in growth rate of larval northern anchovy (*Engraulis mordax*) to anomalous upwelling in the northern California Current. Fish Oceanogr 21:393–404

Takasuka A, Sakai A, Aoki I (2017) Dynamics of growth-based survival mechanisms in japanese anchovy (*Engraulis japonicus*) larvae. Can J Fish Aquat Sci 74:812–823

Thompson AR, Schroeder ID, Bograd SJ, Hazen EL, Jacox MG, Leising A, Wells BK, Largier JL, Fisher JL, Jacobson KC, Zeman SM, Bjorktedt EP, Robertson RR, Kahru M, Goericke R, Peabody CE, Baumgartner T, Lavaniegos BE, Miranda LE, Gómez-Ocampo E, Gómez-Valdés J, Auth TD, Daly EA, Morgan CA, Burke JB, Field JC, Sakuma K, Weber ED, Watson W, Porquez JM, Dolliver J, Lyons DE, Orben RA, Zamon J, Warybok P, Jahncke J, Santora JA, Thompson SA, Hoover B, Sydeman WJ, Melin S (2019) State of the California current 2018-19: a novel anchovy regime and a new marine heat wave? CalCOFI Rep 60:1–65

Tomaro L, Teel D, Peterson W, Miller J (2012) When is bigger better? Early marine residence of middle and upper Columbia River spring Chinook salmon. Mar Ecol Prog Ser 452:237–252

Vrooman AM, Paloma PA, Zweifel JR (1981) Electrophoretic, morphometric, and meristic studies of subpopulations of northern anchovy, *Engraulis mordax*. Calif Fish Game 67:39–51

Wood S (2021) mgcv. R package version 1.8-38. https://cran.r project.org/web/packages/mgcv /mgcv.pdf

Zuur AF, Leno EN, Elphick CS (2010) A protocol for data exploration to avoid common

statistical problems. Methods Ecol Evol 1:3–14

Table 3.1. Northern anchovy (*Engraulis mordax*) concentration, temperature, chlorophyll *a* concentration, depth of the chlorophyll max, and concentrations of environmental prey and potential predators at three cross-shelf locations along the Newport Hydrographic Line, Oregon, in the summers of 2018 and 2019.

	2018				2019			
	All	**Inshore**	**Shelf-break**	**Offshore**	**All**	**Inshore**	**Shelf-break**	**Offshore**
Northern anchovy (ind. 1000 m^{-3})	**233.3 (±90.8)**	89.2(±48.2)	320.0 (±254.4)	389.8 (±221.9)	**32.9 (±8.5)**	9.8 (±6.3)	57.7 (±21.2)	38.8(±15.0)
Temperature (°C)	**13.0 (±0.4)**	11.2 (±0.4)	14.2 (±0.6)	14.5 (±0.4)	**12.6 (±0.4)**	11.2 (±0.8)	12.1 (±0.3)	14.1(±0.3)
Chlorophyll *a* (mg m^{-3})	**1.4 (±0.1)**	1.7 (±0.2)	1.3 (±0.2)	1.1 (±0.1)	**1.1 (±0.2)**	2.0 (±0.2)	0.7 (±0.1)	0.4 (±0.1)
Depth of chlorophyll max (m)	**10.7 (±1.6)**	5.8 (±0.7)	10.1 (±1.1)	17.8 (±2.6)	**23.8 (±2.1)**	14.1 (±2.0)	27.7 (±0.9)	31.5 (±1.5)
Prey								
Protists (ind. m^{-3})	**2323.6 (±305.1)**	1426.7 (±250.6)	3588.7 (±31.4)	2588.0 (±277.7)	**1374.0 (±369.4)**	619.0 (±245.1)	1972.9 (±1127.8)	1735.1 (±632.8)
Calanoid copepods (ind. m^{-3})	**134.5 (±16.9)**	182.9 (±3.2)	151.8 (±9.7)	77.3 (±14.1)	**85.1 (±9.9)**	117.3 (±12.7)	93.1 (±22.9)	53.0(±9.4)
Cyclopoid copepods (ind. m^{-3})	**87.7 (±6.3)**	77.6 (±2.2)	110.9 (±5.6)	86.1 (±12.6)	**69.5 (±6.6)**	89.7 (±10.2)	81.6 (±13.7)	45.9 (±3.0)
Predators								
Chaetognaths (ind. m^{-3})	**2.0 (±0.4)**	1.0 (±0.3)	1.7 (±0.0)	3.2 (±0.6)	**2.7 (±0.4)**	0.6 (±0.0)	2.7 (±0.4)	4.6 (±0.4)
Ctenophores (ind. m^{-3})	**1.2 (±0.5)**	0.2 (±0.0)	0.2 (±0.0)	2.6 (±0.6)	**1.6 (±0.1)**	1.6 (±0.2)	1.7 (±0.3)	1.6 (±0.1)
Hydromedusae (ind. m^{-3})	**1.3 (±0.5)**	0.4 (±0.0)	0.5 (±0.0)	2.6 (±0.8)	**6.5 (±1.2)**	3.1 (±0.3)	1.8 (±0.4)	11.9 (±1.0)
Siphonophores (ind. m^{-3})	**1.5 (±0.5)**	0.5 (±0.1)	0.5 (±0.0)	3.0 (±0.9)	**3.6 (±1.2)**	0.8 (±0.1)	2.5 (±0.9)	11.3 (±0.9)
Predators pooled (ind. m^{-3})	**6.0 (±1.8)**	2.0 (±0.4)	2.9 (±0.0)	11.4 (±2.9)	**16.5 (±2.8)**	6.1 (±0.3)	8.6 (±1.4)	29.4 (±2.2)

Northern anchovy larvae were sampled with a MOCNESS and all other taxa with the *In situ* Ichthyoplankton Imaging System (ISIIS). Temperature values are the mean per MOCNESS net and chlorophyll *a* concentration and depth of the chlorophyll max are derived from CTD

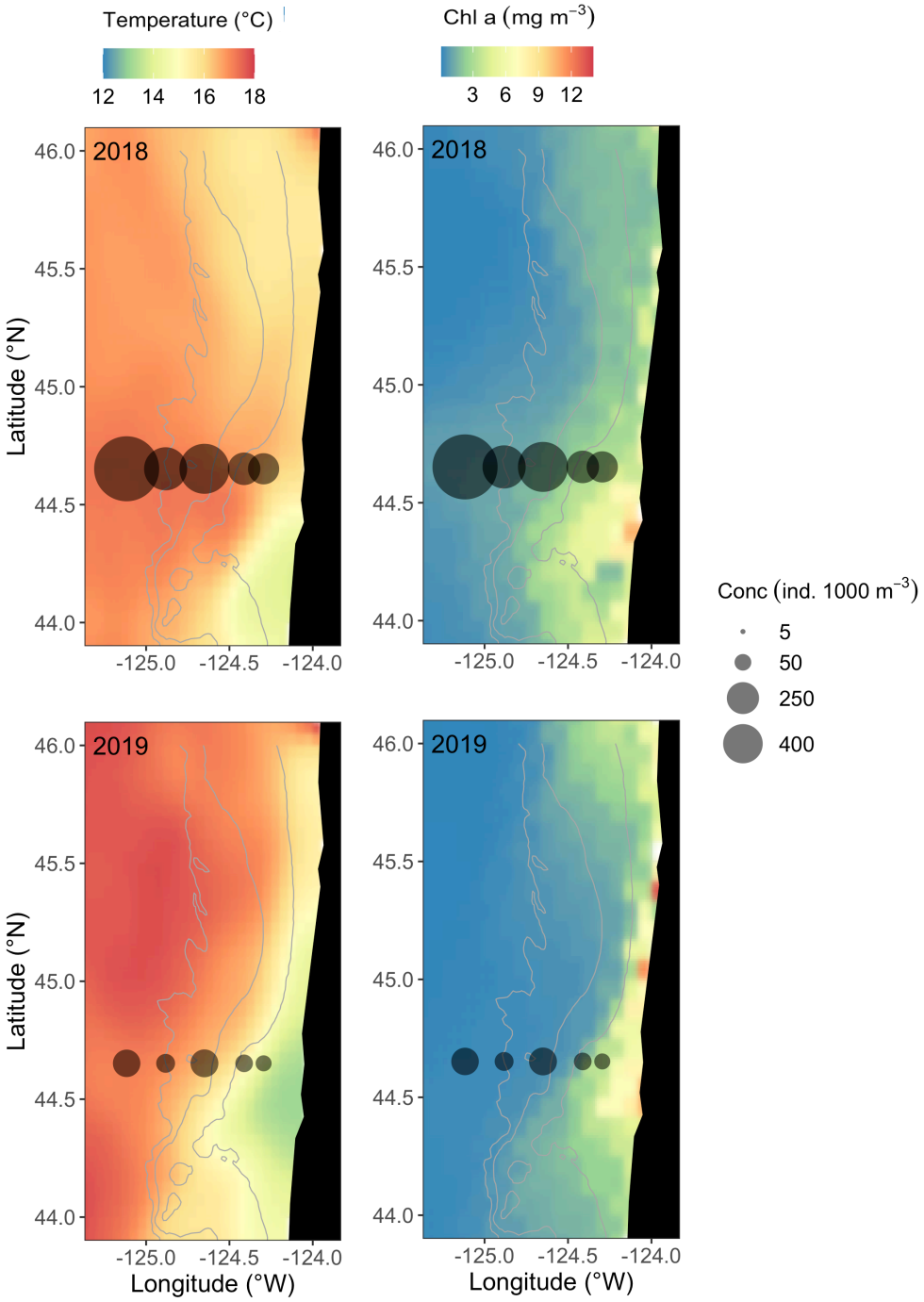

Fig. 3.1. Mean concentration of northern anchovy (*Engraulis mordax*) larvae (individuals 1000 m $^{-3}$) in the top 50 m of the water column sampled along the Newport Hydrographic Line during the summers of 2018 (Jul 3-11) and 2019 (Jul 16-25). Data are overlaid on satellite derived sea surface temperature (left) and chlorophyll (chl) *a* concentration (right). Contour lines represent the 100-, 200-, and 500-m isobaths

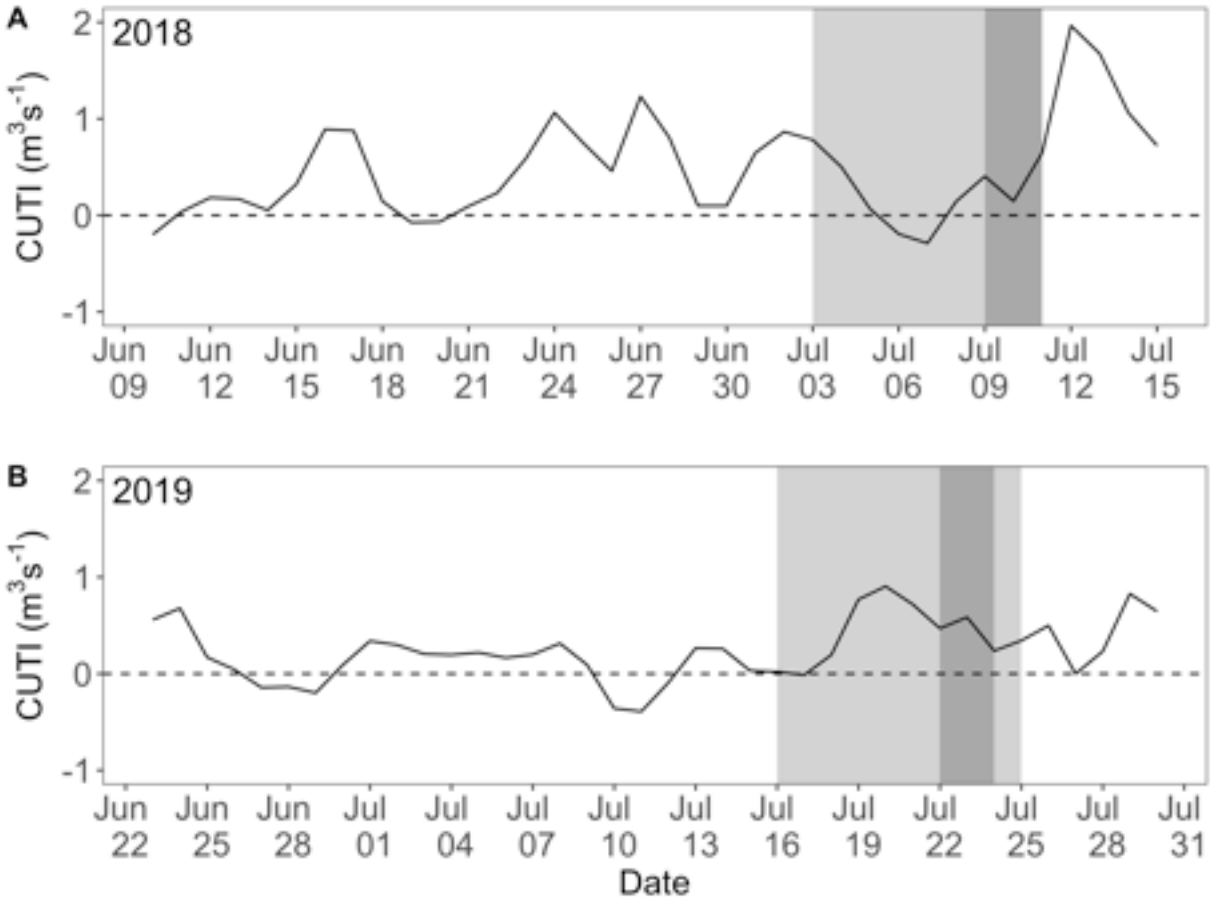

Fig. 3.2. Daily Coastal Upwelling Transport Index (CUTI) for the Newport Hydrographic Line (45° N) prior to and during sampling in the summers of (A) 2018 and (B) 2019, with cruise dates highlighted in light gray and days northern anchovy (*Engraulis mordax*) were collected for otolith analysis in dark gray. Positive values signify upwelling, zero are neutral conditions, and negative values are downwelling.

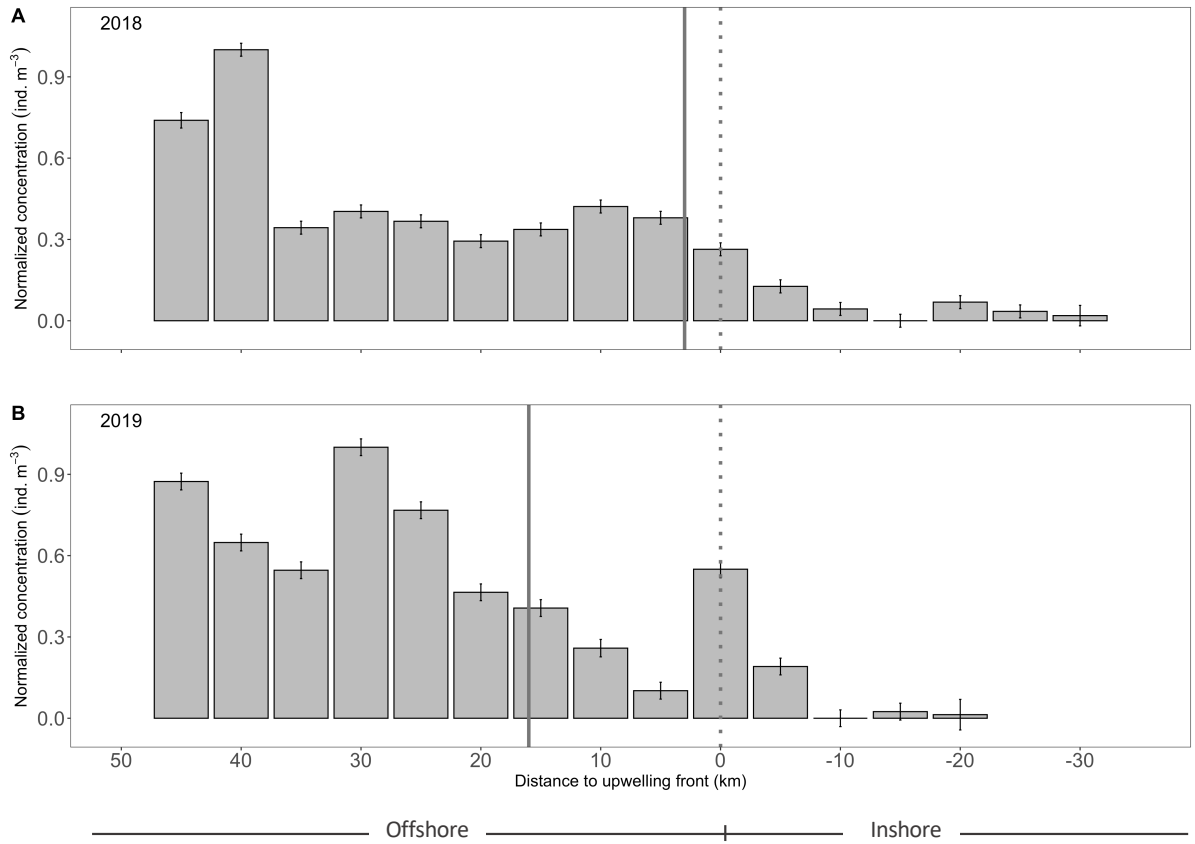

Fig. 3.3. Mean (± SE) concentration of northern anchovy (*Engraulis mordax*) larvae relative to the upwelling front along the Newport Hydrographic Line in the summers of (A) 2018 and (B) 2019. Data were normalized to the maximum value each year. Solid vertical line denotes the location of the continental shelf-break and the dotted vertical line denotes the position of the upwelling front.

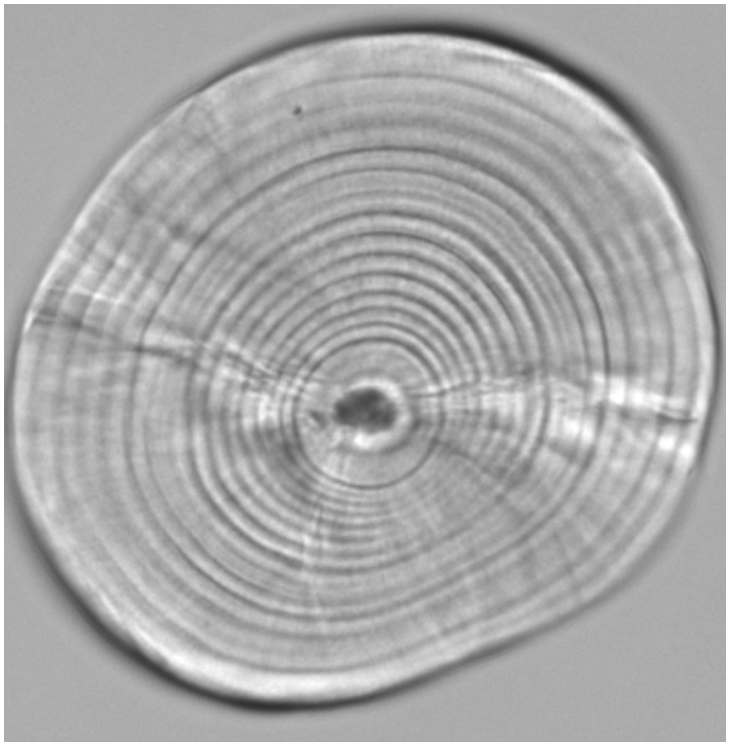

Fig. 3.4. Larval northern anchovy (*Engraulis mordax*) sagittal otolith under 400x oil immersion magnification.

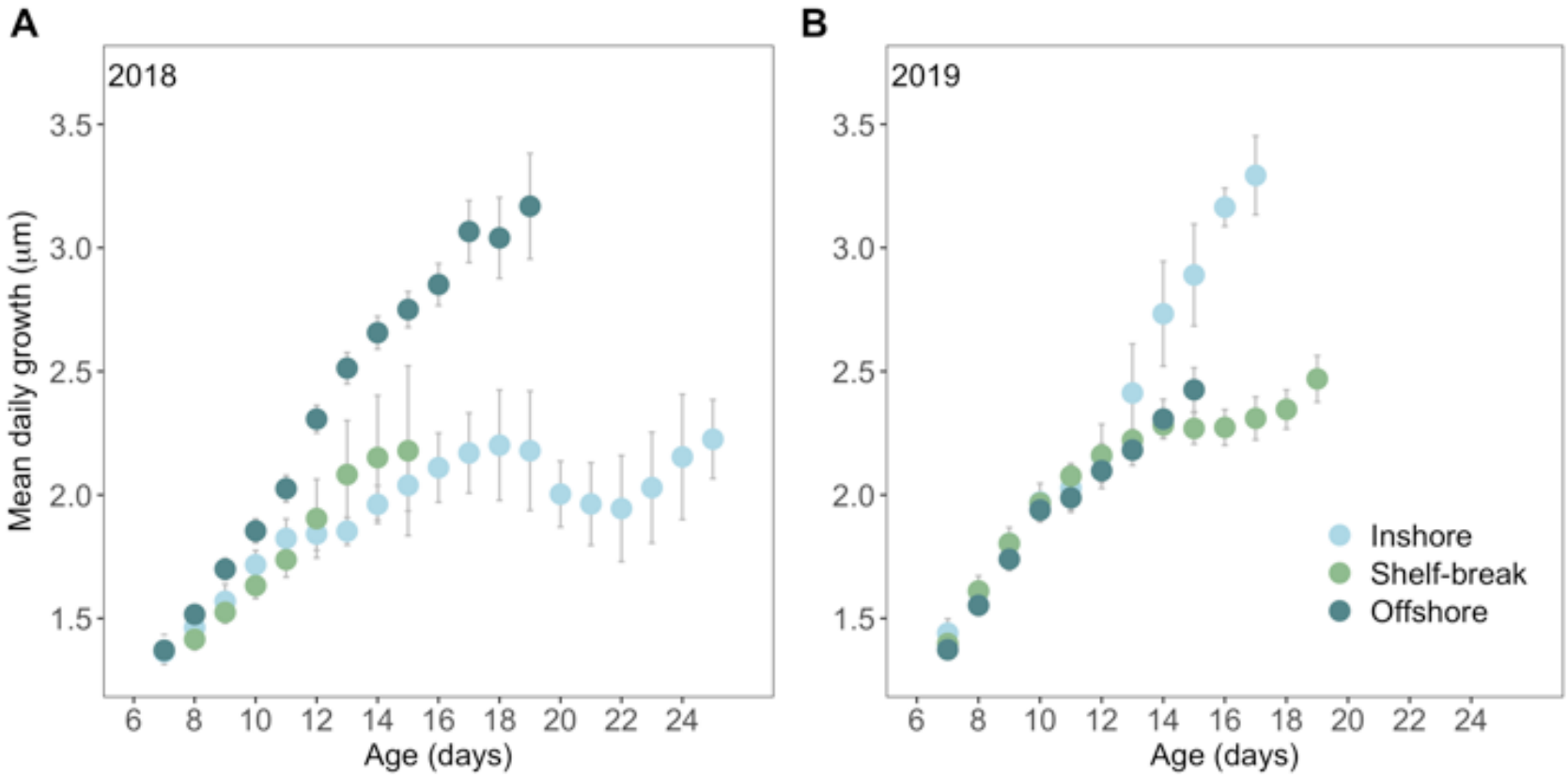

Fig. 3.5. Mean (± SE) daily growth (otolith increment width) of northern anchovy (*Engraulis mordax*) collected along the Newport Hydrographic Line in the summers of (A) 2018 and (B) 2019 at three cross-shelf locations. Ages were truncated when n < 3 observations.

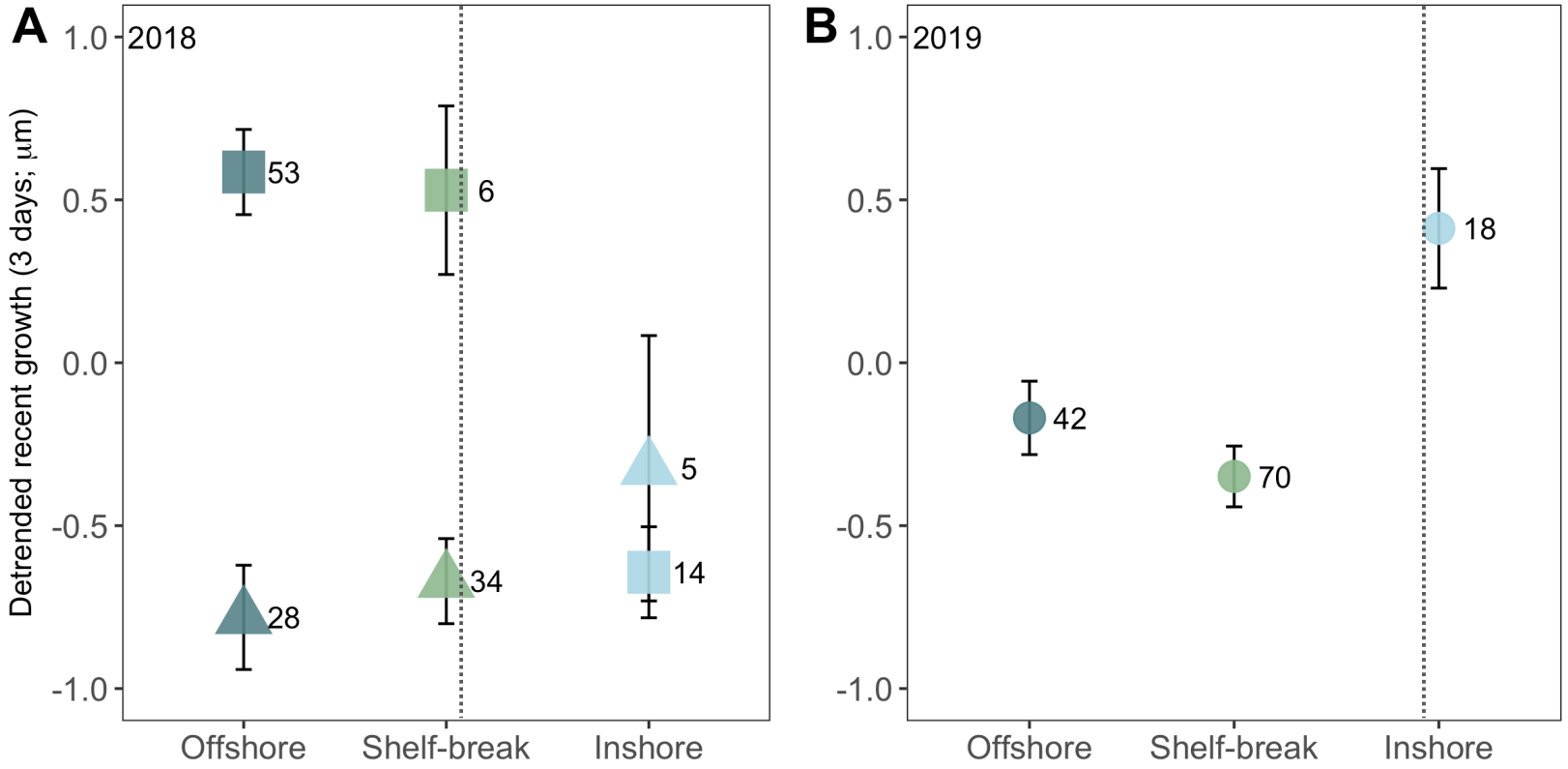

Fig. 3.6. Mean (± SE) detrended growth during the last three complete days of life (mean recent growth; MRG) of northern anchovy (*Engraulis mordax*) collected along the Newport Hydrographic Line in the summers of (A) 2018 and (B) 2019 at three cross-shelf locations. The dotted line denotes the general position of the upwelling front. Circles are comparisons with all ages included; squares, old (≥ 14 d) age group only; and triangles, young (< 14 d) age group only. Samples size indicated to the right of each data point.

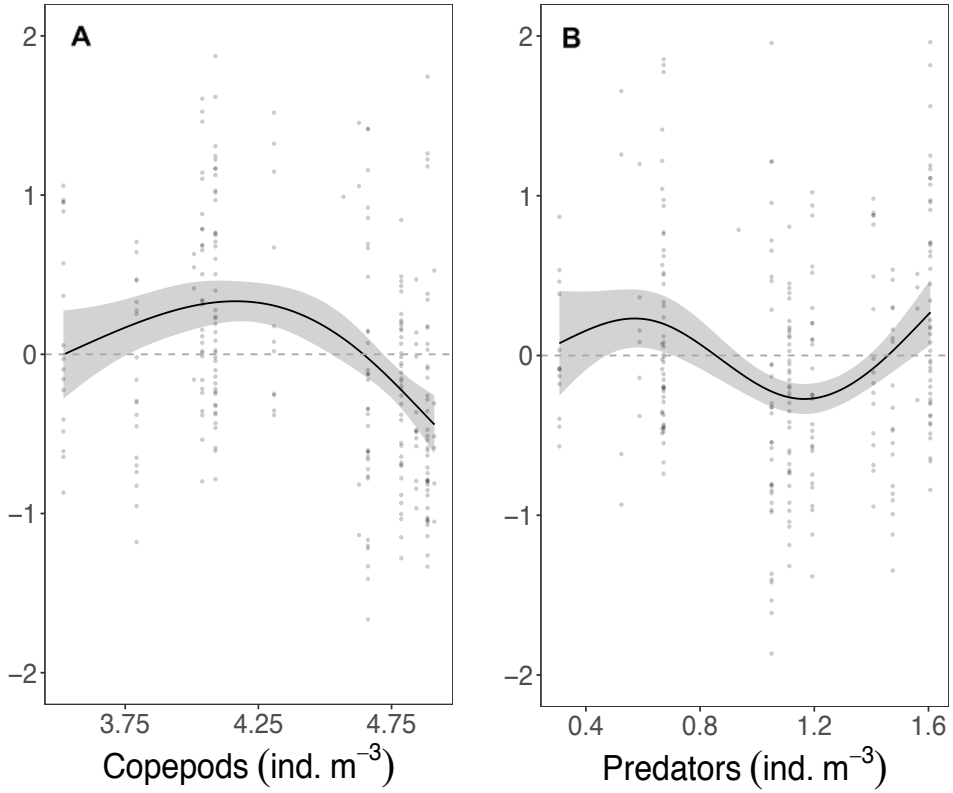

Fig. 3.7. GAM smooth functions showing the partial effects of each covariate after accounting for the other covariate effects on the mean recent growth (MRG; last three complete days) of individual larval northern anchovy (*Engraulis mordax*; n= 270). Copepod (calanoid and cyclopoid) and potential predator (chaetognaths, ctenophores) concentrations are log+1 transformed. 95% confidence intervals (gray shading) and partial residuals (points) are shown for each covariate. Model deviance explained = 39.9%

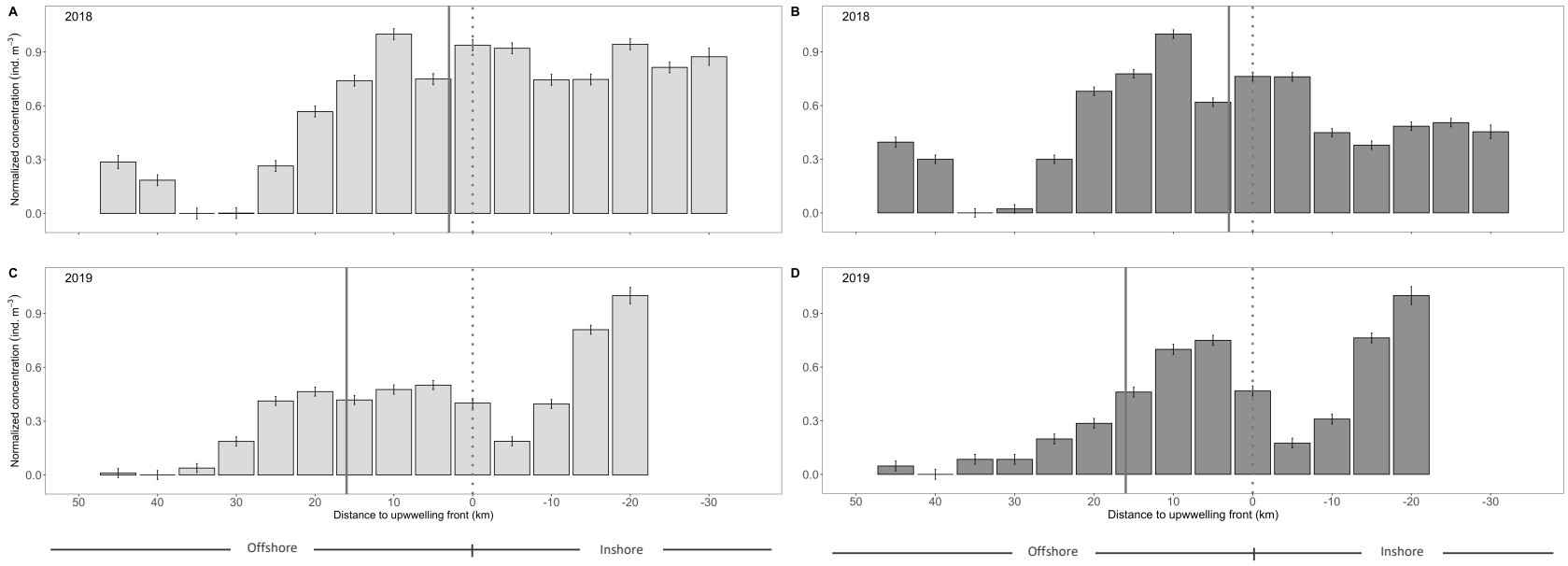

Fig. 3.8. Mean (± SE) concentration of (A,C) calanoid copepods and (B, D) cyclopoid copepods relative to the upwelling front along the Newport Hydrographic Line in the summers of (A,B) 2018 and (C,D) 2019. Data are normalized to the maximum value each year. Solid vertical line denotes the location of the continental shelf-break and the dotted vertical line denotes the position of the upwelling front

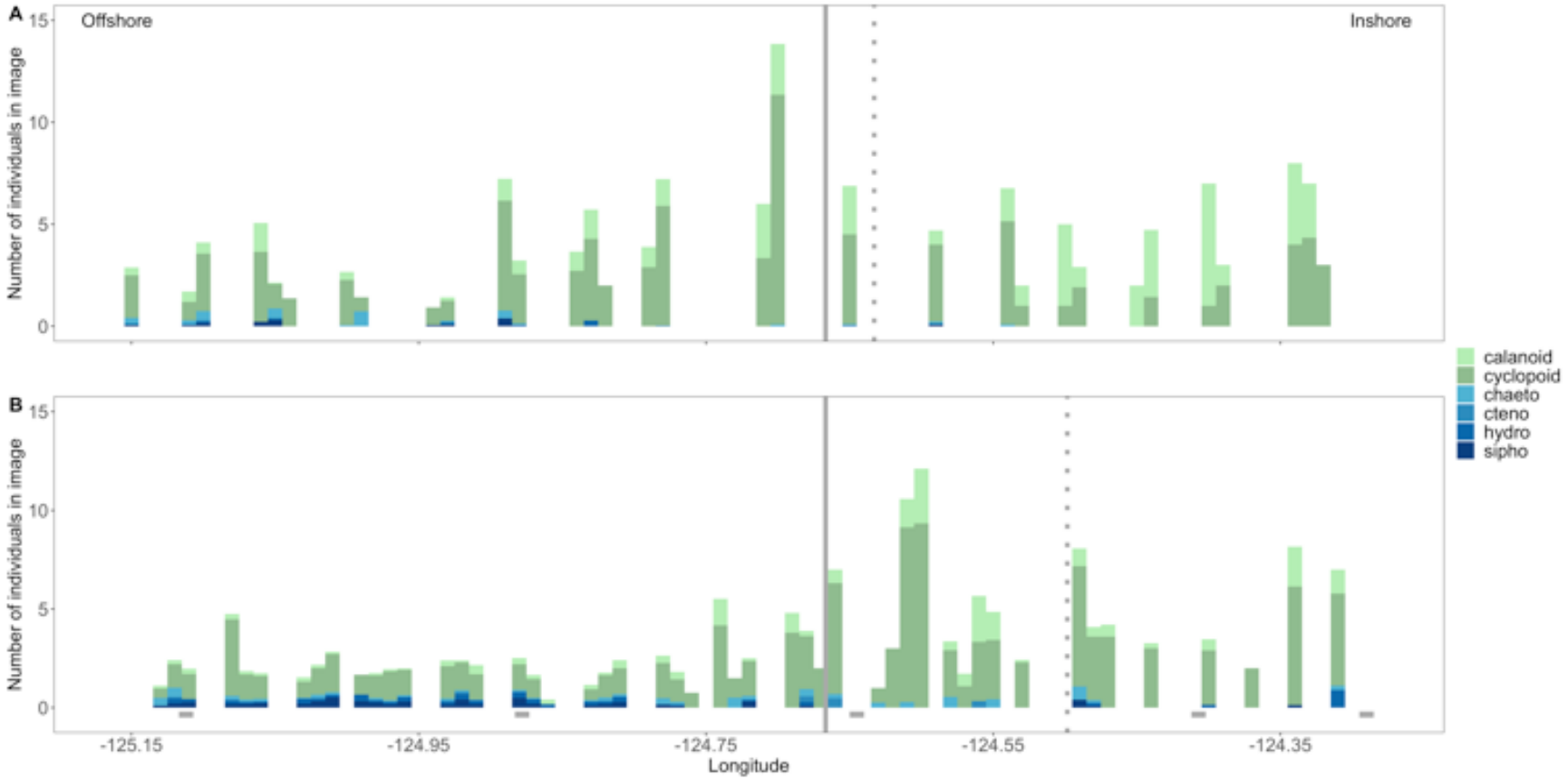

Fig. 3.9. Mean number of zooplankton by taxonomic group found in a plankton imagery frame (13 x 13 x 50 cm) with a northern anchovy (*Engraulis mordax*) larva along the Newport Hydrographic line in the summers of 2018 (A) and 2019 (B). Potential zooplankton prey groups are coded in greens and predators in blues. Solid vertical line denotes the location of the continental shelf-break, the dotted vertical line denotes the position of the upwelling front during sampling each year, and grey squares along the x-axis in (B) mark the locations of biological sampling stations. Calanoid = calanoid copepods, cyclopoid = cyclopoid copepods, chaeto = chaetognaths, cteno = ctenophores, hydro = hydromedusae, sipho = siphonophores

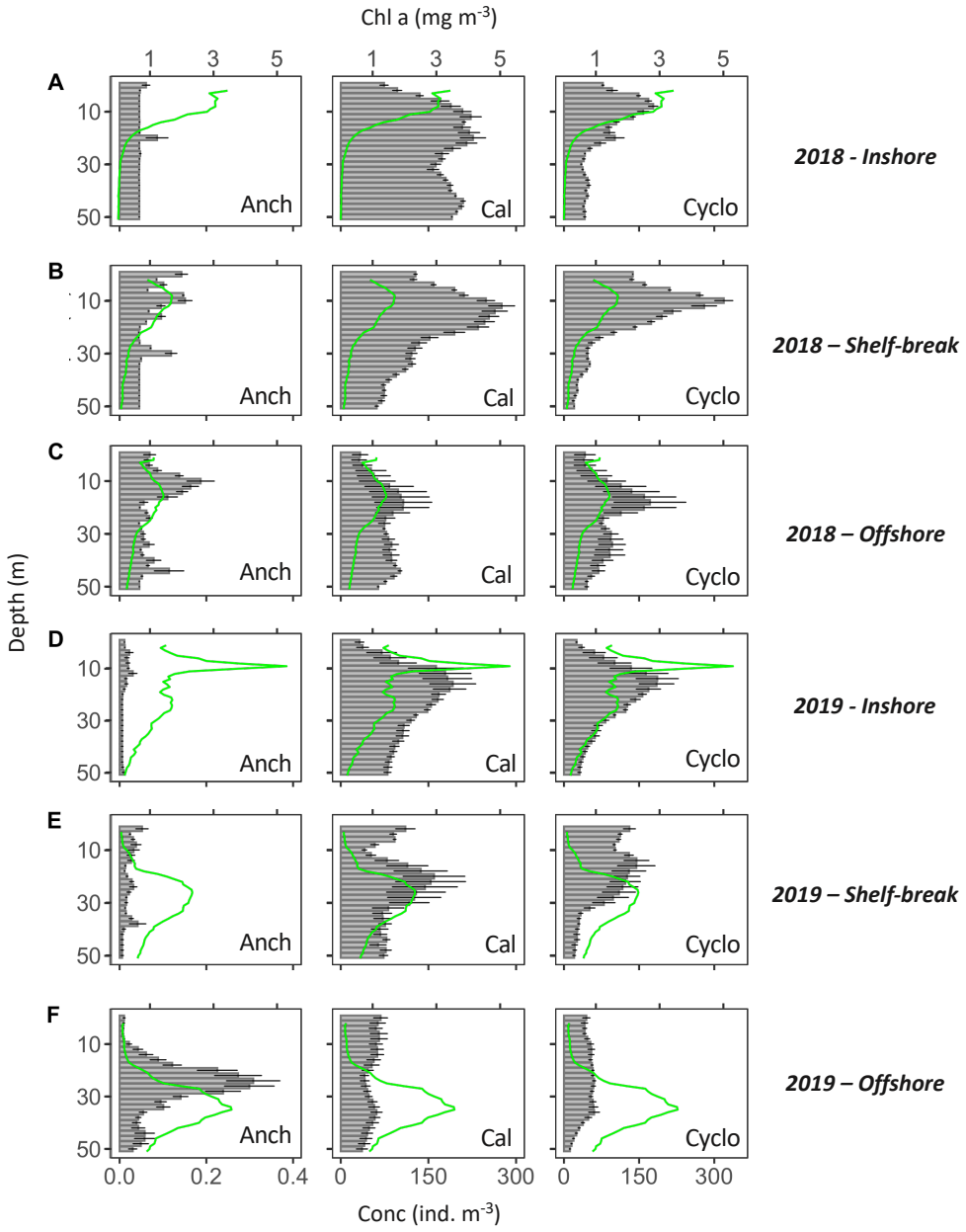

Fig. 3.10. Mean concentration (± SE) of northern anchovy (*Engraulis mordax*) larvae (Anch), calanoid copepods (Cal), and cyclopoid copepods (Cyclo) in each 2-m depth bin down to 50-m depth during sampling in 2018 (A - C) and 2019 (D - F) inshore (A, D), at the shelf-break (B,E), and offshore (C, F). Mean chlorophyll a profiles are overlaid for each sampling event

Changing with the tides: fine-scale larval fish prey availability and predation pressure near a tidally modulated river plume

Kelsey Swieca, Su Sponaugle, Christian Briseño-Avena, Moritz S. Schmid, Richard D. Brodeur, Robert K. Cowen

Marine Ecology Progress Series
Nordbuente 23, Oldendorf/Luhe, Germany 21385
Available online: https://doi.org/10.3354/meps13367

CHAPTER 4: Changing with the tides: fine-scale larval fish prey availability and predation pressure near a tidally modulated river plume

Abstract

Tidally controlled river plumes form distinct frontal boundaries that can alter the spatial distributions of larval fishes and their planktonic prey and predators. Variable in nature, they may expose larval fishes to different trophic environments over small spatio-temporal scales, with unknown consequences for survival and recruitment. In the northern California Current, the Columbia River Plume is strongly influenced by twice-daily freshwater injections that create a highly dynamic coastal environment. Using the *In situ* Ichthyoplankton Imaging System, we examined changes in the fine-scale horizontal and vertical distributions of larval fishes, their prey, and their predators over space and time (ebb/flood tide). In total, 6095 fish larvae and ~1.5 million prey/predator zooplankton were imaged and measured. Plume regions provided substantially higher concentrations of prey and enhanced spatial overlap between larval fishes and their prey relative to oceanic waters. The functionality of river plumes as a refuge from predators was less clear. Predator concentrations were also higher in plume regions, but overlap with larval fishes was taxon-specific and varied with the tide. Notably, regions of high zooplankton concentrations did not necessarily confer high spatial overlap on small scales (meters vertical, kms horizontal) relevant to trophic interactions. Surface salinity and chlorophyll *a* were the most important factors influencing the spatial overlap of zooplankton with larval fishes. In the vicinity of river plumes, larval fishes experience a diversity of unique prey and predator fields over short spatio-temporal scales, which likely contribute to variable growth and mortality patterns at much finer scales than previously thought.

1. INTRODUCTION

Growth, survival, and recruitment of the critical early life stages of fishes is contingent upon their ability to find food and avoid predation in a physically and biologically heterogeneous environment (Bailey & Houde 1989, Houde 2008). Consequently, the spatio-temporal distributions of prey and predator zooplankton taxa can significantly influence fish population dynamics. Spatial variability in plankton distributions is often attributed to physical gradients in density, temperature, and/or salinity that vary over a wide range of spatial and temporal scales (Graham et al. 2001, Benoit-Bird & McManus 2012, Acha et al. 2015). When abrupt, these gradients can concentrate zooplankton and larval fishes (Grimes & Finucane 1991, Morgan et al. 2005, Munk 2007), creating regions of intensified biological interaction that may disproportionately affect larval fish survival.

Physical features that aggregate prey resources are thought to allow larval fishes to grow quickly and increase survival through their most vulnerable life stages (Lasker 1975). High prey availability typically leads to high feeding success, fast growth, and large size-at-age of larvae (Sponaugle et al. 2009, Pepin et al. 2015). Consequently, oceanographic features that concentrate plankton may lead to heightened recruitment success (Lasker 1975, Shulzitski et al. 2015, 2016). However, this may not always be the case, as the same features that aggregate prey and enhance larval fish feeding also typically concentrate known larval fish predators, especially gelatinous zooplankton (Purcell & Arai 2001, Bakun 2006, McClatchie et al. 2012, Luo et al. 2014). The potentially confounding effects of increased predator abundances are not well understood, due, in part, to the difficulty of sampling fragile gelatinous taxa with traditional net-based techniques. Detailed studies on the fine-scale spatial distributions of larval fishes, their prey, and their predators are needed to understand the mechanisms of larval success and relationships to physical processes.

In many coastal ecosystems, riverine discharge into the ocean creates a shallow, low-salinity, high-turbidity plume that is marked by sharp physical gradients at the plume fronts. Characterized by density discontinuities and hydrodynamic convergence, plume fronts have been shown to aggregate phyto-, zoo-, and ichthyoplankton in a variety of systems including the Gulf of Mexico (Grimes & Finucane 1991, Govoni 1997),

Chesapeake Bay (Reiss & McConaugha 1999, Roman et al. 2005), the Gulf of Ancud (Castro et al. 2011), the Sea of Japan (Watanabe et al. 2014), and the Columbia River in the northern California Current (NCC; Morgan et al. 2005, Peterson & Peterson 2008). River plumes are important habitats for larval fishes, and several studies have demonstrated increased encounter rates leading to higher feeding success in larval fish associated with a plume compared to their non-plume-associated conspecifics (e.g. Govoni & Chester 1990, Govoni 1997, Lochmann et al. 1997). Through the accumulation and retention of zooplankton, the location of plume fronts may play an important role in fish population dynamics.

While plume fronts can alter the spatial distributions of zooplankton and are suspected to influence larval fish survival, they are highly variable and often ephemeral in nature. This is particularly true for tidally modulated river plumes where once- or twice-daily freshwater injections modify the strength and location of plume fronts (Acha et al. 2015). One such plume is the Columbia River Plume (CRP) in the NCC. The NCC is oceanographically complex and characterized by dynamic wind-driven upwelling and downwelling processes that support a dense planktonic community (Peterson & Miller 1975). Within the NCC, the Oregon–Washington coastal ecosystem is further complicated by significant freshwater inputs from the second largest runoff river in the USA, the Columbia River (Federal Columbia River Power System; https://www.bpa.gov/news/pubs/GeneralPublications/edu-The-Federal-Columbia-River-Power-System-Inside-Story.pdf). Here, riverine outflow is modulated by large tides that create a plume that varies in volume from 2 to 11 × 10^{10} m^3 (Hickey et al. 1998), is typically on the order of 20 m deep (Bowman 1988), and can extend hundreds of kilometers beyond the continental shelf (García Berdeal et al. 2002, Hickey et al. 2005). The plume region within 50 km of the river mouth is particularly dynamic and varies over small spatial and temporal scales as a result of twice-daily tidal pulses that modify the plume structure (Horner-Devine et al. 2009). At peak ebb tide, the outflow velocity can exceed 3 m s^{-1}, creating strong frontal gradients that have been shown to transport zooplankton off the continental shelf at a rate 5 times faster than typical wind-driven transport (Horner-Devine et al. 2009, Peterson & Peterson 2009). During coastal

upwelling events, the plume is diverted southward where it has a longer residency time and is characterized as a far-field 'aged' plume (Horner-Devine et al. 2009).

In systems such as the CRP, fronts are often defined by and sampled along their visually observable surface discontinuity that marks the vertical plume front (Grimes & Finucane 1991, Morgan et al. 2005). However, frontal boundaries occur along both the vertical and horizontal margins, and because plumes are shallow features, the frontal gradient along their horizontal plane is often much larger than the vertical gradient. In the CRP, the formation of distinct vertical and horizontal fronts can change the spatial distributions of zooplankton and may be important features structuring zooplankton communities. Where strong vertical fronts have been shown to aggregate plankton along the leading edge of the plume, strong horizontal gradients are thought to vertically compress phyto- and zooplankton beneath the plume. For example, in the absence of plume waters, zooplankton tend to aggregate in the upper 25 m of the water column, but when the plume is present, zooplankton aggregate at 10 m depth beneath the base of the plume (Peterson & Peterson 2008, 2009).

The Columbia River and its associated plume are a biological hotspot in the Northeast Pacific Ocean. Not only does this region support many important marine fisheries, including Dungeness crab *Cancer magister* and the largest runs of Pacific salmon (*Oncorhynchus* spp.) in the continental USA, it also serves as an important spawning and nursery habitat for the northern stock of northern anchovy *Engraulis mordax* (Richardson 1981, Emmett et al. 1997, 2005, 2006). In contrast to many other riverine dominated coastal systems, intense hydroelectric regulation of the Columbia River creates artificially high summer flows resulting in a dominant and year-round influence on NCC waters (Henderikx Freitas et al. 2018). Thus, the CRP is a particularly useful system to study how river plumes influence the spatial distributions of zooplankton communities and how those spatial distributions may impact larval fish trophic interactions and population dynamics.

While decades of work have demonstrated that river plumes serve an important role in structuring coastal ecosystems, the physical effects of tidally controlled river plumes on zooplankton spatial distributions, larval fish trophic interactions, and ultimately survival remain poorly understood. This is likely due to the highly dynamic

nature of river plumes and the inability of many traditional sampling techniques to resolve both the vertical and horizontal plume margins and fine-scale biological processes. Elucidating these requires high-resolution sampling that can be achieved with underwater imaging, where, with recent technological advancements, data are collected at the scale of an individual larva. We used the high-resolution *In situ* Ichthyoplankton Imaging System (ISIIS) coupled with state-of-the-art machine learning techniques to investigate the fine-scale spatial distribution of larval fishes, their prey, and their predators in the CRP over space (inshore versus offshore) and time (through the progression of a tidal series). Our goal was to measure how various zooplankton and larval fish distributions respond to changes in physical variables. By examining individuals of a diversity of taxonomic groups over time and space, we aimed to determine the degree to which larval fishes overlap with their prey and predators in this dynamic system.

2. MATERIALS AND METHODS

2.1. Data collection

Towed *in situ* imagery data were collected in the NCC just south and offshore of the Oregon–Washington state boundary aboard the NOAA Fisheries RV 'Bell M. Shimada,' as part of the NOAA Northwest Fisheries Science Center Pre-Recruitment Survey (Brodeur et al. 2019). Sampling occurred during daylight hours (08:00–19:00 h PDT) on 23–24 June 2016, and included 2 sequential 25 km cross-plume (parallel to the coastline) transects 10 km offshore of the Columbia River mouth and one 60 km cross-shelf transect south of the river mouth (perpendicular to the coastline), which was split into inshore and offshore sections for further analyses, to capture the plume influence nearshore (Fig. 4.1A). During the former transect, we transited the same cross-plume line through the progression of the Columbia River ebb-flood tide series (Fig. 4.1C). The imager was towed at a speed of 2.5 m s^{-1} in a tight undulating fashion from the surface to 100 m depth or within a few meters of the seafloor in shallower regions. Each undulation provided 2 quasi-vertical profiles of the water column. Our sampling resulted in 76 full undulations or 152 quasi-vertical profiles.

2.2. ISIIS

ISIIS (Cowen & Guigand 2008) is a towed, low turbulence, high-resolution *in situ* shadowgraph imaging system. It has a large sampling volume (150–185 l s^{-1}) and is capable of capturing and quantifying both rare plankters, like larval fishes, and their more abundant prey and predators. Additionally, its large field of view (13 × 13 × 50 cm) allows the system to image fragile gelatinous taxa (McClatchie et al. 2012, Luo et al. 2014, 2018), which can be important prey and predators of larval fishes but are difficult to enumerate with traditional net-based sampling techniques (Fig. 4.2). Sensors on ISIIS include a CTD (Sea-Bird SBE 49 FastCAT), dissolved oxygen (Sea-Bird 43), chlorophyll *a* (chl *a*) fluorescence (Wetlabs FLRT), and photosynthetically active radiation (E_{PAR}; Biospherical QCP-2300). Data from ISIIS are transferred via fiber optic cable to a ship-board computer where images are time-stamped and stored. Imagery data are processed, trained, and tested for automated classification following protocols detailed by Luo et al. (2018). These methods are briefly described below.

2.2.1. Image processing

ISIIS files (AVI stacks) were parsed into single frames and flat-fielded to subtract background noise using a *k*-harmonic means clustering algorithm. Individual plankters, known as regions of interest, were detected, segmented from the full frame, assigned a unique name identifier (including a detailed time stamp), and saved as jpg files. Each jpg file contains an individual plankter and will hereafter be referred to as a vignette.

2.2.2. Classification training

A sparse convolutional neural network (sCNN) was used for automated classification of vignettes (single organism images) into taxa categories. sCNNs are state-of-the-art for the automated identification of *in situ* plankton imagery (Graham 2015, LeCun et al. 2015, Luo et al. 2018). The sCNN is a deep learning tool and was trained using 'SparseConvNets' with 'Fractional Max-Pooling' (Graham 2015) with a customized NCC training library that consisted of 161 categories including phyto-, zoo-, and ichthyoplankton, particles, and noise artifacts (e.g. bubbles at the surface; Table C1 in the Supplement at www.int-res.com/articles/suppl/m000p000_supp.pdf). This training

library was built by extracting and manually identifying 51870 vignettes from the entire NCC imagery collection (including the 3 transects analyzed in this study) to accurately capture the diversity of organisms in our sampling region. Both clear and noisy images were included to account for the different water masses sampled, and training of the sCNN continued until an error rate of ≤5% at 400 epochs was attained. An epoch is when the entire dataset is passed though the sCNN once, and the weights, which contain the information that the CNN learned during that epoch, are updated.

The sCNN assigned 161 probabilities to each vignette, indicating to which one of the 161 categories the vignette likely belonged. The category with the highest probability was selected as the predicted identification. Following automated classification, the 161 categories were mapped onto 72 final groups due to the consolidation of multiple categories of the same taxa that needed to be kept separate for automated classification because of differences in orientation, life-stage, or size (Table C1).

2.2.3. Classification testing

Filter-thresholding (*sensu* Faillettaz et al. 2016, Schmid et al. 2020) was applied to remove low-confidence vignettes using a LOESS model. The model calculates a probability threshold cutoff for 90% classification precision at the broader group level. Vignettes with a maximum probability of less than or equal to the calculated cutoff for their category were re-classified as 'unknown' (Table C1). Applying this thresholding reduces the occurrence of false positive identifications substantially. Prediction of true spatial distributions is still possible after removing low classification confidence vignettes (Faillettaz et al. 2016).

The final classification pipeline performance was evaluated using a confusion matrix (Hu & Davis 2006, Tharwat 2018). We compared the results of 86681 randomly selected and manually identified vignettes to their automated predicted classification from the sCNN. This provided a number of true positives (TPs), false positives (FPs), and false negatives (FNs) in our dataset, and performance for each class was then calculated based on precision ($P = TP/(TP+FP)$), recall ($R = TP/(TP+FN)$), and F-score, which is the first harmonic mean of precision and recall ($F\text{-score} = 2\times P\times R/(P+R)$).

2.2.4. Image post-processing and concentration estimates

Final vignettes were merged with simultaneously collected environmental data using the time stamp and binned into 1 m vertical depths along the ISIIS towpath. Fluorescence volts were converted to chl *a* concentrations based on a calibration for our instrument done by SeaBird on 29 January 2016, and environmental data were kriged (Matlab package 'EasyKrig' v.3.0) onto a grid equal to the length of each transect at 1 m vertical and 500 m horizontal resolution. Plume waters were defined using the reference salinity of ≤32.5 for the CRP (Barnes et al. 1972).

Taxa concentrations (ind. m^{-3}) were estimated using the volume of water imaged, average tow speed, and time spent in each 1 m bin. A correction factor based on the confusion matrix results (Hu & Davis 2006, Schmid et al. 2020) was applied to the calculated concentrations according to the following equation

$$Correction\ factor_{taxon} = \frac{Precision\ rate_{taxon}}{Recall\ rate_{taxon}} \quad (1)$$

2.3. Ecological analyses

Key taxonomic groups were selected for analysis based on their ecological significance as potential prey or predator groups of larval fishes. Calanoid copepods and appendicularians are frequently found in the guts of larval fishes (Baier & Purcell 1997, reviewed by Llopiz 2013). Appendicularians, in particular, are estimated to comprise 97% of the diet of a pleuronectid in this region (Gadomski & Boehlert 1984). Calanoid copepods dominate the plankton off Oregon (Peterson & Miller 1975) and are a more important prey resource than cyclopoid copepods at mid- and high latitudes (Llopiz 2013). Chaetognaths are primarily carnivorous, and several studies suggest that based on their high abundance and the presence of fish larvae in their guts, they may cause significant mortality (reviewed by Alvarino 1985). Finally, larval fishes make up a significant portion of the diets of some gelatinous taxa, including ctenophores, siphonophores, and hydromedusae (reviewed by Purcell 1985). With few notable exceptions (Gadomski & Boehlert 1984), there is a lack of information on the diets of and predation upon larval fishes in the NCC compared to other regions (e.g. the Straits of

Florida; see Llopiz & Cowen 2009). To account for this knowledge gap, zooplankton were combined into the following higher taxonomic groupings for all analyses: larval fishes, calanoid copepods, appendicularians, chaetognaths, ctenophores, hydromedusae, and siphonophores. Concentrations of each taxon per depth bin along the sampling transects were calculated, and Kruskal-Wallis tests were used to compare the mean concentrations in plume (salinity ≤32.5) and non-plume waters (salinity >32.5). Finally, each individual within these taxa was measured along its major axis. Taxa size distribution plots were created to evaluate the potential for predator–prey interactions.

2.3.1. Zooplankton community analyses

Ordination was used to determine if the zooplankton community structure differed between the 2 plume types (tidal plume and far-field plume) and oceanic habitat. Data were binned into 1 m vertical depth bins across each transect. Tidal plume habitats were defined as those directly off of the river mouth (Transects 1 and 2) where salinity was ≤32.5, far-field plume habitats were classified by the same salinity value but located inshore, south of the river mouth (Transect 3 inshore), and oceanic habitats were where salinity was >32.5.

Ordination was done using non-metric multidimensional scaling (NMDS) in the R (v. 3.5.2) package ‘vegan’ v. 2.5-6 (Oksanen et al. 2019) with a Bray-Curtis distance measure. NMDS ordinates sample units (1 m depth bins across each transect) in multidimensional species space to identify samples with similar zooplankton communities, where the more similar in composition 2 samples are, the closer they appear in space. The relationship between stress and dimensionality was examined to find the smallest number of axes where the reduction in stress (a measure of the goodness-of-fit between the species data and the final ordination) adequately plateaued (Mather 1976). The 2 dominant ordination axes are presented graphically for ease of visualization. We tested the null hypothesis of no difference in zooplankton communities among tidal plume, far-field plume, and oceanic habitats using the ‘adonis’ function in ‘vegan,’ which computes a non-parametric permutational multivariate analysis of variance (Anderson 2001).

2.3.2. Fine-scale vertical distributions

Mean concentrations per 1 m depth bin of larval fishes, their prey, and their predators were examined to investigate the effect of plume waters on taxa vertical distributions. The weighted mean depth (WMD) of the vertical distribution of larval fishes and their potential prey and predators was calculated following Frost & Bollens (1992):

$$WMD = \frac{\Sigma(n_i \times d_i)}{\Sigma n_i} \qquad (2)$$

where n_i is the concentration of individuals per cubic meter of taxon i at depth d_i, which is taken to be the shallowest point of each 1 m depth stratum. WMDs were calculated for the full transects as well as the deeper southern and shallower northern portions of the cross-plume transects separately to ensure that patterns were not significantly influenced by the bathymetry of the region.

2.3.3. Larval fish prey/predator spatial overlap

Relationships of larval fish prey/predator taxa throughout the water column were evaluated using the spatial overlap index described by Williamson & Stoeckel (1990):

$$O_{ij} = \frac{\sum_{z=1}^{m}\left(N_{jz} \times n_{iz}\right)m}{\sum_{z=1}^{m}\left(N_{jz}\right) \times \sum_{z=1}^{m}\left(n_{iz}\right)} \qquad (3)$$

where z is the depth stratum, m is the number of sampled depths, N_{jz} is the concentration of larval fish at a given depth, and n_{iz} is the concentration of the select prey or predator taxon at a given depth. Overlap index values of 1 indicate that fish larvae and/or the select taxonomic group are evenly distributed in the water column; index values <1 indicate vertical spatial separation between fish larvae and the select taxa; and index values >1 indicate vertical spatial overlap of fish larvae and the select taxa, where the theoretical upper limit is defined by the number of points sampled. The spatial

overlap index of Williamson & Stoeckel (1990) takes into account prey and predator concentrations in addition to spatial and temporal overlap and has been used in a variety of systems to evaluate trophic interactions among zooplanktonic organisms (Bezerra-Neto & Pinto-Coelho 2007, Möller et al. 2012, Picapedra et al. 2015). Overlap indices for larval fishes and each of their prey/predator groups were determined for every quasi-vertical profile (2 per undulation) resulting in horizontally stratified index values. Median transect-wide integrated values with their corresponding standard errors were calculated based on the individual quasi-vertical profile spatial overlap values and are also reported to provide an overall statistical description of overlap in each transect.

2.3.4. Overlap-environment modeling

Boosted regression tree (BRT) analysis was used to evaluate how the presence of surface plume waters affected the likelihood of spatial overlap between larval fishes and their prey/predator taxa in the water column. BRTs are an ensemble statistical modeling method capable of fitting complex nonlinear relationships (Luo et al. 2014, Lieske et al. 2018). Instead of attempting to fit a single parsimonious model like traditional techniques, BRTs use random subsets of data to construct a large number of simple regression trees. These trees are then combined using machine learning (boosting) to optimize predictive performance (Elith et al. 2008). Similar to other tree-based methods, BRTs provide an estimate of the relative importance of each explanatory variable as well as partial dependence plots that show how the influence of the variable varies over its range.

Six BRT models (1 for each prey/predator taxon) were constructed to predict the horizontally stratified spatial overlap index based on 5 explanatory variables: mean salinity, temperature, dissolved oxygen, chl *a* concentration, and photosynthetically active radiation (E_{PAR}) in surface waters. Specifically, each row in the model matrix consisted of the calculated spatial overlap index for 1 quasi-vertical profile and the mean environmental parameters in the top 5 m of the water column for that profile. We used the top 5 m to indicate surface waters because plumes are shallow features; during sampling, the maximum depth of the plume was 3.7 m in some regions, and the plume signal was quickly lost beyond this depth during the ebb tide due to sharp physical

gradients. All models were built using the R (v.3.5.2) package 'dismo' v.1.1-4 (Hijmans et al. 2017), and model performances were evaluated using an estimate of deviance explained (D^2 = 1 – residual deviance/null deviance). Partial dependence plots were created for the top 3 most important explanatory variables for each prey/predator taxon using the R (v.3.5.2) package 'gbm' v.2.1.5 (Greenwell et al. 2019). Partial dependence plots show the effect of environmental variables on the likelihood of spatial overlap between larval fish and each prey/predator group.

3. RESULTS

3.1. Environmental setting

Mean Columbia River discharge during the study period was 5478 m^3 s^{-1}, with a maximum flow volume of 11100 m^3 s^{-1}. Winds reversed from weakly downwelling-favorable to upwelling-favorable 8 d prior to sampling and remained weakly upwelling-favorable throughout the sampling period (Fig. 4.1B). The sampling period encompassed spring tides; the semidiurnal tides were unequal in magnitude, with the larger ebb occurring during daytime hours and coinciding with sampling (Fig. 4.1C). Transect 1 data were primarily collected during slack ebb and Transect 2 during slack flood. Transect 3 (cross-shelf) sampling began just before slack ebb and continued through maximum flood, when sampling was nearest to shore. Plume waters (defined as salinity ≤32.5) were present at the surface and captured in sampling during all transects.

3.2. Automated classification performance

Imagery data yielded 24.7 million vignettes, including numerous representatives of all taxa of interest (6095 fish larvae and ~1.5 million prey/predator zooplankton; Fig. 4.2). After filtering thresholds were applied and the original 161 classes were mapped onto their broader groups, the weighted average model precision (number of true positives/number of true and false positives) was 77%, recall (number of true positives/number of true positives and false negatives) was 73%, and F-score (harmonic mean of precision and recall) was 67%. Note that a correction factor (precision/recall, see Section 2.2.4) was applied prior to calculating final concentrations (Table C2, Fig. C1). These evaluation metrics are strong, especially given the large number of classes

included in our training library (n = 161). As the number of classes in a model increases, classification becomes more difficult. Yet, our model precision is comparable to studies with far fewer classes. For example, Gorsky et al. (2010) achieved a mean model precision of ~80% (precision calculated as recall/[recall + contamination] in their study) with just 8 classes, while our mean model precision of 77% was achieved with 161 classes. Our model also performed well compared to more recent studies that use CNNs. Orenstein et al. (2015) presented a comparison of different classifiers, of which the best one had 70 classes, and had an unweighted mean F-score of 42%.

3.3. Taxa concentrations

A total of 6095 fish larvae were identified in the automated image classification. The most abundant groups accounted for 83.86% of the catch and were comprised of Sebastidae (43.58%), Clupeiformes (19.76%), 'long slender' (10.19%), Pleuronectiformes (8.33%), and Myctophidae (2.00%). Based on the literature in this region, we suspect that the group 'long slender' was possibly dominated by Bathylagidae (Parnel et al. 2008). Mean concentrations of taxa of interest during all sampling varied over 3 orders of magnitude (Table 4.1). Corrected larval fish concentrations ranged from 0.09 ± 0.00 ind. m^{-3} in Transect 1, to 0.16 ± 0.01 ind. m^{-3} in the inshore region of Transect 3. Appendicularians were the most abundant overall (81.14 ± 1.26 ind. m^{-3}) followed by calanoid copepods (15.05 ± 0.22 ind. m^{-3}). Calanoid copepods and appendicularians were also most abundant in all individual transects with the exception of Transect 2, where the concentration of hydromedusae (13.43 ± 0.62 ind. m^{-3}) exceeded that of calanoid copepods (11.85 ± 0.33 ind. m^{-3}). Predator groups were dominated by hydromedusae and chaetognaths, with total mean concentrations of 9.06 ± 0.24 and 7.04 ± 0.12 ind. m^{-3}, respectively. The offshore region of Transect 3 had the lowest abundances of copepods (8.25 ± 0.20 ind. m^{-3}), chaetognaths (1.34 ± 0.04 ind. m^{-3}), ctenophores (0.86 ± 0.03 ind. m^{-3}), hydromedusae (2.59 ± 0.10 ind. m^{-3}), and siphonophores (1.18 ± 0.04 ind. m^{-3}), and the second lowest concentration of fish larvae (0.10 ± 0.01 ind. m^{-3}).

Concentrations of all taxa differed significantly between the plume and non-plume water masses in regions where the plume was present, with the exception of

hydromedusae in the inshore region of Transect 3 (Kruskal-Wallis test; Table 4.1). In all other cases, taxa concentrations were significantly higher in non-plume water compared to plume water.

3.4. Taxa size distributions

The size (total length; TL) of larval fishes ranged from 1.00 to 38.75 mm, with a mean TL of 6.44 mm (Table 4.2). Fishes south of the river mouth were larger than those directly off of the river mouth. The size of prey and predator taxa also varied across transects, but both prey groups (calanoid copepods and appendicularians) were substantially smaller than larval fishes in all sampling. Mean larval fish TL ranged from 2.74–5.11 mm larger than the mean size of their prey. In general, potential predator size distributions were more protracted and their distributions overlapped with, and often exceeded, those of larval fishes (Fig. C2). The exceptions to this were ctenophores, whose size distributions were more compressed and had a mean size that was smaller than those of larval fishes in all plume regions. Conversely, the mean size of hydromedusae exceeded that of larval fishes in all plume regions (i.e. in all sampling but the offshore region of Transect 3). While chaetognaths were on average larger than larval fishes throughout the entirety of sampling, siphonophores were larger than larval fishes only directly off of the river mouth (Table 4.2).

3.5. Plume structure, community composition, and fine-scale vertical distributions

The distribution of larval fishes, their prey, and their predators in relation to the CRP was documented for 4 distinct water column structures observed throughout sampling.

3.5.1. Transect 1: ebb tidal plume—low surface salinity and strong shallow stratification

Low-salinity plume waters were present at the sea surface along the entire length of Transect 1. The plume was highly stratified and restricted to the upper 20 m of the water column with vertical salinity gradients of up to 4.4 m^{-1} and a maximum depth of 19.6 m. Minimum depth of the plume was 4.5 m (Fig. 4.3A).

With the exception of a small pocket of fresher water extending to 19.6 m depth on the southern end of the transect, the plume was deeper in the northern than the southern extremes of the transect. Salinity values ranged from 12.68 at the surface to 34.39 at depth. The freshest water was located directly offshore of the river mouth, in the upper 3 m of the water column. Surface salinity was higher in the southern portion of the transect, with a minimum salinity of 25.23 in the upper 20 m. Temperature varied from 7.55 to 15.0°C, with the warmest waters in the top 15 m on the northern end of the transect. A thin phytoplankton layer (as indicated by chl *a* concentration) extended approximately 6 km into the southern portion of the transect. The entire water column was normoxic, with oxygen values exceeding 1.43 ml l^{-1} (Fig. 4.3A; Grantham et al. 2004).

During the ebb tide when there was strong, but shallow, stratification of the water column, larval fishes did not occupy the shallowest 5 m, but were relatively evenly distributed below this depth with a slight peak in abundance ~10 m below the base of the plume (Fig. 4.4A). While prey groups (calanoid copepods and appendicularians) were broadly distributed below 5 m depth, their WMDs were slightly deeper than that of larval fishes, with the exception of appendicularians in the southern region. Predator distributions were more dynamic but were generally most abundant in the top 25 m of the water column. The WMD of predators was, on average, 7.85 m shallower than the WMD of fish larvae in the southern region and 1.30 m shallower in the northern region. Chaetognath and hydromedusae distributions formed distinct concentration peaks near the base of the plume, while the distributions of ctenophores and siphonophores were more protracted. Notably, chaetognaths were the only taxon present in significant concentrations at the shallowest depths and some of the lowest salinities in this transect (~15; Fig. 4.4A, C3A).

3.5.2. Transect 2: flood tidal plume—moderately low surface salinity and stratification

Plume waters remained at the sea surface along the entirety of Transect 2. While still highly stratified, the plume was more mixed during the flood than the ebb tide, with a maximum vertical salinity gradient of 2.1 m^{-1} and salinity values ranging from 17.94

within the surface plume to 35.02 at depth. Again, the plume was restricted to the top 20 m of the water column varying in depth from 3.7 m in the south to 17.6 m in the north. While the temperature range during the flood tide was similar to the ebb (7.58–14.93°C), the extent of the 'warm pool' of water in the northern portion of the transect surface waters increased both vertically and horizontally. Similarly, the phytoplankton layer on the southern end of the transect became more well-defined and increased in thickness from around 5 to 10 m depth. Oxygen values ranged from 1.67 to 7.62 ml l^{-1} (Fig. 4.3B).

There was a distinct deepening (>6 m) of the vertical distribution of larval fishes from a WMD of 25.39 m during the ebb tide to 31.51 m during the flood tide when low-salinity water extended deeper into the water column (Figs. 4.3B, 4.4B). This pattern held in the deep and shallow portions of the transect where the WMD of larval fishes deepened 5.01 m in the south and 7.87 m in the north. Larval fish concentrations were negligible above 20 m depth, and there was a broad peak in abundance at the 20–50 m depth range, indicating possible vertical compression. WMDs of calanoid copepod and appendicularian prey deepened by approximately 3 m, creating moderate abundance peaks at depth that roughly coincided with the peak in larval fish abundance. When the transect was split into deep and shallow sections, the WMD of fish larvae closely adhered to both prey groups, especially calanoid copepods. One predator taxon, ctenophores, exhibited a vertical distribution markedly similar to larval fishes. Chaetognath, hydromedusae, and siphonophore WMDs were, at a minimum, 6.44 m shallower than the WMD of fish in the northern region and 8.94 m shallower in the southern region. Interestingly, the distribution of hydromedusae was virtually the same in the ebb and flood stages of sampling, with a strong peak in concentration around 20 m depth. Although there remained some degree of overlap with the vertical distribution of fish larvae, the highest peak in larval fish abundance was nearly 10 m deeper than the region of highest hydromedusae concentrations (Figs. 4.4B, C3B).

3.5.3. Transect 3 (inshore): far-field plume—intermediate surface salinity and weak stratification

Low-salinity waters extended 18 km into Transect 3 (cross-shelf, south of the river mouth) on the inshore end (Fig. 4.3C). Salinity values within the plume reached a

minimum of 25.1, and the maximum depth of the plume was 15.5 m. The maximum vertical salinity gradient was 0.5 m^{-1}. Temperature was moderately cooler in this region south of the river mouth and ranged from 6.97 to 15.19°C. The highest phytoplankton signal was located closest to shore, with a maximum chl *a* concentration of 10.39 µg l^{-1} . Bottom water beneath the plume was mildly hypoxic, reaching a minimum of 1.36 ml l^{-1}.

High abundances of larval fishes were relatively evenly distributed throughout the water column. WMD of fish larvae was deepest in this region at 58.24 m (Fig. 4.4C). The same was true for calanoid copepods (62.96 m) and appendicularians (52.15 m), yet their distributions appeared to be more structured. Calanoid copepod abundance increased slightly with depth, and appendicularians peaked in the 20–60 m depth range. The 1 m depth bin with the highest concentration of fish larvae coincided with a 6 m peak in copepod abundance. WMD of fish larvae was <1.5 m deeper than the mean for prey, but was nearly 8 m deeper than the mean for predators. Again, hydromedusae exhibited the most contracted distribution of any taxon, displaying a sharp, shallow concentration peak. Their WMD was >30 m shallower than the WMD of fish larvae (Figs. 4.4C, C3C).

3.5.4. Transect 3 (offshore): negligible plume

In the cross-shelf offshore region, salinity ranged from 31.58 to 33.92. Despite the relatively minor salinity variability, the water column was moderately structured by thermo- and oxyclines shoaling toward the shelf, with values ranging from 7.11 to 15.75°C and 1.53 to 6.70 ml l^{-1}, respectively (Fig. 4.3C). The maximum phytoplankton chl *a* concentration of 4.63 µg l^{-1} was substantially lower than in all other regions. In the absence of surface plume waters, larval fishes and all zooplankton were relatively evenly distributed in the water column (Figs. 4.4D, C3D).

3.5.5. Community composition

Non-metric multidimensional scaling (NMDS) revealed significant differences in the community compositions among the 2 types of plume habitats (tidal and far-field plume) and oceanic waters (Fig. 4.5). The ordination performed well with a stress value of 0.08, which is in the ‘good’ criteria range (McCune & Grace 2002). Non-parametric statistical analysis (‘adonis’) indicated that the zooplankton community structure was

significantly different among the tidal plume, far-field plume, and oceanic habitats ($p = 0.001$).

3.6. Larval fish prey/predator spatial overlap

As an indication of the potential for trophic interactions between larval fishes and their prey/predators, we calculated an index of vertical overlap for each sampling quasi-vertical profile ($n = 152$) along every transect. Median transect-wide overlap indices ranged from 1.14 to 1.89 for prey groups and from 0.88 to 1.77 for predator groups (Fig. 4.6). Taxa spatial overlap with larval fishes varied significantly over space (Transect 3: inshore vs. offshore) and time (Transect 1: ebb tide vs. Transect 2: flood tide; Figs. 4.6, 4.7).

3.6.1. Variation in overlap over space

When no plume waters were present, there was some degree of spatial overlap between larval fishes and all prey and predator taxa (Fig. 4.6). Overlap between prey/predator taxa and fish larvae was more dynamic in regions where the water column was structured by the inshore plume, as evident by the overlap of larval fishes with some taxa and the separation from others. Where plume waters were present at the surface, south of the river mouth (i.e. Transect 3 inshore), there was a small degree of vertical alignment between fish larvae and calanoid copepods, appendicularians, chaetognaths, ctenophores, and siphonophores, while there was vertical separation between fish larvae and hydromedusae (Fig. 4.6).

Across Transect 3, prey groups overlapped with fish larvae throughout the entire length of the inshore region, but there were instances of separation from fish larvae in the offshore region. With the exception of chaetognaths, all taxa anomalously overlapped with fish larvae in 1 quasi-vertical profile offshore (Fig. 4.7C,D).

Interestingly, along the leading edge of the plume (i.e. the vertical plume front; second to farthest west quasi-vertical profile in Fig. 4.7C), spatial overlap of prey taxa with larval fishes was nearly 2 standard deviations above the mean of adjacent waters. There was an even greater increase (2.5 standard deviations above the mean) in spatial overlap with predator taxa near the vertical plume front. A few kilometers offshore of this

frontal region, prey groups only slightly co-occurred with or were separated from fish larvae, while predator groups highly co-occurred with fish larvae (Fig. 4.7C, D).

3.6.2. Variation in overlap over time

Median overlap values indicated that all prey and predator taxa were positively correlated with fish larvae during the ebb tide (Transect 1; Fig. 4.6). During the flood tide (Transect 2) a few hours later, while both prey taxa (calanoid copepods and appendicularians) became more strongly correlated with fish larvae, 3 out of 4 predator groups became less correlated with fish larvae (chaetognaths and siphonophores) or even showed some degree of vertical separation (hydromedusae; Fig. 4.6).

Notably, where plume waters were the freshest and very shallow during the ebb tide, all taxa were correlated with fish larvae (Figs. 4.3A, 4.7A). This contrasts with both north and south of this region where there was a mixture of overlap and separation across taxa (Fig. 4.7A). When the river was flooding and low-salinity water was pushed deeper into the water column (Fig. 4.3B), there was a high overlap of larval fishes with both prey groups (calanoid copepods and appendicularians) but separation between fish larvae and some predator taxa, especially hydromedusae (Fig. 4.7B).

Spatial overlap of taxa with larval fishes was more accentuated in the shallower northern portion of Transects 1 and 2. Generally, in the deeper portion of the transect to the south, prey groups overlapped with fish larvae and predator groups were separated from fish larvae (Fig. 4.7A,B).

3.7. Overlap-environment modeling

The number of regression trees fit to BRT models ranged from 1100 for the overlap model of larval fishes with appendicularians, to 3000 for the overlap model of larval fishes with ctenophores. All models performed well, with a mean D^2 of 0.48. Ctenophore and hydromedusae models performed best, with D^2 values of 0.65 and 0.62, respectively (Fig. 4.8).

Model results indicate that salinity and chl *a* concentration had the highest relative influence on spatial overlap with larval fishes for the largest number of taxa. Salinity was the most important variable influencing overlap for 3 taxa and was in the top 3 most

important for all taxa (Fig. 4.8). The next most influential explanatory variables, based on rank importance, in decreasing order, were chl *a* concentration, temperature/oxygen, and E_{PAR}.

The mean relative influence of salinity on spatial overlap with larval fishes was greater for prey groups (33.95%) compared to predator groups (24.08%; Fig. 4.8). Chaetognath overlap with fish larvae was the least influenced by salinity (18.7%), and they were the only group to not have salinity in the top 2 most important variables (Fig. 4.8).

Partial dependence plots showing the effect of environmental variables on the spatial overlap index relative to the model mean indicated that all taxa were predicted to have above-average spatial overlap with larval fishes when surface salinity was ≤24 (Fig. 4.9). Maximum overlap of larval fishes with copepods occurred when surface salinity was ~24, while overlap with appendicularians was greatest when surface salinities were ~25.5–27. Chaetognath overlap with larval fishes was at a maximum at ~26.5, ctenophores and siphonophores at ~20–24, and hydromedusae at ~24.5–26. When surface salinity approached the reference plume cut off for the CRP (≤32.5), all taxa were predicted to have below-average overlap with larval fishes (Fig. 4.9).

Copepods and appendicularians showed above-average spatial overlap with larval fishes at high surface chl *a* concentrations, while chaetognaths, ctenophores, and hydromedusae demonstrated below-average overlap at these values (Fig. 4.9). In general, intermediate surface temperatures (~13–15°C), high surface oxygen (~6 ml l^{-1}), and the highest surface E_{PAR} values (>0.002) predicted above-average spatial overlap with larval fishes (Fig. 4.9).

4. DISCUSSION

Using a high-resolution *in situ* imaging system, we documented changes in the fine-scale horizontal (km) and vertical (m) distributions and spatial overlap of larval fishes with their zooplankton prey and predators in a highly dynamic river plume system. Our analyses demonstrated substantial changes in concentrations, distributions, and spatial overlap with larval fishes among different zooplankton taxa over small spatial and temporal scales.

Our results are consistent with previous findings that suggested chl *a*, zoo-, and ichthyoplankton concentrations are higher in plume-influenced regions (St. John et al. 1992, Albaina & Irigoien 2004, Morgan et al. 2005), yet emphasize that zoo- and ichthyoplankton were primarily found aggregated beneath, and not within, the plume at the horizontal plume front. Fish larvae and their prey (calanoid copepods and appendicularians) were generally distributed deeper in the water column than their potential predators (chaetognaths, ctenophores, hydromedusae, and siphonophores). However, the presence of a shallow horizontal plume front reduced the magnitude of this difference, contributing to high spatial overlap of larval fishes with their prey and predators (although overlap with predators was taxon-specific and varied with the tide and depth of the horizontal front). Further, regions of high taxa concentration did not necessarily lead to high fine-scale spatial overlap of larval fishes with their prey/predators. Surface salinity and chl *a* concentration were the most important factors influencing spatial overlap of larval fishes and zooplankton taxa.

Larval fishes must find food and avoid predators in heterogeneous environments (Lasker 1975, Bailey & Houde 1989, Cushing 1990). In highly dynamic systems such as riverine plumes, the trophic environment can quickly shift from favorable (high prey, low predator concentration) to poor (low prey, high predator concentration). Riverine plumes are important habitats for larval fishes and are thought to provide mechanisms of favorable transport (i.e. nearshore retention) and high food availability (Grimes & Finucane 1991, Govoni 1997, Eggleston et al. 1998), but traditional sampling techniques have not adequately examined the fine-scale distributions of larval fishes, their prey, and their predators in relation to highly dynamic and 3-dimensional riverine plumes. Results of our study demonstrate the effect of this dynamic physical system on the distributions and overlap of biological constituents over space (inshore versus offshore) and time (ebb versus flood tide), with potential consequences on larval fish prey/predator interactions.

4.1. Larval fish distributions

Distributions of larval fish taxa (Sebastidae, Clupeiformes, ‘long slender’ [possibly Bathylagidae, see Section 3.3], Pleuronectiformes, and Myctophidae) varied in space and time in both horizontal and vertical dimensions. On a broad scale, the highest

concentrations of fish larvae were found in the inshore region of Transect 3, ~20 km south of the river mouth. This was consistent with expectations, as during the study period there was weak upwelling driven by northern winds that have previously been shown to divert the CRP and zooplankton southward and offshore (Hickey et al. 2005, Peterson & Peterson 2008, 2009). Further, some species, notably northern anchovy, are known to spawn in the far-field 'aged' plume waters, which may account for higher concentrations in this region compared to directly off of the river mouth (Richardson 1981, Emmett et al. 1997).

The distribution of fish larvae also changed vertically in relation to the horizontal plume front. Throughout sampling, larval fish concentrations peaked at around 10 m below the base of the plume. Although this peak was moderate in some transects, larval fishes were consistently found in higher abundances beneath fresher plume waters with negligible, near-zero concentrations within the shallow surface plume. As such, when plume waters extended deeper into the water column (Transect 2, flood tide), larval fishes were distributed deeper and appeared to be vertically compressed on short time scales (hours). Vertical plume avoidance could be due to (1) physiological limitations, (2) physical displacement, (3) biological factors, or some combination of these. Northern anchovy are euryhaline, and given that some *Sebastes* and Pleuronectiformes species use the estuary as juveniles, they may also tolerate a wide salinity range (Allen & Baltz 1997, Oh et al. 2014). However, Bathylagidae and Myctophidae are mesopelagic taxa and thus are unlikely to tolerate low salinity. Myctophidae were primarily found offshore. Our sampling did not enable us to definitively address why larval fishes were not found in surface plume waters. However, because most taxa responded to the deepening of the horizontal front in a similar manner (i.e. their distributions deepened) regardless of their varied ability to withstand a wide range of salinities, we hypothesize that physical displacement and biological factors may have played a larger role than physiological limitations in the CRP.

4.2. Fine-scale habitat partitioning beneath the plume

All prey and predator taxa were primarily distributed beneath fresher plume waters. Much like the larval fishes, vertical distributions changed with the depth of the

horizontal plume front. For example, when the horizontal front extended deeper into the water column during the flood tide, all taxa were distributed at greater depths and vice versa, suggesting that broad taxa distributions were set by the physical environment, likely through density gradients or sheer at the horizontal front. Adherence of zooplankton distributions to the depth of the horizontal front due to strong density gradients has been observed in previous studies in the region (Peterson & Peterson 2008). The role of density gradients in maintaining taxa distributions is illustrated with the distribution of chaetognaths. Chaetognaths were the only taxon consistently found above negligible concentrations within the plume water at the shallowest depths. Chaetognaths are highly active ambush predators; laboratory studies found chaetognath swimming speeds to be as high as 6.2–22.5 cm s^{-1} for *Sagitta* spp., a common genus in this region (Ignatyev 1997). While these swimming speeds are similar to those of some large fish larvae, they are significantly higher than the swimming speeds attained by the relatively small fish larvae (~6 mm TL) observed in this study (Hunter 1972, Kashef et al. 2014). With strong swimming capabilities, chaetognaths may be the only taxon able to access regions above the horizontal plume front, although the advantages for doing so are unclear.

Recent *in situ* studies suggest that physical oceanographic features broadly determine the distribution of taxa, but within those distributions, zoo- and ichthyoplankton exhibit fine-scale habitat partitioning (Benoit-Bird et al. 2009, Greer et al. 2013). Concentrations of predator taxa, especially hydromedusae, peaked directly under the horizontal plume front. This is not surprising, since many of our predator groups have highly buoyant bodies that have a tendency to get ‘stuck’ at density discontinuities (Graham et al. 2001). Interestingly, however, the bulk of larval fishes and their prey (calanoid copepods and appendicularians) were often found below the highest peaks in predator concentrations. Further, throughout the study, fish larvae vertically overlapped with both of their prey groups, but were vertically separated from hydromedusae during both the flood tide as well as in the inshore region south of the river mouth. The vertical separation between fish larvae and hydromedusae, and simultaneous overlap with their prey, suggests that there may be some degree of habitat partitioning beneath the river plume. Although we cannot discern whether vertical spatial

separation with hydromedusae and overlap with calanoid copepods and appendicularians was due to active or passive processes, we suspect that physical conditions at the horizontal front set the ultimate limits for zoo- and ichthyoplankton distributions, while beneath the plume, biological interactions acted to optimize feeding and reduce predation pressure. Given the timescale of this study (hours between Transect 1 and Transect 2), partitioning of the water column beneath the plume is unlikely to be due to the predatory 'top-down effect' of one population on another. By distinguishing patterns of different taxa on fine spatial scales, our results build upon previous findings of broad aggregations of phyto- and zooplankton near or within the density discontinuity along the horizontal plume margin of the CRP (Peterson & Peterson 2008).

4.3. Trophic interactions in space and time

Based on the observed distributions and fine-scale spatial overlap of larval fishes and their prey, most fish larvae in the vicinity of the CRP should experience high concentrations of appropriately sized copepod and appendicularian prey, especially directly off of the river mouth and during the flood tide. Since calanoid copepods and appendicularians are important prey resources for larval fishes (Gadomski & Boehlert 1984, Llopiz et al. 2010, Llopiz 2013), these spatial and temporal conditions can be considered favorable feeding environments.

Potential predators were also concentrated in plume regions. Although ctenophores can be predators of larval fishes (reviewed by Purcell 1985), the ctenophores encountered in the plume regions of this study are unlikely to have functioned as prominent larval fish predators given their small mean body size compared to that of the larval fishes. The remaining predators showed some degree of vertical overlap with larval fishes in all plume regions, with the exception of hydromedusae in the flood tide and in the inshore region south of the river mouth. In the latter, fish larvae also experienced low overlap with many other predator taxa, and there was a mismatch in size with siphonophores, making trophic interactions between them and larval fishes less likely here. This lack of overlap suggests that potential predation pressure on larval fishes by a broad range of predatory taxa was reduced in the inshore region south of the river mouth relative to directly off the river mouth and offshore.

While our results indicate that larval fishes experienced the most favorable feeding conditions seaward of the river mouth, potential predation pressure (measured by fine-scale spatial overlap) in this area fluctuated on short time scales (hours) over the progression of a tidal series. Overall conditions for larval fishes may have been more favorable for survival during the flood tide when there were higher prey concentrations, higher spatial overlap of larval fishes and their prey, and reduced overlap with most of their predators, relative to during the ebb tide.

Larval fishes also experienced variable trophic environments over space. To survive, larval fishes must both find food and avoid predation and there may frequently be times where these constraints necessitate trade-offs. We hypothesize that the inshore region south of the river mouth may have provided conditions most conducive for larval survival. Although larval fish overlap with prey was substantially reduced in this region relative to near the river mouth, overlap with potential zooplanktonic predators was also lower. Considering the size of the planktonic predators in addition to overlap, chaetognaths may have been the only prominent predators of larval fishes in this region. Farther offshore, chaetognaths and ctenophores overlap with and are the appropriate size to function as predators of larval fishes. Predation is thought to be the primary agent of larval fish mortality, and baseline prey levels necessary for larval fish survival have probably been over-estimated in lab-based experiments, as larvae may forage more effectively in the wild than expected (Bailey & Houde 1989). With this in mind, food availability may have been sufficiently high and predation pressure sufficiently low to sustain larval fishes nearshore south of the river mouth. This favorable trophic environment may underlie the spawning of northern anchovy in this region (Richardson 1981, Emmett et al. 1997). The degree to which such regions of potentially enhanced larval fish success are common in nearshore regions of other systems remains to be examined.

4.4. Trophic interactions and the physical environment

BRTs, which allowed us to model the relative importance of a variety of surface physical variables on the spatial overlap of larval fish and their prey/predators, revealed that surface salinity and chl *a* concentration were the most important factors influencing

taxa overlap with fish larvae. Surface salinity was especially important for prey groups (calanoid copepods and appendicularians), and it was in the top 3 most important predictors for all taxa. Additional BRT analyses (not shown) incorporating sub-surface data (5–10 and 20–40 m) explained less deviance than the presented top 5 m surface model.

In the CRP, the highest zooplankton abundance and biovolume were reported to occur at surface salinities of between 26 and 30, which is characteristic of the far-field 'aged' plume (Peterson & Peterson 2008, Horner-Devine et al. 2009). Our data are consistent with this pattern in that zooplankton concentrations were enhanced for many taxa within this surface salinity range. However, BRTs revealed that high zooplankton concentrations may not confer high overlap on small scales (meters in the vertical, kms in the horizontal) relevant to trophic interactions. We found that at salinities of 27 and above, spatial overlap with fish larvae was below model average for all prey and predator taxa regardless of their high concentrations in these regions. When surface salinities were within this range, the WMD of some zooplankton was up to 30 m shallower than that of larval fishes, though this varied greatly across taxa. This fine-scale difference could explain why at even higher prey concentrations in plume-influenced waters elsewhere, larval fish had slower growth (Axler et al. 2020).

Interestingly, high surface chl *a* concentrations were predicted to lead to above model average overlap of larval fishes with their prey groups, but below-average overlap with their potential predator groups. While the reasoning behind this relationship is unclear, it suggests that there are complex interactions between adjacent trophic levels in dynamic river plume systems.

4.5. River plumes as important larval fish habitats

Many species (e.g. the northern anchovy in the NCC) use river plumes as spawning and nursery habitats (Richardson 1981, Emmett et al. 1997, Parnel et al. 2008) and thus it is often assumed that plumes provide favorable conditions for the vulnerable early life stages of larval fishes. It is thought that river plumes may offer (1) nearshore retention mechanisms, (2) high food availability, and/or (3) reduced predation pressure (Grimes & Finucane 1991, Govoni 1997, Eggleston et al. 1998). Indeed, we found that

river plumes provided substantially higher concentrations of prey resources and enhanced spatial coherence between larval fishes and their prey relative to oceanic waters. The functionality of river plumes as a refuge from predation was less clear. Importantly, high concentrations of larval fishes and zooplankton did not necessarily lead to high spatial overlap on fine scales (meters) relevant to larval fish trophic interactions, but these relationships were highly nuanced in space and time.

Our results help to fill gaps in our knowledge on how the physical environment can influence larval fish trophic interactions on small spatio-temporal scales. However, we also fully acknowledge the limitations of our study: this is a snapshot of a complex system, and trophic interactions are frequently species-specific. Further work would be useful to identify species-specific larval fish prey and predators in the NCC and to investigate annual variation in fine-scale larval fish prey availability and predation pressure near important habitats, like river plumes.

4.6. ISIIS and the importance of predation

High-resolution *in situ* sampling allowed us to evaluate the relationships between larval fishes, their prey, and their predators on fine spatial and temporal scales. Further, using ISIIS allowed us to explicitly investigate the role of potential predation in river plumes, an often-overlooked process determining larval fish survival. Traditional sampling techniques vastly underestimate fragile gelatinous taxa and thus the potential for predation on larval fishes. It is suggested that nets underestimate some groups of gelatinous zooplankton by 12 times (Remsen et al. 2004). Because predation may be the primary agent of larval fish mortality (Bailey & Houde 1989), understanding variations in growth, survival, and recruitment requires including accurate estimates of predation potential on fine scales.

Our sampling occurred during anomalously warm conditions in the NCC associated with a large-scale marine heatwave and El Niño forcing. This resulted in a shift in the zooplankton community from crustacean to gelatinous dominated (Brodeur et al. 2019), which likely contributed to the extremely high concentrations of some gelatinous predators observed in our sampling. Although it is difficult to say if the distributions we observed were typical for the NCC, our study certainly highlights the

need for better quantification of potential predation, especially in the context of changing ocean conditions that may favor gelatinous predator taxa. This will provide a better baseline for understanding how oceanographic conditions structure fine-scale zooplankton communities, which is critical for understanding the processes that drive adult population dynamics (Houde 2008).

5. ACKNOWLEDGEMENTS

We thank the 3 anonymous reviewers whose comments greatly improved this manuscript. We are grateful for the opportunity to have joined the 2016 NOAA-funded pre-recruit cruise. We thank the captain and crew of the RV 'Bell M. Shimada,' as well as those involved in the shore-based operations necessary for the successful completion of this work. We are particularly indebted to Jessica Luo, Kelly Robinson, H. William Fennie, Daniel Ottmann, and Toby Auth for their contributions in the field and lab. Finally, this work could not have been completed without image processing help from Christopher Sullivan and Michaela Buchanan at Oregon State University's Center for Genomic Research and Biocomputing. While preparing this manuscript, R.K.C., S.S., M.S.S., and C.B.A. were supported by NSF OCE 1737399.

6. REFERENCES

Acha EM, Piola A, Iribarne O, Mianzan H (2015) Ecological processes at marine fronts: oases in the ocean. Springer International Publishing, New York, NY

Albaina A, Irigoien X (2004) Relationships between frontal structures and zooplankton communities along a cross- shelf transect in the Bay of Biscay (1995 to 2003). Mar Ecol Prog Ser 284:65−75

Allen RL, Baltz DM (1997) Distribution and microhabitat use by flatfishes in a Louisiana estuary. Environ Biol Fish 50: 85−103

Alvarino A (1985) Predation in the plankton realm: mainly with reference to fish larvae. Inv Mar CICIMAR 2:1−122

Anderson MJ (2001) A new method for non-parametric multivariate analysis of variance. Austral Ecol 26:32−46

Axler KE, Sponaugle S, Hernandez F Jr, Culpepper C, Cowen RK (2020) Consequences of plume encounter on larval fish growth and condition in the Gulf of Mexico. Mar Ecol Prog Ser (in press) doi:10.3354/meps13396

Baier CT, Purcell JE (1997) Trophic interactions of chaetognaths, larval fish, and zooplankton in the South Atlantic Bight. Mar Ecol Prog Ser 146:43−53

Bailey K, Houde E (1989) Predation on eggs and larvae of marine fishes and the recruitment problem. Adv Mar Biol 25:1−83

Bakun A (2006) Fronts and eddies as key structures in the habitat of marine fish larvae: opportunity, adaptive response and competitive advantage. Sci Mar 70:105−122

Barnes C, Duxbury A, Morse B (1972) Circulation and selected properties of the Columbia River effluent at sea. In: Pruter A, Alveison D (eds) The Columbia River Estuary and adjacent ocean waters: bioenvironmental studies. University of Washington Press, Seattle, WA, p 71−80

Benoit-Bird KJ, McManus MA (2012) Bottom-up regulation of a pelagic community through spatial aggregations. Biol Lett 8:813−816

Benoit-Bird KJ, Cowles TJ, Wingard CE (2009) Edge gradients provide evidence of ecological interactions in planktonic thin layers. Limnol Oceanogr 54:1382−1392

Bezerra-Neto JF, Pinto-Coelho RM (2007) Diel vertical migration of the copepod *Thermocyclops inversus* (Kiefer, 1936) in a tropical reservoir: the role of oxygen and the spatial overlap with *Chaoborus*. Aquat Ecol 41: 535−545

Bowman M (1988) Estuarine fronts. In: Kjerfve B (ed) Hydrodynamics of estuaries. CRC Press, Boca Raton, FL, p 85−132

Brodeur RD, Auth TD, Phillips A (2019) Major shifts in pelagic micronekton and macrozooplankton community structure in an upwelling ecosystem related to an unprecedented marine heatwave. Front Mar Sci 6:212

Castro L, Cáceres M, Silva N, Muñoz M, León R, Landaeta M, Soto-Mendoza S (2011) Short-term variations in mesozooplankton, ichthyoplankton, and nutrients associated with semi-diurnal tides in a Patagonian Gulf. Cont Shelf Res 31:282−292

Cowen RK, Guigand CM (2008) *In situ* ichthyoplankton imaging system (ISIIS): system design and preliminary results. Limnol Oceanogr Methods 6:126−132

Cushing D (1990) Plankton production and year-class strength in fish populations: an update of the match/mis- match hypothesis. Adv Mar Biol 26:249−293

Eggleston DB, Armstrong DA, Elis WE, Patton WS (1998) Estuarine fronts as conduits for larval transport: hydrodynamics and spatial distribution of Dungeness crab

postlarvae. Mar Ecol Prog Ser 164:73−82
Elith J, Leathwick JR, Hastie T (2008) A working guide to boosted regression trees. J Anim Ecol 77:802−813
Emmett RL, Bentley PJ, Schiewe MH (1997) Abundance and distribution of northern anchovy eggs and larvae (*Engraulis mordax*) off the Oregon coast, mid-1970s vs.1994 and 1995. In: Proceedings of the International Symposium on the Role of Forage Fishes in Marine Eco- systems. Alaska Sea Grant College Program Rep 97-01. Alaska Sea Grant College Program, Fairbanks, AK, p 505−508
Emmett RL, Brodeur RD, Miller TW, Pool SS, Krutzikowsky GK, Bentley PJ, McCrae J (2005) Pacific sardine (*Sardinops sagax*) abundance, distribution, and ecological relationships in the Pacific Northwest. Calif Coop Ocean Fish Invest Rep 46:122−143
Emmett RL, Krutzikowsky GK, Bentley P (2006) Abundance and distribution of pelagic piscivorous fishes in the Columbia River plume during spring/early summer 1998−2003: relationship to oceanographic conditions, forage fishes, and juvenile salmonids. Prog Oceanogr 68:1−26
Faillettaz R, Picheral M, Luo JY, Guigand C, Cowen RK, Irisson JO (2016) Imperfect automatic image classification successfully describes plankton distribution patterns. Methods Oceanogr 15−16:60−77
Frost BW, Bollens SM (1992) Variability of diel vertical migration in the marine planktonic copepod *Pseudocalanus newmani* in relation to its predators. Can J Fish Aquat Sci 49:1137−1141
Gadomski DM, Boehlert GW (1984) Feeding ecology of pelagic larvae of English sole *Parophrys vetulus* and butter sole *Isopsetta isolepis* off the Oregon coast. Mar Ecol Prog Ser 20:1−12
García Berdeal I, Hickey B, Kawase M (2002) Influence of wind stress and ambient flow on a high discharge river plume. J Geophys Res 107:13−24
Gorsky G, Ohman MD, Picheral M, Gasparini S and others (2010) Digital zooplankton image analysis using the ZooScan integrated system. J Plankton Res 32: 285−303
Govoni JJ (1997) The association of the population recruitment of gulf menhaden, *Brevoortia patronus*, with Mississippi River discharge. J Mar Syst 12:101−108
Govoni JJ, Chester AJ (1990) Diet composition of larval *Leiostomus xanthurus* in and about the Mississippi River plume. J Plankton Res 12:819−830
Graham B (2015) Fractional max-pooling. arXiv:1412.6071
Graham WM, Pagès F, Hamner WM (2001) A physical context for gelatinous zooplankton aggregations: a review. Hydrobiologia 451:199−212
Grantham BA, Chan F, Nielsen KJ, Fox DS and others (2004) Upwelling-driven nearshore hypoxia signals ecosystem and oceanographic changes in the northeast Pacific. Nature 429:749−754
Greenwell B, Boehmke B, Cunningham J (2019) gbm: generalized boosted regression models. R package version 2.1.5. https://cran.r-project.org/web/packages/gbm/index.html
Greer AT, Cowen RK, Guigand CM, McManus MA, Sevadjian JC, Timmerman AH (2013) Relationships between phytoplankton thin layers and the fine-scale vertical dis- tributions of two trophic levels of zooplankton. J Plankton Res 35:939−956
Grimes CB, Finucane JH (1991) Spatial distribution and abundance of larval and juvenile fish, chlorophyll and macrozooplankton around the Mississippi River dis-

charge plume, and the role of the plume in fish recruitment. Mar Ecol Prog Ser 75:109−119

Henderikx Freitas F, Salidas GS, Goni M, Shearman RK, White AE (2018) Temporal and spatial dynamics of physical and biological properties along the endurance array of the Cal- ifornia Current ecosystem. Oceanography 31:80−89

Hickey B, Pietrafesa L, Jay D, Boicourt W (1998) The Columbia River Plume study: subtidal variability in the velocity and salinity fields. J Geophys Res 103:10339−10368

Hickey B, Geier S, Kachel N, MacFadyen A (2005) A bi- directional river plume: the Columbia in summer. Cont Shelf Res 25:1631−1656

Hijmans RJ, Phillips S, Leathwick J, Maintainer JE (2017) dismo: species distribution modeling. R package version 1.1-4. https://cran.r-project.org/web/packages/dismo/dismo.pdf

Horner-Devine AR, Jay DA, Orton PM, Spahn EY (2009) A conceptual model of the strongly tidal Columbia River plume. J Mar Syst 78:460−475

Houde ED (2008) Emerging from Hjort's shadow. J Northw Atl Fish Sci 41:53−70

Hu Q, Davis C (2006) Accurate automatic quantification of taxa-specific plankton abundance using dual classification with correction. Mar Ecol Prog Ser 306:51−61

Hunter JR (1972) Swimming and feeding behavior of larval anchovy *Engraulis mordax*. Fish Bull 70:821−838

Ignatyev S (1997) Pelagic fishes and their macroplankton prey: swimming speeds. In: Proceedings of the International Symposium on the Role of Forage Fishes in Marine Ecosystems. Alaska Sea Grant College Program Rep 97-01. Alaska Sea Grant College Program, Fairbanks, AK, p 31−39

Kashef NS, Sogard SM, Fisher R, Largier JL (2014) Ontogeny of critical swimming speeds for larval and pelagic juvenile rockfishes (*Sebastes* spp., family Scorpaenidae). Mar Ecol Prog Ser 500:231−243

Lasker R (1975) Field criteria for survival of anchovy larvae: the relation between inshore chlorophyll maximum layers and successful first feeding. Fish Bull 73:453−462

LeCun Y, Bengio Y, Hinton G (2015) Deep learning. Nature 521:436−444

Lieske DJ, Schmid MS, Mahoney M (2018) Ensembles of ensembles: combining the predictions from multiple machine learning methods. In: Humphries G, Magness D, Huettmann F (eds) Machine learning for ecology and sustainable natural resource management. Springer International Publishing, Cham, p 109−121

Llopiz J (2013) Latitudinal and taxonomic patterns in the feeding ecologies of fish larvae: a literature synthesis. J Mar Syst 109−110:69−77

Llopiz JK, Cowen RK (2009) Variability in the trophic role of coral reef fish larvae in the oceanic plankton. Mar Ecol Prog Ser 381:259−272

Llopiz JK, Richardson DE, Shiroza A, Smith SL, Cowen RK (2010) Distinctions in the diets and distributions of larval tunas and the important role of appendicularians. Limnol Oceanogr 55:983−996

Lochmann S, Taggart C, Griffin D, Thompson K, Maillet G (1997) Abundance and condition of larval cod (*Gadus morhua*) at a convergent front on Western Bank, Scotian Shelf. Can J Fish Aquat Sci 54:1461−1479

Luo JY, Grassian B, Tang D, Irisson JO and others (2014) Environmental drivers of the

fine-scale distribution of a gelatinous zooplankton community across a mesoscale front. Mar Ecol Prog Ser 510:129−149

Luo JY, Irisson JO, Graham B, Guigand C, Sarafraz A, Mader C, Cowen RK (2018) Automated plankton image analysis using convolutional neural networks. Limnol Oceanogr Methods 16:814−827

Mather PM (1976) Computational methods of multivariate analysis in physical geography. John Wiley & Sons, London

McClatchie S, Cowen R, Nieto K, Greer A and others (2012) Resolution of fine biological structure including small narcomedusae across a front in the Southern California Bight. J Geophys Res 117:C04020

McCune B, Grace JB (2002) Analysis of ecological communities. MJM Software Design, Gleneden Beach, OR

Möller KO, St. John M, Temming A, Floeter J, Sell AF, Herrmann JP, Möllmann C (2012) Marine snow, zooplankton and thin layers: indications of a trophic link from small- scale sampling with the Video Plankton Recorder. Mar Ecol Prog Ser 468:57−69

Morgan CA, De Robertis A, Zabel RW (2005) Columbia River plume fronts. I. Hydrography, zooplankton distribution, and community composition. Mar Ecol Prog Ser 299:19−31

Munk P (2007) Cross-frontal variation in growth rate and prey availability of larval North Sea cod *Gadus morhua*. Mar Ecol Prog Ser 334:225−235

Oh SY, Kim CK, Jang YS, Choi HJ, Myoung JG (2014) Effect of salinity on survival, oxygen consumption and blood physiology of Korean rockfish *Sebastes schlegelii*. Ocean Polar Res 36:135−143

Oksanen J, Blanchet FG, Friendly M, Kindt R and others (2019) Vegan: community ecology package. R package version 2.5-6. https://cran.r-project.org/web/packages/vegan/vegan.pdf

Orenstein EC, Beijbom O, Peacock EE, Sosik HM (2015) WHOI-Plankton— a large scale fine grained visual recognition benchmark dataset for plankton classification.arXiv:1510.00745v1

Parnel MM, Emmett RL, Brodeur RD (2008) Ichthyoplankton community in the Columbia River plume off Oregon: effects of fluctuating oceanographic conditions. Fish Bull 106:161−173

Pepin P, Robert D, Bouchard C, Dower JF and others (2015) Once upon a larva: revisiting the relationship between feeding success and growth in fish larvae. ICES J Mar Sci 72:359−373

Peterson WT, Miller CB (1975) Year-to-year variations in the planktology of the Oregon upwelling zone. Fish Bull 73: 642−653

Peterson JO, Peterson WT (2008) Influence of the Columbia River plume (USA) on the vertical and horizontal distribution of mesozooplankton over the Washington and Oregon shelf. ICES J Mar Sci 65:477−483

Peterson JO, Peterson WT (2009) Influence of the Columbia River plume on cross-shelf transport of zooplankton. J Geophys Res 114:1−11

Picapedra PHS, Lansac-Tôha FA, Bialetzki A (2015) Diel vertical migration and spatial overlap between fish larvae and zooplankton in two tropical lakes, Brazil. Braz J Biol 75:352−361

Purcell J (1985) Predation on fish eggs and larvae by pelagic cnidarians and ctenophores. Bull Mar Sci 37:739−755

Purcell JE, Arai MN (2001) Interactions of pelagic cnidarians and ctenophores with fish: a review. Hydrobiologia 451: 27−44

Reiss CS, McConaugha JR (1999) Cross-frontal transport and distribution of ichthyoplankton associated with Chesapeake Bay plume dynamics. Cont Shelf Res 19:151−170

Remsen A, Hopkins TL, Samson S (2004) What you see is not what you catch: a comparison of concurrently collected net, Optical Plankton Counter, and Shadowed Image Particle Profiling Evaluation Recorder data from the northeast Gulf of Mexico. Deep Sea Res I 51:129−151

Richardson SL (1981) Spawning biomass and early life of northern anchovy, *Engraulis mordax*, in the northern subpopulation off Oregon and Washington. Fish Bull 78: 855−876

Roman M, Zhang X, McGilliard C, Boicourt W (2005) Seasonal and annual variability in the spatial patterns of plankton biomass in Chesapeake Bay. Limnol Oceanogr 50:480−492

Schmid MS, Cowen RK, Robinson K, Luo JY, Briseño-Avena C, Sponaugle S (2020) Prey and predator overlap at the edge of a mesoscale eddy: fine-scale, in-situ distributions to inform our understanding of oceanographic processes. Sci Rep 10:921

Shulzitski K, Sponaugle S, Hauff M, Walter K, D'Alessandro EK, Cowen RK (2015) Close encounters with eddies: oceanographic features increase growth of larval reef fishes during their journey to the reef. Biol Lett 11:20140746

Shulzitski K, Sponaugle S, Hauff M, Walter KD, Cowen RK (2016) Encounter with mesoscale eddies enhances survival to settlement in larval coral reef fishes. Proc Natl Acad Sci USA 113:6928−6933

Sponaugle S, Llopiz JK, Havel LN, Rankin TL (2009) Spatial variation in larval growth and gut fullness in a coral reef fish. Mar Ecol Prog Ser 383:239−249

St. John MA, MacDonald JS, Harrison PJ, Beamish RJ, Choromanski E (1992) The Fraser River plume: some preliminary observations on the distribution of juvenile salmon, herring, and their prey. Fish Oceanogr 1: 153−162

Tharwat A (2018) Classification assessment methods. Appl Comput Inf, https://doi.org/10.1016/j.aci.2018.08.003

Watanabe K, Kasai A, Antonio ES, Suzuki K, Ueno M, Yamashita Y (2014) Influence of salt-wedge intrusion on eco- logical processes at lower trophic levels in the Yura Estuary, Japan. Estuar Coast Shelf Sci 139:67−77

Williamson CE, Stoeckel ME (1990) Estimating predation risk in zooplankton communities: the importance of vertical overlap. Hydrobiologia 198:125−131

Table 4.1. Mean (SE) taxa concentrations per depth bin along the sampling transect for all sampling (total) and each sampling transect near the Columbia River Plume including the significance of a Kruskal-Wallis (K-W) test for differences in mean concentrations in the plume (P) vs. outside of the plume (NP). Taxa are in descending order based on their concentrations within each sampling regime. K-W test significance: *p < 0.001, **p < 0.0001, (–): not significant. Sample sizes for concentration (n1) and K-W estimates (n2) are indicated under each transect. NA: no K-W test was performed due to a lack of plume waters

Transect	Taxon	Mean concentration (ind. m^{-3})	SE	K-W (P/NP)
Total	Appendicularians	81.14	1.26	**
n1 = 7504	Calanoid copepods	15.05	0.22	**
n2 (P/NP) = 2459/5045	Hydromedusae	9.06	0.24	**
	Chaetognaths	7.04	0.12	**
	Ctenophores	2.01	0.04	**
	Siphonophores	1.97	0.03	**
	Fish larvae	0.11	0.00	**
Transect 1 (Ebb)	Appendicularians	50.04	1.09	**
n1= 1835	Calanoid copepods	14.06	0.40	**
n2 (P/NP) = 575/1260	Hydromedusae	11.79	0.45	**
	Chaetognaths	9.30	0.27	**
	Ctenophores	2.41	0.08	**
	Siphonophores	2.11	0.07	**
	Fish larvae	0.09	0.00	**
Transect 2 (Flood)	Appendicularians	50.04	1.15	**
n1 = 2337	Hydromedusae	13.43	0.62	**
n2 (P/NP) = 838/1499	Calanoid copepods	11.85	0.33	**
	Chaetognaths	11.45	0.27	**
	Ctenophores	2.51	0.08	**
	Siphonophores	2.32	0.06	**
	Fish larvae	0.12	0.01	**
Transect 3 (inshore)	Appendicularians	219.56	5.24	**
n1 = 1211	Calanoid copepods	33.86	0.78	**
n2 (P/NP) = 213/998	Hydromedusae	7.64	0.49	—
	Chaetognaths	5.01	0.15	**
	Siphonophores	2.41	0.09	*
	Ctenophores	2.37	0.08	**
	Fish larvae	0.16	0.01	**
Transect 3 (offshore)	Appendicularians	61.26	1.25	NA
n1 = 2121	Calanoid copepods	8.25	0.20	NA
	Hydromedusae	2.59	0.10	NA
	Chaetognaths	1.34	0.04	NA
	Siphonophores	1.18	0.04	NA
	Ctenophores	0.86	0.03	NA
	Fish larvae	0.10	0.01	NA

Table 4.2. Mean taxa size (mm) and standard error for each sampling transect near the Columbia River Plume

	Transect 1 (Ebb)		Transect 2 (Flood)		Transect 3 (inshore)		Transect 3 (offshore)	
	Mean	SE	Mean	SE	Mean	SE	Mean	SE
Fish larvae	5.70	0.09	5.54	0.08	7.88	0.12	6.63	0.09
Calanoid Copepods	2.72	0.01	2.77	0.01	3.64	0.01	2.22	0.01
Appendicularians	2.80	0.00	2.80	0.00	2.77	0.00	2.73	0.00
Chaetognaths	6.59	0.01	7.03	0.02	8.36	0.03	8.29	0.04
Ctenophores	4.51	0.03	4.18	0.03	4.50	0.04	8.62	0.11
Hydromedusae	14.67	0.05	15.28	0.05	12.18	0.08	5.31	0.05
Siphonophores	9.42	0.03	9.08	0.04	6.93	0.06	6.16	0.07

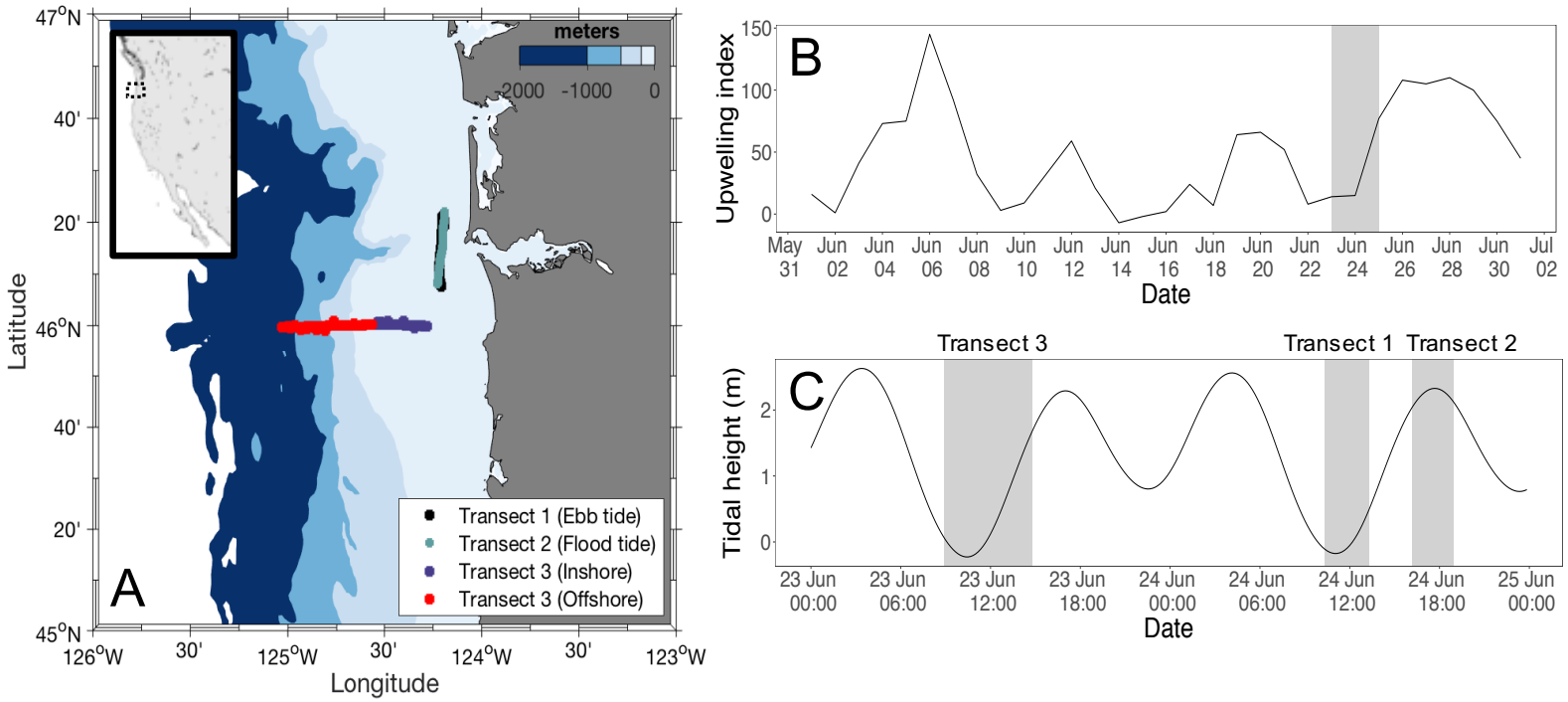

Fig. 4.1. (A) Study area, showing the 2 cross-plume transects and the cross-shelf transect in relation to the mouth of the Columbia River on 23–24 June 2016. Depth contours are the 200, 500, 1000, and 2000 m isobaths. (B) Bakun upwelling index values for 45° N during the month that sampling occurred, with the grey box highlighting our sampling dates. (C) Tidal height estimates (meters above Mean Lower Low Water) for Astoria, Oregon (CoOp, National Ocean Service, NOAA, Station 9349040). Grey shaded regions indicate sampling periods during the transects (shown in A). Times are in Pacific Daylight Time (PDT)

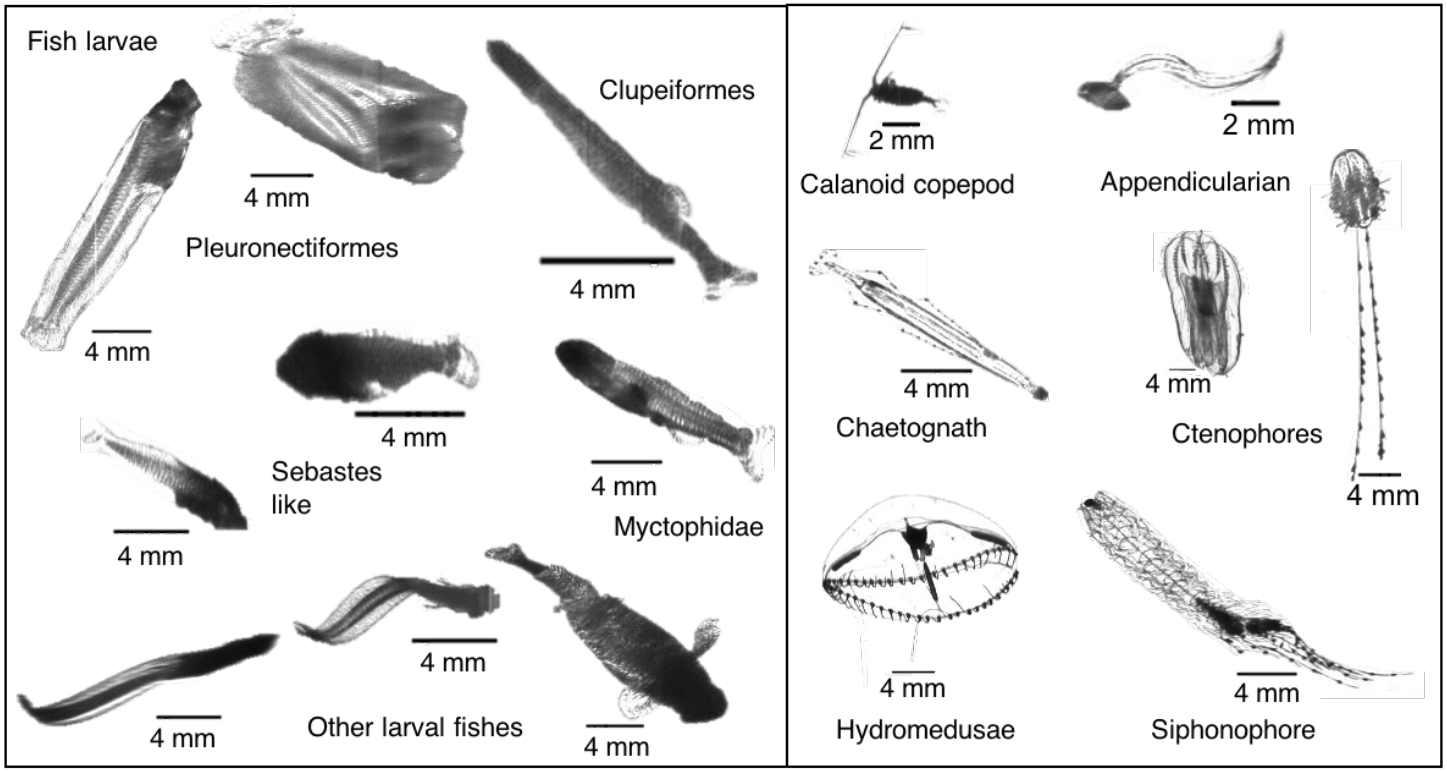

Fig. 4.2. Images of representative plankton taxa taken by the *In situ* Ichthyoplankton Imaging System (ISIIS) in the northern California Current

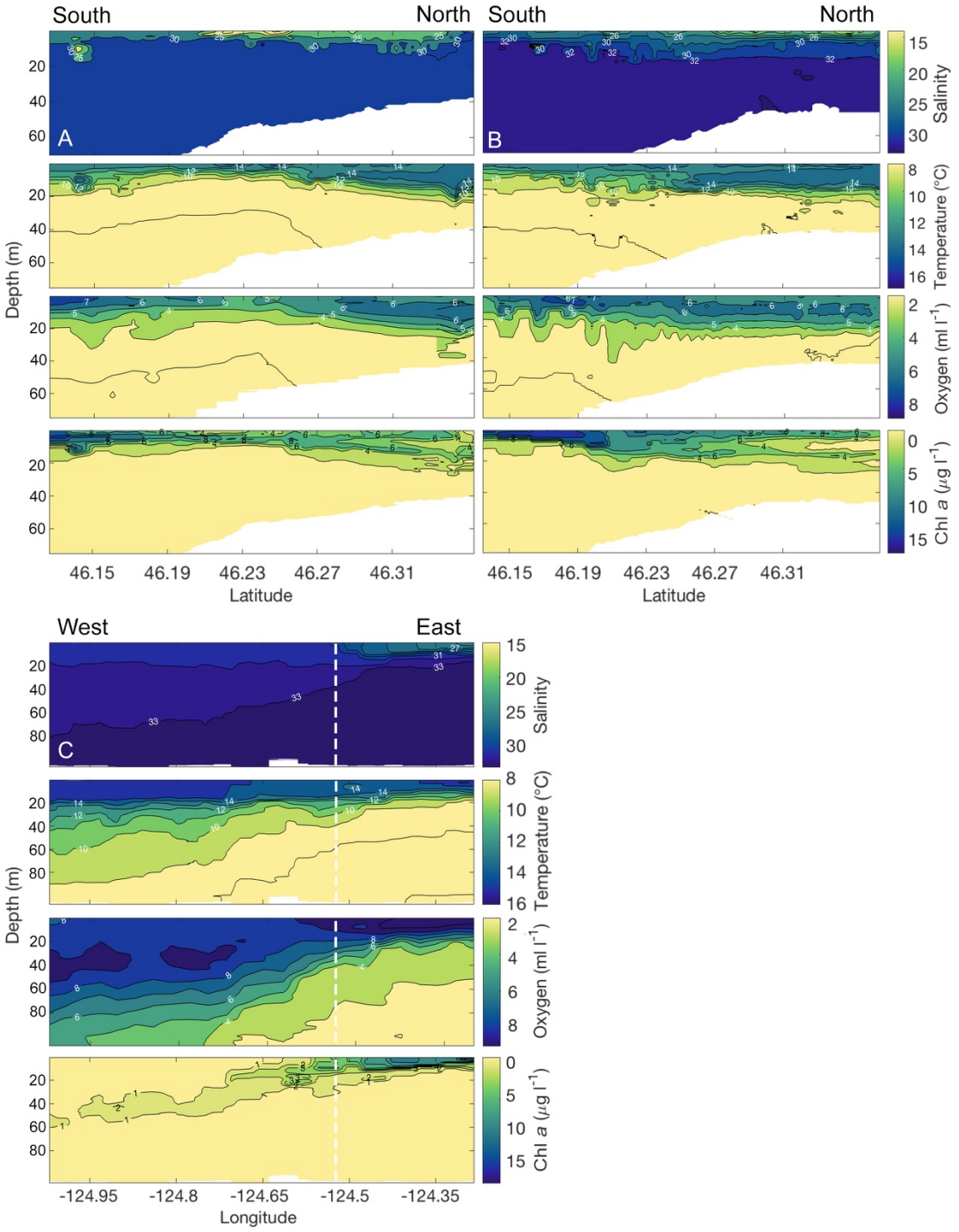

Fig. 4.3. Kriged contour plots of environmental parameters during (A) Transect 1 (ebb), (B) Transect 2 (flood), and (C) Transect 3 near and within the Columbia River Plume. The dashed line in C indicates the cutoff between the inshore and offshore regions used in analyses. Chl *a*: chlorophyll *a* concentration.

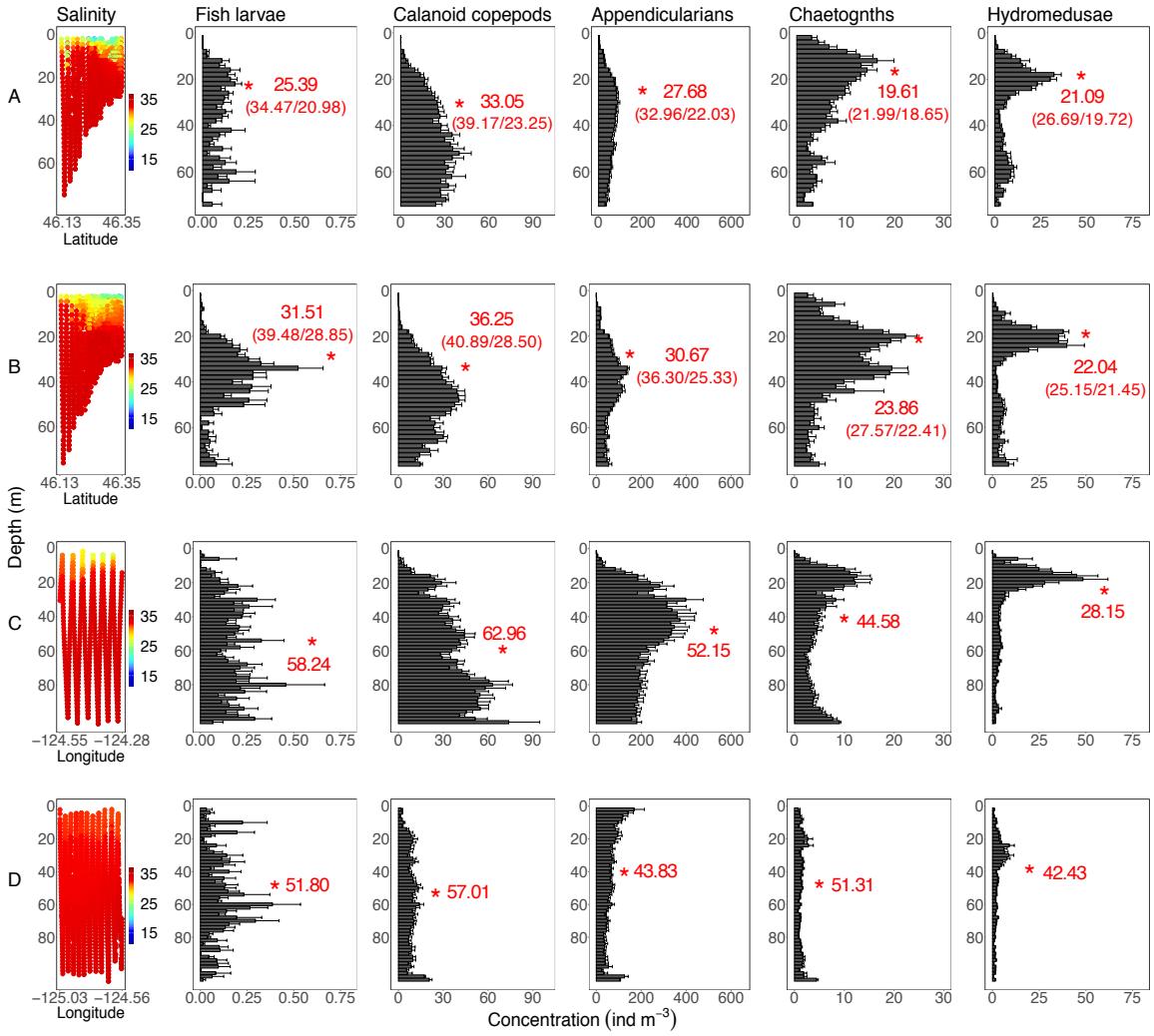

Fig. 4.4. Mean concentration of each taxonomic group in every other 1 m depth bin during (A) Transect 1, (B) Transect 2, (C) Transect 3 inshore, and (D) Transect 3 offshore of the Columbia River, with transect salinity profiles shown in the far left column. Error bars are standard error, and red asterisks indicate the weighted mean depth (WMD; in meters) of taxa distributions. For transects (A) and (B), we also give separate WMDs for the southern (deep) and northern (shallow) sections of the transect separately as (south/north)

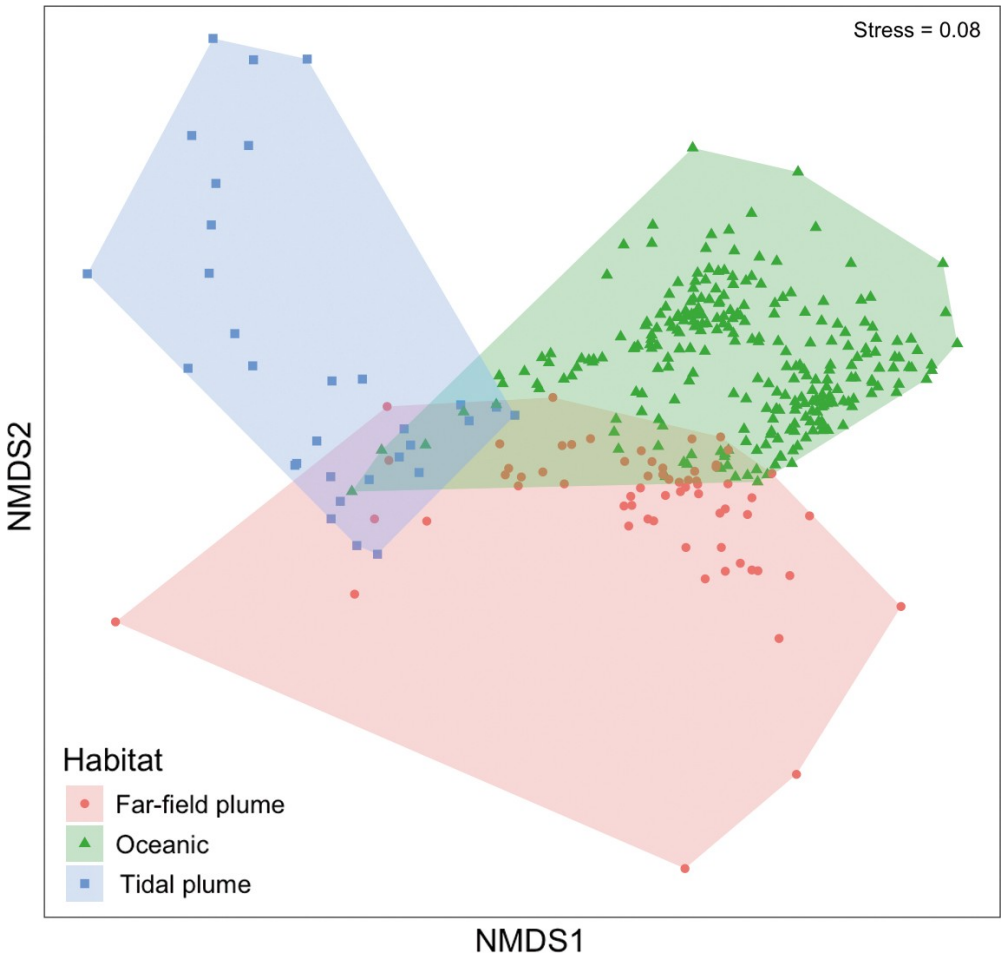

Fig. 4.5. Non-metric multidimensional scaling (NMDS) ordination of zooplankton taxa concentrations in 3 different habitats near the Columbia River Plume. Each data point represents the community composition in a 1 m vertical depth bin along the sampling transects. Tidal plume samples are those within plume waters directly off of the river mouth, far-field plume samples are plume waters south of the river mouth, and oceanic samples are those with salinity >32.5. Stress (a measure of goodness-of-fit) is indicated in the top right corner

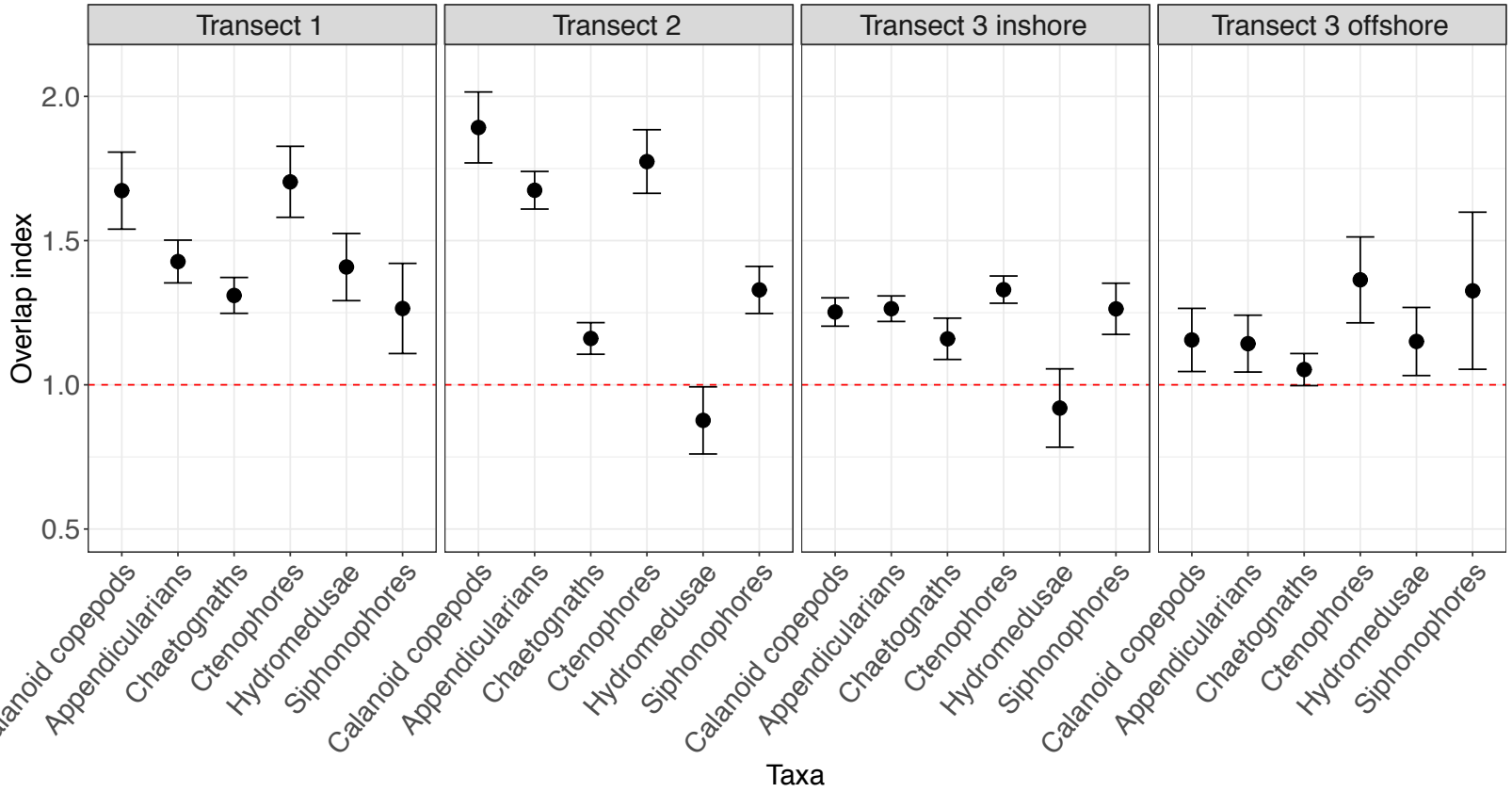

Fig. 4.6. Median spatial overlap of selected prey and predator groups with fish larvae in transects near and within the Columbia River Plume. Black markers are estimates of the Williamson spatial overlap index during each sampling transect. Overlap index values = 1 (red dashed line) indicate that fish larvae and the taxonomic group are evenly distributed in the water column; index values <1 indicate some degree of vertical separation between fish larvae and the group; index values >1 indicate some degree of vertical overlap of fish larvae and the group in any layer of the water column. Error bars are standard error

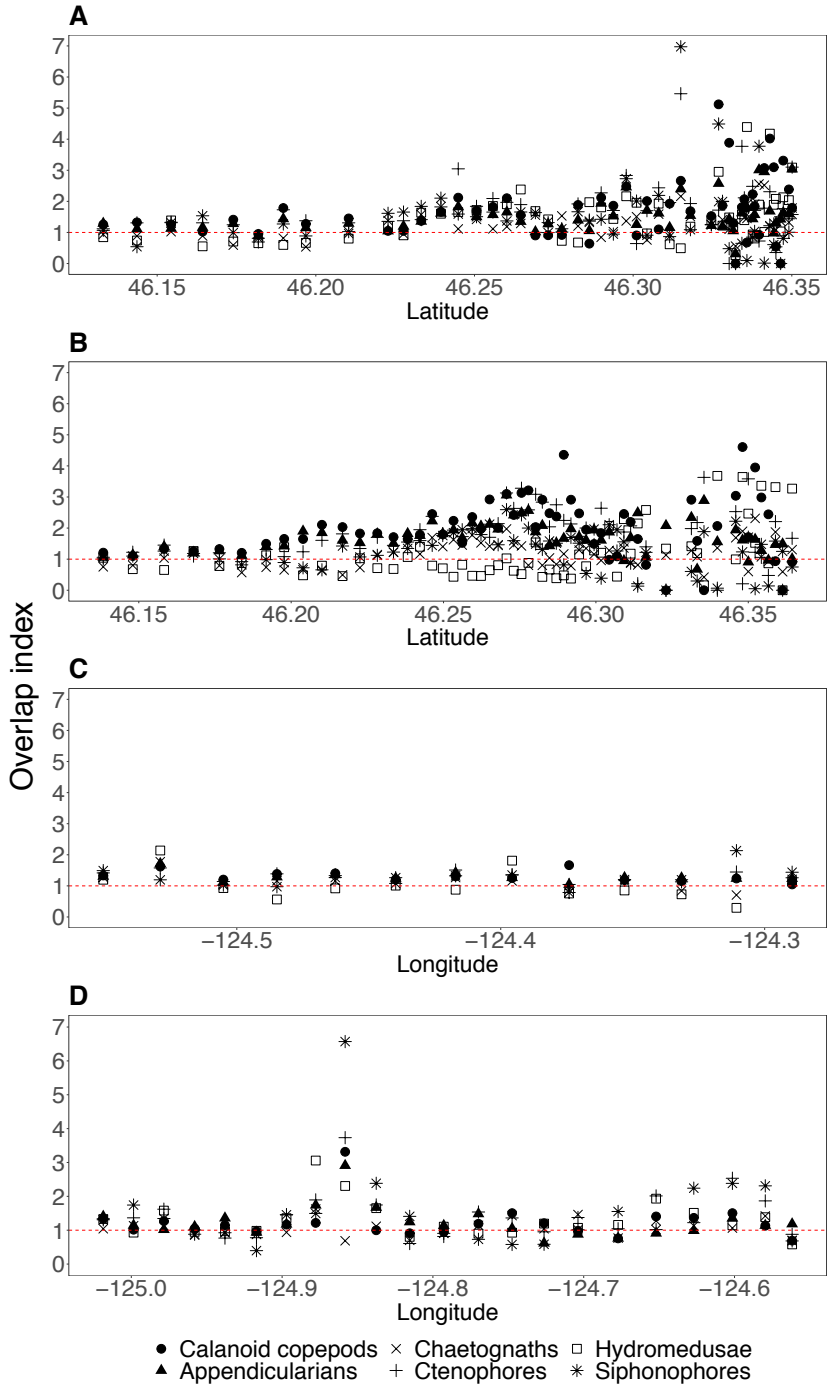

Fig. 4.7. Spatial overlap between fish larvae and selected prey and predator groups along (A) Transect 1, (B) Transect 2, (C) Transect 3 inshore, and (D) Transect 3 offshore near and within the Columbia River Plume. Markers are estimates of the Williamson spatial overlap index for each quasi-vertical profile; details as in Fig. 4.6.

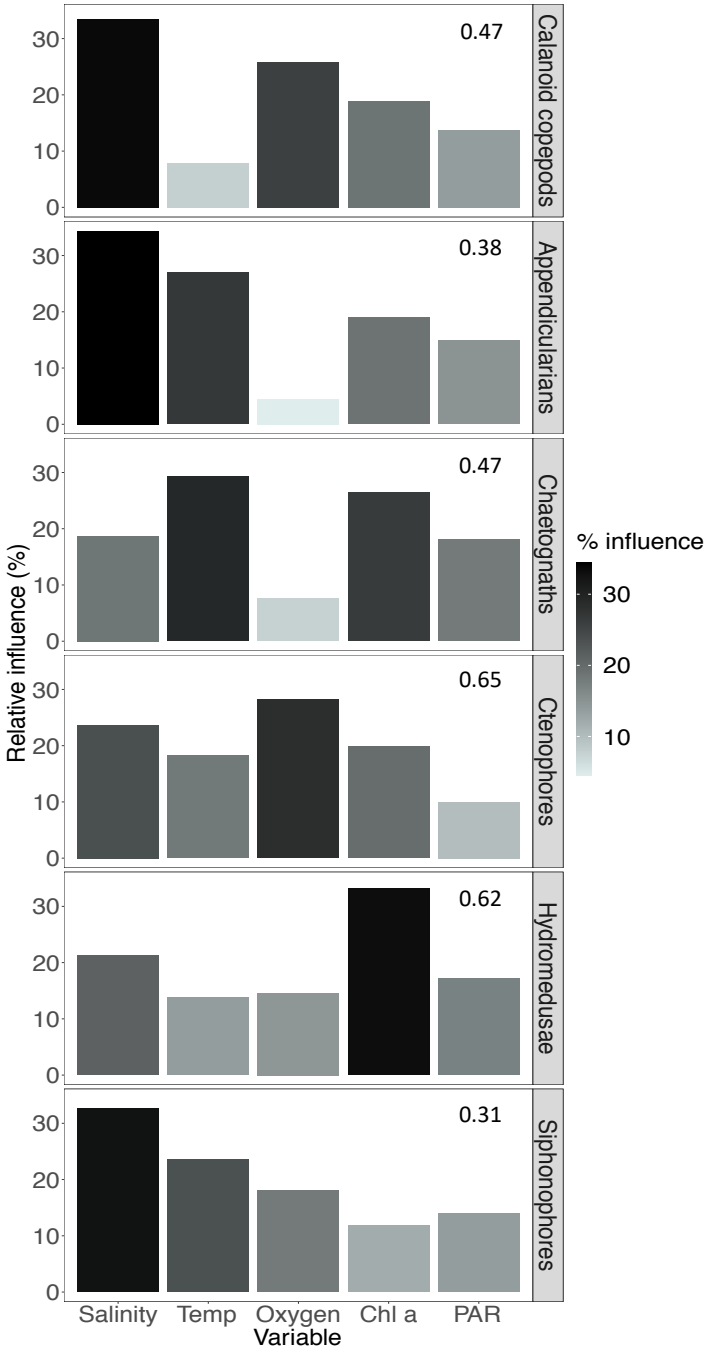

Fig. 4.8. Results of the boosted regression tree (BRT) analysis showing the relative influence of surface physical variables on the spatial overlap of each taxon with fish larvae near and within the Columbia River Plume. Associated model deviance explained (D^2) values are in the top right corner of each plot. Chl *a*: chlorophyll *a* concentration; PAR: photosynthetically active radiation

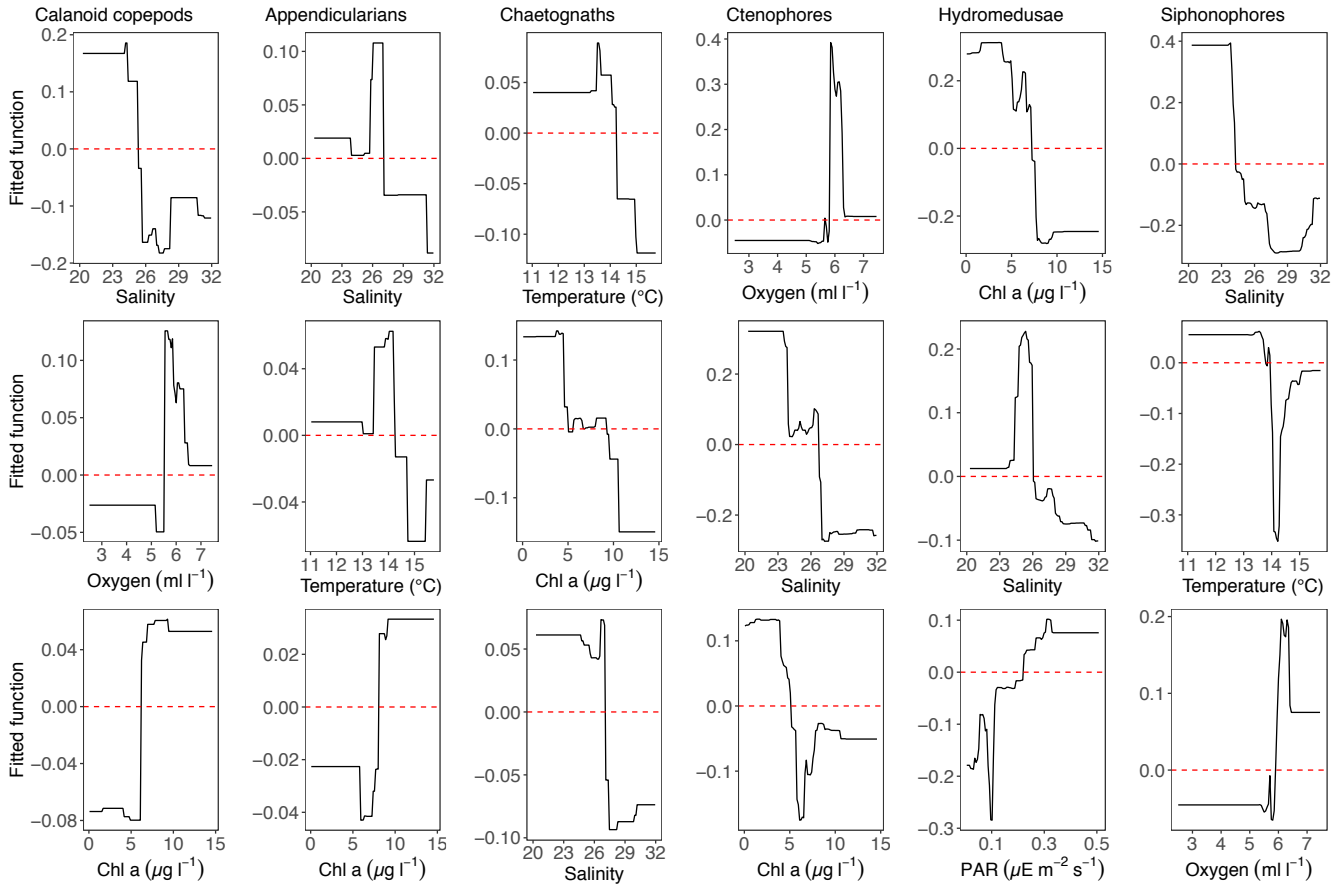

Fig. 4.9. Partial dependence plots of the top 3 most important explanatory variables in the likelihood of spatial overlap of larval fishes and each taxon sampled in the vicinity of the Columbia River from the boosted regression tree (BRT) analysis. Each column shows the results from a particular model and is organized in descending order of importance from top to bottom. A fitted value of 0 (red dotted line) represents a model prediction of average spatial overlap of the taxa with fish larvae; negative fitted values indicate below-average predicted overlap; positive fitted values indicate above-average predicted overlap. Chl *a*: chlorophyll *a* concentration; PAR: photosynthetically active radiation

Chapter 5: Offshore distribution of Dungeness crab zoea in the northern California Current

This chapter was completed in partial fulfillment of the National Science Foundation Research Traineeship (NRT) program at Oregon State University.

CHAPTER 5 CONTEXT

The following study was done in partial fulfillment of the National Science Foundation Research Traineeship (NRT) program at Oregon State University. This novel program was designed to foster the development of innovative and collaborative natural resource scientists and managers. Participating students are trained to holistically tackle complex environmental issues using a transdisciplinary approach and in the context of coupled human-natural systems. NRT programmatic elements include a year-long cross-disciplinary research project supported by a competitive fellowship, coursework focused on the themes of 'big data', 'risk and uncertainty', 'earth systems', and 'social systems', professional development seminars emphasizing collaborative working structures and the communication of risk and uncertainty, and an internship. NRT products include: (1) a graduate minor in Risk and Uncertainty Quantification and Communication in Earth Systems, (2) a group project Transdisciplinary Report, and (3) an individual Interdisciplinary Thesis Chapter.

I was part of a team that consisted of ecologists, geneticists, social scientists, and mathematicians. We investigated how changing ocean conditions affect commercial catch of Dungeness crab (*Cancer magister*) and the associated fishing communities of the U.S. West coast. We found that oceanographic conditions substantially impact Dungeness crab catch per unit effort (CPUE). In particular, modeling revealed that sea surface temperature scenarios for 2080 (+1.7 °C and +2.8 °C) reduced Dungeness crab CPUE by 30-100%, depending on fishing port latitude. This finding suggests that U.S. West Coast communities are differentially susceptible to a decline in Dungeness crab catch. Importantly, varying levels of risk (a combination of exposure and susceptibility) for fishing ports did not necessarily align with regional or fishery management boundaries thereby reducing this fisheries adaptability under future climate scenarios. Our transdisciplinary report was published in *Frontiers in Marine Science* (Magel et al. 2020).

The following study constitutes my Interdisciplinary Thesis Chapter which builds upon our project Transdisciplinary Report and subsequent publication to emphasize my area of expertise, plankton ecology and fisheries oceanography. I focus on describing the poorly understood offshore distribution of larval Dungeness crab. Late-stage megalopal recruitment to nearshore environments has been linked to lagged fishery production

(Shanks & Roegner 2007, Shanks et al. 2010, Shanks 2013), but these studies only indirectly address the most vulnerable earlier pelagic larval stages. A missing piece of information that could improve our understanding of adult crab supply to U.S. West coast communities is knowledge of the spatial and temporal distribution and survival of the vulnerable early (zoeal) pelagic stages.

CHAPTER 5: Offshore distribution of Dungeness crab zoea in the northern California Current

Abstract

Dungeness crab (*Cancer magister*) is frequently the most lucrative fishery on the U.S. West coast, yet landings can fluctuate by an order of magnitude over both spatial and temporal scales. Like most marine taxa with bi-phasic life histories, the pelagic larval stages of Dungeness crab experience high rates of mortality and are considered a bottleneck for fishery production. As such, nearshore arrival of late-stage megalopae has been used to predict lagged commercial catch. However, this approach only indirectly addresses the most vulnerable early pelagic stages (zoea) and assumes a uniform larval distribution offshore. We examined the interannual, latitudinal, cross-shelf, vertical, and diel distributions of Dungeness crab zoea along two historically sampled transects in the northern California Current during the winters of 2018 and 2019. In total, we collected 14,314 Dungeness crab zoea from 102 depth-stratified samples. These data revealed that zoeal abundance was significantly negatively correlated with *in situ* temperature and salinity throughout ontogeny. Zoea were not uniformly distributed in time or space, but exhibited distinct spatial distributions within the water column, over the continental shelf, and across latitudes each year. Zoea were significantly more abundant off Oregon than northern California during both years of sampling. Larvae generally exhibited an ontogenetic shift in their cross-shelf distribution, with later stage zoea found progressively farther offshore. Zoea were concentrated in the upper 25 m of the water column throughout sampling, but concentrations within the top 100 m were substantially greater during the night compared to the day, suggesting that zoea may undergo substantial diel vertical migrations. These fine-scale offshore zoeal distributions provide context for previously described patterns between oceanographic conditions, megalopal recruitment, and fishery catch.

1. INTRODUCTION

Dungeness crab (*Cancer magister*) is often the most economically valuable single-species fishery in the California Current Ecosystem. Although the fishery frequently boasts an annual coastwide ex-vessel value >$90 million, interannual landings of Dungeness crab can fluctuate by an order of magnitude (reviewed in Rasmuson 2013, CDFW 2018, ODFW 2018, WDFW 2018). The implications of dramatic fluctuations in Dungeness crab catch propagate through ecological and social systems, affecting management strategies, the fishing industry, and the livelihoods of local communities (Botsford et al. 1983, Methot 1986, Rasmuson 2013). Because fishing pressure is high – more than 90% of all legally sized male crabs are harvested each year – fluctuations in catch are thought to accurately reflect changes in adult year class strength (Hackett et al. 2003).

Harvest variability (proxy for adult abundance) is linked to Dungeness crab early life history success (McKelvey et al. 1980, Shanks et al. 2010, Shanks 2013). Like most marine taxa with bi-phasic life cycles, the larval stages of Dungeness crab experience high rates of mortality and are considered to be a bottleneck for fishery production. Survival during these stages is strongly impacted by the prevailing ocean conditions which affect larval vital rates and distributions (Thorson 1946, reviewed in Botsford et al. 1989, and Rasmuson 2013).

The early life history dynamics of Dungeness crab are complex because of its long pelagic larval duration. In the California Current, Dungeness crab eggs hatch in January-March and then pass through five pelagic zoeal stages (Z1 - Z5) and one pelagic megalopal stage over a period of 3-4 months (Poole 1966, Shanks 2009). As they develop, zoea move progressively farther offshore and are transported northward by the Davidson Current and then back southward by the California Current. It is generally thought that southward transport occurs after the annual spring transition with the onset of north winds when the southward flowing California Current extends onto the continental shelf. However, some southward transport may occur prior to the spring transition if larvae are transported far enough offshore (Lough 1975, Wild & Tasto 1983, Shanks & Roegner 2007, Shanks 2013). After metamorphosis, megalopae recruit to nearshore environments via internal waves during upwelling events (Jamieson & Phillips

1988, Shanks 2006, Rasmuson 2013). Settled megalopae continue to grow as juveniles and subadults, becoming available to the fishery at age 4.

Nearshore megalopal abundance has been used to predict California Current Dungeness crab commercial catch, lagged by 4 yrs (i.e., age of entry to the fishery; Shanks & Roegner 2007, Shanks et al. 2010, Shanks 2013). Megalopal recruitment patterns are influenced by a series of atmospheric and climatic forces through their impacts on larval transport. Recruitment is high in years with an early spring transition (Shanks & Roegner 2007), negative Pacific Decadal Oscillation (PDO; Shanks et al. 2010), and strong upwelling (Shanks 2013). It is hypothesized that in years with a positive PDO, the southward flowing California Current is weaker (Minobe & Mantua 1999) and larvae transported northward in the Davidson Current may not experience enough southward transport to return to Oregon and California coasts for settlement.

These studies provide valuable insights into the relationship between recruitment and oceanographic conditions, yet they fail to directly address the most vulnerable pelagic larval stages. By sampling only megalopae and correlating their nearshore patterns of abundance to offshore physical processes most studies have assumed a uniform distribution of zoea in space. A missing piece of information that could improve commercial catch predictions is detailed knowledge of the offshore distribution of pelagic Dungeness crab zoea and how zoeal distributions are related to physical parameters. Depth-stratified winter sampling of zooplankton is not frequently conducted in the northern California Current even though knowledge of the fine-scale zoeal distributions would provide context for the patterns described between Dungeness crab recruitment and oceanographic conditions.

Laboratory-based experiments indicate that Dungeness crab zoea are sensitive to temperature and, to a lesser extent, salinity. Normal zoeal development occurs over a temperature range of 10.0-13.9°C and a salinity range of 25-30, with the duration of each developmental stage decreasing as water temperature increases. Zoea experience the highest rates of survival at 10°C. At temperatures > 14°C zoea experience substantial mortality increasing to 100% mortality by 20°C (Des Voigne 1973, Ebert et al. 1983, Sulkin & McKeen 1989). After recruitment, juvenile Dungeness crabs experience little to no mortality at temperatures up to 25°C (Des Voigne 1973). These data suggest that the

pelagic zoeal stage is most vulnerable to ocean temperature, with implications for mortality and subsequent recruitment. While field-based attempts to comprehensively describe offshore zoeal distributions suggest a lack of correlation between zoeal abundance and temperature, these studies were based on surface hydrographic data and coarse sampling with oblique and neuston tows (Hobbs et al. 1992). Such methods may obscure real relationships between zoeal distributions and physical parameters.

The paucity of data on the Dungeness crab zoeal stages has limited our ability to predict the effects of ocean conditions on one of the U.S. West coast's most valuable fisheries. Investigating relationships between the offshore distribution of zoea and the physical conditions in which they exist is necessary to ultimately understand how oceanography affects the fishery and the coastal communities that rely on it for their livelihoods. The present study examines the offshore latitudinal, cross-shelf, vertical, and diel distribution of Dungeness crab zoea in the context of oceanographic parameters in the northern California Current. Through this baseline work we hope to contribute to our understanding of how future ocean conditions may impact this important fishery.

2. MATERIALS AND METHODS

2.1 Field sampling

To describe the offshore distribution of Dungeness crab (*Cancer magister*) zoea, we collected depth-discrete zooplankton samples during two northern California Current research cruises in the winters of 2018 (15-23 Feb) and 2019 (3-11 Mar). Sampling occurred at six stations along two historically sampled cross-shelf transects: the Newport Hydrographic Line (NH) off the central coast of Oregon and the Trinidad Head Line (TR) off of northern California. Station locations were selected to capture shelf (Station 1), shelf-break (Station 3), and offshore (Station 5) environments on each transect (Fig. D1). Samples were collected at night in 2018 and during the day and night in 2019, with day and night sampling occurring within a 24 h period. All sampling excluded dawn and dusk when vertical movement by zoea may be most pronounced. Replicate tows were performed at every station in 2019, but 2018 sampling was limited by extreme winter storm conditions.

Zooplankton tows were conducted with a Multiple Opening/Closing Net and Environmental Sensing System (MOCNESS; Guigand et al. 2005) with a 1 m^2 opening and 333 μm mesh nets. The system was fit with a flowmeter and conductivity, temperature, salinity, and depth sensors. While the MOCNESS was towed at approximately 2.5 m s^{-1}, ship and wire retrieval speeds were continuously adjusted to maintain a MOCNESS angle as close to 45° as possible, which ensures a 1 m^2 net mouth opening. To aid in the visualization of physical parameters, MOCNESS physical data were supplemented by sampling in an undulating fashion with a separately towed sensor system. This undulating system collected high resolution physical data across the length of each transect within 24 h of each biological sample collection. Detailed descriptions of this sampling effort conducted concurrently with the MOCNESS sampling described herein can be found in Swieca et al. (*in prep* A, B).

The MOCNESS sampled at 25-m depth bins down to a maximum depth of 100 m. Immediately after net retrieval all MOCNESS nets were rinsed with seawater, sieved, and individually preserved in 95% ethanol. Ethanol was changed within 48 h of sample collection and again within 2 mo. to ensure sufficient preservation. Samples were sorted in the laboratory to remove crab larvae, and when necessary, net samples were subsampled with a plankton box splitter until the sample contained approximately 500 zooplankton individuals. Crab larvae were identified to the lowest possible taxonomic level and staged (Z1 - Z5, megalopae) following Lough (1975).

2.2 Physical data analysis

All raw MOCNESS and undulating sensor data were converted to variables of interest based on factory calibrations. Mean MOCNESS temperature and salinity were averaged per depth-discrete net sample, with vertically integrated haul values calculated as the mean of all depth-discrete nets within each haul. Undulating tow data were kriged onto a grid equal to the length of each transect at 2-m vertical and 500-m horizontal resolution. In addition to investigating the effects of temperature and salinity, we quantified the strength of upwelling immediately prior to sample collection to understand how local oceanography influences larval Dungeness crab distributions. We used the cumulative daily Coastal Upwelling Transport Index (CUTI;

https://mjacox.com/upwelling-indices/) 10 d prior to sampling as a measure of upwelling strength, with positive values indicating upwelling and negative values downwelling. This time period was selected to account for the lag between physical wind-stress, water movement, and phyto- and zooplankton abundances (Spitz & Allen 2005).

We assessed the relationship between stage specific zoea concentrations and *in situ* environmental parameters using non-parametric Spearman rank correlations. Variable measures were mean stage-specific zoea concentrations, temperature, and salinity per depth-stratified MOCNESS sample. Correlation significance was set at $p < 0.05$ and determined using the 'Hmisc' R package (Harrell & Dupont 2021).

2.3 Ecological data analyses

While species level identification necessitates staging zoea as Z1 - Z5, for data analysis, we pooled Dungeness crab zoea into early- (Z1 - Z2), mid- (Z3), and late-stages (Z4 - Z5). Early-, mid-, and late-stage zoea abundances for each depth-stratified sample were standardized to concentration per 1000 m^{-3} using the biological count divided by the volume of water filtered through the net. Because depth bin size was consistent (25 m) throughout sampling, mean vertically integrated haul concentrations were calculated as the mean of all depth-stratified samples in each haul. To facilitate vertical distribution analyses, we also calculated zoea weighted mean depths (WMD) following Frost & Bollens (1992):

$$WMD = \frac{\Sigma(n_i \times d_i)}{\Sigma n_i} \qquad (1)$$

where n_i is the concentration of individuals per cubic meter of taxon i at depth d_i, which is taken to be the midpoint of each 25-m depth stratum. Stage-specific WMDs were calculated for each haul.

Broad patterns in stage-specific zoea distributions were visualized by overlaying vertically integrated abundances on sampling maps and depth-discrete abundances on loess interpolated MOCNESS temperature cross-sections. Non-parametric Wilcoxon rank sum tests (two test groups) or Kruskal-Wallis tests (>two test groups) were applied to both depth-stratified and vertically integrated haul concentrations to test for significant

differences between years (2018, 2019) and transects (NH, TR), and among stations (1, 3, 5) and depth strata (0-25, 25-50, 50-75, 75-100). When applicable, Kruskal-Wallis tests were following by a Dunn post-hoc test.

Plots of mean stage-specific station concentrations were constructed for each year and transect. There was no significant difference in early-, mid-, late-stage, or total zoea WMD between years, locations, or stations within each location (all p's >0.05), so these groups were pooled when plotting mean concentrations per 25 m depth bin.

Zoea diel vertical migration (DVM) behavior was investigated using 2019 data, when samples were collected along each transect during day and night within a 24 h period. Differences in stage-specific day and night vertical WMDs were tested using non-parametric Wilcoxon rank sum tests, and zoea were determined to undergo DVM if the difference in day and night WMD was significant ($p < 0.05$). If DVM behavior was detected, the migration amplitude was calculated as the difference between day and night WMDs, with positive values indicating 'normal' DVM (i.e., move up during night, down during day) and negative values indicating 'reverse' DVM (i.e., move down during night, up during day; Bezerra-Neto & Pinto-Coelho 2007, Picapedra et al. 2015).

3. RESULTS

3.1 Environmental setting

In situ water temperature and salinity varied significantly in time and space, differing more across latitudinal [Newport Hydrographic (NH) and Trinidad Head (TR) Lines] than cross-shelf or vertical scales. In 2018, ocean conditions were generally colder and saltier than 2019 ($p < 0.001$, Wilcoxon). Interannual differences were most evident at TR, where 2018 temperatures were as much as 2.4 °C colder than in 2019 (Table 5.1, Fig. D2). Water temperatures were cooler at TR than at NH in 2018, but the reverse was true in 2019. In both years, salinity was higher at TR compared to NH (Table 5.1). Consistent with expectations, the winter water column was relatively well mixed throughout sampling. Surface waters were moderately cooler than at depth and there was a persistent band of warm water at mid-depth, but the water column lacked defined vertical thermal stratification in both years and locations (Fig. D2). This was especially true in 2018, when sampling occurred during winter storm conditions that typically lead to deep

mixing of the water column and strong turbulence in the surface layer (Bograd et al. 2009, Checkley Jr. & Barth 2009, García-Reyes & Largier 2012).

Upwelling was roughly 3x stronger in 2018 compared to 2019 and at TR relative to NH each year (Table 5.1). In 2018, TR experienced strong and persistent upwelling during and prior to sample collection. Upwelling was more dynamic in NH, where conditions were downwelling or relatively neutral until approximately 5 d prior to sampling when the CUTI began to fluctuate between upwelling and downwelling or neutral conditions on 3-5 d time scales (Fig. 5.1A). In 2019, NH and TR conditions were more similar to one another, with both locations exhibiting downwelling immediately prior to sample collection, followed by moderate upwelling at the start of sampling before returning to weak downwelling conditions (Fig. 5.1B). Mean cumulative upwelling 10 d prior to sampling ranged from 0.8 to 12.9 m^3s^{-1}, with the lowest value occurring in 2019 at NH and the highest in 2018 at TR. While both locations experienced interannual variability in upwelling, the magnitude of interannual variability was much greater in TR (9.8 m^3s^{-1}) than NH (2.2 m^3s^{-1}; Table 5.1).

3.2 Overall zoea abundance, relationship with oceanography, and distribution over time and latitude

After adjusting for split samples, a total of 14,314 Dungeness crab (*Cancer magister*) zoea were collected over the two cruises, almost half (46.9%) of the total catch of larval crabs. The overall mean concentration of zoea was 133.4 (± 40.0) ind. 1000 m^{-3} and ranged from 63.7 (±23.2) ind. 1000 m^{-3} in 2018 to 150.8 (±49.3) ind. 1000 m^{-3} in 2019 (Table 5.1). While zoea were significantly more abundant in 2019 compared to 2018 ($p = 0.003$), the relative contribution of each stage varied across years. Mean abundance of early-stage zoea was greater in 2018 than 2019 ($p < 0.001$), while the abundances of mid- ($p = 0.03$) and late-stage ($p = 0.005$) zoea were higher in 2019. Finally, zoea abundance was significantly higher at NH than at TR in both years, with NH concentrations exceeding those at TR by nearly two orders of magnitude ($p < 0.001$). This general latitudinal pattern held for early-, mid-, and late-stage zoea (Table 5.1, Fig. 5.2; all p's < 0.001). Finally, the mean concentration of early- ($p = 0.005$, $p = 0.02$), mid- ($p < 0.001$, $p = 0.001$), late-stage (both p's < 0.001), and total zoea (both p's < 0.001)

were significantly negatively correlated with temperature and salinity, respectively. Correlation strength increased throughout ontogeny, with later stage larvae being more strongly negatively correlated with temperature and salinity than earlier stage larvae (Table 5.3).

3.3 Cross-shelf distributions of zoea

Larval crab concentrations exhibited cross-shelf variability along the NH Line, but not the TR Line (Figs. 5.2, 5.3). There was no significant difference in early-, mid-, late-stage, or total zoea abundance among stations on the TR Line in either year (Fig. 5.3B; $p > 0.05$ for all stages and both years). Note that zoea abundances were very low overall at TR, and interestingly, zoea were often entirely absent from nearshore (inshore and shelf-break) stations.

At NH, cross-shelf distributions of zoea varied interannually. During strong upwelling in 2018, zoea were evenly distributed across the shelf, with no significant difference in stage-specific or total zoea abundance among stations (Figs. 5.2, 5.3A; all p's > 0.05). While offshore sampling was not possible due to extreme storm conditions that year, interannual differences in the relative concentration of zoea between inshore and shelf-break stations is consistent with a lack of pattern. Conversely, in 2019, the abundance of zoea increased along an offshore - nearshore gradient to a maximum at our most inshore station (Fig. 5.2). While all stages of zoea were concentrated inshore, later-stage larvae were more broadly distributed across the shelf, with offshore concentrations increasing through ontogeny. No early-stage larvae were found offshore that year (Figs. 5.2, 5.3A).

3.4 Vertical and diel distributions of zoea

Abundances of Dungeness crab zoea varied across depth-stratified and diel scales (Figs. 5.4-5.6). Vertical distributions were highly nuanced in time and space, with zoea appearing to be slightly more uniformly distributed throughout the water column in 2018 compared to 2019, at NH compared to TR, and on the continental shelf compared to at the shelf-break or offshore (Figs. 5.4, 5.5). Zoea displayed the most consistent vertical distribution at the shelf-break station, especially at NH where they were typically

concentrated in the top 25 m of the water column (Figs. 5.4A, 5.5A). However, there was ultimately no significant difference in early-, mid-, late-stage, or total zoea weighted mean depths (WMDs) between years, transects, or stations along each transect (all p's > 0.50). As a result, these groups were pooled to examine general patterns in zoea abundances among depth-strata.

Zoea were distributed from the surface to our maximum sampling depth of 100 m but were most concentrated in the upper 50 m of the water column. Total zoea WMD was 35.5 m, but WMD increased moderately though ontogeny. This is evidenced by substantially higher abundances of late-stage zoea in the 25-50 m depth bin compared to early- and mid-stage zoea who were more restricted to the top 25 m of the water column (Fig. 5.5A, 5.6).

The overall mean abundance of zoea in the top 100 m of the water column was significantly greater at night than during the day, especially for late-stage larvae (Table 5.2, Fig. 5.5; $p = 0.02$). Within this pattern of total abundance, zoea exhibited unique day and night distributions among depth strata within our sampling range. Nighttime weighted mean depths (MWDs) of early-, mid-, and late-stage zoea were 21.3, 8.3, and 8.1 m deeper than daytime WMDs, respectively. Early-stage zoea displayed the most prominent change in diel vertical distribution with 97.9% of their abundance occurring in the top 25 m of the water column during the day, but only 61.9% occurring in this upper layer at night when they were more broadly distributed over the top 100 m (Fig. 5.7A). Similarly, the relative abundance of mid-stage zoea in the top 25 m increased during the day compared to night (Fig. 5.7B). Late-stage zoea were fairly evenly distributed in the top 50 m of the water column during the night but shifted to have 76.1% of their relative abundance concentrated in the top 25 m during the day (Fig. 5.7C). Although all stages of zoea appear to exhibit diel changes in their vertical distributions such that within the top 100 m of the water column they were shallower during the day and deeper at night, the differences in day and night WMDs for early-, mid- , and late-stage zoea were not significant (all p's > 0.05).

4. DISCUSSION

Dungeness crab (*Cancer magister*) is frequently the most valuable single-species commercial fishery in the California Current. Because harvest pressure is high (>90% of the population is harvested each year), commercial catch can be used as a proxy for adult population size (Hackett et al. 2003). Commercial fishery data from recent decades indicate that there are large annual fluctuations in Dungeness crab year-class strength (Shanks & Roegner 2007, reviewed in Rasmuson 2013). Understanding the drivers underlying these fluctuations is important for determining sustainable management strategies for this economically important species.

Evidence from megalopal recruitment and commercial catch dynamics underscore the importance of the early life history stages in determining the abundance and distribution of adult Dungeness crab in the California Current (Shanks & Roegner 2007, Shanks et al. 2010), with implications for the coastal communities that rely on this species for their livelihoods. Yet, correlations between offshore physical processes, megalopal recruitment, and commercial catch only indirectly address the most vulnerable pelagic zoeal stages: zoea are assumed to be evenly distributed offshore such that megalopal recruitment to a single coastal Oregon bay is representative of the California Current system.

Our replicated depth-discrete winter sampling revealed that Dungeness crab zoea are not uniformly distributed in time or space, but exhibit distinct spatial distributions interannually, latitudinally, across the shelf, and within the water column. Considering all of the data, zoeal abundances were significantly negatively correlated with *in situ* temperature and salinity throughout ontogeny. During both years of sampling, zoea were substantially more abundant off Oregon (NH) than northern California (TR). Similar to previous studies, zoea generally exhibited an ontogenetic shift in their cross-shelf distribution, with later stage zoea found progressively farther offshore. Additionally, zoea abundances were strongly vertically structured. Large-scale patterns in vertical distribution may change over diel scales but were generally consistent in the top 100 m of the water column. Consistency in these spatial patterns together with the strong relationship with physical parameters provides a valuable opportunity to incorporate the youngest life stages into distribution and population modelling.

4.1 Interannual and latitudinal variability

Zoea were significantly more abundant in 2019 compared to 2018 and at the Newport Hydrographic Line (NH) compared to the Trinidad Head Line (TR) both years. The relative contribution of each zoeal stage to the total abundance also varied across years, with early-stage zoea dominating in 2018 and mid- and late-stage zoea in 2019. Because the duration of each Dungeness crab larval stage decreases as temperature increases (Ebert et al. 1983, Sulkin & McKeen 1989), an argument could be made that the warmer 2019 water temperatures contributed to faster development in 2019. However, interannual temperature differences were primarily driven by temperatures at TR, where zoea abundances were relatively low. Mean temperature on the NH line varied only by 0.1 °C between years. Thus, it is more likely that differences in stage-specific abundances were due to the timing of sample collection, which was two weeks earlier in 2018 (15-23 Feb) than in 2019 (3-11 Mar). Early-stage zoea include Z1 and Z2 individuals and at 10°C, the mean duration of these stages is 13.2 d and 11.3 d, respectively (Sulkin & McKeen 1989). Assuming hatch timing was roughly consistent within each location both years, developmental time accounts for the observed variability in the relative stage-specific abundances.

With only 2 yrs of data it is not possible to determine the specific mechanism(s) underlying interannual differences in total zoeal abundance. Notably, limited sampling over time precludes our ability to examine the effects of large-scale physical drivers that have been shown to impact the distributions of Dungeness crab megalopae but often operate on decadal time scales (i.e., Pacific Decadal Oscillation, North Pacific Gyre Oscillation, etc; Shanks et al. 2010, Magel et al. 2020). Nonetheless, *in situ* oceanographic conditions vary substantially throughout the latitudinal range of Dungeness crab providing insights into the physical parameters playing an important role.

Zoea were significantly negatively correlated with water temperature and salinity throughout ontogeny. Normal zoeal development occurs over a temperature range of 10.0-13.9°C and a salinity range of 25-30 (Ebert et al. 1983, reviewed in Rasmuson 2013). During our sampling, water temperature and salinity ranged from 8.8 - 11.2 °C and 31.7 - 33.8, respectively. While mean temperature only deviated from the typical range of crab development at TR in 2018, salinity exceeded the range for normal

development across all sampling efforts. Both the highest temperature and highest salinity values were recorded at TR. While these unfavorable conditions may have contributed to low zoeal abundances at TR relative to NH, other factors such as upwelling induced offshore advection probably also contributed to the observed patterns.

4.2 Vertical and cross-shelf distributions

Within our sampling depth range (100 m), maximum total zoea concentrations occurred in the top 25 m of the water column. This is consistent with expectations (Reilly 1983, Booth et al. 1986, Jamieson & Phillips 1993). By concentrating at this depth, zoea are subject to surface currents which likely impact their horizontal distributions. Dungeness crab zoea are present in the northern California Current during the winter months, when the coastal ocean is typically characterized by net northward surface flow (the Davidson Current). Though the mechanisms of cross-shelf dispersal in this current system are unclear, it is hypothesized that this flow regime results in the gradual offshore and northward transport of crab zoea (reviewed in Rasmuson 2013). Our stage-specific cross-shelf zoea distributions are consistent with this theory. Early stage zoea (Z1-Z2) were typically concentrated on the continental shelf, while mid- (Z3) and late-stage (Z4-Z5) larvae were often found farther offshore.

Our observed patterns in stage-specific zoea cross-shelf distributions at NH agree with the previous findings that suggest later stage larvae are found progressively farther offshore (Lough 1976, Reilly 1983, Hobbs et al. 1992). However, at TR crab zoea were often absent from nearshore waters or were evenly distributed among cross-shelf stations. This system (northern California) experiences strong and persistent upwelling (Checkley Jr. & Barth 2009, García-Reyes & Largier 2012), as evidenced by CUTI values that were 2-3x greater at TR than NH during sampling. Upwelling is associated with high production, but also offshore transport of the surface layer. It is possible that the observed TR cross-shelf zoea distributions are due to higher rates of upwelling circulation that rapidly advected larvae across the shelf either evenly distributing zoea or transporting them offshore and entirely out of our sampling domain. This upwelling-induced movement of surface waters may also underlie the overall low zoea abundances at TR

and the more even distributions of zoea across the NH shelf in 2018 compared to 2019, as upwelling at NH was 2x greater in 2018 than in 2019.

4.3 Diel vertical migration (DMV)

Although there were no significant differences in the day and night weighted mean depths of Dungeness crab zoea within our sampling range, the total abundance of larvae in the upper 100 m of the water column was significantly higher at night compared to day, especially for late-stage larvae. Day and night samples were collected at each location within 24 h. Thus, our observation of ~2x greater nighttime total abundance compared to daytime total abundance suggests that zoea may be migrating into our sampling range at night and out of our sampling range during the day. This finding provides some evidence for type-I DVM, with large abundances of zoea migrating to the upper 50 m of the water column at night and down to depths > 100 m during the day. This migration pattern would not be captured by comparing WMDs, as the vertical structure of zoeal distributions was consistent in the upper 100 m of the water column but there was a significant diel change in total larval abundance.

While type-I DVM has been reported for Dungeness crab zoea and megalopae (Reilly 1983, Booth et al. 1986, Hobbs & Botsford 1992), the observed day and night differences in abundance within the upper 100 m the water column would constitute a larger magnitude of vertical migration than is typically reported. For example, most studies examining zoeal DVM have reported vertical migrations on the order of 10s of meters (Reilly 1983, Booth et al. 1986, Hobbs & Botsford 1992), whereas our results would suggest that vertical migrations of at least 50 m occur. However, the majority of these previous studies coupled neuston and oblique tows, comparing the surface-most layer to an integrated water column of a pre-determined depth. This approach examines diel movements in and out of the neuston but may obscure larger migrations. Dungeness crab larvae are considered to be relatively strong swimmers within the plankton community with zoea swimming at a speeds of 1.5 cm s^{-1} and megalopae swimming at 12 cm s^{-1} on average, but up to 44 cm s^{-1} (reviewed in Rasmuson 2013). *Cancer* spp. larvae have been shown to migrate from the surface to >50 m depth on the shelf and up to 80 m depth offshore (Shanks 1986). In the Strait of Georgia, Dungeness crab larvae display

diel migrations between 1 m from the surface and 160 m depth (Jamieson & Phillips 1993). These two studies suggest our observations of heightened nighttime abundances could be due to large (>50 m) vertical migrations and thus may capture type-I DVM behavior in Dungeness crab zoea. Deeper sampling is needed to confirm and fully examine the extent of larval Dungeness crab DVM.

DVM is well documented for many marine larvae, but particularly for those with bi-phasic life histories. A variety of hypotheses have been put forth to explain the drivers behind this behavior including the metabolic advantages of oscillating between two temperature regimes (McLaren 1963), predator avoidance (Lyczkowski-Shultz & Steen 1991, Brodeur & Rugen 1994), prey availability (Lampert 1989), and favorable larval transport (Hobbs & Botsford 1992, Hare & Govoni 2005, Auth et al. 2007). The latter is most frequently invoked to describe the underlying driver of Dungeness crab vertical migrations (Shanks 1986, Jamieson & Phillips 1993).

5. CONCLUSIONS

It is widely accepted that spatial and temporal fluctuations in Dungeness crab harvest are due to factors influencing the early life history stages (McKelvey et al. 1980, Shanks 2013, Shanks et al. 2010). Yet, we lack a clear understanding of how oceanography and physical parameters impact the offshore distributions of the youngest and most vulnerable pelagic stages. Nonetheless, these data are needed to elucidate the mechanisms underlying recruitment variability to more accurately predict adult year-class size in the future. Using fine-scale depth-discrete sampling we found that Dungeness crab zoea were not evenly distributed in the horizontal (latitudinal, cross-shelf) or vertical dimension, and their distributions were significantly impacted by ocean conditions. Specifically, high larval crab abundances were associated with low water temperature and salinity. This association is especially important under the context of changing ocean conditions, which are predicted to result in increasing ocean temperatures and a subsequent northward shift in Dungeness crab distribution (Magel et al. 2020). On a regional scale, the increasing frequency of marine heat waves is also likely to influence these early stages. The implication of temperature induced changes will cascade through

ecological and social systems, impacting the coastal ocean, fishing communities, and all others who rely on this species for their livelihoods.

6. ACKNOWLEDGEMENTS

We are grateful for the captain and crew of the R/V Sikuliaq for their contributions to at-sea sampling. Special thanks to the Oregon State University National Science Foundation Research Traineeship staff and faculty, especially L. Ciannelli and K. Hoffman. This project was greatly improved through input on Dungeness crab identification by J. Fisher, S. Zeman, and C. Morgan. Finally, we thank REU student A. Chin, J. Ivory, M. Schmid, H.W. Fennie, M. Wilson, K. Axler, M. Gleiber, and C. Briseño-Avena for their dedication to this study, which included spending up to 20 d at sea. This study was funded by NSF OCE 1737399 and NSF NRT 1545188. KS was also supported through the HMSC Markham Award, the Walter G. Jones Fishery Development Award, the Hannah-Jones Award, and Integrative Biology Research Funds.

7. REFERENCES

Auth TD, Brodeur RD, Fisher KM (2007) Diel variation in vertical distribution of an offshore ichthyoplankton community off the Oregon coast. Fish Bull 105:313–326

Bezerra-Neto JF, Pinto-Coelho RM (2007) Diel vertical migration of the copepod *Thermocyclops inversus* (Kiefer, 1936) in a tropical reservoir: the role of oxygen and the spatial overlap with *Chaoborus*. Aquat Ecol 41:535–545

Bograd SJ, Schroeder I, Sarkar N, Qiu X, Sydeman WJ, Schwing FB (2009) Phenology of coastal upwelling in the California Current. Geophys Res Lett 36:1–5

Booth J, Phillips A, Jamieson G (1986) Fine scale spatial distribution of *Cancer magister* megalopae and its relevance to sampling methodology. In: Melteff B (ed) Proceedings of the Symposium on Dungeness Crab Biology and Management. Alaska Sea Grant, Anchorage, Alaska, p 273–286

Botsford LW, Armstrong DA, Shenker JM (1989) Oceanographic influences on the dynamics of commercially fished populations. Elsevier Oceanogr Ser 47:511–565

Botsford LW, Methot Jr. RD, Johnston WE (1983) Effort dynamics of the northern California Dungeness crab (*Cancer magister*) fishery. Can J Fish Aquat Sci 40:337–346

Brodeur RD, Rugen WC (1994) Diel vertical distribution of ichthyoplankton in the northern Gulf of Alaska. Fish Bull 92:223–235

CDFW (2018) California Commercial Landings. https://wildlife.ca.gov/Fishing/Commercial /Landings

Checkley Jr. DM, Barth JA (2009) Patterns and processes in the California Current System. Prog Oceanogr 83:49–64

Des Voigne (1973) Influence of temperature and photoperiod upon the Dungeness crab *Cancer magister*. Ph.D. Dissertation, University of Washington

Ebert E, Haseltine A, Houk J, Kelly R (1983) Labratory cultivation of the Dungeness crab, *Cancer magister*. Fish Bull 172:259–310

Frost BW, Bollens SM (1992) Variability of diel vertical migration in the marine planktonic copepod *Pseudocalanus newmani* in relation to its predators. Can J Fish Aquat Sci 49:1137–1141

García-Reyes M, Largier J (2012) Seasonality of coastal upwelling off central and northern California: new insights, including temporal and spatial variability. J Geophys Res Ocean 117:1–17

Guigand CM, Cowen RK, Llopiz JK, Richardson DE (2005) A coupled asymmetrical multiple opening closing net with environmental sampling system. Mar Technol Soc J 39:22–24

Hackett S, Krachey M, Dewees C, Hankin D, Sortais K (2003) An economic overview of Dungeness crab (*Cancer magister*) processing in California. CalCOFI Reports 44:86–93

Hare JA, Govoni JJ (2005) Comparison of average larval fish vertical distributions among species exhibiting different transport pathways on the southeast United States continental shelf. Fish Bull 103:728–736

Harrell F, Dupont C (2021) Hmisc. R package version 4.6-0. In: p 1–452

Hobbs RC, Botsford LW (1992) Diel vertical migration and timing of metamorphosis of larvae of the Dungeness crab *Cancer magister*. Mar Biol 112:417–428

Hobbs RC, Botsford LW, Thomas A (1992) Influence of hydrographic conditions and

wind forcing on the distribution and abundance of Dungeness crab, *Cancer magister*, larvae. Can J Fish Aquat Sci 49:1379–1388
Jamieson G, Phillips A (1988) Occurence of cancer crab (*C. magister* and *C. oregonensis*) megalopae off of the west coast of Vancouver Island, British Columbia. Fish Bull 86:525–542
Jamieson G, Phillips A (1993) Megalopal spatial distribution and stock separation in Dungeness crab (*Cancer magister*). Can J Fish Aquat Sci 50:416–429
Lampert W (1989) The adaptive significance of diel vertical migration of zooplankton. Funct Ecol 3:21–27
Lough R (1975) Dynamics of crab larvae (Anomura, Brachyura) off the central Oregon coast, 1969-1971. Ph.D Dissertation, Oregon State University
Lough R (1976) Larval dynamics of the Dungeness crab, *Cancer magister*, off the central Oregon coast, 1970-71. Fish Bull 74:353–376
Lyczkowski-Shultz J, Steen J (1991) Diel vertical distribution of red drum *Sciaenops ocellatus* larvae in the northcentral Gulf of Mexico. Fish Bull 89.4:631–641
Magel CL, Lee EMJ, Strawn AM, Swieca K, Jensen AD (2020) Connecting crabs, currents, and coastal communities: examining the impacts of changing ocean conditions on the distribution of U.S. West Coast Dungeness crab commercial catch. Front Mar Sci 7:401. doi: 10.3389/fmars.2020.00401
McKelvey R, Hankin D, Yanosko K, Snygg C (1980) Stable cycles in multistage recruitment models: an application to the northern California Dungeness crab (*Cancer magister*) fishery. Can J Fish Aquat Sci 37:2323–2345
McLaren IA (1963) Effects of temperature on growth of zooplankton, and the adaptive value of vertical migration. J Fish Res Board Canada 20:685–727
Methot R (1986) Management of Dungeness crab fisheries in North Pacific Workshop on Stock Assessment and Management of Invertebrates (G Jamieson and N Bourne, Eds.). Ottawa: Department of Fisheries and Oceans 326-384
Minobe S, Mantua N (1999) Interdecadal modulation of interannual atmospheric and oceanic variability over the North Pacific. Prog Oceanogr 43:163–192
ODFW (2018) Commercial Dungeness crab fishery. https://wildlife.ca.gov/Fishing/Commercial/Landings
Picapedra P, Lansac-Tôha F, Bialetzki A (2015) Diel vertical migration and spatial overlap between fish larvae and zooplankton in two tropical lakes, Brazil. Braz J Biol 75:352–361
Poole RL (1966) A description of laboratory-reared zoeae of *Cancer magister* Dana, and megalopae taken under natural conditions (Decapoda Brachyura). Crustaceana 11:83–97
Rasmuson LK (2013) The Biology, ecology and fishery of the Dungeness crab, *Cancer magister*. Adv Mar Biol 65:95–148
Reilly P (1983) Dynamics of Dungeness crab, *Cancer magister*, larvae off central and Northern California. In: Wild P, Tasto R (eds) Life History, Environment, and Mariculture Studies of the Dungeness crab, *Cancer magister*, with Emphasis on the Central California Fishery Resource. California Department of Fish and Game, Sacramento, p 57–84
Shanks AL (1986) Vertical migration and cross-shelf dispersal of larval *Cancer* spp. and *Randallia ornata* (Crustacea: Brachyura) off the coast of southern California. Mar

Biol 92:189–199
Shanks AL (2006) Mechanisms of cross-shelf transport of crab megalopae inferred from a time series of daily abundance. Mar Biol 148:1383–1398
Shanks AL (2009) Pelagic larval duration and dispersal distance revisited. Biol Bull 216:373–85
Shanks A (2013) Atmospheric forcing drives recruitment variation in the Dungeness crab (*Cancer magister*), revisited. Fish Oceanogr 22:263–272
Shanks A, Roegner G (2007) Recruitment limitation in Dungeness crab populations is driven by variation in atmospheric forcing. Ecology 88:1726–1737
Shanks A, Roegner G, Miller J (2010) Using megalopae abundance to predict future commercial catches of Dungness crabs (*Cancer magister*) in Oregon. CalCOFI Reports 51:1–13
Spitz Y, Allen J (2005) Modeling of ecosystem processes on the Oregon shelf during the 2001 summer upwelling. J Geophys Res 110:C10S17
Sulkin S, McKeen G (1989) Laboratory study of survival and duration of individual zoeal stages as a function of temperature in the brachyuran crab *Cancer magister*. Mar Biol 103:31–37
Thorson G (1946) Reproduction and larval development of Danish marine bottom invertebrates, with special reference to the planktonic larvae in the Sound (Øresund). Meddelelser fra Kommissionen Danmarks Fisk og havundersøgelser Ser Plankt 4:1–523
WDFW (2018) Coastal commercial Dungeness crab fishery. https://wdfw.wa.gov/fishing/commercial/crab/coastal
Wild P, Tasto R (1983) Life history, environment, and mariculture studies of the Dungeness crab, *Cancer magister*, with empahsis on the central California fishery resource. Calif Dep Fish Game, Fish Bull 172:1–352

Table 5.1. Temperature, salinity, and upwelling during sampling, and concentrations of early- (Z1-Z2), mid- (Z3), late-stage (Z4-Z5), and total Dungeness crab (*Cancer magister*) zoea sampled along the Newport Hydrographic Line (NH) and the Trinidad Head Line (TR) during the winters of 2018 and 2019.

	2018			**2019**		
	All	**NH**	**TR**	**All**	**NH**	**TR**
Temperature (°C)	**10.0 (8.8 - 11.2)**	10.2 (9.6 - 10.5)	9.7 (8.8 - 10.4)	**10.5 (9.45 - 11.2)**	10.1 (9.4 - 10.7)	10.8 (10.0 - 11.2)
Salinity	**33.0 (31.7 - 33.8)**	32.6 (31.7 - 33.5)	33.4 (33.0 - 33.8)	**32.7 (31.8 - 33.6)**	32.6 (31.8 - 33.3)	32.8 (31.8 - 33.6)
Upwelling (CUTI; m^3s^{-1})	**6.7 (2.9 - 12.9)**	3.6 (2.9 - 4.3)	12.9 (NA)	**2.2 (0.8 - 3.2)**	1.4 (0.8 - 2.0)	3.1 (2.9 - 3.2)
Zoea (ind. 1000 m^{-3})						
Early-stage	**78.7 (±24.0)**	153.9 (±41.9)	3.5 (±1.3)	**28.4 (±11.1)**	55.6 (±21.8)	1.3 (±0.8)
Mid-stage	**99.8 (±39.6)**	197.3 (±67.0)	2.3 (±1.1)	**129.0 (±60.4)**	258.0 (±118.0)	0.1 (±0.1)
Late-stage	**30.6 (±16.9)**	60.8 (±32.7)	0.3 (±0.2)	**284.0 (±67.3)**	567.0 (±127.3)	1.1 (±0.6)
Total	**63.7 (±23.2)**	125.4 (±37.7)	2.0 (±0.7)	**150.8 (±49.3)**	300.6 (±93.3)	1.0 (±0.4)

Zoea concentrations, temperature, and salinity are from the MOCNESS. Upwelling values are the cumulative daily CUTI (Coastal Upwelling Transport Index; https://mjacox.com/upwelling-indices/) 10 d prior to each sampling event. Concentrations are reported as mean (± SE) and physical data are mean and range. NA = no range of values due to one day of sampling.

Table 5.2. Mean (±SE) day and night concentrations of early- (Z1-Z2), mid- (Z3), late-stage (Z4-Z5), and total Dungeness crab (*Cancer magister*) zoea collected within 24-h periods along the Newport Hydrographic Line (NH) and the Trinidad Head Line (TR) during the winter of 2019

	Day	**Night**
Zoea (ind. 1000 m-3)		
Early-stage	31.8 (±18.5)	25.1 (±12.4)
Mid-stage	76.9 (±33.7)	181.2 (±116.2)
Late-stage	153.9 (±46.2)	414.4 (±125.2)
Total	89.6 (±34.6)	211.9 (±92.0)

Table 5.3. Correlation coefficients for depth-stratified sample means (n = 102) collected along the Newport Hydrographic Line (NH) and the Trinidad Head Line (TR) in the winters of 2018 and 2019: *in situ* temperature (°C), salinity, and concentrations (ind. 1000 m^{-3}) of early- (Z1-Z2), mid- (Z3), and late-stage (Z4-Z5) Dungeness crab (*Cancer magister*) zoea, as well as total zoea. *p < 0.05, **p < 0.01, ***p < 0.001

	Temperature	Salinity
Early-stage	-0.28**	-0.24*
Mid-stage	-0.37***	-0.32**
Late-stage	-0.40***	-0.40***
Total zoea	-0.48***	-0.40***

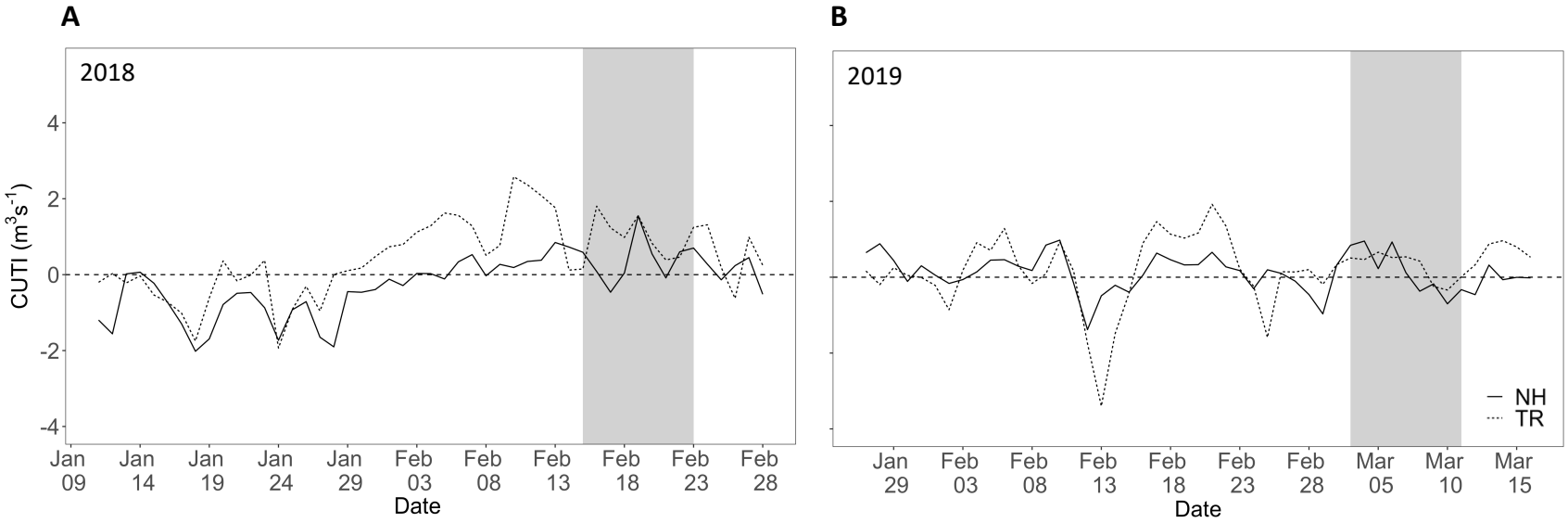

Fig. 5.1. Daily Coastal Upwelling Transport Index (CUTI) for the Newport Hydrographic Line (NH; 45° N; solid line) and the Trinidad Head Line (TR; 41° N; dotted line) during winter of (A) 2018 and (B) 2019, with sampling dates highlighted in gray. Positive values signify upwelling, zero are neutral conditions, and negative values are downwelling

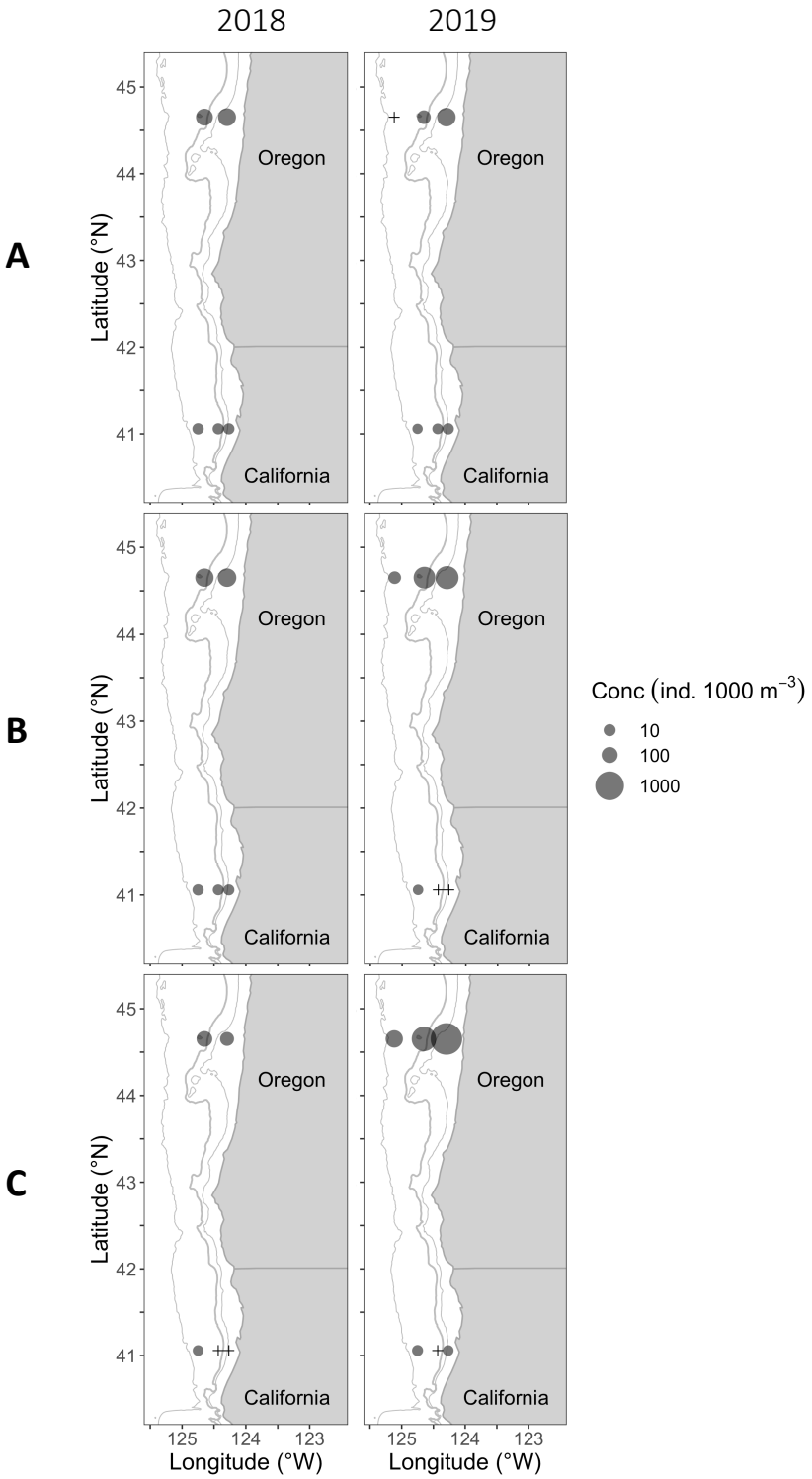

Fig. 5.2. Cross-shelf distributions of (A) early- (Z1-Z2), (B) mid- (Z3), and (C) late-stage (Z4-Z5) Dungeness crab (*Cancer magister*) zoea collected along the Newport Hydrographic Line (NH) and the Trinidad Head Line (TR) in the winters of 2018 (left) and 2019 (right). Empty regions represent unsampled locations and '+' denote true zeros. Contour lines represent the 100-, 200-, and 2000-m isobaths.

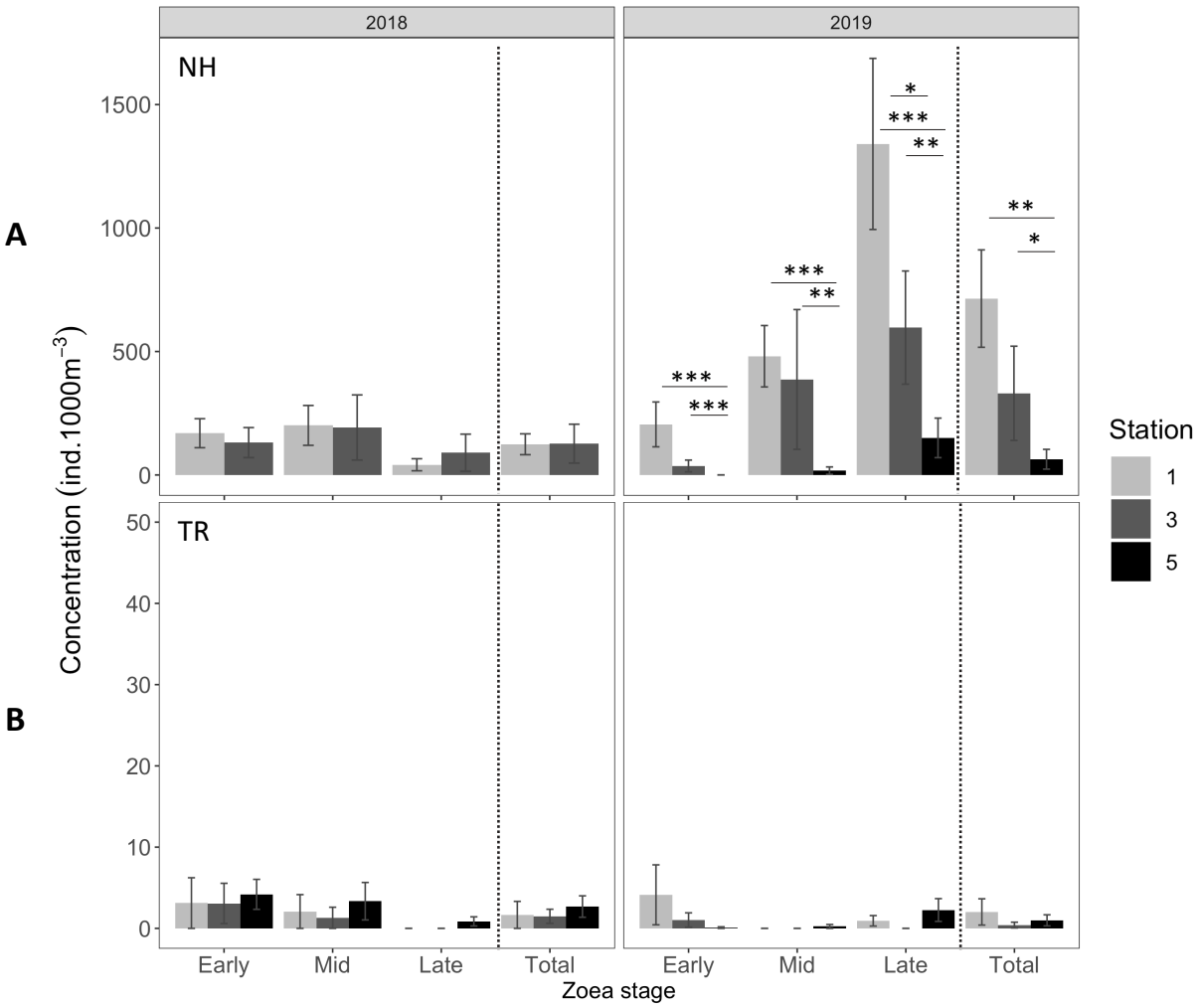

Fig. 5.3. Mean (±SE) concentration of early- (Z1-Z2), mid- (Z3), late-stage (Z4-Z5) and total Dungeness crab (*Cancer magister*) zoea collected at three cross-shelf stations along the (A) Newport Hydrographic Line (NH) and the (B) Trinidad Head Line (TR) in the winters of 2018 (left) and 2019 (right). Station 1 = inshore, station 3 = shelf-break, station 5 = offshore. Note that y-axis scales differ. *$p < 0.05$, **$p < 0.01$, ***$p< 0.001$

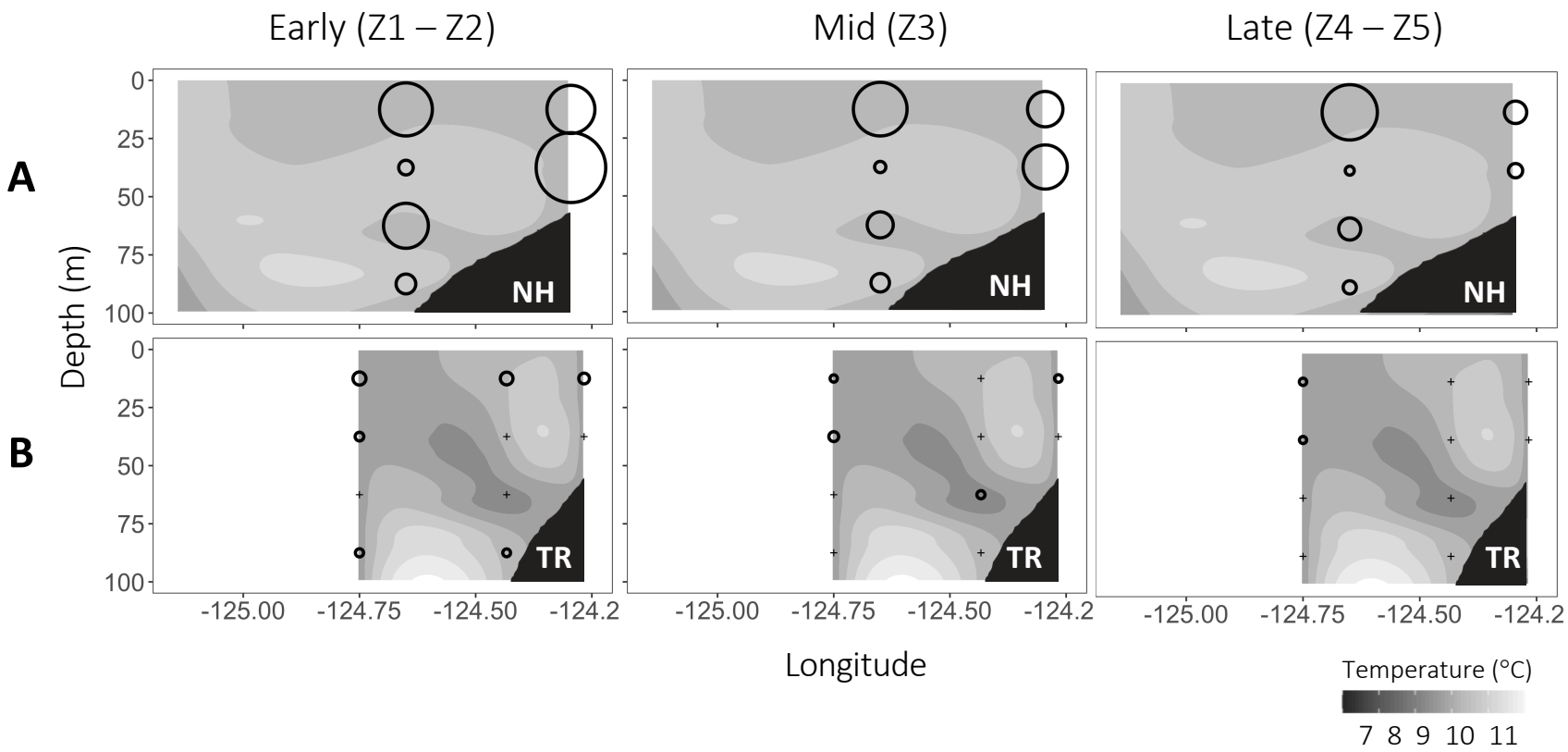

Fig. 5.4. Cross-sections of night transects sampled during winter of 2018 along the (A) Newport Hydrographic Line (NH) and the (B) Trinidad Head Line (TR) depicting thermal contours and concentrations (ind. 1000 m^{-3}) of early- (Z1-Z2), mid- (Z3), and late-stage (Z4-Z5) Dungeness crab (*Cancer magister*) zoea throughout the water column. Empty regions represent unsampled locations while '+' denote true zeros. Black polygons show the approximate location of the continental shelf.

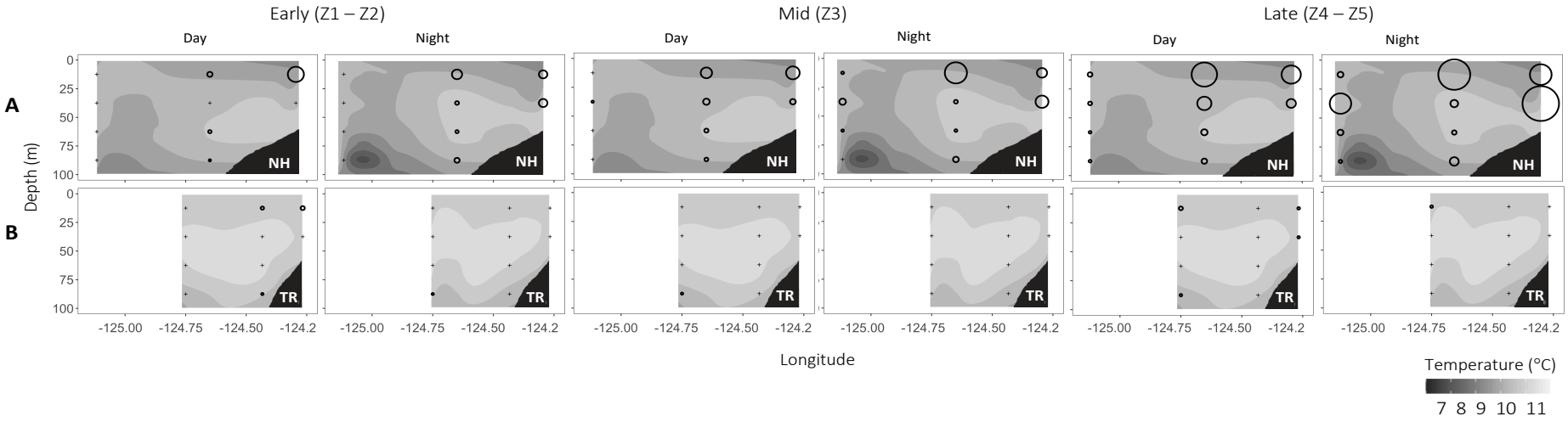

Fig. 5.5. Cross-sections of day and night transects sampled during the winter of 2019 along the (A) Newport Hydrographic Line (NH) and the (B) Trinidad Head Line (TR) depicting thermal contours and concentrations (ind. 1000 m^{-3}) of early- (Z1-Z2), mid- (Z3), and late-stage (Z4-Z5) Dungeness crab (*Cancer magister*) zoea throughout the water column. Empty regions represent unsampled locations and '+' denote true zeros. Black polygons show the approximate location of the continental shelf

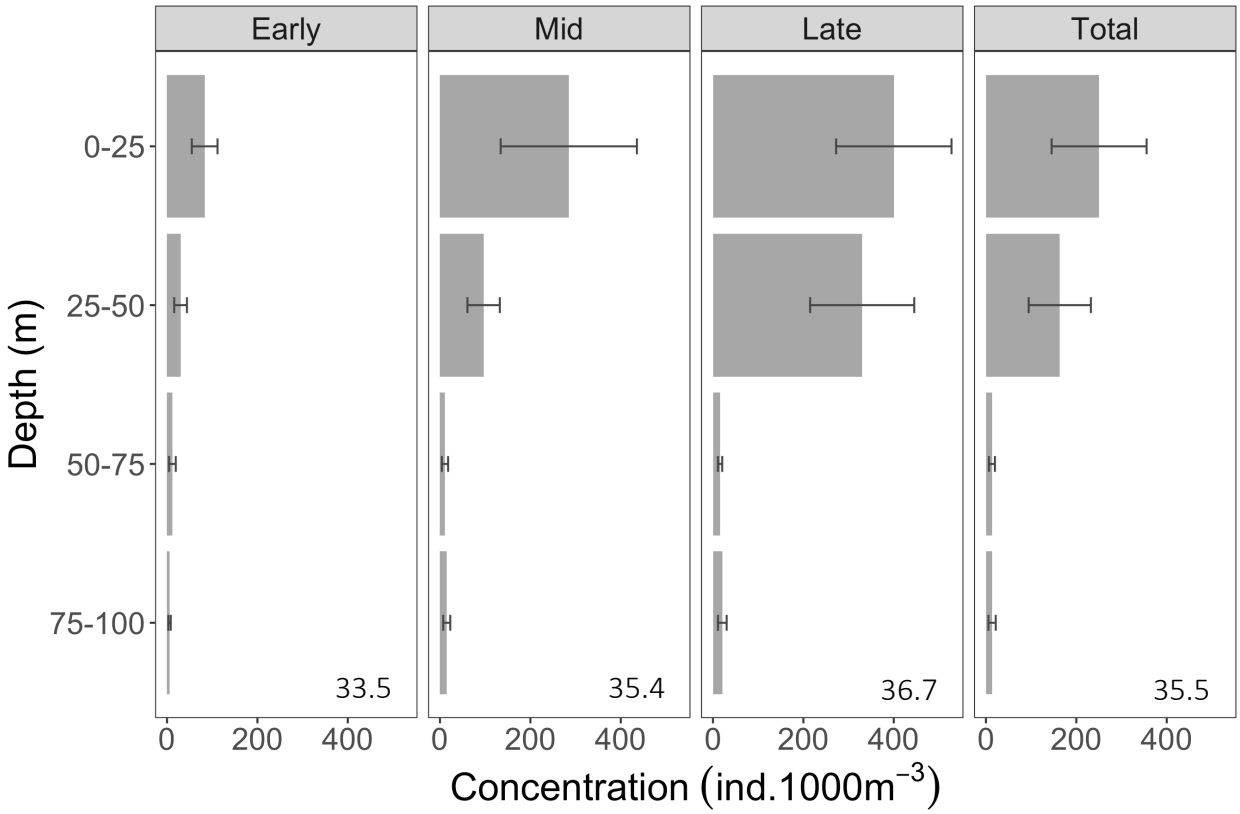

Fig. 5.6. Mean (±SE) concentration of early- (Z1-Z2), mid- (Z3), late-stage (Z4-Z5), and total Dungeness crab (*Cancer magister*) zoea per 25-m vertical depth bin, with stage-specific weighted mean depths (m) indicated in the bottom right of each plot

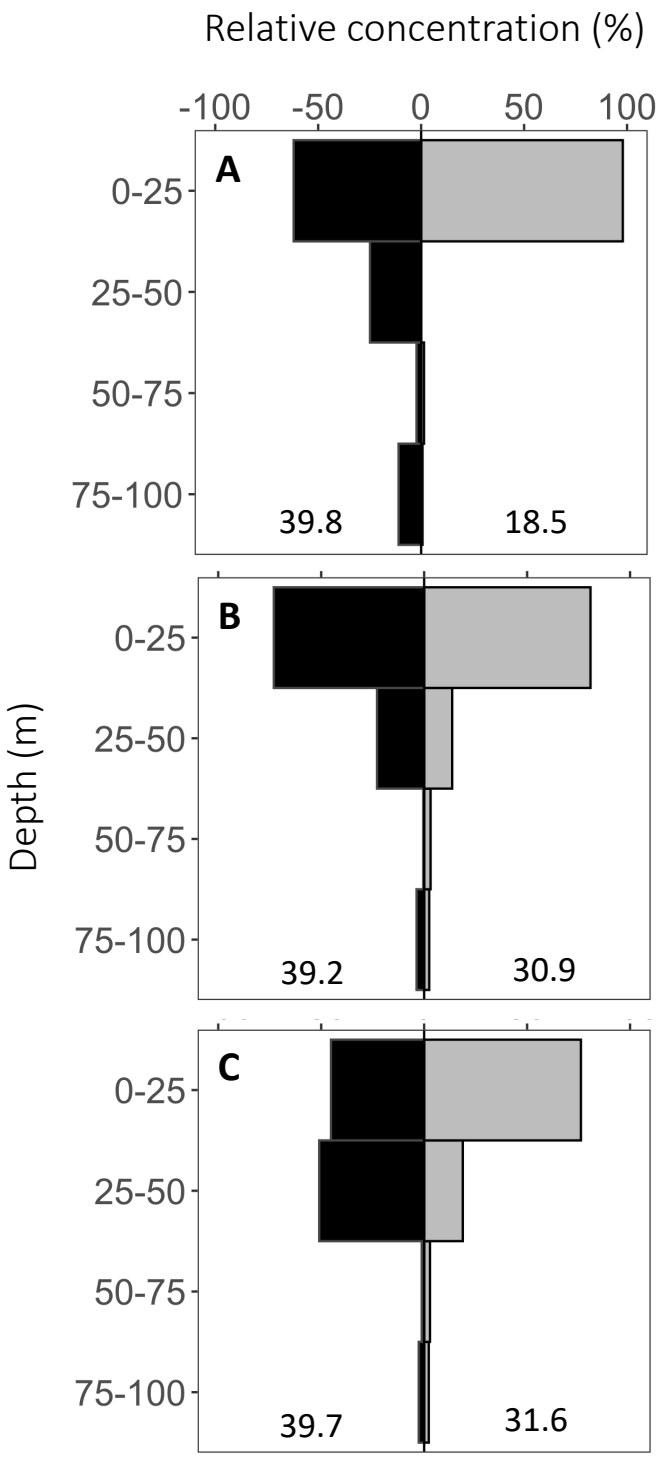

Fig. 5.7. Diel vertical distributions of the relative day and night concentration (%) of (A) early-, (B) mid-, and (C) late-stage Dungeness crab (*Cancer magister*) zoea collected within 24 h periods along the Newport Hydrographic Line and Trinidad Head Line (combined) in the winter of 2019. Black bars = night; gray bars = day, excluding dusk and dawn. Stage-specific night and day weighted mean depths (m) are indicated at the bottom of each plot. There was no significant difference in night and day WMDs for any stage.

CHAPTER 6: General conclusions

A fundamental goal of the field of fisheries oceanography is to understand the specific mechanisms through which variability in the environment translates into recruitment variability. Survival to recruitment ultimately depends on larva-prey and larva-predator encounter rates, which are subject to the prevailing oceanographic conditions that dictate overall abundances as well as spatial distributions among taxa (Lasker 1975, Bailey & Houde 1989). However, our knowledge of the fine-scale distributions and realized diets and growth of the early life history stages of fishes in the northern California Current (NCC) is limited. Here, we used novel sampling (depth-discrete net collections, *in situ* plankton imagery) and lab analyses (gut content and otolith-derived growth analyses) to holistically address the biophysical drivers of larval success. Together, the four chapters of this dissertation answer important questions about larval fish survivorship that contribute to our understanding of recruitment variability in the NCC.

The NCC is a highly dynamic and productive Eastern Boundary Current System that supports robust populations of ecologically and economically important species. There are multiple research programs in this system dedicated to examining the effects of oceanographic variability on the spatio-temporal distributions of the early life history stages of fishes. From these studies, we know that fish larvae are strongly impacted by oceanographic conditions; however, teasing apart the mechanisms relating the physical environment to survival in this dynamic system has been difficult. Recently, the NCC experienced a severe marine heatwave that led to unusual ecological occurrences. One such unpredictable occurrence was the dominance of species typically associated with cool and productive conditions, such as northern anchovy and rockfishes (Thompson et al. 2019). The breakdown of correlative relationships between species and their environment under novel conditions (Muhling et al. 2020) challenges our current understanding of the role of oceanographic conditions and illustrates the importance of considering the indirect influence of oceanography on food-web dynamics.

Consequences of oceanographic conditions in the NCC

Temperature is widely recognized to be a central physical parameter affecting vital rates (Gillooly et al. 2001). Higher temperatures typically lead to faster larval growth and development. This has been confirmed for northern anchovy (*Engraulis mordax;* Methot & Kramer 1979) and Dungeness crab (*Cancer magister;* Des Voigne 1973, Ebert et al. 1983, Sulkin & McKeen 1989) larvae under laboratory conditions. Not surprisingly, modeling results in Chapter 2 indicated that larval northern lampfish (*Stenobrachius leucopsarus*) growth was significantly positively related to temperature. Importantly, all of these positive relationships between temperature and growth control for larval fish feeding. The above northern anchovy and Dungeness crab relationships were obtained in regimented lab-based settings where larvae were supplied with ad libitum food and our northern lampfish relationship accounted for prey availablility by including prey density as a covariate in the growth model. In contrast, Chapter 3 revealed that water temperature did not significantly affect northern anchovy growth after accounting for ambient prey availability, suggesting that the direct effects of temperature may not always be observed in the wild. This finding is an illustration of how the relationship between growth and temperature is constrained by sufficient feeding and the metabolic needs of ectotherms increase with temperature (Gillooly et al. 2001). In upwelling systems, temperature and production usually have an inverse relationship and it is relatively atypical for the 'best' feeding opportunities to co-occur with warm temperaures. As such, directly relating growth to temperature can be misleading in upwelling systems without explicitly accounting for changes in prey availabililty. Measuring the combined effects of temperature and food-web dynamics on larval fishes in the NCC is integral to predicting the impacts of changing ocean conditions on fish populations. Such data would likely help us understand the underlying cause of the 'cold water' species booms during anomolously warm marine heatwave conditions.

This dissertation revealed that upwelling strongly affected the distributions, diets, and growth of planktonic larvae. Upwelling had a larger influence on the cross-shelf distribution of taxa that occupied the surface layer (i.e., northern anchovy and crab zoea) than those that are more broadly distributed throughout the water column (i.e., northern lampfish, Chapter 2). Interestingly, upwelling influenced larval distributions in two distinct ways that varied based on species spawning location. Upwelling appeared to

advect coastal taxa (i.e., Dungeness crab, Chapter 5) seaward while at the same time restricting the shoreward distribution of offshore taxa (i.e., northern anchovy, Chapter 3). As a result, the cross-shelf extent of upwelled waters mediated coastal and offshore species interactions which contributed to spatially variable patterns in northern anchovy growth (Chapter 3).

The *Optimal Environmental Window Hypothesis* (Cury & Roy 1989, Roy et al. 1992) predicts that there is a dome-shaped relationship between upwelling intensity and recruitment. In Chapter 2, we found that the fastest northern lampfish larval growth occurred at moderate upwelling intensity. Despite similar ambient prey densities between moderate and intense upwelling conditions, fish that experienced the latter consumed an order of magnitude lower prey biomass resulting in significantly slower larval growth. We hypothesize that while upwelling is necessary to replenish surface nutrients, too much upwelling can disrupt larval feeding. More broadly, these data indicate that foraging success is a function of local productivity and the factors that influence larva-prey encounter rates. This notion is echoed in Chapter 3 where we found that although prey densities were highest at the location of the upwelling front, northern anchovy larval growth was not. High abundances of zooplankton predators led to above average growth for northern lampfish and anchovy, which may indicate the consistent selective predation loss of slower-growing larvae in this system.

Upwelling clearly plays an important role in larval trophodynamics and growth. Yet, the NCC is a seasonally driven system with larvae experiencing vastly different upwelling conditions depending on the timing of spawning. The focal fish species in this dissertation are unusual in that they are not solely winter spawners like most NCC species. Northern anchovy are considered one of the only summer spawners in the system and northern lampfish have a protracted spawning season that encompasses both winter (downwelling) and summer (upwelling) conditions (Richardson 1973, Richardson & Pearcy 1977, Auth & Brodeur 2006, Auth et al. 2007, Brodeur et al. 2008, Auth 2009). Examining patterns of feeding and growth in the latter allowed us to investigate the trade-offs between winter and summer spawning in this seasonal system. In Chapter 2, we found that northern lampfish larvae consumed fewer and lower trophic level prey in the winter than in the summer, resulting in significantly slower growth in the winter. This

begs the question: what is the benefit of winter spawning? We hypothesize that winter-spawning may confer a survival advantage to young later in life, as they will be larger juveniles and subject to less gape-limitation when the large, lipid-rich copepod community dominates the system in summer. Such a tradeoff between fast and slow larval growth and subsequent juvenile success may underlie the persistence of a protracted spawning behavior in seasonally driven systems. How this tradeoff carries over to successful recruitment to the adult population each year is unclear, though this likely varies among years.

Fish larvae responded similarly to densities of their zooplankton prey at a major river plume as they did during upwelling along the coast, and results of Chapter 4 may help explain the observed phenomenon that larval fish feeding success is not solely determined by prey abundance. In this study of zooplankton dynamics in and around the Columbia River Plume, we found that although plume frontal regions concentrated prey, they did not necessarily confer the highest larval fish-prey overlap on fine scales relevant to trophic interactions. Also analogous to our upwelling findings, high densities of gelatinous predators co-occurred with high densities of prey throughout the Columbia River Plume region, but overlap with larval fishes was taxon-specific and varied through the progression of a tidal cycle.

Together, this work connects larval fish trophodynamics to oceanographic processes, illustrating how variability in the physical environment affects patterns of feeding, growth, and survival of the early life history stages of fishes in the NCC. Three dominant themes emerged from this dissertation and were evident across a range of oceanographic processes: (1) high prey densities do not always contribute to high larva-prey encounter rates or heightened feeding success, (2) high predator densities co-occur with high prey densities and affect larval growth of survivors, and (3) patterns of larval feeding and growth are sensitive to the prevailing environmental conditions on fine spatial and temporal scales. Specifically, local oceanography is an important factor affecting growth, and presumably, recruitment. Changes in vital rates with local oceanography and fine-scale distributions of prey and predators contributes to a mechanistic understanding of how variability in the environment translates into recruitment variability.

Anticipated impacts of climate change

Climate change is leading to novel conditions in the NCC that are becoming increasingly difficult to anticipate and manage. One of the most apparent is an increase in the frequency and intensity of marine heatwaves (Frölicher & Laufkötter 2018). Conditions during the 2014-2016 California Current severe marine heatwave resulted in reduced productivity (Kahru et al. 2018), low quality copepod prey (Peterson et al. 2015a, b, 2017), and a shift in the zooplankton community from crustacean to gelatinous dominated (Brodeur et al. 2019). While each of these processes have the potential to affect larval fish growth and mortality rates, their synergistic effects compound the consequences of marine heatwaves. For example, the metabolic needs of ectotherms increase with temperature (Gillooly et al. 2001). High marine heatwave temperatures coupled with low prey quantity and/or quality may lead to significantly reduced larval fish growth and condition (Gleiber et al. 2020), with implications for vulnerability to size-specific predation (Chapter 2,3; Anderson 1988).

Future climate scenarios are also predicted to change upwelling conditions, though the response is likely to be system- and latitude-specific (Sydeman et al. 2014). It was originally hypothesized that upwelling would universally intensify with climate change, as air over land should warm more quickly than air over the ocean, resulting in an increase in the cross-shore pressure gradients that drive upwelling-favorable winds (Bakun 1990). However, more recent modelling efforts suggest that the upwelling response is spatially variable and will intensify toward the poles in some Eastern Boundary Current Systems, including the NCC (Sydeman et al. 2014, Rykaczewski et al. 2015, García-Reyes et al. 2015). Intensified upwelling may increase production and shorten coastal food-webs, but it will also result in turbulence in the upper water column and increased offshore advection. Because the fastest larval fish growth occurred at moderate upwelling intensity and larval fish feeding and growth were diminished during the most intense upwelling conditions (Chapter 2), enhanced upwelling-induced production may not be a hallmark for increased larval fish feeding success as is often hypothesized. Further, the characteristics of upwelled water are likely to change into the future. Strong thermal stratification due to warming ocean temperatures can limit the

depth of the upwelling cell. This may result in warmer and less productive future upwelled waters. A shallower upwelling cell would impact food-web dynamics and limit the potential for intensified upwelling to counteract warming ocean temperatures, though there is still much uncertainty surrounding this hypothesis (Chhak & Di Lorenzo 2007, Jacox & Edwards 2011, Jacox et al. 2015). Upwelling phenology will also be impacted by climate change. The NCC is trending toward later and shorter upwelling seasons (Snyder et al. 2003, Bograd et al. 2009). Delayed upwelling-favorable winds may impact the arrival of the lipid-rich copepod prey base that is transported south from subarctic source waters after the onset of the upwelling season (Peterson & Miller 1977, Hooff & Peterson 2006). Access to the early life stages (nauplii and copepodite) of this nutritious prey-base is important for larval fish feeding (Chapter 2, 3).

In addition to the direct effects of climate change on the ocean, changing inland conditions trickle down to impact the coastal environment. In contrast to many other riverine dominated coastal systems, the Columbia River effluence is heavily regulated by 14 federal and a handful of privately owned hydroelectric dams. These dams participate in flow augmentation programs to aid in the migration of ESA listed juvenile salmonids from upper tributaries to the ocean. As inland drought conditions increase in frequency and intensity, some dams store water through the winter to be released during spring and summer, when sufficient flows are needed for the passage of out-migrating salmonids. These operations reduce winter flow and create artificially high spring and summer flow, with implications for the total volume and seasonality of the Columbia River Plume (Henderikx Freitas et al. 2018, NMFS 2020). Outflow volumes affect the strength and location of the plume fronts which directly impact larval fish trophic environments by modifying the spatial distributions of larvae, their prey, and their potential predators (Chapter 4). Changes to plume characteristics will especially impact taxa who use the Columbia River Plume as spawning and nursery habitat, such as northern anchovy (Richardson 1981, Emmett et al. 1997, 2006, Brodeur et al. 2005).

Future directions

The results of this dissertation highlight a few promising avenues for further study. The most apparent is a general need to increase our knowledge about the diets and

growth of forage fishes in the NCC. Northern lampfish (Chapter 2) and northern anchovy (Chapter 3, 4) are both constituents of this small-bodied and short-lived group. Given their life histories, their populations respond rapidly to changing oceanographic conditions (Baumgartner et al. 1992, Emmett et al. 2005, Brodeur et al. 2008) affording researchers the opportunity to more closely link observations to the environment. While the sheer biomass of these taxa in the ichthyoplankton points to the critical role they play in NCC oceanic food-webs, information about their diets and growth in this system is scant. Most diet and growth analyses are from studies in southern California for northern anchovy or Alaska for northern lampfish. Given the differences in planktonic communities and temperature between these regions and the NCC, we should expect variability in forage fish diets and growth across systems. This may be especially true for northern anchovy, who have genetically distinct sub-populations in the NCC and southern California. Unfortunately, we were unable to investigate northern anchovy diets in this dissertation because their long and fragile guts require preservation in formalin which precludes otolith-based growth analysis or the use of methods such as fatty acids or stable isotopes which were beyond the scope of this dissertation. Nonetheless, this would be an exciting extension of our work and extremely beneficial to parameterizing estimates of prey availability and to teasing apart the forces guiding northern anchovy recruitment variability in the NCC.

Another line of future research involves otolith-based growth analysis across life history stages. Specifically, in Chapter 2 we hypothesize that there may be a trade-off between fast larval and juvenile growth for winter-spawned species in seasonally driven upwelling systems. An extension of growth and diet analyses across these life history stages would address this hypothesis. This work might be most easily achieved by examining myctophids, such as northern lampfish, that have a protracted spawning season and are highly abundant. Further, myctophids are rarely targeted for 'higher-order' lab analyses and so it is possible that such a study could be accomplished using existing collections without the need to acquire expensive ship-time.

Finally, high-resolution *in situ* sampling allowed us to evaluate the relationships between larval fishes, their prey, and their predators on the fine spatial and temporal scales relevant to trophic interactions. Additionally, imagery allowed us to explicitly

investigate the role of potential predation, an often-overlooked process determining larval fish survival. Due to their fragile morphologies, gelatinous taxa are typically vastly underestimated by traditional sampling techniques, and thus is the potential for their predation on larval fishes. Because predation may be the primary agent of larval fish mortality (Bailey & Houde 1989), understanding variations in growth, survival, and recruitment requires the inclusion of accurate estimates of predation potential. When these data are coupled with depth-discrete sampling we can mechanistically relate the physical environment to recruitment by investigating the biological consequences (feeding and growth) of species distributions in space and time. Importantly, this sampling approach allows for the incorporation of *in situ* physical data. Because physical parameters attenuate quickly with depth in upwelling systems like the NCC, surface data (sea surface temperature, salinity, etc.) may not accurately capture conditions experienced by non-neustonic larvae. With new technologies and lab analyses, we can tackle previously unanswered questions about how variability in the environment translates into recruitment variability in the NCC. This knowledge is imperative to accurately predicting the effects of climate variability on fish populations both now and into the future.

REFERENCES

Anderson JT (1988) A review of size dependent survival during pre-recruit stages of fishes in relation to recruitment. J Northwest Atl Fish Sci 8:55–66

Auth TD (2009) Importance of far-offshore sampling in evaluating the ichthyoplankton community in the northern California Current. Calif Coop Ocean Fish Investig Reports 50:107–117

Auth TD, Brodeur RD (2006) Distribution and community structure of ichthyoplankton off the coast of Oregon, USA, in 2000 and 2002. Mar Ecol Prog Ser 319:199–213

Auth TD, Brodeur RD, Fisher KM (2007) Diel variation in vertical distribution of an offshore ichthyoplankton community off the Oregon coast. Fish Bull 105:313–326

Bailey K, Houde E (1989) Predation on eggs and larvae of marine fishes and the recruitment problem. Adv Mar Biol 25:1–83

Bakun A (1990) Global climate change and intensification of coastal ocean upwelling. Sci 247:198–201

Baumgartner T, Soutar A, Ferreira-Bartina V (1992) Reconstruction of the history of Pacific sardine and northern anchovy populations over the past two millennia from sediments of Santa Barbara Basin, California. CalCOFI Reports 33:24–40

Bograd SJ, Schroeder I, Sarkar N, Qiu X, Sydeman WJ, Schwing FB (2009) Phenology of coastal upwelling in the California Current. Geophys Res Lett 36:1–5

Brodeur RD, Auth TD, Phillips A (2019) Major shifts in pelagic micronekton and macrozooplankton community structure in an upwelling ecosystem related to an unprecedented marine heatwave. Front Mar Sci 6:212

Brodeur RD, Fisher JP, Emmett RL, Morgan CA, Casillas E (2005) Species composition and community structure of pelagic nekton off Oregon and Washington under variable oceanographic conditions. Mar Ecol Prog Ser 298:41–57

Brodeur RD, Peterson WT, Auth TD, Soulen HL, Parnel MM, Emerson AA (2008) Abundance and diversity of coastal fish larvae as indicators of recent changes in ocean and climate conditions in the Oregon upwelling zone. Mar Ecol Prog Ser 366:187–202

Chhak K, Lorenzo E Di (2007) Decadal variations in the California Current upwelling cells. Geophys Res Lett 34: L14604

Cury P, Roy C (1989) Optimal environmental window and pelagic fish recruitment success in upwelling areas. Can J Fish Aquat Sci 46:670–680

Des Voigne (1973) Influence of temperature and photoperiod upon the Dungeness crab *Cancer magister*. Ph.D. Dissertation, University of Washington

Ebert E, Haseltine A, Houk J, Kelly R (1983) Labratory cultivation of the Dungeness crab, *Cancer magister*. Fish Bull 172:259–310

Emmett RL, Bentley PJ, Schiewe MH (1997) Abundance and distribution of northern anchovy eggs and larvae (*Engraulis mordax*) off the Oregon coast, mid-1970s-1994 and 1995. Alaska Sea Grant College Program, Fairbanks, AK

Emmett RL, Brodeur RD, Miller TW, Pool SS, Krutzikowsky GK, Bentley PJ, McCrae J (2005) Pacific sardine (*Sardinops sagax*) abundance, distribution, and ecological relationships in the Pacific Northwest. CalCOFI Rep 46:122–143

Emmett RL, Krutzikowsky GK, Bentley P (2006) Abundance and distribution of pelagic piscivorous fishes in the Columbia River plume during spring/early summer 1998–

2003: relationship to oceanographic conditions, forage fishes, and juvenile salmonids. Prog Oceanogr 68:1–26
Frölicher TL, Laufkötter C (2018) Emerging risks from marine heat waves. Nat Commun 9:2015–2018
García-Reyes M, Sydeman W, Schoeman D, Rykaczewski R, Black B, Smit A, Bograd S (2015) Under pressure: climate change, upwelling, and eastern boundary upwelling ecosystems. Front Mar Sci 2:109
Gillooly J, Brown J, West G, Savage V, Charnov E (2001) Effects of size and temperature on metabolic rate. Science 293:2248–2251
Gleiber MR, Sponaugle S, Cowen RK (2020) Some like it hot, hungry tunas do not! Implications of temperature and plankton food web dynamics on growth and diet of tropical tuna larvae. ICES J Mar Sci 77:3058–3073
Henderikx Freitas F, Saldías GS, Goni M, Shearman RK, White AE (2018) Temporal and spatial dynamics of physical and biological properties along the endurance array of the California Current ecosystem. Oceanography 31:80–89
Hooff RC, Peterson WT (2006) Copepod biodiversity as an indicator of changes in ocean and climate conditions of the northern California current ecosystem. Limnol Oceanogr 51:2607–2620
Jacox MG, Bograd SJ, Hazen EL, Fiechter J (2015) Sensitivity of the California Current nutrient supply to wind, heat, and remote ocean forcing. Geophys Res Lett 42:5950–5957
Jacox MG, Edwards CA (2011) Effects of stratification and shelf slope on nutrient supply in coastal upwelling regions. J Geophys Res Ocean 116:3019
Kahru M, Jacox MG, Ohman MD (2018) CCE1: Decrease in the frequency of oceanic fronts and surface chlorophyll concentration in the California Current System during the 2014-2016 northeast Pacific warm anomalies. Deep Sea Res Part I Oceanogr Res Pap 140:4–13
Lasker R (1975) Field criteria for survival of anchovy larvae: the relation between inshore chlorophyll maximum layers and successful first feeding. Fish Bull US 73:453–462
Methot RD, Kramer D (1979) Growth of northern anchovy, *Engraulis mordax*, larvae in the sea. Fish Bull 77:413–423
Muhling BA, Brodie S, Smith JA, Tommasi D, Gaitan CF, Hazen EL, Jacox MG, Auth TD, Brodeur RD (2020) Predictability of species distributions deteriorates under novel environmental conditions in the California Current System. Front Mar Sci 7:589
NMFS (2020) Endangered Species Act Section 7(a)(2) Biological Opinion and Magnuson-Stevens Fishery Conservation and Management Act Essential Fish Habitat Response for the Continued Operation and Maintenance of the Columbia River System. https://www. fisheries.noaa.gov/national/endangered-species-conservation/biological-opinions
Peterson WT, Fisher JL, Strub PT, Du X, Risien C, Peterson J, Shaw CT (2017) The pelagic ecosystem in the Northern California Current off Oregon during the 2014-2016 warm anomalies within the context of the past 20 years. J Geophys Res Ocean 122:7267–7290
Peterson WT, Miller CB (1977) Seasonal cycle of zooplankton abundance and species

composition along the central Oregon coast. Fish Bull 75:717–724
Peterson WT, Robert M, Bond N (2015a) The warm Blob- conditions in the northeastern Pacific ocean. PICES Press 23
Peterson WT, Robert M, Bond N (2015b) The warm Blob continues to dominate the ecosystem of the northern California Current. PICES Press 23
Richardson SL (1973) Abundance and distribution of larval fishes in waters off Oregon, May - October 1969, with special emphasis on the northern anchovy, *Engraulis mordax*. Fish Bull 71:697–711
Richardson SL (1981) Spawning biomass and early life of northern anchovy, *Engraulis mordax*, in the northern subpopulation off Oregon and Washington. Fish Bull 78:855–876
Richardson SL, Pearcy WG (1977) Coastal and oceanic fish larvae in an area of upwelling off Yaquina Bay, Oregon. Fish Bull 75:125–145
Roy C, Cury P, Kifani S (1992) Pelagic fish recruitment success and reproductive strategy in upwelling areas: environmental compromises. South African J Mar Sci 12:135–146
Rykaczewski RR, Dunne JP, Sydeman WJ, García-Reyes M, Black BA, Bograd SJ (2015) Poleward displacement of coastal upwelling-favorable winds in the ocean's eastern boundary currents through the 21st century. Geophys Res Lett 42:6424–6431
Snyder MA, Sloan LC, Diffenbaugh NS, Bell JL (2003) Future climate change and upwelling in the California Current. Geophys Res Lett 30:1823
Sulkin S, McKeen G (1989) Laboratory study of survival and duration of individual zoeal stages as a function of temperature in the brachyuran crab *Cancer magister*. Mar Biol 103:31–37
Sydeman W, Garcia-Reyes M, Schoeman D, Rykaczewski D, Thompson S, Black B, Bograd S (2014) Climate change and wind intensification in coastal upwelling ecosystems. Science 345:1750-377–80
Thompson AR, Schroeder ID, Bograd SJ, Hazen EL, Jacox MG, Leising A, Wells BK, Largier JL, Fisher JL, Jacobson KC, Zeman SM, Bjorktedt EP, Robertson RR, Kahru M, Goericke R, Peabody CE, Baumgartner T, Lavaniegos BE, Miranda LE, Gómez-Ocampo E, Gómez-Valdés J, Authy TD, Daly EA, Morgan CA, Burke JB, Field JC, Sakuma K, Weber ED, Watson W, Porquez JM, Dolliver J, Lyons DE, Orben RA, Zamon J, Warybok P, Jahncke J, Santora JA, Thompson SA, Hoover B, Sydeman WJ, Melin S (2019) State of the California Current 2018-19: a novel anchovy regime and a new marine heat wave? CalCOFI Rep 60:1–65

APPENDICES

APPENDIX A – Chapter 2 supplementary tables and figures

Table A1. Summary of linear regressions between northern lampfish (*Stenobrachius leucopsarus*) size (standard length * body depth; mm) vs. age (d), otolith radius (um) vs. age, and size-at-age residuals vs. radius-at-age residuals. NH = Newport Hydrographic Line and TR = Trinidad Head Line.

				Slope			
Relationship	Year	Season	Location	Est.	SE	R^2	p
Size vs. Age	2018	Winter	NH	0.16	0.01	0.83	<0.001
	2018	Winter	TR	0.18	0.05	0.7	0.02
	2018	Summer	NH	0.59	0.06	0.79	<0.001
	2018	Summer	TR	0.46	0.05	0.78	<0.001
	2019	Winter	NH	0.23	0.02	0.82	<0.001
	2019	Winter	TR	0.19	0.02	0.82	<0.001
	2019	Summer	NH	0.43	0.04	0.83	<0.001
	2019	Summer	TR	0.57	0.05	0.84	<0.001
Radius vs. Age	2018	Winter	NH	1.08	0.06	0.91	<0.001
	2018	Winter	TR	1.49	0.14	0.96	<0.001
	2018	Summer	NH	2.21	0.17	0.85	<0.001
	2018	Summer	TR	1.95	0.21	0.76	<0.001
	2019	Winter	NH	1.14	0.05	0.95	<0.001
	2019	Winter	TR	1.08	0.07	0.91	<0.001
	2019	Summer	NH	1.97	0.11	0.92	<0.001
	2019	Summer	TR	2.44	0.18	0.87	<0.001
Size-at-age residuals vs.	2018	Winter	NH	3.46	0.62	0.54	<0.001
radius-at-age residuals	2018	Winter	TR	-0.64	1.34	-0.19	0.67
	2018	Summer	NH	1.85	0.47	0.34	<0.001
	2018	Summer	TR	2.52	0.75	0.28	0.002
	2019	Winter	NH	1.28	0.38	0.26	0.002
	2019	Winter	TR	2.08	0.65	0.25	0.003
	2019	Summer	NH	2.25	0.39	0.54	<0.001
	2019	Summer	TR	2.85	0.49	0.55	<0.001

Table A2. Northern lampfish (*Stenobrachius leucopsarus*) concentration, upwelling during sampling, and concentrations of environmental prey (protists, copepod nauplii, and calanoid copepods) and predators (chaetognaths and ctenophores) sampled along the Newport Hydrographic Line (NH) and Trinidad Head Line (TR) during the winter and summer of 2018 and 2019.

	Winter			Summer		
	All	**NH**	**TR**	**All**	**NH**	**TR**
2018						
Northern lampfish (ind. 1000 m^{-3})	2.2 (±1.3)	2.4 (±1.7)	1.6 (±1.3)	55.0 (±8.7)	32.0 (±13.0)	74.4 (±11.2)
Upwelling (CUTI; m^3s^{-1})	6.7 (2.9 - 12.9)	3.6 (2.9 - 4.3)	12.9 (NA)	11.3 (3.0 - 21.0)	3.1 (3.0 - 3.1)	19.6 (18.2 - 21.0)
Prey						
Protists (ind. m^{-3})	8.9 (±3.0)	10.9 (±4.7)	6.8 (±4.9)	15.1 (±3.8)	7.3 (±3.0)	19.0 (±4.5)
Copepod nauplii (ind. m^{-3})	NA	NA	NA	9551.1 (±1443.2)	9416.6 (±2660.9)	9685.6 (±1821.1)
Calanoid copepods (ind. m^{-3})	59.5 (±46.8)	13.4 (±3.2)	105.6 (±94.3)	49.9 (±18.5)	98.8 (±35.0)	25.4 (±7.1)
Predators						
Chaetognaths, ctneophores (ind. m^{-3})	2.4 (±0.5)	3.0 (±0.2)	1.9 (±1.0)	2.2 (±0.5)	2.5 (±1.8)	2.1 (±0.4)
2019						
Northern lampfish (ind. 1000 m^{-3})	19.6 (±5.4)	18.6 (±3.3)	20.6 (±9.3)	14.1 (±1.8)	11.2 (±2.7)	16.9 (±2.4)
Upwelling (CUTI; m^3s^{-1})	2.2 (0.8 - 3.2)	1.4 (0.8 - 2.0)	3.1 (2.9 - 3.2)	5.0 (3.6 - 7.0)	3.8 (3.6 - 3.9)	6.2 (5.5 - 7.0)
Prey						
Protists (ind. m^{-3})	10.2 (±2.0)	13.6 (±2.5)	6.9 (±2.3)	25.6 (±4.4)	23.1 (±8.6)	28.1 (±3.6)
Copepod nauplii (ind. m^{-3})	3754.7 (±644.5)	4146.3 (±1298.0)	3363.1 (±488.6)	4439.2 (±719.8)	3931.0 (±754.5)	4947.4 (±1327.8)
Calanoid copepods (ind. m^{-3})	13.7 (±3.2)	18.9 (±5.3)	8.6 (±0.8)	39.6 (±9.4)	56.8 (± 14.2)	22.4 (±3.4)
Predators						
Chaetognaths, ctneophores (ind. m^{-3})	3.1 (±0.8)	5.1 (±0.3)	1.1 (±0.1)	4.2 (±0.7)	3.2 (±0.9)	5.2 (±1.0)

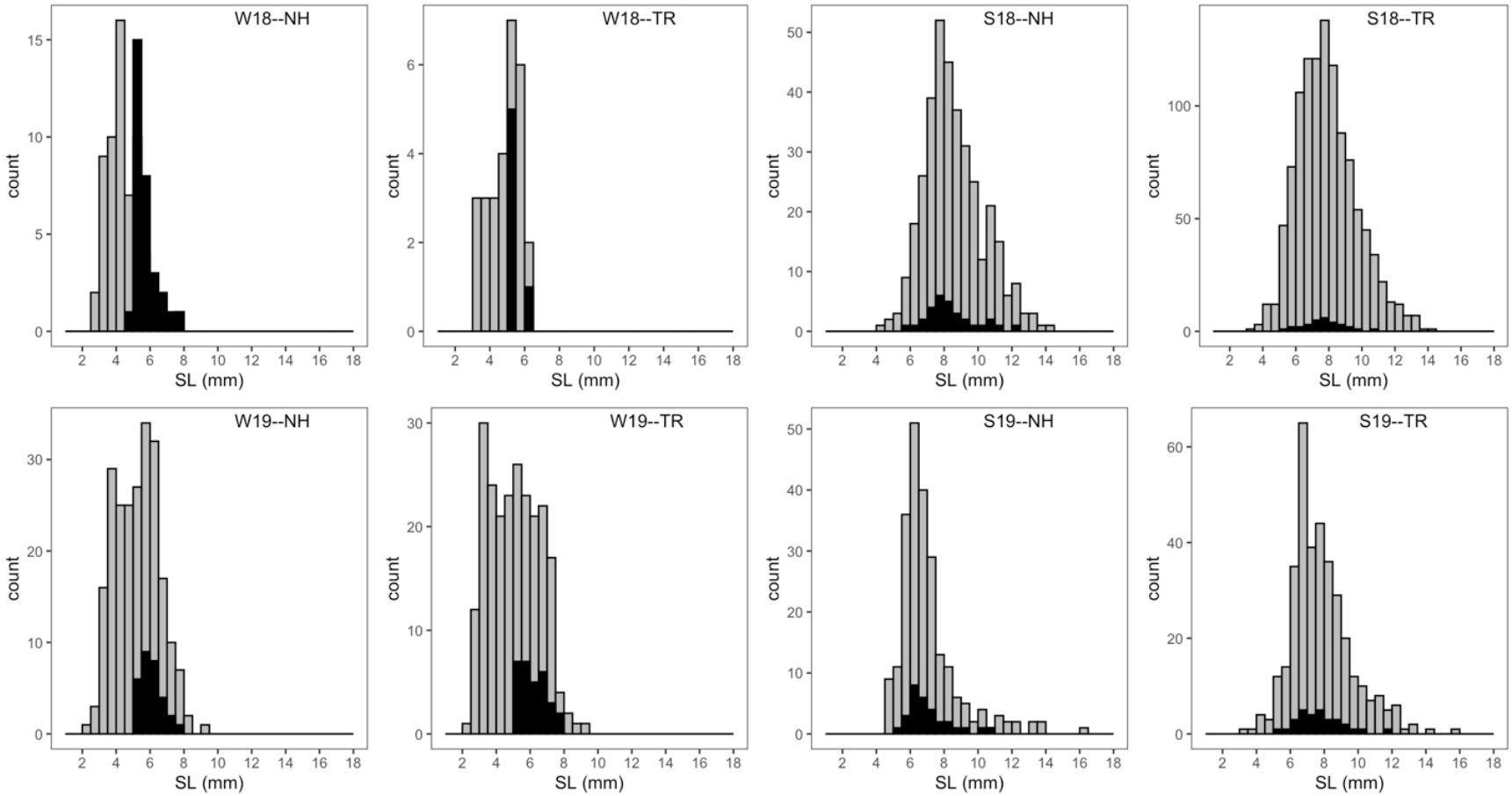

Fig. A1. Size (SL; standard length) frequency distribution of larval *Stenobrachius leucopsarus* collected in the winter and summer of 2018 and 2019 along the Newport Hydrographic Line (NH) and the Trinidad Head Line (TR). Grey bars indicate larvae collected in the top 50 m of the water column in all tows (n = 2,620), black bars indicate larvae selected for otolith and diet analysis. W18 = winter 2018, W19 = winter 2019, S18 = summer 2018, S19 = summer 2019

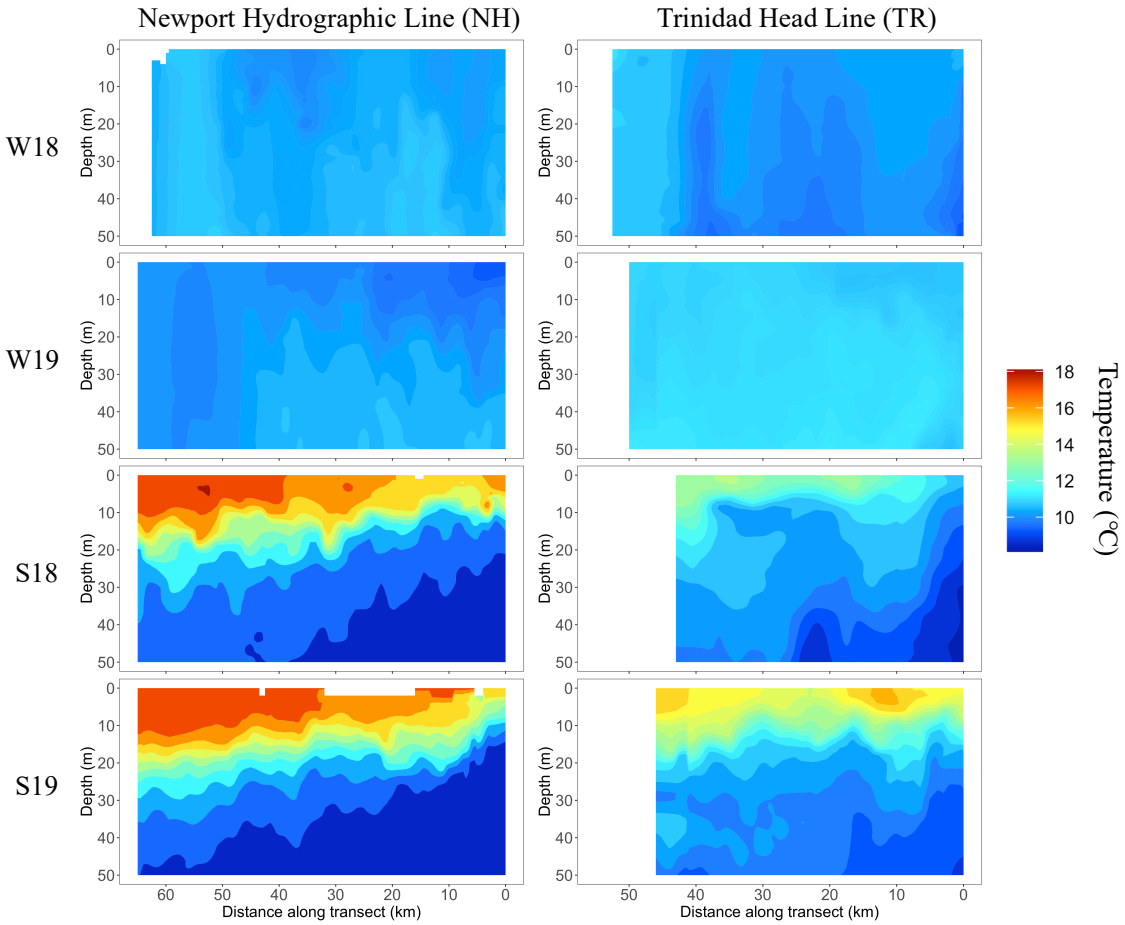

Fig. A2. Cross-shelf mean temperature profiles from the *In situ* Ichthyoplankton Imaging System (ISIIS) for each cruise and location, with the inshore most point on the right and offshore on the left. Values are kriged at a 2 m vertical, 500 m horizontal resolution the length of each transect. W18 = winter 2018, W19 = winter 2019, S18 = summer 2018, S19 = summer 2019

APPENDIX B – Chapter 3 supplementary tables and figures

Table B1. Summary of linear regressions between northern anchovy (*Engraulis mordax*) size (standard length; SL, mm) vs. age (d), otolith radius (um) vs. age, and size-at-age residuals vs. radius-at-age residuals

			Slope		
Relationship	Year	Location	Est.	SE	p
Size vs. Age	2018	Inshore	0.48	0.04	<0.001
	2018	Shelf-break	0.6	0.03	<0.001
	2018	Offshore	0.73	0.03	<0.001
	2019	Inshore	0.6	0.06	<0.001
	2019	Shelf-break	0.62	0.03	<0.001
	2019	Offshore	0.64	0.09	<0.001
Radius vs. Age	2018	Inshore	2.13	0.09	<0.001
	2018	Shelf-break	2.57	0.09	<0.001
	2018	Offshore	3.03	0.12	<0.001
	2019	Inshore	2.94	0.2	<0.001
	2019	Shelf-break	2.4	0.13	<0.001
	2019	Offshore	2.61	0.2	<0.001
Size-at-age residuals vs.	2018	Inshore	1.67	0.55	0.009
radius-at-age residuals	2018	Shelf-break	1.25	0.38	0.002
	2018	Offshore	2.21	0.3	<0.001
	2019	Inshore	1.77	0.68	0.02
	2019	Shelf-break	1.61	0.43	<0.001
	2019	Offshore	0.81	0.36	0.03

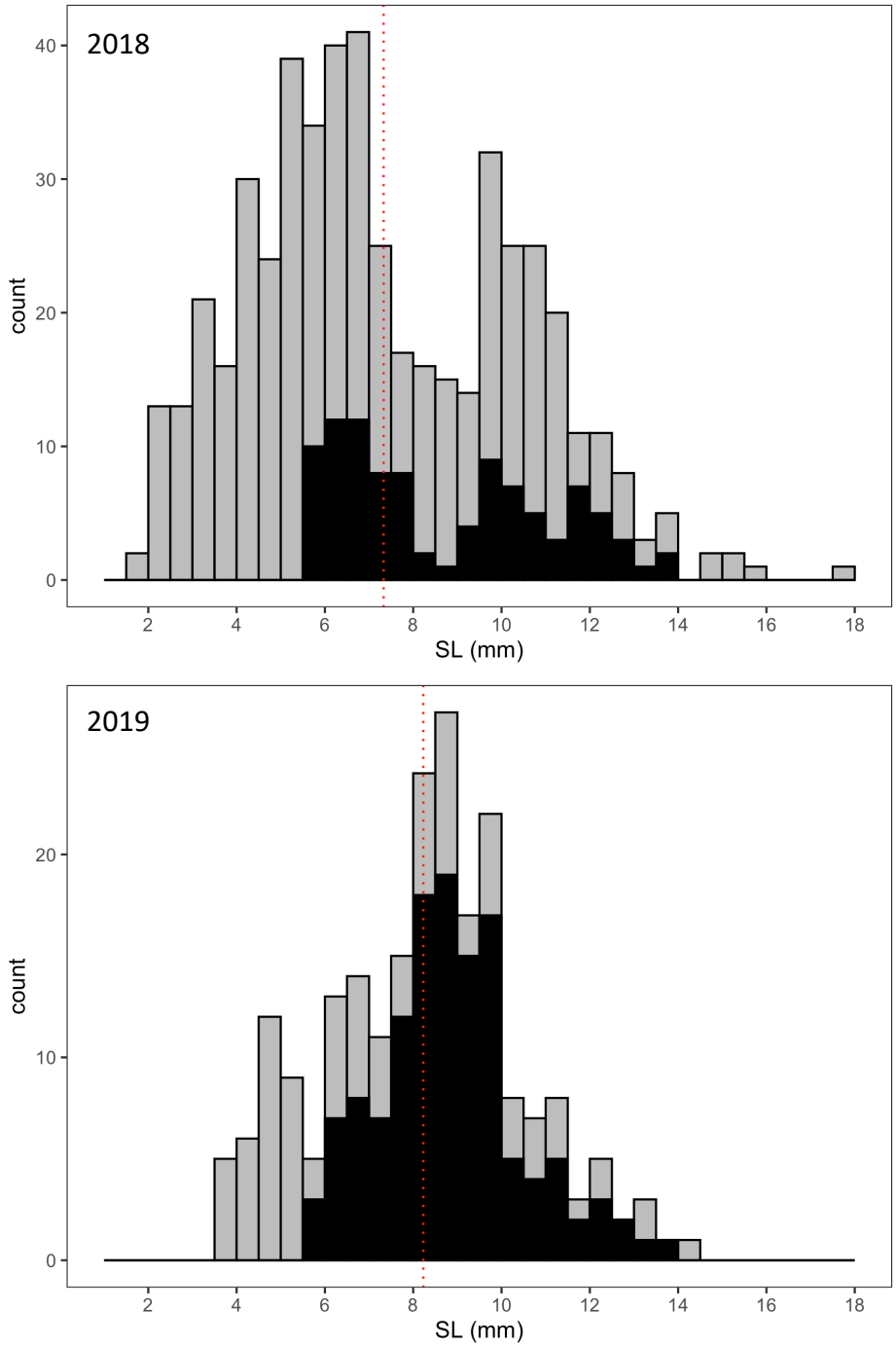

Fig. B1. Size (SL; standard length) frequency distribution of larval *Engraulis mordax* collected along the Newport Hydrographic Line in the summers of 2018 (top) and 2019 (bottom). Gray bars indicate larvae collected in the top 50 m of the water column in all tows, black bars indicate larvae selected for otolith analysis (n = 270). Red dotted line denotes the mean size each year.

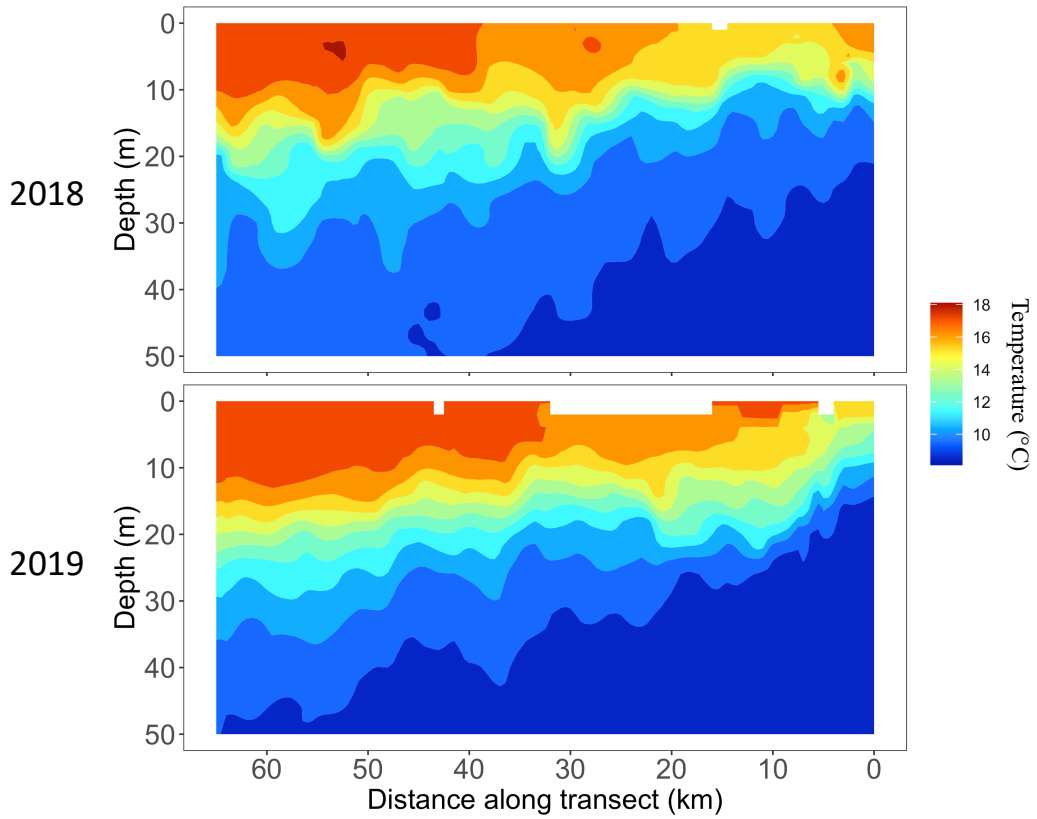

Fig. B2. Cross-shelf mean temperature profiles from the *In situ* Ichthyoplankton Imaging System (ISIIS) for each year, with the inshore most point on the right and offshore on the left. Values are kriged at a 2-m vertical, 500-m horizontal resolution the length of each transect.

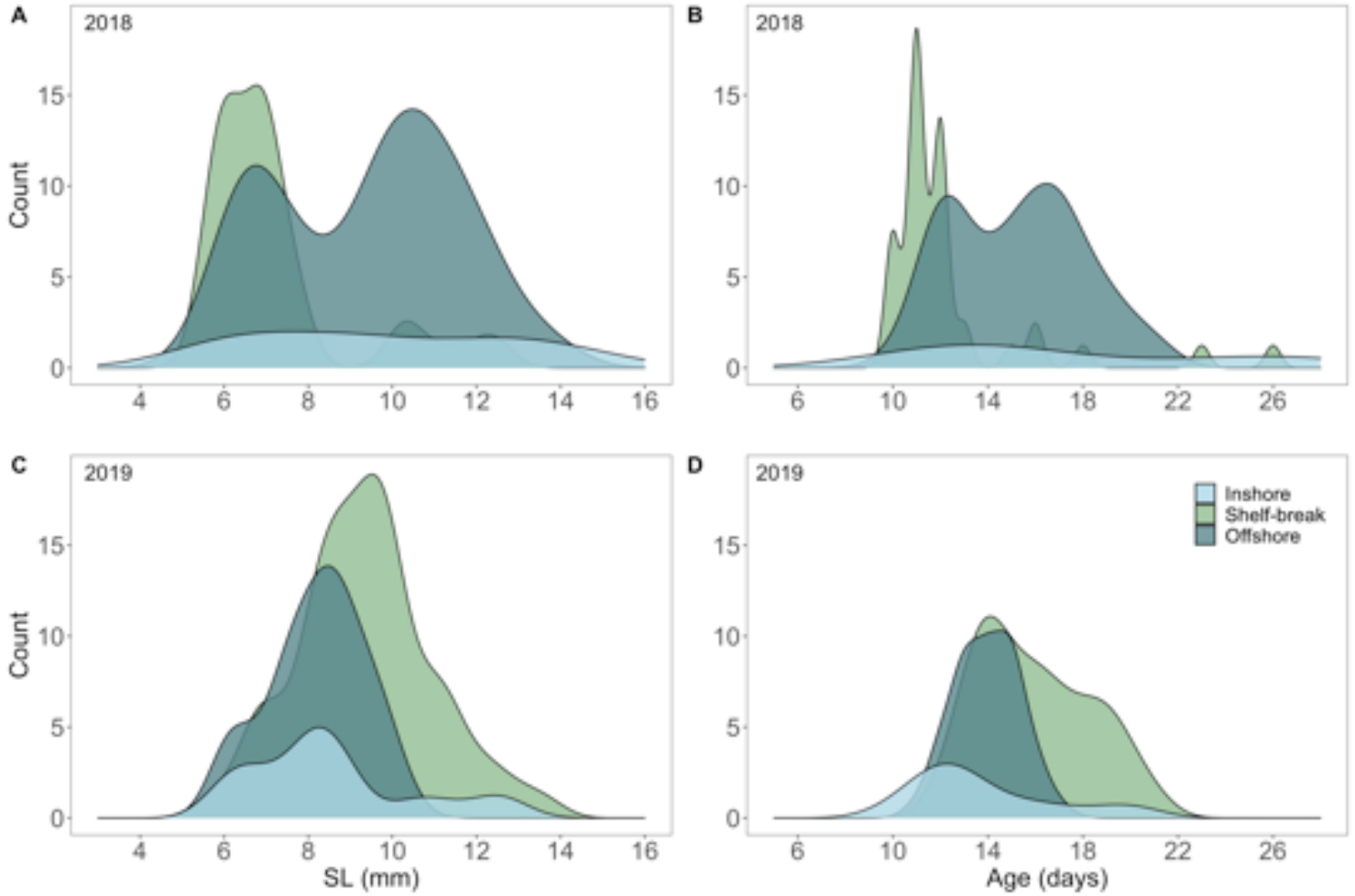

Fig. B3. Size (standard length; SL; A,C) and age (days post hatch; B,D) frequency distributions of larval northern anchovy (*Engraulis mordax*) examined for otolith microstructure analysis. Fish were collected along the Newport Hydrographic Line during the summers of (A, B) 2018 and (C,D) 2019 inshore (light blue), at the shelf-break (green), and offshore (dark blue).

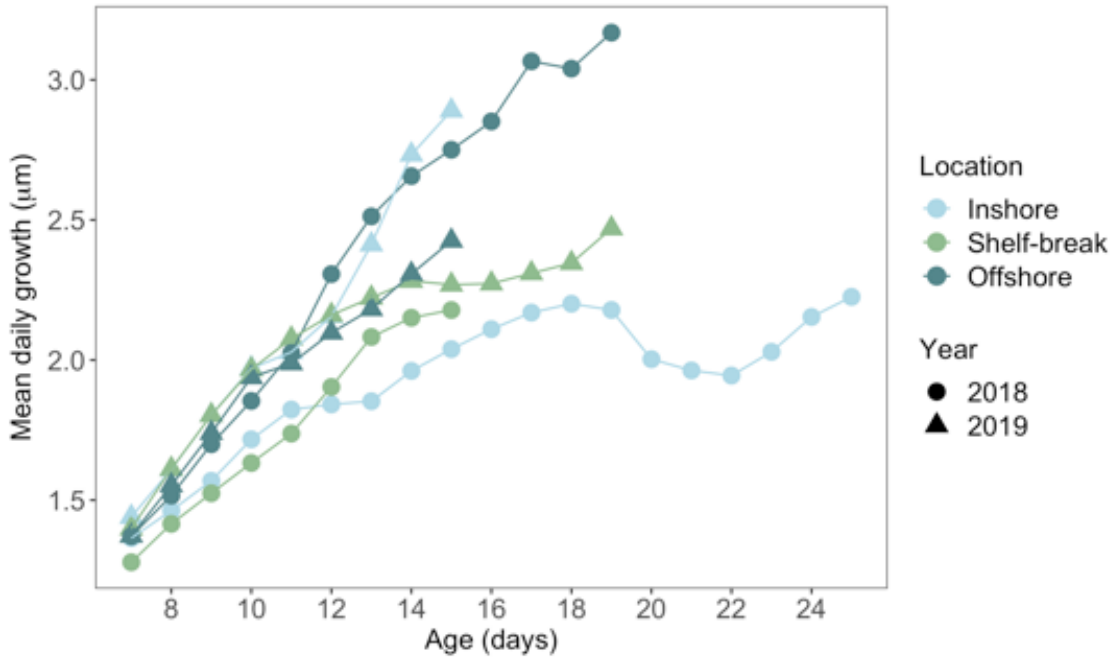

Fig. B4. Mean daily growth (otolith increment width) of northern anchovy (*Engraulis mordax*) collected along the Newport Hydrographic Line in the summers of 2018 (circles) and 2019 (triangles) at three cross-shelf locations. Ages were truncated when n < 3 observations

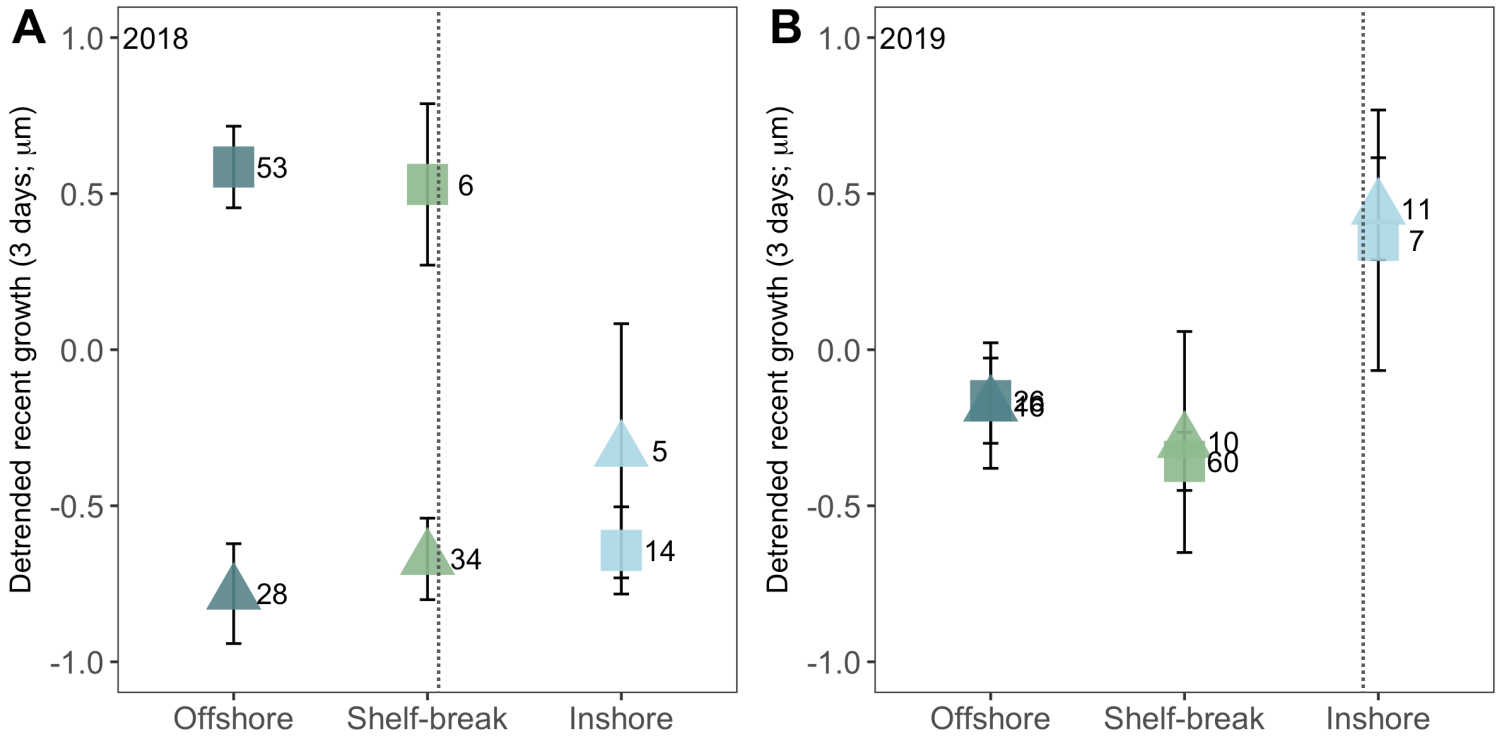

Fig. B5. Mean (± SE) detrended growth during the last three complete days of life (mean recent growth) of northern anchovy (*Engraulis mordax*) collected along the Newport Hydrographic Line in the summers of 2018 (A) and 2019 (B) at three cross-shelf locations. The dotted line denotes the general position of the upwelling front during sampling each year. Squares, old (≥ 14 d) age group only and triangles, young (< 14 d) age group only. Samples size indicated to the right of each data point

APPENDIX C – Chapter 4 supplementary tables and figures

Table C1. Original categories used by the sparse Convolutional Neural Net (sCNN) in the training library for the Columbia River Plume study and the corresponding filtering threshold (FT) applied to that category prior to condensing to their final categories. See Methods section for more details on this process.

Original category	FT	Final category
Anemone ceriantharia	1.00	Anemone ceriantharia
Appendicularian Fritillaridae	0.25	Appendicularian
Appendicularian s shape	0.36	Appendicularian
Appendicularian slight curve	0.85	Appendicularian
Appendicularian straight	0.30	Appendicularian
Appendicularian tadpole	0.49	Detritus
Artifacts bubble	0.99	Artifacts
Artifacts marbled	0.85	Artifacts
Chaetognath curve	0.99	Chaetognath
Chaetognath head	0.98	Chaetognath
Chaetognath “s” shape	0.96	Chaetognath
Chaetognath straight	0.23	Chaetognath
Chaetognath tail	0.42	Chaetognath
Copepod Calanoid Calanus	0.67	Copepod Calanoid Calanus
Copepod Calanoid diaptomoidea	0.93	Copepod Calanoid diaptomoidea
Copepod Calanoid eggs	0.99	Copepod Calanoid eggs
Copepod Calanoid long antennae	0.99	Unknown
Copepod Calanoid Mesocalanus	0.96	Copepod Calanoid Mesocalanus
Copepod Calanoid Metridia	0.99	Copepod Calanoid Metridia
Copepod Calanoid oblong	0.99	Copepod Calanoid Calanus-like
Copepod Calanoid oval	0.61	Copepod other
Copepod Calanoid paracalanidae	0.96	Copepod Calanoid paracalanidae
Copepod Calanoid Paracalanus	0.99	Copepod Calanoid paracalanidae
Copepod Calanoid Paraeuchaeta a	0.35	Copepod Calanoid Paraeuchaeta
Copepod Calanoid Paraeuchaeta b	0.27	Copepod Calanoid Paraeuchaeta
Copepod Calanoid Pseudocalanus	0.35	Copepod Calanoid Pseudocalanus
Copepod Cyclopoid Copilia female	0.84	Detritus
Copepod Cyclopoid Copilia male	0.38	Tunicate doliolid
Copepod Cyclopoid Oithona	0.62	Copepod Cyclopoid Oithona
Copepod Cyclopoid Oithona eggs	0.96	Copepod Cyclopoid Oithona eggs

Copepod Cyclopoid oithona eggs sideview	0.52	Copepod Cyclopoid oithona_eggs
Copepod Eucalaniid complex	0.97	Copepod Eucalaniid
Copepod Eucalaniid escape a	0.59	Copepod Eucalaniid
Copepod Eucalaniid escape b	0.66	Copepod Eucalaniid
Copepod Eucalaniid Eucalanus	0.42	Copepod Eucalaniid
Copepod Eucalaniid sideview	0.27	Copepod Eucalaniid
Copepod head on	0.99	Copepod other
Copepod humpback	0.55	Copepod other
Copepod other	0.46	Copepod other
Copepod poecilostomatoid	0.92	Copepod poecilostomatoid
Copepod poecilostomatoid eggs	0.56	Copepod poecilostomatoid
Copepod side view	0.23	Copepod other
Crustacean megalopae	0.83	Crustacean megalopae
Crustacean ostracod	0.47	Detritus
Crustacean other	0.27	Crustacean other
Crustacean shrimp Benthesicymidae	0.99	Crustacean shrimp other
Crustacean shrimp Caridean	0.47	Crustacean shrimp Caridean
Crustacean shrimp escape fully folded	0.32	Crustacean euphausiid
Crustacean shrimp escape partially folded	0.27	Crustacean euphausiid
Crustacean shrimp euphausiid	0.36	Crustacean euphausiid
Crustacean shrimp lg other	0.73	Crustacean other
Crustacean shrimp molt	0.96	Crustacean shrimp molt
Crustacean shrimp molt folded	0.96	Crustacean shrimp molt
Crustacean shrimp sm other	0.38	Crustacean other
Crustacean shrimp spiny	0.91	Crustacean other
Crustacean stomatopod	0.22	Detritus
Crustacean zoea crab	0.99	Crustacean zoea
Crustacean zoea shrimp	0.18	Crustacean zoea
Crustacean zoea tail	0.35	Crustacean zoea
Ctenophore Beroe	0.82	Ctenophore Beroe
Ctenophore cestid	0.56	Unknown
Ctenophore cydippid no tentacles	0.99	Ctenophore cydippid
Ctenophore cydippid tentacles	0.87	Ctenophore cydippid
Ctenophore lobate	0.79	Ctenophore lobate
Detritus bowtie	0.30	Detritus
Detritus “copepodmorph”	0.99	Detritus
Detritus “crustaceanmorph”	0.91	Detritus
Detritus dark	0.99	Detritus
Detritus partial	0.74	Detritus
Detritus “shooting star” shape	0.24	Detritus
Detritus small	0.98	Detritus

Detritus snow	0.95	Detritus
Detritus splotchy	0.32	Detritus
Diatom multiple	0.84	Phytoplankton mats
Diatom slight curve	0.99	Phytoplankton mats
Diatom stringy	0.24	Phytoplankton mats
Diatom “u” shape	0.98	Phytoplankton mats
Echinoderm holothurian auricularian	0.43	Echinoderm holothurian auricularian
Echinoderm pluteus	0.93	Echinoderm larvae
Echinoderm brachiolaria	0.67	Echinoderm larvae
Fish Engraulids	0.26	Fish Engraulids
Fish large flat	0.69	Fish large flat
Fish Leptocephlii	0.99	Fish Leptocephalii
Fish-like	0.28	Detritus
Fish long slender	0.48	Fish long slender
Fish Myctophid postflexion	0.48	Fish Myctophid
Fish Myctophid preflexion	0.99	Fish Myctophid
Fish Pleuronectiformes	0.36	Fish Pleuronectiformes
Fish Sebastes-like	0.28	Fish Sebastes-like
Fish unknown	0.40	Fish Unknown
Fish unknown type I	0.37	Fish Unknown
Foraminifera	0.46	Protist Foraminifera
Heteropod	0.99	Detritus
Hydromedusae Aegina	0.98	Hydromedusae Narcomedusae Aegina
Hydromedusae Aglantha dark	0.69	Hydromedusae Trachymedusae Aglantha
Hydromedusae Aglantha long tentacles	0.84	Hydromedusae Trachymedusae Aglantha
Hydromedusae Aglantha short tentacles	0.88	Hydromedusae Trachymedusae Aglantha
Hydromedusae Aglaura	0.37	Hydromedusae Trachymedusae Aglaura
Hydromedusae Arctapodema	0.91	Hydromedusae Trachymedusae Arctapodema
Hydromedusae big bulbous bell	0.79	Hydromedusae Leptomedusae Clytia
Hydromedusae big partial bell	0.21	Hydromedusae Leptomedusae Clytia
Hydromedusae big thin bell	0.92	Hydromedusae Leptomedusae Clytia
Hydromedusae Cunina or Pegantha	0.61	Hydromedusae Narcomedusae other
Hydromedusae Euphysa or Sarsia	0.89	Hydromedusae Anthomedusae
Hydromedusae Halitholus	0.98	Hydromedusae Anthomedusae
Hydromedusae Liriope	0.99	Hydromedusae Trachymedusae_other
Hydromedusae other	0.99	Hydromedusae Unknown
Hydromedusae sm bell	0.99	Hydromedusae Unknown
Hydromedusae Solmaris	0.45	Hydromedusae Narcomedusae Solmaris

Hydromedusae Solmundella	0.92	Hydromedusae Narcomedusae Solmundella
Hydromedusae Unknown I	0.42	Hydromedusae Unknown
Hydromedusae Unknown II	0.99	Hydromedusae Unknown
Hydromedusae Velella conaria-like	0.32	Hydromedusae Anthomedusae
Hydromedusae Velella medusae-like	0.99	Hydromedusae Anthomedusae
Jellyfish ephyra	0.45	Detritus
Jellyfish tentacles	0.99	Unknown gelatinous pieces
Jellyfish tentacles type II	0.42	Unknown gelatinous pieces
Nemertean pilidium	0.95	Nemertean pilidium
Phytoplankton Diatom chain string	0.99	Phytoplankton chains
Phytoplankton Diatom chain tube	0.99	Phytoplankton chains
Polychaete fat	0.99	Polychaete
Polychaete nectochaete magelona	0.33	Polychaete larvae
Polychaete snakey	0.88	Polychaete
Polychaete tomopteridae type I	0.72	Polychaete
Polychaete tomopteridae type II	0.77	Polychaete
Protist acantharia	0.33	Protist acantharia
Protist acantharia big center	0.30	Protist acantharia
Protist dark center	0.99	Protist other
Protist fuzzy olive	0.99	Protist radiolarian
Protist noctiluca	0.77	Protist other
Protist noctiluca long flagella	0.88	Protist other
Protist other	0.99	Protist other
Protist radiolarian chain	0.30	Protist other
Protist radiolarian colony	0.96	Protist other
Pteropod Cavoliniidae	0.44	Pteropod
Pteropod Clinoe	0.55	Pteropod
Pteropod Corolla	0.99	Pteropod
Pteropod tail	0.18	Pteropod
Pyrosome-like	0.39	Protist other
Siphonophore Calycophoran Abylidae	0.38	Siphonophore Calycophoran Abylidae
Siphonophore Calycophoran box	0.76	Siphonophore Calycophoran Abylidae
Siphonophore Calycophoran Muggiaea	0.28	Siphonophore Calycophoran Muggiaea
Siphonophore Calycophoran Muggiaea young	0.88	Siphonophore Calycophoran Muggiaea
Siphonophore Calycophoran Sphaeronectes doublebell	0.99	Siphonophore Calycophoran Sphaeronectes
Siphonophore Calycophoran Sphaeronectes singlebell	0.96	Siphonophore Calycophoran Sphaeronectes
Siphonophore other	0.37	Siphonophore other
Siphonophore partial	0.32	Siphonophore other
Siphonophore physonect	0.77	Siphonophore physonect

Tunicate doliolid	0.39	Tunicate doliolid
Tunicate doliolid budding	0.42	Tunicate doliolid budding
Tunicate doliolid dark	0.67	Tunicate doliolid
Tunicate doliolid multiple	0.48	Tunicate doliolid multiple
Tunicate doliolid sm	0.99	Tunicate doliolid
Tunicate doliolid with nurse	0.99	Tunicate doliolid with nurse
Tunicate partial body	0.99	Tunicate partial body
Tunicate partial zooids	0.99	Tunicate partial body
Tunicate salp	0.36	Tunicate salp
Unknown dark circles	0.22	Unknown
Unknown gelatinous pieces	0.33	Unknown
Unknown triangle	0.61	Unknown
Unknown unclassified	N/A	Unknown

Table C2. Confusion Matrix analysis results including the correction factor (CF) applied to concentration estimates for each final category. See Methods for a detailed description of each parameter.

No.	Category	Precision	Recall	F-score	CF
1	Anemone Ceriantharia	1.00	1.00	1.00	1.00
2	Appendicularian	0.25	0.47	0.33	0.54
3	Artifacts	0.80	0.68	0.73	1.18
4	Chaetognath	0.18	0.91	0.31	0.20
5	Copepod Calanoid Calanus	1.00	0.98	0.99	1.02
6	Copepod Calanoid Calanus-like	1.00	0.95	0.98	1.05
7	Copepod Calanoid Diaptomoidea	0.48	0.99	0.65	0.48
8	Copepod Calanoid eggs	0.97	0.99	0.98	0.98
9	Copepod Calanoid Mesocalanus	0.92	0.98	0.95	0.94
10	Copepod Calanoid Metridia	1.00	0.99	0.99	1.01
11	Copepod Calanoid Paracalanidae	0.61	0.92	0.73	0.67
12	Copepod Calanoid Paraeuchaeta	0.92	1.00	0.96	0.92
13	Copepod Calanoid Pseudocalanus	0.98	1.00	0.99	0.98
14	Copepod Cyclopoid Oithona	0.21	1.00	0.34	0.21
15	Copepod Cyclopoid Oithona eggs	0.16	1.00	0.27	0.16
16	Copepod Eucalaniid	0.75	0.99	0.86	0.76
17	Copepod other	0.59	0.88	0.70	0.66
18	Copepod Poecilostomatoid	0.12	0.99	0.21	0.12
19	Crustacean euphausiid	0.86	0.96	0.90	0.90
20	Crustacean megalopae	0.08	0.98	0.14	0.08
21	Crustacean other	0.09	0.74	0.15	0.12
22	Crustacean shrimp Caridean	0.36	1.00	0.53	0.36
23	Crustacean shrimp molt	0.29	0.97	0.45	0.30
24	Crustacean shrimp other	0.99	0.70	0.82	1.40
25	Crustacean zoea	0.59	0.99	0.74	0.60
26	Ctenophore Beroe	0.16	0.97	0.28	0.17
27	Ctenophore Cydippid	0.23	0.79	0.36	0.29
28	Ctenophore Lobate	0.81	0.92	0.86	0.88
29	Detritus	0.96	0.28	0.44	3.39
30	Echinoderm Holothurian Auricularian	0.03	1.00	0.07	0.03
31	Echinoderm larvae	0.01	0.93	0.02	0.01
32	Fish Engraulids	0.09	1.00	0.17	0.09
33	Fish large flat	0.19	0.50	0.27	0.38
34	Fish Leptocephalii	1.00	1.00	1.00	1.00
35	Fish long slender	0.14	0.96	0.24	0.14
36	Fish Myctophid	0.89	1.00	0.94	0.90
37	Fish Pleuronectiformes	0.06	0.96	0.11	0.06

38	Fish Sebastes-like	0.11	1.00	0.20	0.11
39	Fish Unknown	0.02	0.87	0.03	0.02
40	Hydromedusae Narcomedusae Solmundella	0.61	1.00	0.76	0.61
41	Hydromedusae Anthomedusae	0.75	0.98	0.85	0.76
42	Hydromedusae Leptomedusae Clytia	0.68	0.87	0.76	0.78
43	Hydromedusae Narcomedusae Aegina	0.80	0.99	0.89	0.81
44	Hydromedusae Narcomedusae other	0.40	1.00	0.57	0.40
45	Hydromedusae Narcomedusae Solmaris	0.25	1.00	0.40	0.25
46	Hydromedusae Trachymedusae Aglantha	0.63	0.95	0.75	0.66
47	Hydromedusae Trachymedusae Aglaura	0.03	0.83	0.05	0.03
48	Hydromedusae Trachymedusae Arctapodema	0.31	1.00	0.48	0.31
49	Hydromedusae Trachymedusae other	1.00	0.60	0.75	1.67
50	Hydromedusae Unknown	0.54	0.88	0.67	0.62
51	Nemertean pilidium	0.02	1.00	0.05	0.02
52	Phytoplankton chains	0.96	0.62	0.76	1.55
53	Phytoplankton mats	0.78	0.78	0.78	1.00
54	Polychaete	0.26	0.99	0.41	0.26
55	Polychaete larvae	0.01	1.00	0.01	0.01
56	Protist Acantharia	0.26	0.78	0.39	0.34
57	Protist Foraminifera	0.26	0.99	0.42	0.27
58	Protist other	0.48	0.98	0.64	0.49
59	Protist Radiolarian	0.80	0.97	0.88	0.82
60	Pteropod	0.04	0.96	0.07	0.04
61	Siphonophore Calycophoran Abylidae	0.33	0.99	0.49	0.33
62	Siphonophore Calycophoran Muggiaea	0.62	0.89	0.73	0.69
63	Siphonophore Calycophoran Sphaeronectes	0.91	0.99	0.95	0.91
64	Siphonophore other	0.01	0.74	0.02	0.02
65	Siphonophore Physonect	0.39	0.95	0.55	0.41
66	Tunicate doliolid	0.54	0.36	0.43	1.50
67	Tunicate doliolid budding	1.00	0.82	0.90	1.21
68	Tunicate doliolid multiple	0.25	0.98	0.39	0.25
69	Tunicate doliolid with nurse	1.00	0.98	0.99	1.02
70	Tunicate partial body	0.81	0.99	0.89	0.81
71	Tunicate salp	0.01	0.81	0.03	0.02
72	Unknown	0.84	0.59	0.69	1.43

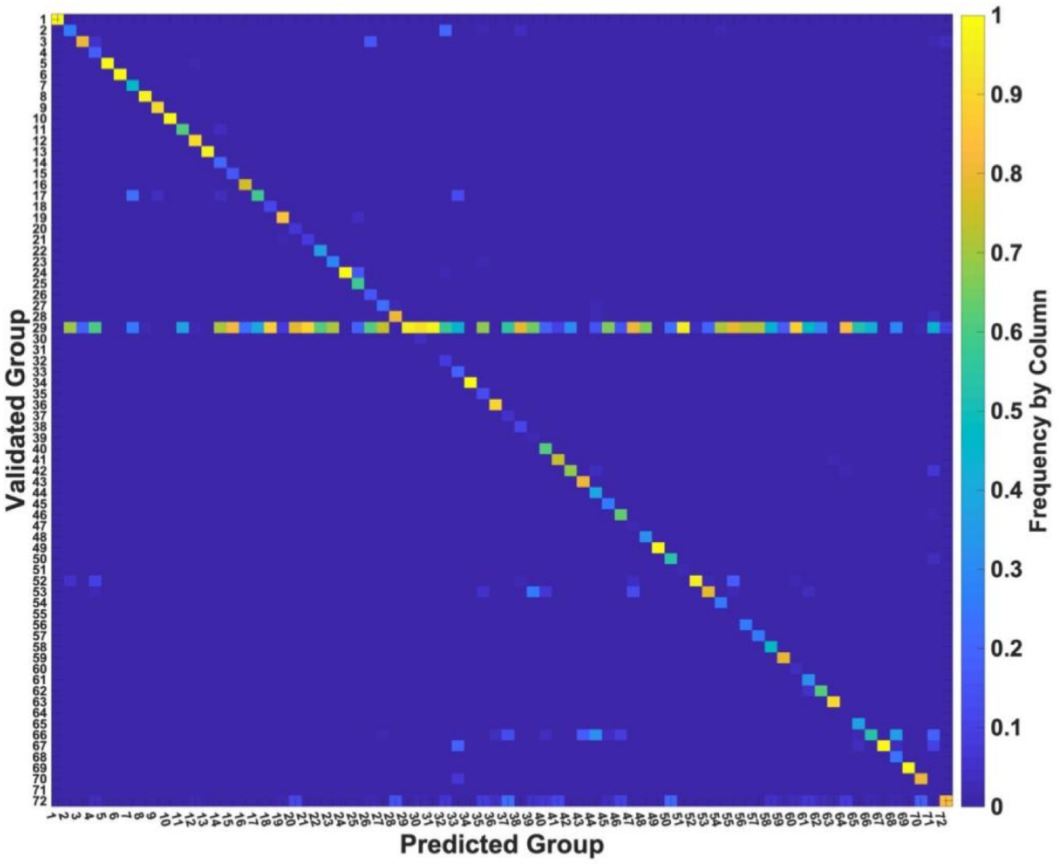

Fig. C1. Heat map of model Confusion Matrix showing predicted versus human expert validation of 86 681 randomly selected vignettes from all predicted groups. See Table S2 for category index numbers.

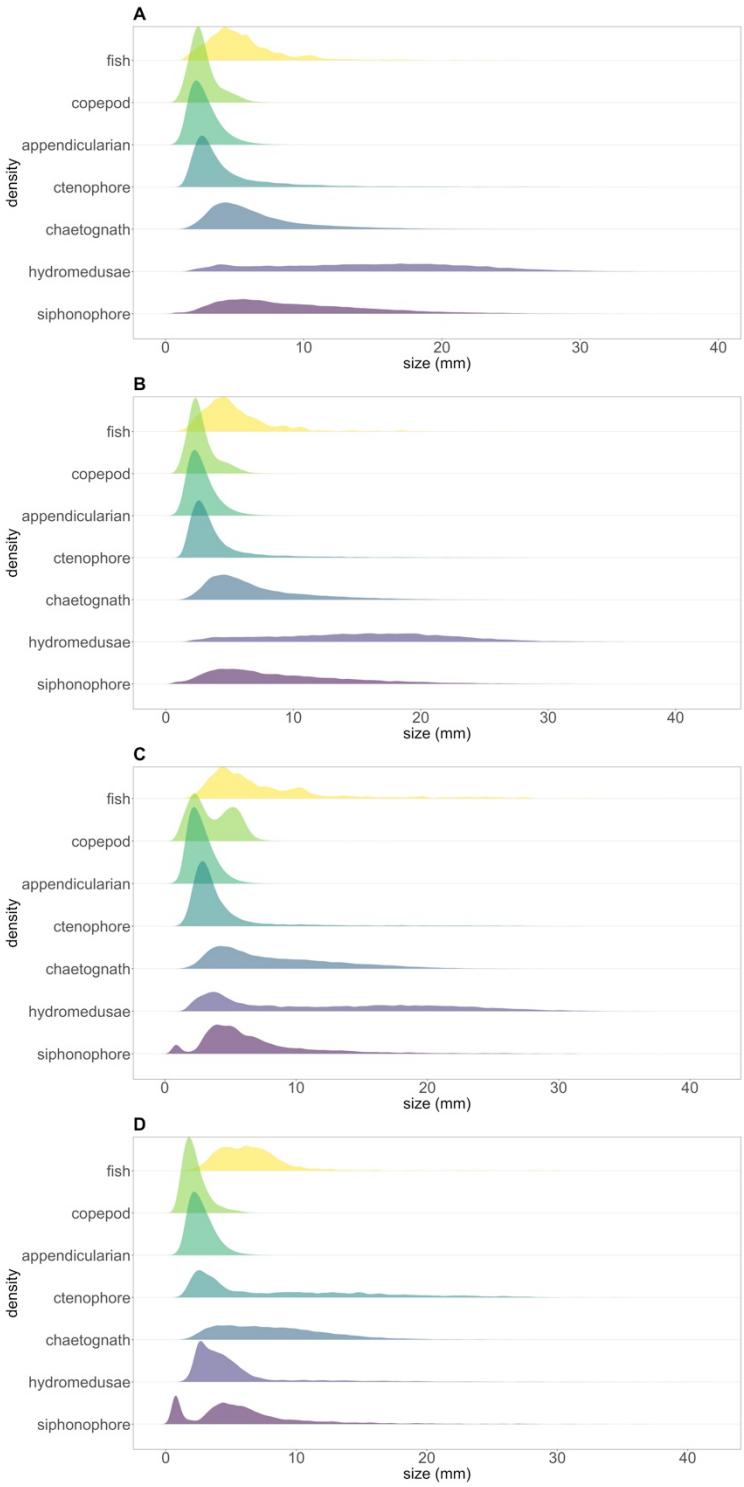

Fig. C2. Taxa size density distributions in (A) transect 1, (B) transect 2, (C) transect 3 inshore, and (D) transect 3 offshore.

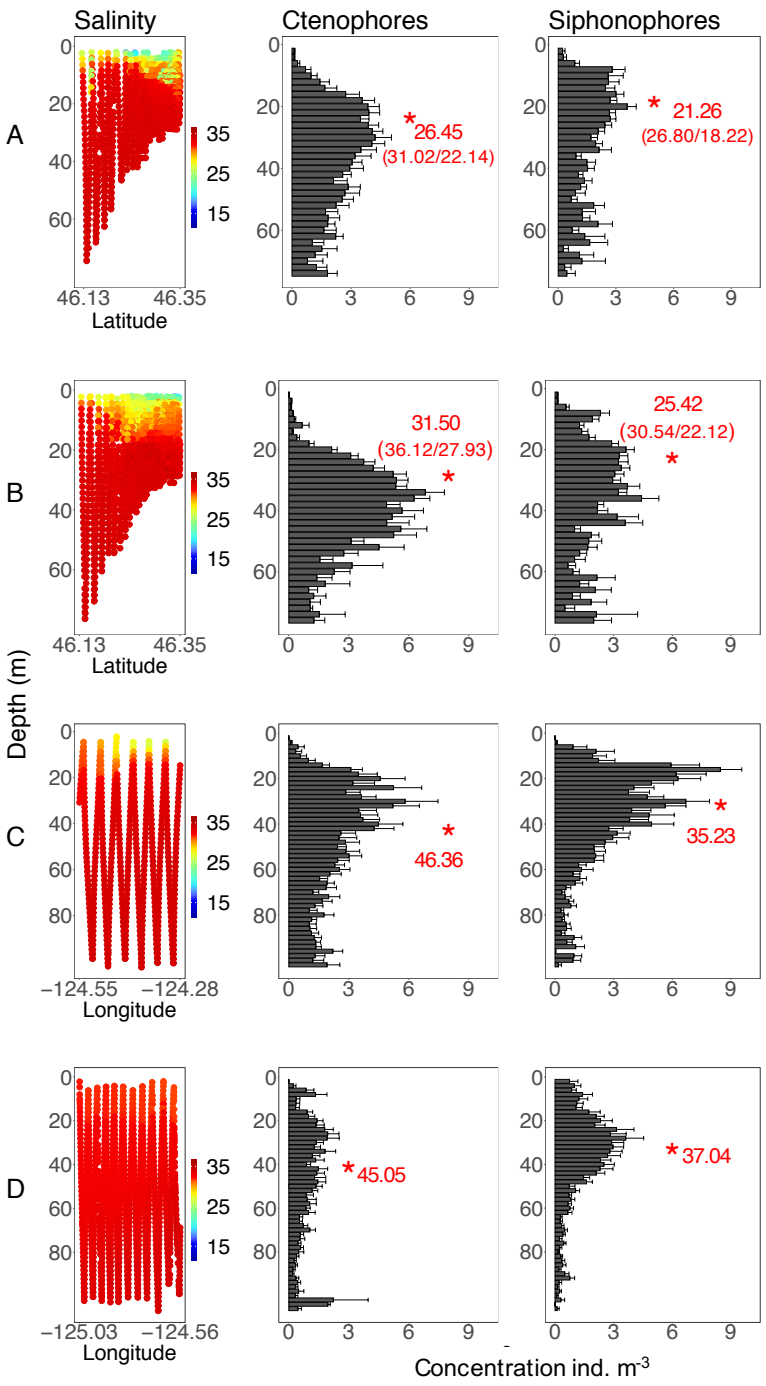

Fig. C3. Mean concentration of each taxa group in every other 1 m depth bin during (A) transect 1, (B) transect 2, (C) transect 3 inshore, and (D) transect 3 offshore of the Columbia River, with transect salinity profiles shown in the far left column. Error bars are standard error and red asterisks indicate the weighted mean depth (WMD; in meters) of taxa distributions. For transects (A) and (B) we also give separate WMDs for the southern (deep) and northern (shallow) sections of the transect separately as (south/north). Latitude is degrees north and longitude is degrees west.

APPENDIX D – Chapter 5 supplementary tables and figures

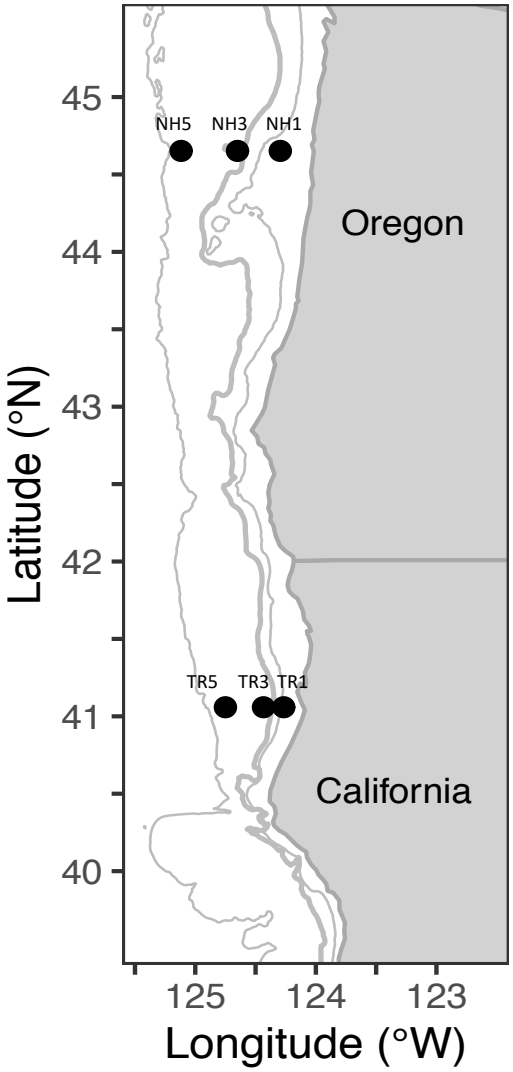

Fig. D1. Locations of stations sampled for Dungeness crab (*Cancer magister*) zoea along the Newport Hydrographic Line (NH) off the coast of Oregon and the Trinidad Head Line (TR) off the coast of California in winters of 2018 (Feb 15-23) and 2019 (Mar 3-11). Contour lines represent the 100-, 200-, and 2000-m isobaths

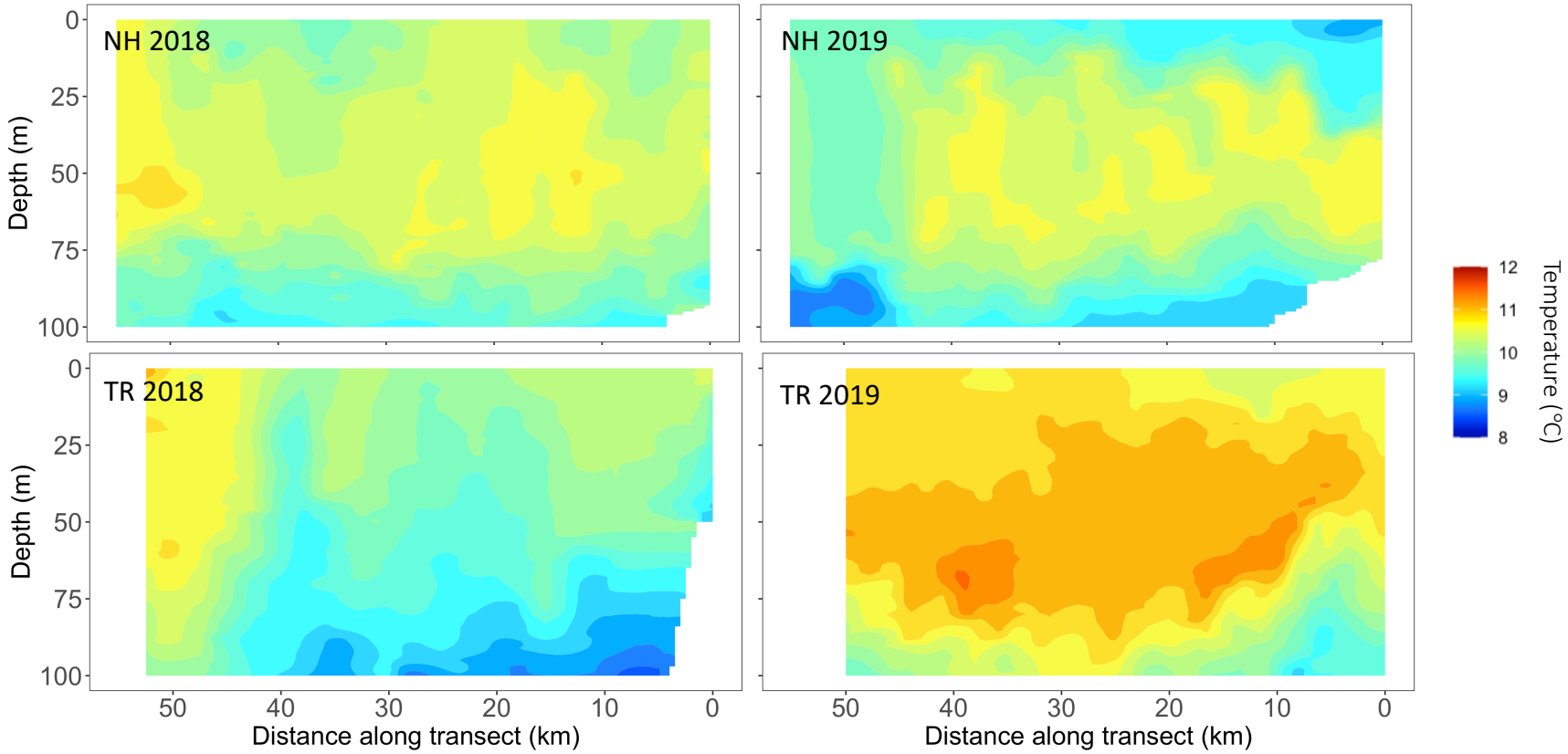

Fig. D2. Cross-shelf mean temperature profiles from the undulating sensor system for the Newport Hydrographic Line (NH) and the Trinidad Head Line (TR) during the winters of 2018 and 2019, with the inshore-most point on the right and offshore on the left. Values are kriged at a 2 m vertical, 500 m horizontal resolution the length of each transect